A PROPOSED GROUND MOTION SELECTION AND SCALING PROCEDURE FOR STRUCTURAL SYSTEMS

A THESIS SUBMITTED TO
THE GRADUATE SCHOOL OF NATURAL AND APPLIED SCIENCES
OF
MIDDLE EAST TECHNICAL UNIVERSITY

BY

BEKİR ÖZER AY

IN PARTIAL FULFILLMENT OF THE REQUIREMENTS
FOR
THE DEGREE OF DOCTOR OF PHILOSOPHY
IN
CIVIL ENGINEERING

DECEMBER 2012

Approval of the thesis:

A PROPOSED GROUND MOTION SELECTION AND SCALING PROCEDURE FOR STRUCTURAL SYSTEMS

submitted by **BEKİR ÖZER AY** in partial fulfillment of the requirements for the degree of **Doctor of Philosophy in Civil Engineering Department, Middle East Technical University** by,

Prof. Dr. Canan Özgen _____
Dean, Graduate School of **Natural and Applied Sciences**

Prof. Dr. Ahmet Cevdet Yalçıner _____
Head of Department, **Civil Engineering**

Prof. Dr. Sinan Akkar _____
Supervisor, **Civil Engineering Dept., METU**

Examining Committee Members:

Assoc. Prof. Dr. Murat Altuğ Erberik _____
Civil Engineering Dept., METU

Prof. Dr. Sinan Akkar _____
Civil Engineering Dept., METU

Assoc. Prof. Dr. Mehmet İnel _____
Civil Engineering Dept., Pamukkale University

Prof. Dr. Ahmet Yakut _____
Civil Engineering Dept., METU

Prof. Dr. Barış Binici _____
Civil Engineering Dept., METU

Date: 27.12.2012

I hereby declare that all information in this document has been obtained and presented in accordance with academic rules and ethical conduct. I also declare that, as required by these rules and conduct, I have fully cited and referenced all material and results that are not original to this work.

Name, Last Name : Bekir Özer Ay

Signature :

ABSTRACT

A PROPOSED GROUND MOTION SELECTION AND SCALING PROCEDURE FOR STRUCTURAL SYSTEMS

Ay, Bekir Özer
Ph.D., Department of Civil Engineering
Supervisor : Prof. Dr. Sinan Akkar

December 2012, 196 pages

This study presents a ground-motion selection and scaling procedure that preserves the inherent uncertainty in the modified recordings. The proposed procedure provides a set of scaled ground-motion records to be used in the response estimation of structural systems for a pre-defined earthquake hazard level. Given a relatively larger ground-motion dataset, the methodology constrains the selection and scaling of the accelerograms to the differences between individual records and corresponding estimations from a representative ground-motion predictive model. The procedure precisely calculates the distribution parameters of linear structural systems whereas it provides estimations of these parameters for nonlinear structural response. Thus this method is not only useful for ground-motion selection and scaling but also for probability based performance assessment studies. The proposed procedure is also capable of matching with a pre-defined target elastic response spectrum and

corresponding variance over a period range. Case studies that compare the performance of the proposed procedure with some other record selection and scaling methods suggest its usefulness for the accurate verification of structural systems and rapid loss estimation studies.

Keywords: Ground-motion record selection and scaling, linear and nonlinear structural response, record-to-record variability, target response spectrum and variance matching, structural performance assessment

ÖZ

YAPISAL SİSTEMLER İÇİN YER HAREKETİ KAYDI SEÇME VE ÖLÇEKLENDİRME YÖNTEMİ

Ay, Bekir Özer
Doktora, İnşaat Mühendisliği Bölümü
Tez Yöneticisi : Prof. Dr. Sinan Akkar

Aralık 2012, 196 sayfa

Bu çalışma yer hareketinin doğasında var olan rassal belirsizliği koruyan bir kayıt seçme ve ölçeklendirme yöntemi sunmaktadır. Yöntem yapısal sistemlerin belirli bir sismik tehlike seviyesindeki davranışını doğru tespiti etmek için kullanılacak yer hareketi kayıtlarını elde eder. Önerilen metot sismolojik parametreleri belli kayıtları sayıca daha fazla aday kayıt arasından seçip ölçeklendirirken yer hareketi tahmin denklemlerini kullanır. Bu yöntem herhangi bir kayıt seti için ortalama doğrusal spektral tepki değerini ve buna bağlı standart sapma değerini zaman-tanım alanı analizlerine gerek olmaksızın hesaplar, doğrusal olmayan davranım için bu değerleri yaklaşık olarak tahmin eder. Bu sayede, yapılardaki hasar seviyelerinin olasılık esaslı yöntemler ile tahmin edilmesinde kullanılabilir. Ayrıca yer hareketi kayıtlarının belirli bir periyot bandı içerisinde hedef medyan spektrum ve buna bağlı varyansa göre seçilip ölçeklendirilmesine de olanak sağlar. Önerilen yöntem ile yer hareketi kayıtlarının seçilmesi ve ölçeklendirmesi

için kullanılan diğer bazı yöntemler arasında yapılan karşılaştırmalar, bu çalışmada önerilen seçme ve ölçeklendirme yönteminin yapıların performans tespiti ve hasar tahmini çalışmaları için kullanışlı olduğunu ortaya koymaktadır.

Anahtar Sözcükler: Yer hareketi seçme ve ölçeklendirme, doğrusal ve doğrusal olmayan yapısal davranış, yer hareketinin doğasında var olan rassal belirsizlik, hedef davranış spektrumu ve varyans eşleme, yapısal performans tespiti

To My Family

ACKNOWLEDGMENTS

This PhD study was carried out under the supervision of Prof. Dr. Sinan Akkar. I gratefully acknowledge his guidance, criticism, advice and enthusiasm throughout this study. It was a great chance to work with him.

I want to thank Assoc. Prof. Dr. Altuğ Erberik and Assoc. Prof. Dr. Mehmet İnel for their support and advice during this research.

I also appreciate the insightful comments of Prof. Dr. Ahmet Yakut and Prof. Dr. Barış Binici to increase the technical quality of this dissertation.

Thanks to Prof. Dr. Güney Özcebe for his inspiring wisdom and personality. I would like to extend my thanks to Assoc. Prof. Dr. Mehmet Halis Günel, Assoc. Prof. Dr. Ayşegül Askan Gündoğan, Prof. Dr. İsmail Özgür Yaman and Asst. Prof. Dr. Hediye Tüydeş Yaman. It has been a privilege to work with them.

I also owe thanks to Tuba Eroğlu Azak, Salim Azak, Özkan Kale and Abdullah Sandıkkaya for their friendship and support whenever I needed.

I would like to express my deepest appreciation to my parents Hasan Hüseyin Ay and Güler Ay and my grandmother Hidayet Özdenler for their endless love, care, and understanding throughout my whole life.

Meral Başak Ay, my lovely wife deserves special thanks for her love, patience and understanding. She gave me encouragement and support in the most difficult times of this study.

TABLE OF CONTENTS

LIST OF TABLES

TABLES

LIST OF FIGURES

FIGURES

CHAPTER 1

INTRODUCTION

1.1 General

Currently one of the major practices in earthquake engineering and engineering seismologists is to focus on the quantification of site-specific hazard and corresponding performance assessment of structural systems. Probabilistic and deterministic seismic hazard analyses (PSHA and DSHA, respectively), as well as rigorous code-based approaches can be employed in order to represent the hazard of an earthquake prone site. Provided that the target seismic demand is quantified, the nonlinear static and dynamic analyses are used for assessing the performance of existing structures.

Despite the prevalence of nonlinear static procedures in the performance evaluation of conventional structural systems, the use of response history analysis (RHA) is appealing and sometimes inevitable for various critical projects (e.g., design of power plants, dams, lifeline systems, tall buildings, structures of strategic importance, etc.). If nonlinear RHA is of concern, an ensemble of accelerograms representing the pre-defined earthquake hazard (seismic demand) is required. This requirement brings forward the significance of obtaining a suitable set of accelerograms since nonlinear structural response can be very sensitive to the employed ground motion time-series.

Generating synthetic ground motions, frequency modification of accelerograms conditioned on a given spectrum or selection and amplitude scaling of recorded acceleration time-series can be described as the main procedures of establishing a set of accelerograms suitable for a pre-defined earthquake hazard level.

Synthetic accelerograms are artificial acceleration time-series that are generated according to the seismological source models, travel path functions and site effects. Despite the continuous improvement in ground motion databanks, generating synthetic accelerograms is still advantageous due to the limited number of useful records satisfying all the ground motion and geophysical parameters suitable for the target earthquake scenario which can be determined by the deaggregation of PSHA or direct results of DSHA. On the other hand, the sensitivity of the resulting accelerograms to the source characterization parameters and difficulties in the determination of these parameters (usually requires expert judgment) are the main disadvantages of these procedures (Bommer and Acevedo, 2004).

Another way of obtaining a set of accelerograms for RHA of structural systems is spectrum matching of ground motion time-series via frequency content modification. Such modifications make the accelerograms match with the target spectrum perfectly, whereas number of artificial waves embedded may produce unrealistic structural response especially for nonlinear dynamic analysis of degrading systems.

The most common and practical way of establishing a ground-motion bin for RHA is selection and amplitude scaling of recorded time-series. This kind of modification neither requires comprehensive expert opinion to fulfill the operational features nor includes peculiar aspects related with the fundamental frequency characteristics of ground motions. Nevertheless, reliability of metadata information and data processing of subject records are the main issues in the selection of recorded acceleration time-series. Inherently, amplitude scaling of

these records raises further concerns related with the source kinematics and the bias (if any) due to excessive scaling (manipulation) of records.

Generating synthetic ground motions and frequency modification of acceleration time-series are out of scope of this study. Selection and amplitude scaling of recorded accelerograms are investigated in this dissertation. In fact, selection and amplitude scaling of records, corresponding seismological constraints and issues associated with random nature of ground motions have been popular research subjects among earthquake engineers and engineering seismologists over a decade with an increasing interest.

The objective of ground motion selection and scaling methodologies is to provide a suitable set of recordings to be used in RHA either to estimate median structural response accurately or to predict the full probability distribution of response for a given scenario event. Current approach in accurate estimation of the median structural response is to eliminate the dispersion about the median by selecting and scaling the subject records conditioned either on a target intensity level (the quantity of site-specific seismic hazard) or on a desired response spectrum. Although such procedures reduce the scatter to particular levels depending on the nonlinearity level and hysteretic behavior of structural system, some objections arise against these methods as they tend to ignore the inherent variance that may exist in the response spectrum (Jayaram et al., 2011). These objections are mainly based on the possibility of obtaining biased response estimations due to zero variance that is also a contradiction in terms of the inherent random nature of earthquake mechanism. Moreover, instead of accurate estimation of median response, most of the earthquake engineering applications, such as seismic performance evaluation of structural systems require the determination of full probability distribution. This way, the integration of PSHA outcomes with risk assessment studies could be accomplished.

The aim of this study is to introduce a ground-motion selection and scaling procedure with a geophysical rationale to be used in the response estimation of structural systems for a given scenario event. Within a relatively larger ground-motion dataset, the proposed method selects the optimum ground-motion bin that satisfies the conditional requirements described by the RHA objective. The procedure scales the ground-motion time-series according to the differences between individual ground motions and their estimations from a representative ground-motion predictive model such that average spectral ordinate of scaled accelerograms matches the target hazard level. This way, the proposed method aims to preserve the inherent aleatory variability in the selected and scaled recordings without manipulating their inherent features excessively. The method can precisely calculate the dispersion about the median structural response when the structure behaves in the elastic range. Moreover, it can provide estimations of median structural response and corresponding dispersion for systems responding beyond their elastic range. This feature makes it as a useful tool for damage assessment or loss estimation studies.

1.2 Literature Survey

Studies on the selection and scaling of recorded accelerograms date back to mid-80s. Search for an "efficient" and "sufficient" intensity measure to be used in the accurate estimation of median structural response is of particular interest for decades. This terminology mainly based on the study conducted by Luco (2002). Luco (2002) describes an "efficient" intensity measure as the one that yields relatively smaller dispersion on the structural response whereas he classifies an intensity measure as "sufficient" if can characterize the seismic demand independent of magnitude or source-to-site distance information. From this theoretical point of view, the best intensity measure is the demand measure itself. However, the practical constraints on the computation of an intensity measure require a trade-off between the practicality and efficiency and sufficiency of the

intensity measure (Luco, 2002). With the aim of having such a quantity, initial tendency of using instrumental peak values is associated or replaced with the use of parameters that are based on energy content (e.g., Arias Intensity (Arias, 1970)) or frequency content during the evaluation of these studies. Eventually, Nau and Hall (1984) concluded that record scaling with respect to spectral ordinates reduce the dispersion on the structural response for low to moderate ductility levels. In his study, Martinez-Rueda (1998) proposed using the spectrum intensity scales (e.g., spectrum intensity scales proposed by Housner (1952), Matsumura (1992) and Martinez-Rueda (1996)) that are well correlated to displacement ductility demand for a given structure. Similarly, Kappos and Kyriakakis (2000) emphasized proper scaling of records with respect to the spectrum intensity (i.e. area under the pseudovelocity spectrum) in order to reduce the dispersion on structural response.

Shome et al. (1998) highlighted the correlation between the dispersion (standard deviation) in the structural response and number of ground motions to be used in RHA to assess damage measures for a given confidence level with emphasis on the choice of an efficient and sufficient intensity measure. Shome et al. (1998) indicated that scaling of recordings by considering the median spectral ordinate of the ground-motion bin at the fundamental period of the structure would result in a median structural response with lesser dispersion. Shome et al. (1998) also discussed the concerns about matching the geophysical parameters of selected records with target earthquake scenario and stressed on the lesser significance of such restrictions in the implementation of their methodology. On the other hand, Stewart et al. (2001) and Bommer and Acevedo (2004) pointed the importance of magnitude match between the selected recordings and target earthquake scenario due to the strong influence of magnitude on duration and frequency content of the ground motion. Krawinkler et al. (2003) discussed the inadequacy of the mere consideration of spectral quantities at the fundamental period for near-fault ground motions for evaluation of structural response. Naeim et al. (2004) emphasized that not only the magnitude but also a proper distance interval that

matches the target hazard scenario is advantageous while selecting the ground motions. Recently, Cimellaro et al. (2011) observed that the magnitude and distance properties of the selected ground motions affect the dispersion on the damage indices.

Another important concern about ground motion scaling is the possible bias of using large scaling factors. In their study, Watson-Lamprey and Abrahamson (2006) highlighted the shortcomings of excessive scaling that may invoke the bias in the structural response. Notwithstanding other studies (e.g., Luco and Bazzurro, 2007) advocated that large amounts of scaling would not produce biased nonlinear structural response unless the spectral shapes of the chosen recordings follow trends significantly different than the target spectrum. Hancock et al. (2008) quantified the upper limit of scaling factor as 10 without introducing bias in structural response given that the records are initially selected to match not only a spectral shape but also the target magnitude. Consequently, spectral shape or epsilon as a proxy for the spectral shape is being increasingly used in the selection and scaling of accelerograms in order to eliminate the bias in structural response statistics. As a matter of fact, Baker (2011) proposed conditional mean spectrum (CMS) on the selection and scaling of ground-motion records. The early phases of spectral shape effect or epsilon were discussed in the consecutive studies of Baker and Cornell (2005; 2006a). Basically, the CMS provides a spectral shape conditioned on the occurrence of a target intensity level associated with deaggregation results.

There are also some other selection and scaling studies aiming to describe the full probability of structural response (e.g., Buratti et al., 2011 and Jayaram et al., 2011). This motivation allows the analyst to consider a reasonable dispersion about target intensity as a proxy of structural response distribution. Hence, selection and scaling of recordings with respect to the target intensity level and corresponding dispersion yield a set of accelerograms suitable to obtain the full probability distribution of structural response that is required for earthquake loss

assessment studies (Huang et al., 2011). Thus the previous selection and scaling procedures provide estimations on the possible standard deviation with the primary objective of obtaining accurate median structural response estimation and reduced dispersion about median response (e.g., Shome et al., 1998). On the other hand, the current studies (e.g., Jayaram et al., 2011; Baker et al., 2011; Baker, 2011) based on the random nature of earthquakes and interaction between ground motions and structural response, show that artificial suppression of variability in the selected recordings imposes some limitations in the accurate quantification of uncertainty in structural response.

Haselton (2009) has recently classified the above methodologies (and many others) into five major groups according to their fundamental features. Almost all methods in these groups primarily intend to obtain recordings with magnitude and distance properties closely matching the scenario event of interest. However, each group differs in several points as they impose numerous constraints on the proposed selection and scaling approach to obtain an optimum ground-motion bin that comply with the objectives of RHA.

Methods in the first group simply scale each ground motion to a target spectral level after selecting the recordings having similar magnitude ranges of the scenario earthquake. The method proposed by Shome et al. (1998) is the benchmark study for the procedures in this group. Although the essential component in Shome et al. (1998) is to have zero dispersion of scaled recordings about the target spectral level, it also approximates the standard deviation of the nonlinear structural response subjected to the scaled recordings. Its simplicity and the use of concepts familiar to engineers are the advantages of this procedure.

The second group methods are the code procedures (e.g., ASCE 7-05 (ASCE, 2006); Eurocode 8 (CEN, 2004)). According to the code-based procedures, records are scaled appropriately such that the average values of response spectra of the scaled recordings closely follow the target design spectrum within a period

interval. Recordings scaled by these methods may lead to conservative median structural response for severe earthquake scenarios as scaling is commonly done over a wide range of spectral periods using the Uniform Hazard Spectrum (UHS) that is associated with large spectral ordinates (Baker, 2011).

The third group methods use the CMS concept of Baker (2011) for selecting the ground motions. This method uses simple amplitude scaling of ground motions over a period range and aims at obtaining reliable estimations of the median structural response without describing the probability distribution of structural response at the target hazard level.

The selection and scaling methods in the fourth group consider the epsilon at the fundamental period of the structure that is obtained from the deaggregation of a site-specific probabilistic hazard analysis (e.g., Baker and Cornell, 2005). They use the epsilon as a proxy for the spectral shape and select ground motions with epsilon values that closely match with the epsilon value determined from deaggregation. These methods are easy to implement because they only try to match the epsilon instead of matching a range of spectral ordinates in selection and scaling. However, they may result in variations in the median structural response among different sets of ground motions assembled for the same hazard level (Haselton, 2009).

Different than the above four groups, the methods in the fifth group consider a close match between inelastic spectral ordinates of target scenario and selected ground motions (e.g., Kalkan and Chopra, 2010; Kalkan and Chopra, 2011). These methods consider the factors important to nonlinear structural response that may result in optimum selection and scaling of recordings to render a better assessment of inelastic structural behavior. However, if the target scenario is based on elastic spectral ordinates, common in many seismic hazard studies, these methods require realistic estimations of inelastic target. Therefore, the

accuracy of these methods is limited to the performance of the tools used to relate elastic and inelastic spectral ordinates in such cases.

1.3 Objective and Scope

Selection and amplitude scaling of ground-motion records are frequently used tools for obtaining a set of accelerograms suitable for the accurate verification of structural systems for a given earthquake scenario. Consequently, this subject is of increasing interest of researchers, code developers and practicing engineers. The primary objective of this study is to introduce a selection and scaling methodology that preserves the basic seismological features of the modified records and leads unbiased median structural response estimations.

This dissertation is composed of seven chapters. The first chapter gives a general overview for the need of obtaining a suitable set of accelerograms and includes a literature survey on ground motion selection and scaling methodologies. The last section of this chapter presents the general features of the ground-motion library used throughout this study.

Chapter 2 presents the general concepts of establishing a candidate ground-motion dataset and selecting the optimum ground-motion bin. Chapter 2 also discusses the current ground-motion record selection and scaling strategies and discusses the concerns related with the modification of ground-motion records.

Chapter 3 introduces the proposed selection and scaling procedure for linear systems. The evaluation of the proposed methodology is addressed by comparing the response statistics obtained by the proposed procedure with those of current scaling methodologies. Besides, this chapter demonstrates the application of the proposed scaling procedure to alternative ground-motion values. Finally,

Chapter 3 investigates some rules to establish the most appropriate candidate ground-motion dataset and the required number of candidate accelerograms.

The proposed selection and scaling procedure is improved for nonlinear structural systems in Chapter 4. In this chapter, the proposed methodology is tested by comparing the proposed methodology with other selection and scaling procedures employing nonlinear single-degree-of-freedom systems.

Chapter 5 investigates the effectiveness of the procedure for the verification of non-degrading, simple (first-mode dominant) multi-degree-of-freedom structural systems. This chapter presents a brief discussion on the statistical features of the Turkish building stock and the analytical building models that reflect the observed characteristics of the examined building stock. The second part of this chapter is devoted on the evaluation of the proposed methodology for MDOF systems and compares the results with alternative selection and scaling procedures. The discussions in the second part of Chapter 5 convey the limitations of the procedure as a tool for probabilistic vulnerability assessment studies.

Chapter 6 discusses the implementation (modification) of the proposed procedure to the spectrum matching concept. Compatibility with a target response spectrum median and corresponding variance conditioned on a given target intensity level is discussed. A new parameter is introduced in this chapter for its use in the modified selection and scaling procedure for cases where target response spectrum and variance matching is desired over a pre-defined period range. The performance of the modified selection and scaling procedure is investigated and corresponding limitations are discussed at the end of Chapter 6.

Finally, Chapter 7 concludes the observations on the selection and amplitude scaling procedure presented in this dissertation. This chapter summarizes the comparisons, evaluations and investigations on alternative selection and scaling

procedures. The last section of Chapter 7 includes some recommendations for future studies related with the procedure presented in this dissertation.

1.4 Ground-Motion Record Library Used in This Study

The ground-motion record library used in this study is gathered from the Turkish national strong ground-motion (http://kyh.deprem.gov.tr/ftpe.htm), PEER-NGA (http://peer.berkeley.edu) and the European strong-motion (http://www.isesd.cv.ic.ac.uk) databases. The reliability and consistency of data processing and uniformity of records in terms of magnitude scales and distance metrics are considered as the major concerns while compiling the ground-motion record library. Records within a moment magnitude (M_w) range of $5.0 \leq M_w < 7.7$ and source-to-site distance (R_{JB}, the closest distance from the vertical projection of ruptured fault (Joyner and Boore, 1981)) interval from 0 km to 100 km are selected to focus on seismic excitations that are of engineering significance. The selected accelerograms satisfy NEHRP C and NEHRP D (see BSSC, 2009 for NEHRP site classifications) soil conditions.

The selected ground motions are clustered for specific M_w and R_{JB} intervals. Clustering in five magnitude bins is utilized in order to account for the frequency content and strong-motion duration characteristics of records. Similarly, records are grouped into three R_{JB} bins for a reasonably fair consideration of distance effects on ground-motion bins. A total of 260 accelerograms from 113 different events are compiled. Table 1.1 lists the number of records in each M_w–R_{JB} bin whereas Figure 1.1 displays site conditions of records as well as the magnitude and distance boundaries of these bins. As it is inferred from Table 1.1 and Figure 1.1, fifteen ground-motion bins of different magnitude and distance intervals are used for clustering the ground-motion library. The magnitude intervals are identified by indices M1 to M5 whereas the indices used for distance intervals are designated as SR, IR and LR. The identification of a particular

M_w–R_{JB} bin is done by combining the magnitude and distance indices. For example, M1SR cluster refers to the ground-motion subset having recordings of $5.0 \leq M_w < 5.5$ and $R_{JB} < 20$ km. This naming convention is used throughout the dissertation while referring to specific clusters of the compiled ground-motion library.

Table 1.1 Number of accelerograms in each ground-motion bin

		SR	IR	LR
		$0\text{km} \leq R_{JB} < 20\text{km}$	$20\text{km} \leq R_{JB} < 50\text{km}$	$50\text{km} \leq R_{JB} < 100\text{km}$
M1	$5.0 \leq M_w < 5.5$	17	17	22
M2	$5.5 \leq M_w < 6.0$	15	17	15
M3	$6.0 \leq M_w < 6.5$	22	21	27
M4	$6.5 \leq M_w < 7.0$	13	16	13
M5	$7.0 \leq M_w < 7.7$	14	16	15
TOTAL		81	87	92

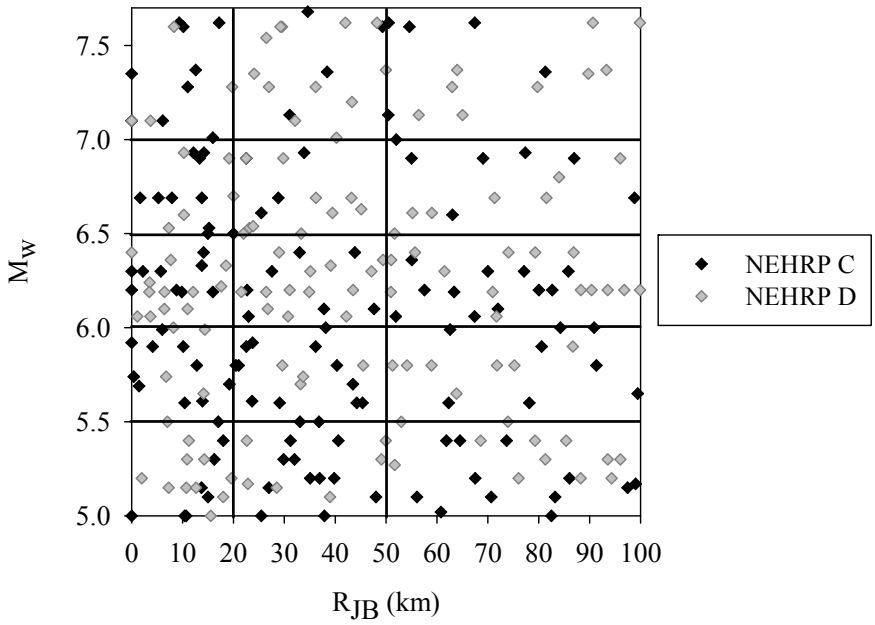

Figure 1.1 M_w versus R_{JB} distribution and NEHRP soil type information of records in each ground-motion bin (horizontal and vertical lines represent magnitude and distance interval boundaries, respectively)

The accelerograms in the ground-motion library, their important properties (M_w, R_{JB}, soil type and style-of-faulting), peak ground-motion values (PGA, PGV) and elastic spectral displacement ordinates are given in Appendix A.

CHAPTER 2

GROUND-MOTION RECORD SELECTION AND SCALING

2.1 Ground-Motion Record Selection for Response History Analysis

The identification of ground-motion records to be used in the evaluation of structures is a critical issue as it directly influences the structural response estimations. The literature for selecting a pre-defined number of recordings within a candidate ground-motion dataset is developing consistently due to the advances in engineering practice such as improvements in nonlinear RHA, faster computers for running RHA, etc. Although there is a consensus on the importance of this subject in earthquake engineering and engineering seismology communities, the ways of achieving this goal differ due to theoretical and practical constraints of engineers and seismologists. For instance, the primary concern of earthquake engineers is accurate estimation of structural response by performing a limited number of RHA whereas engineering seismologists also consider the importance of selecting ground-motion records having comparable seismological features with target earthquake scenario. This section discusses the limitations of record selection strategies in terms of earthquake kinematics and presents common ground-motion selection principles.

2.1.1 Assembling Candidate Ground-Motion Dataset

Using real records for RHA of structures is still the most popular way of assembling the input ground-motion dataset because no consensus has been reached among the engineering community on the use of synthetic accelerograms for structural analysis. This is because generating synthetic accelerograms that can properly represent the high- and low-frequency ground-motion components is still considered as an expensive and challenging task (Akkar et al., 2012).

Despite the rapid increase of real accelerograms and relative ease of obtaining them from different online sources (e.g., http://kyh.deprem.gov.tr/ftpe.htm), the current resolution of the strong-motion datasets usually does not provide sufficient number of recordings that fully comply with the geophysical and seismological constraints of a given scenario earthquake. This is particularly valid for large magnitude events for which the data distribution is sparse and relatively non-uniform. Consequently, the common approach in earthquake engineering community is to assemble a candidate (preliminary) accelerogram bin that can fairly address the overall seismological and geophysical features of the scenario earthquake. The final selection and scaling of recordings among the candidate accelerograms are then accomplished to have an optimum ground-motion bin that fully matches with the target intensity level of the scenario earthquake.

Among seismological features, the earthquake magnitude is a primary search parameter because it is the best proxy of ground-motion frequency content and duration. The latter two parameters have a significant effect on nonlinear structural response. As a result, there is a general consensus among most of the record selection strategies as well as building codes (e.g., ATC-58 50% Draft (ATC, 2009)) to select the recordings from a magnitude interval that is representative of the scenario event. This can be accomplished by selecting accelerograms with magnitudes closely matching the target magnitude. The

criterion satisfying this objective is quantified as 0.25 units and 0.20 units at either side of the target magnitude by Stewart et al. (2001) and Bommer and Acevedo (2004), respectively. Note that Bommer and Acevedo (2004) also discusses the objections against using such narrow magnitude intervals. Bearing these debates in mind, ±0.5 units of magnitude might be forced as limiting values for the magnitude interval from which the candidate records are selected. In any case, such an approach should be applied with caution for cases where the structural response is assumed to be less sensitive to earthquake duration (e.g., non-degrading and regular structures are relatively less sensitive to the number of cycles of earthquake ground motions).

In addition to magnitude, source-to-site distance is also used as a constraint in database queries while assembling the candidate ground-motion dataset. However, it is widely accepted that the sensitivity of dynamic structural response to source-to-site distance is less significant (e.g., Bommer and Acevedo, 2004; Stewart et al., 2001). Consequently, for cases where the number of candidate accelerograms has to be increased, relaxing the source-to-site distance constraint is more reasonable than increasing the magnitude interval. Nevertheless, some building codes (e.g., ASCE 7-05 (ASCE, 2006), FEMA P-750 (BSSC, 2009)) require the analyst to use records of events having source-to-site distance that is consistent with the target earthquake scenario.

Finally, the influence of style-of-faulting (rupture mechanism) and soil type on structural response may also be taken into consideration in record selection strategies. Inherently, the style-of faulting and soil class affect the ground-motion amplitude. However, the influence of style-of faulting on structural response is rather complicated and depends on the fundamental period of the structure. Except for very soft (modifying either low- or high-frequency ground motions depending on their level of amplitude or resulting in narrow-band accelerograms) or rock sites (amplifying high frequency ground motions), the effect of soil is limited on structural response with respect to magnitude and distance. Besides,

the number of candidate accelerograms may decrease significantly (even if the strong motion databank is extensive) when these criteria are considered together with the major ones discussed in the previous part. Thus the tendency among engineers is to exclude these two constraints. This study acknowledges the importance of style-of-faulting as well as the site conditions on ground motion behavior. Consequently, the style-of-faulting and soil class criteria are relaxed partially in favor of obtaining a fair amount of accelerograms while assembling the candidate bin. The scaling methodology proposed in this study preserves the pertinent style-of-faulting and site class features of each candidate accelerogram through the use of ground-motion prediction equations (GMPEs) as discussed in the latter sections.

In addition to the constraints presented, some general requirements on records should also be taken into account. Main issues to be addressed while selecting the records are the consistency of data processing and the metadata quality of records having reliable magnitude, source-to-site distance, site class, style-of-faulting and usable period range information. Near-fault records with pulse effects should be used with caution. Finally, dominancy of records from one single event or one single recording station should be prevented in order not to have biased structural response towards that earthquake (Bommer and Acevedo, 2004).

2.1.2 Final Selection of Ground-Motion Records

Accurate estimation of structural response requires selection of “appropriate records” that represent the target ground-motion hazard. The term “appropriate records” denotes an optimum ground-motion bin that yields the most proper information about dynamic structural response. Theoretically, the optimum dataset contains recordings that match the target intensity level with zero variance or they approximate the target response spectrum median and variance. The former criterion is of particular use when the estimation of median structural

response is of concern. The latter criterion is suitable for probabilistic structural analysis methods that evaluate the likelihood of seismic risk by considering the uncertainties in structural response as well as ground motion.

Among the procedures that aim to evaluate the median structural response, the method proposed by Shome et al. (1998) is one of the benchmark studies in ground-motion selection and scaling. Shome et al. (1998) stated that given a ground-motion bin, scaling each record to target median spectral ordinate (at a given period) produces accurate nonlinear response results even if the records are selected randomly without considering any geophysical or seismological parameter. Other studies (e.g., Shome, 1999; Cordova et al., 2000; Luco, 2002) showed that mere consideration of target elastic spectral ordinate at the fundamental period of the structure may produce biased median response. More recently, Baker (2011) suggested the selection of scenario-specific ground motions that agrees with the CMS in order to estimate the median response more accurately. This way, Baker (2011) constrained the selection of recordings to match a target spectrum for a given period interval with the intention of considering period elongation due to inelastic response and higher mode effects.

With the aim of obtaining full probability response, Buratti et al. (2011) proposed selecting the ground-motion records individually that match a target response spectrum within a period interval. The procedure by Buratti et al. (2011) considers the variance of target response spectrum explicitly. The procedures such as those proposed by Baker (2011) and Buratti et al. (2011) are practical and fast methodologies since each candidate record is evaluated individually in terms of a deviation measurement (e.g., root-mean-square difference) from target spectrum at the final selection. Similar to Buratti et al. (2011), Jayaram et al. (2011) emphasized the importance of considering the variance in target response spectrum. Jayaram et al. (2011) pointed that recordings that match the target response spectrum with zero variance would produce smaller than the actual dispersion about median nonlinear response. This may result in biased

interpretations about the building behavior. In essence, given a relatively large candidate ground-motion dataset, Jayaram et al. (2011) recommended the final selection to be based on median target response spectrum and its variance. Jayaram et al. (2011) also proposed investigation of entire ground-motion dataset instead of dealing with each record individually. Jayaram et al. (2011) indicated that for a given median target spectrum and its variance, the compatibility of an individual accelerogram can only be quantified in the context of recording dataset that contains the subject accelerogram. This type of approach corresponds to a combination problem that may yield excessive number of recording datasets and an indispensable computational effort. Although some solution strategies about this combination problem are previously investigated by various researchers (e.g., Naeim et al., 2004 and Kottke and Rathje, 2008), they still need some further refinement for their wide use among engineers who are involved in probabilistic risk assessment studies.

In the context of above discussions, the selection of final recording set is directly related with the analysis objective and corresponding computational effort. These concerns raise the issue of required number of acceleration time-series to be selected from a candidate ground-motion dataset.

There are various studies in the literature that propose methods for selecting predefined number of accelerograms, n, within a candidate ground-motion dataset that contains "k" accelerograms (e.g., Shome et al., 1998; Baker and Cornell, 2006a; Luco and Bazzurro, 2007; Reyes and Kalkan, 2011; Baker, 2011). However, the literature is relatively limited in determining the required number of recordings. In essence, the required number of records, n, may depend on the codes, analysis methods, the objective of linear/nonlinear RHA, the tolerance level in response accuracy etc. In their study, Shome et al. (1998) showed that halving the dispersion about median target response spectrum decreases the number of required nonlinear RHA by a factor of 4. This observation is the result of standard error (SE) (the standard deviation of the sample mean) computation,

which conveys information about the measure of uncertainty associated with the sample mean. The calculation of SE is given in Equation 2.1, where the standard deviation (σ) of the response is normalized by the number of observations obtained from n recordings.

$$SE = \frac{\sigma}{\sqrt{n}} \tag{2.1}$$

Consequently, for a given level of SE, the number of required acceleration time-series is proportional to the square of observed dispersion in response. By using the relationship between the predictability of the median response and number of observations for a given level of confidence, Hancock et al. (2008) investigated the minimum number of required acceleration time-series. Hancock et al. (2008) showed that the minimum number of required recordings with similar seismological characteristics will reduce from 13 to 3 if they are scaled to a common target spectral level at the fundamental period of the structure. Hancock et al. (2008) also stated that even one unique record will yield this information, if it is scaled to match a target response spectrum over a period range. The numbers proposed by Hancock et al. (2008) were specifically derived for estimating the median maximum roof drift within ±10 % range at 64 % confidence level. More recently, Buratti et al. (2011) highlighted that the number of observations to be used for determining the full probability distribution of response are greater than those that are employed for accurate estimation of median response. For instance, for cases where spectral acceleration is selected as the intensity measure, Cimellaro et al. (2011) indicated that the minimum number of recordings should be 20 to accurately evaluate the fragility curves of a non-degrading, first-mode dominant structure. They also proposed using at least 10 scaled ground-motion records for estimating the first-story drift response with an error of less than 10 %.

In addition to these studies, several codes (e.g., Eurocode 8 (CEN, 2004), FEMA P-750 (BSSC, 2009)) as well as the Turkish earthquake code (TEC, 2007), require selecting at least 7 records (n=7) for accurate median prediction of structural response. Alternatively, ATC-58 50% Draft (ATC, 2009) force the analyst to choose at least 11 accelerograms (n=11) for RHA in order to be used in loss assessment studies. As a matter of fact, ATC-58 35% Draft (ATC, 2007) noted that 11 ground-motion records are required in order to capture the record-to-record variability and hence the dispersion in structural response. Later, ATC-58 50% Draft (ATC, 2009) modified this statement and indicated that using at least 11 recordings in loss assessment studies will convey accurate information of median structural response estimations. Controversially, ATC-58-1 75% Draft (ATC, 2011) pointed that (based on a limited study), even 3 acceleration time-series can be adequate to obtain accurate estimations of median structural response, if the spectral shape of the selected recordings has a good match with the target spectrum. If the agreement between the response spectrum of selected records and target spectrum is poor, then ATC-58-1 75% Draft (ATC, 2011) also requires selecting 11 ground motions to obtain unbiased median structural response estimations. As a side note, this guideline does not specify how to quantify the goodness of fit between target and individual spectra that directly affects the required number of records.

2.2 Scaling of Ground-Motion Records

Amplitude scaling allows the analyst to modify either an individual accelerogram or a set of accelerograms through scalar factors. This way, the analyst would establish a set of acceleration time-series to be used for accurate estimation of either the median response or full probability distribution of response, which conveys important information about the performance of a structure for a future earthquake scenario. This section discusses the need of scaling, introduces common scaling techniques and investigates major concerns of earthquake

engineers and engineering seismologists for linear modification of ground-motion records.

2.2.1 The Need of Scaling

The need for scaling accelerograms stems from the purpose of obtaining a set of records that are compatible with the seismicity of the subject area. In other words, to simulate the future seismic actions and obtain corresponding structural response, recorded (but amplitude wise modified) accelerograms that represent the expected intensities of scenario earthquake should be employed in RHA. The scaling of accelerograms is almost a must for accurate estimation of structural performance. Otherwise, a significant number of RHA is required upon the use of unscaled records due to the large variability in the strong-motion characteristics of the accelerograms. In other words, ensuring a reasonable accuracy in structural response estimations requires either identifying accelerograms that are similar in strong-motion characteristics (which may be difficult to find although they would yield reduced record-to-record variability) or employing relatively larger numbers of ground-motion records. Alternatively, scaling of properly selected ground-motion records can be used to warrant the accelerograms having similar strong-motion characteristics with the aim of accurate estimation of structural response. This way, the analyst can reduce the number of ground motions required to obtain reliable information on the seismic performance of structural systems.

2.2.2 Concerns Regarding Ground-Motion Record Scaling

This dissertation has already addressed several issues of record selection for RHA of structures in previous sections. The problem in this topic is obtaining records that yield unbiased estimations of structural response. The fundamental concerns of ground-motion record scaling also originate from the same reason. Among

these, the possible bias of using large scaling factors and the intensity measure selected as the scaling reference are the main issues raised by engineers and engineering seismologists.

As presented in the previous chapter, various researchers (e.g., Iervolino and Cornell 2005; Watson-Lamprey and Abrahamson, 2006, etc.) investigated whether scaling introduce a bias to the structural response and if so what is the limit of scaling for obtaining unbiased results. Based on these investigations, one would immediately infer that records that are scaled with factors close to 1 are not manipulated significantly (i.e. they still preserve their fundamental seismological features after being scaled). In such cases the analyst would yield relatively more reliable results in terms of structural response. For cases where relatively large scaling factors should be employed, proper selection of records may reduce the possible bias in structural response (Luco and Bazzurro, 2007). Consequently, to increase the accuracy of the structural response estimations, it is advantageous to select records with similar strong-motion characteristics and try to use smaller scaling factors as much as possible.

Another important issue of ground-motion record scaling is the intensity measure used as the target reference. An intensity measure is a ground-motion parameter that relates the effect of record's amplitude to the corresponding structural response. The capability of the intensity measure to reduce the dispersion on damage indices is the indicator of its efficiency. The degree of independency of the resultant response from other ground-motion parameters represents the sufficiency of an intensity measure (Luco and Cornell, 2007). The literature is abundant of proposing alternative intensity measures (e.g., Giovenale et al., 2004; Akkar and Özen, 2005; Vamvatsikos and Cornell, 2005; Tothong and Cornell, 2008; Yang et al., 2009; Kadaş et al., 2011) for a better correlation with structural response. Consequently, an intensity measure that is well correlated with structural response is desired to estimate the structural performance accurately. In this respect, scaling the subject records according to this reference measure will

further increase the reliability of results. Peak ground motion values such as PGA was preferred and used previously due to the code-based spectral shapes anchored to these parameters. Later, various researchers have proven that structure specific intensity measures such as spectral displacement at the fundamental period of structure ($S_d(T_1)$) perform better if the elastic response of non-degrading structures with limited higher mode effects is of concern. Alternatively, instead of using a scalar intensity measure, a vector valued intensity measure as a combination of $S_d(T_1)$ and epsilon is proposed in order to improve the correlation with damage indices (e.g., Baker and Cornell, 2005).

The ease of incorporating the demand measures calculated for a given intensity level into the PSHA studies is another important concern in the choice of intensity measure. To estimate the probabilistic seismic risk of structures, hazard curves derived by using the selected intensity measure is required. Consequently, the target seismic intensity provided by PSHA usually makes the analyst either use the same quantity as the scaling reference or employ additional tools to incorporate the RHA results with the ground motion hazard. The latter option is relatively difficult and less common in current engineering practice. In this respect, peak ground-motion values and elastic spectral quantities are advantageous due to their wide use in ground-motion prediction models. Selection of an intensity measure with the properties described above is a concern in record scaling procedures. Thus scaling procedures which are equally applicable to a variety of intensity measures are advantageous.

Assembling a set of accelerograms for RHA using a single horizontal component or employing both horizontal components is usually a concern related with the complexity of the subject structure and the definition of the target intensity level. The latter topic depends on the employed GMPE that is used to derive the seismic hazard (Beyer and Bommer, 2006 and Beyer and Bommer, 2007). The major horizontal component definitions of spectral quantities used by GMPE's are geometric mean (e.g., Akkar and Bommer, 2010), GMrotI50 (e.g., Campell and

Bozorgnia, 2008), envelope of two components (e.g., Bindi et al., 2010) and randomly chosen component (e.g., Atkinson and Boore, 2003). Among these, GM is the most common horizontal component definition because of its relative simplicity. From amplitude scaling of records point of view, the advantage of using GM is employing a single scaling factor for each of the two horizontal components and applying this factor to both horizontal components simultaneously to preserve the original difference between these components (Bommer and Acevedo, 2004). This study uses GM as the definition of horizontal component for proposed scaling procedure. However, the proposed methodology can be used with other horizontal component definitions to keep the consistency between scaling and the horizontal component definition used in the GMPE.

2.2.3 Common Ground-Motion Record Scaling Techniques

Amplitude scaling of a record is linear modification of original ground-motion amplitude by multiplying the acceleration data with a scalar factor. The factor is called as "scaling factor" which is the ratio of the target intensity level to the recorded (unscaled) amplitude.

In terms of target intensity measure, peak ground-motion values or spectral quantities can be the possible parameters as described in the previous section. Among these, spectral quantities are widely accepted in engineering community as an example of structure specific intensity measures. If these are of concern, a target spectral value at a single period or a target spectrum defined for a given period range affects the calculation of scaling factors and consequently the scaling methodology. Similarly, for a particular set of ground-motion records, the scaling methodology vary depending on either consideration of each record individually, or comparing the median amplitude of subject recording set with the target intensity. This section discusses the common scaling methodologies and

their limitations in terms of accurate estimation of structural response and random nature of strong-motion characteristics.

The current scaling techniques generally modify the amplitude of each record in a ground-motion bin to the target spectral value at the fundamental period of the subject structure. This kind of a scaling is called as stripe-scaling (Jalayer et al., 2007) because structural responses obtained by using these records are aligned on a stripe for the given target intensity level. Among these types of scaling methodologies, the procedure proposed by Shome et al. (1998) is widely accepted by the engineering community as it focuses on the concepts that are familiar to the structural engineers. Basically, Shome et al. (1998) propose to scale each record in a bin to the target median spectral ordinate (at a given period) to reduce dispersion in dynamic response. Accordingly, the calculation of scaling factor (SF) for a record, i, is given in Equation 2.2.

$$SF_{record,i} = \frac{PS_{a,target}(T_1)}{PS_{a,record,i}(T_1)} \tag{2.2}$$

In Equation 2.2, pseudo-spectral acceleration (PS_a) at the fundamental period of structure (T_1) is selected as the subject target spectral quantity ($PS_{a,target}(T_1)$) just for illustrative purposes. Any spectral quantity can be chosen for the calculation of scaling factor. Shome et al. (1998) concluded that such a scaling procedure produces unbiased nonlinear response results. Figure 2.1 shows elastic PS_a values (geometric mean of two horizontal components are used) of records in a ground-motion bin before (left) and after (right) scaling by using the method proposed by Shome et al. (1998) for a vibration period of 1.2 seconds. The example ground-motion bin is composed of 10 records selected according to a fictitious target scenario with a moment magnitude (M_w) value of 6.25, site to source distance (R_{JB}) of 10.5 km and an epsilon (ε) value of 1.25. Corresponding target pseudo-spectral acceleration value is 286 cm/s^2 according to the Akkar and Bommer

(2010) ground-motion prediction model. The moment magnitude interval of subject records is between 6.19 and 6.36 with a median value of 6.26. The minimum R_{JB} distance of the records in the dataset is 2.2 km whereas the maximum R_{JB} distance is 18.5 km. The average of R_{JB} values is 10.4 km. The average scaling factor used for this particular ground-motion record bin is 1.48 with maximum and minimum values equal to 2.78 and 0.75, respectively.

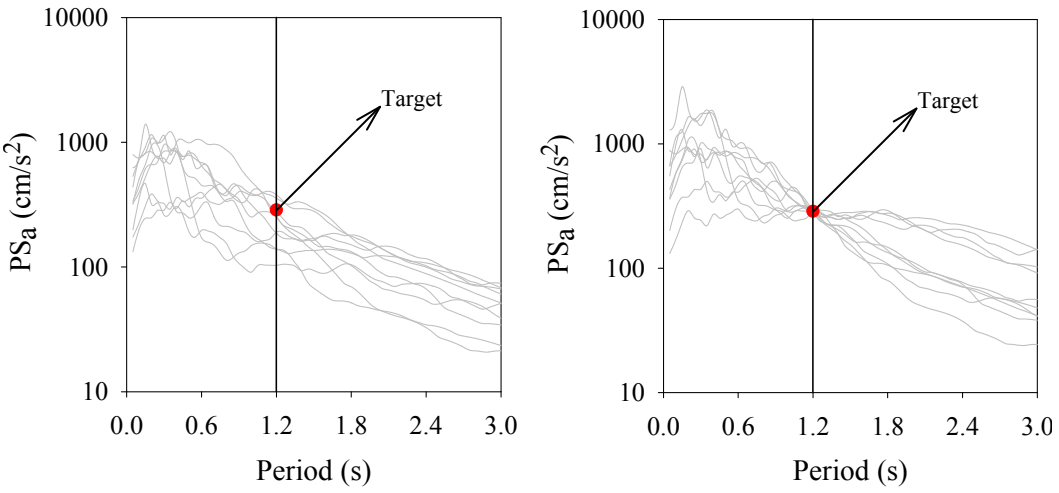

Figure 2.1 Scaling to target median pseudo-spectral acceleration according to the method proposed by Shome et al. (1998)

Although these approaches are proved to be efficient for obtaining suits of scaled records that would yield lower dispersion in elastic spectral response parameters, they do not warrant any seismological basis. Moreover, for stripe-scaling methodology, the uncertainty in structural response is very sensitive to higher-mode effects and/or significant inelastic behavior. Figure 2.2 shows the increase of dispersion with the level of inelasticity for stripe-scaling methodology. The figure shows the results of single-degree-of-freedom (SDOF) RHA using the scaled ground motions described in the previous paragraph. The inelasticity level is represented by strength reduction factor, R (the ratio of elastic strength demand to the yield strength of a SDOF system) in these plots. The panel on the left shows the scatter in pseudo-acceleration spectra for a low-level

inelasticity (mimicked by R=2) whereas the right-hand-side panel exhibits the same dispersion measure for R=4 (moderate-level inelasticity).

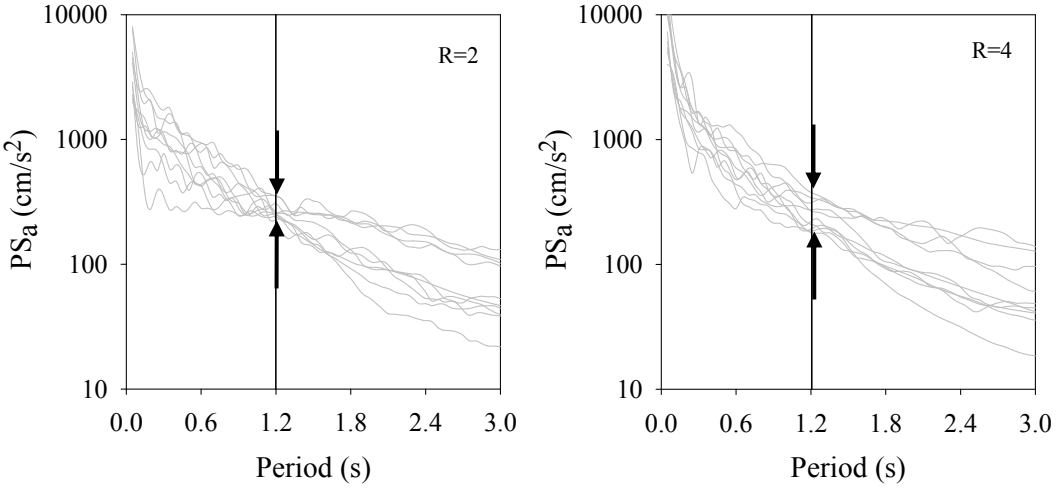

Figure 2.2 The increase in dispersion with increasing level of inelasticity for stripe-scaling

Another way of amplitude scaling is based only on matching the median spectral value of unscaled ground-motion records to the target intensity level. In other words, instead of scaling each accelerogram in a ground motion bin to the target spectral level individually, this scaling method modifies all records with the same scaling factor such that the median spectral level of scaled accelerograms coincides with the target spectral intensity. This type of scaling is named as cloud scaling (Giovenale et al., 2004) where the common scaling factor (SF) of records is calculated as given in Equation 2.3.

$$SF_{record,i} = \frac{PS_{a,target}(T_1)}{\mu_{PS_a(T_1)}} \tag{2.3}$$

In Equation 2.3, $SF_{record,i}$ is the scaling factor that is used to modify the i^{th} record in ground-motion bin, whereas $\mu_{PS_a(T_1)}$ is the average pseudo-spectral

acceleration value of the records. Figure 2.3 displays the unscaled pseudo-spectral acceleration values of the sample group presented in the previous case (left panel) and modified records by using cloud-scaling methodology (right panel) for the same vibration period of 1.2 seconds. The average scaling factor used for this case is 1.26 which is less than the average scaling factor used for stripe-scaling method. So, the manipulation of the subject records is less, whereas the final dispersion is obviously more. Since each record in the bin is modified with the same scaling factor, the dispersion about spectral values before and after cloud-scaling remains the same. Consequently, the observed coefficient of variation (COV) for a series of inelasticity levels is 0.42 both for original (unscaled) records and cloud-scaled ground-motion bin. The COV statistics is a measure of dispersion and displays the standard deviation (scatter) normalized by sample mean.

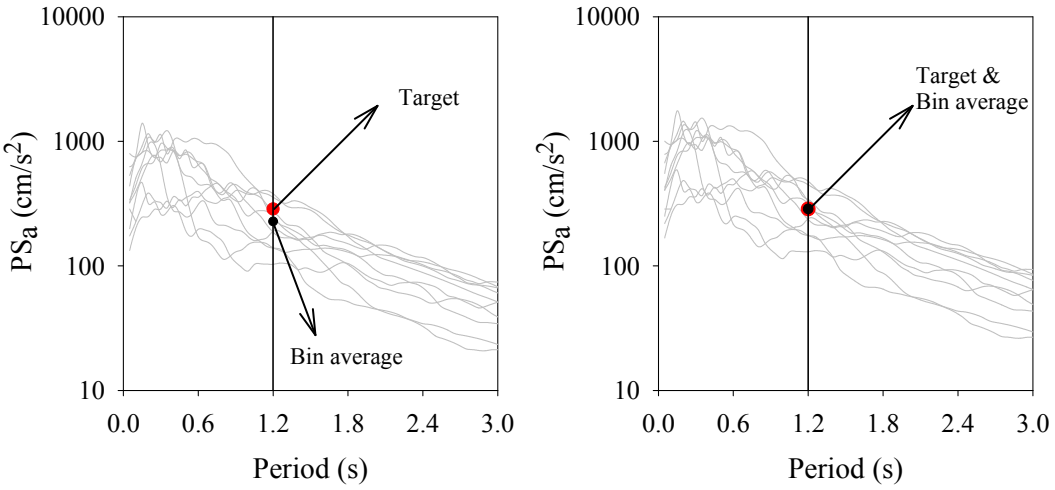

Figure 2.3 Cloud-scaling to target median pseudo-spectral acceleration

Instead of scaling to the target spectral value at the fundamental period of the structural system, a target spectrum defined for a given period range can also be used. This spectrum can be a code-based spectrum, a uniform hazard spectrum or a spectrum conditioned on a target spectral level associated with geophysical parameters that are obtained from deaggregation of PSHA study. The selection of

the target spectrum is a subject of ongoing research and discussion. No matter on which basis the target spectrum is defined, the primary objective of using a target spectrum for a given period interval is to consider the higher mode effects and the period shift due to the inelastic response. This way, the spectral shape is accounted for the modifications made in the acceleration data of the records in order to eliminate the potential scaling bias and reduce the variance. To achieve a match between the target spectral shape and the spectrum of each record, the scaling factor is calculated by using Equation 2.4.

$$SF_{record,i} = \frac{\sum_{i=1}^{t} PS_{a,target}(T_i)}{\sum_{i=1}^{t} PS_{a,record,i}(T_i)} \tag{2.4}$$

In Equation 2.4, "t" is the total number of period values within the pre-defined period interval where the spectral match is of interest. This value is suggested as 50 by Baker (2011) in order to achieve a reasonably smooth match. In his report, Haselton (2009) suggests to use 20 periods with uniform logarithmic spacing for measuring the spectral match. Both studies propose using a period interval ranging from 0.2 T_1 to the 2.0 T_1, where T_1 is the fundamental period of the structure. This criterion is quantified as 0.2 T_1 and 1.5 T_1 in some codes (e.g., ASCE 7-05 (ASCE, 2006)).

Figure 2.4 shows unscaled acceleration spectra of the previously described sample ground-motion bin (left panel) and spectra of the scaled records (right panel) for the fundamental period of 1.2 seconds. The period interval is defined from 0.2 T_1 to 2.0 T_1 for this particular example. The match between original and target spectra are investigated for 45 linearly spaced intermediate period values. In this case, the average scaling factor is found as 1.54, whereas the maximum and minimum scaling factor values are 2.86 and 0.79, respectively. The observed COV at the fundamental period of the structure (T_1 = 1.2 s) is 0.32 which is less

than the unscaled case. Although the level of dispersion is reduced with respect to unscaled case, this is most probably a coincidence as this scaling methodology aims at achieving a match between the scaled spectra of the records and target spectrum. In other words, it does not aim to reduce the dispersion for a single spectral period but for a band of spectral periods. Thus for another ground-motion bin, the COV statistics of scaled records at the fundamental period may be increased with respect to unscaled case. Since each intermediate period value has the same weight, this scaling procedure does not guarantee a perfect match between average spectral value at the fundamental period of the structure and corresponding target. Instead, it provides scaled accelerograms with an optimal match for a certain period interval. For this case, the observed average spectral value at the fundamental period is 315 cm/s^2, whereas the target is 286 cm/s^2.

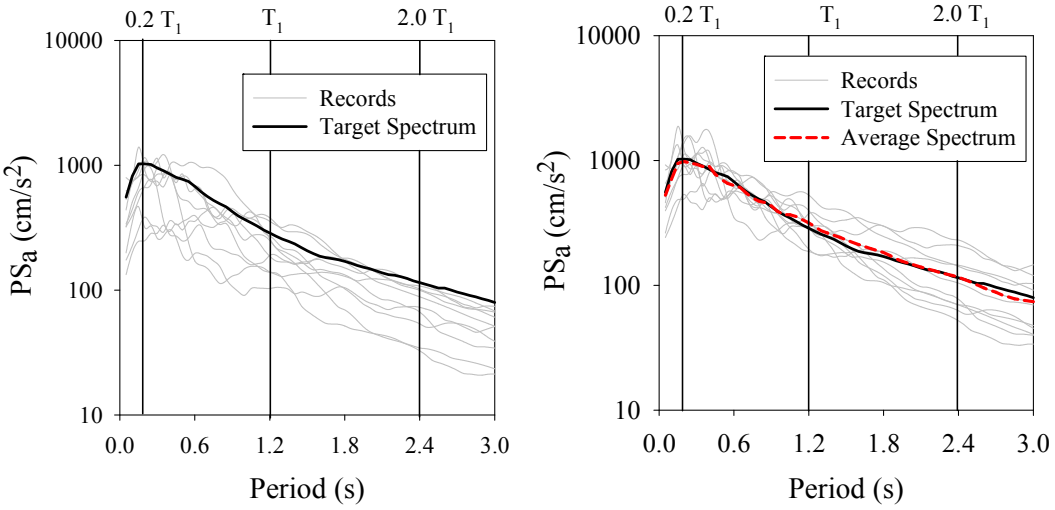

Figure 2.4 Scaling with respect to target spectrum matching

The scaling methodologies presented above use elastic target intensity ordinates and modify the accelerograms according to their elastic properties. As indicated before, procedures that rely on the mere consideration of elastic spectral quantities at the fundamental period of the subject structure yield increasing scatter in dynamic response as inelasticity level increases. To overcome this drawback, some studies suggest scaling the accelerograms according to their

inelastic properties. In this case, the analyst should make some assumptions on the inelastic target intensity from elastic intensity level and the nonlinear behavior of the structure. The accelerograms are then modified such that they yield response values near to the inelastic target level within a specified tolerance for a given nonlinear hysteretic model and level of inelasticity. Such a scaling methodology is recently presented by Kalkan and Chopra (2011). In this procedure, the nonlinear hysteretic model of the structural system is obtained through first-mode pushover analysis. This study assumes that the structure behaves linearly for second- or higher-mode of vibration, whereas the system exhibits nonlinear response associated with the first-mode shape. The method employs nonlinear static pushover analysis with a loading pattern derived from modal analysis to obtain base shear versus top displacement curve (capacity curve) of the structural system. From the idealization of the capacity curve the analyst estimates the yield base shear and post-yield stiffness ratio (α) that dictates the hysteretic modal of this system. The idealized capacity curve is converted to the acceleration-displacement response spectrum (ADRS, Mahaney et al., 1993) format and the yield pseudo-spectral acceleration is obtained. This information is used in order to find R value, which is the ratio of elastic target acceleration to the yield acceleration. As stated in the previous chapter, one of the major shortcomings of the inelastic procedures is that they require intermediate tools in order to relate target elastic and inelastic spectral ordinates. For a given elastic target displacement (associated with elastic target acceleration) and R value, there are various empirical relationships in literature (e.g., Ruiz-García and Miranda, 2003; Chopra and Chintanapakdee, 2004 and Ruiz-García and Miranda, 2007) to estimate the corresponding inelastic displacement. Equation 2.5 presents the calculation of inelastic response ($S_{d,ie}$) for a modification factor, C_R, and target elastic displacement value ($S_{d,e}$).

$$S_{d,ie} = C_R \times S_{d,e} \tag{2.5}$$

The above procedure is also illustrated by a case study. The empirical modification factor C_R proposed by Chopra and Chintanapakdee (2004) is used to estimate the inelastic peak displacement of the SDOF system. Equation 2.6 shows the calculation of C_R value for a given R and α.

$$C_R = 1 + \left[\left(\left(\frac{1}{R} \left(1 + \frac{R-1}{\alpha} \right) \right) - 1 \right)^{-1} + \left(\frac{61}{R^{2.4}} + 1.5 \right) \left(\frac{T_1}{T_c} \right) \right]^{-1} \quad (2.6)$$

In Equation 2.6, T_1 is the fundamental period of the idealized system, whereas T_c is the period separating the acceleration and velocity-sensitive regions of the target spectrum.

Assuming that R = 4 and target elastic spectral displacement ($S_{d,e}$) takes a value of 10.4 cm (provided by the target scenario earthquake; M_w = 6.25, R_{JB} = 10.5 km and ε = 1.25) the target inelastic displacement of the structural system (T_1 = 1.2 seconds and α = 3 %) is estimated as 10.7 cm. According to the hysteretic model that represents nonlinear properties of the first-mode structural response and inelastic target displacement (calculated by Equations 2.5 and 2.6), the scaling factor for each record in the ground-motion bin is determined. However, since the equation of motion of an inelastic structural system is nonlinear, the difficulty in such a methodology comes up during the determination of this scaling factor. Consequently, an iterative code should be developed to find the scaling factor of each record whose inelastic response approximates to the inelastic target within a specified tolerance. Moreover, to achieve this goal, convergence algorithms (e.g., the bisection method (Bradie, 2005)) should be employed to increase the efficiency of the scaling process.

The left panel in Figure 2.5 displays elastic pseudo-spectral acceleration spectra of scaled ground-motion records in the sample group for the fundamental vibration period of 1.2 seconds. The right panel in the same figure shows inelastic pseudo-spectral acceleration spectra for R = 4 and α = 3 %. The average modification factor used for inelastic target scaling is 1.55 with maximum and minimum values as 2.60 and 0.59, respectively.

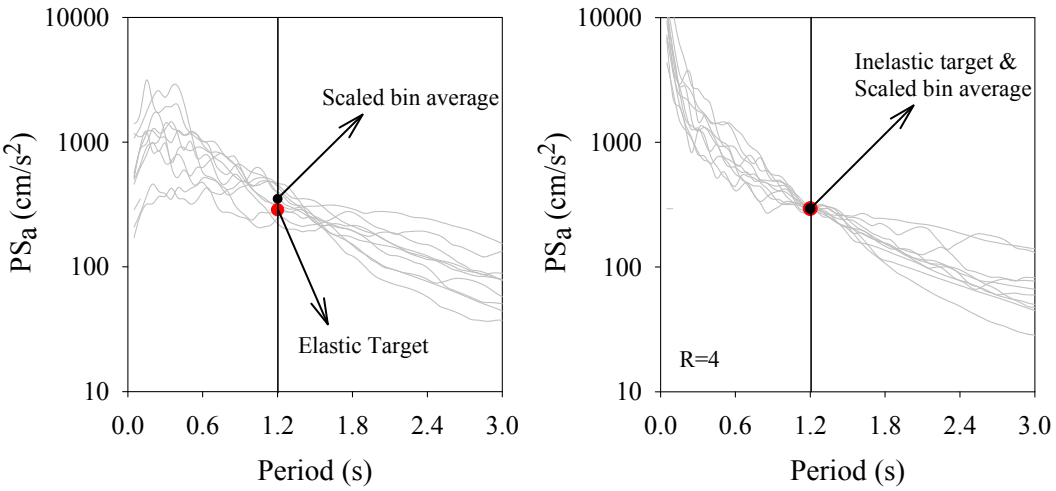

Figure 2.5 The comparison of target and scaled ground motion average values for elastic (left panel) and inelastic (right panel) analysis

Figures 2.6 and 2.7 re-evaluate the features of common scaling methodologies described in previous paragraphs in a generalized frame. The plots illustrate scaled spectra of records for a period interval of 0.05 seconds to 3.0 seconds and compare the linear (Figure 2.6) and nonlinear (Figure 2.7) performance of these scaling methodologies. Figure 2.6 displays the elastic spectra of the given records that are scaled according to the same target hazard level. Assuming that R = 4 and α = 3 %, Figure 2.7 presents the same information for systems responding beyond their elastic range.

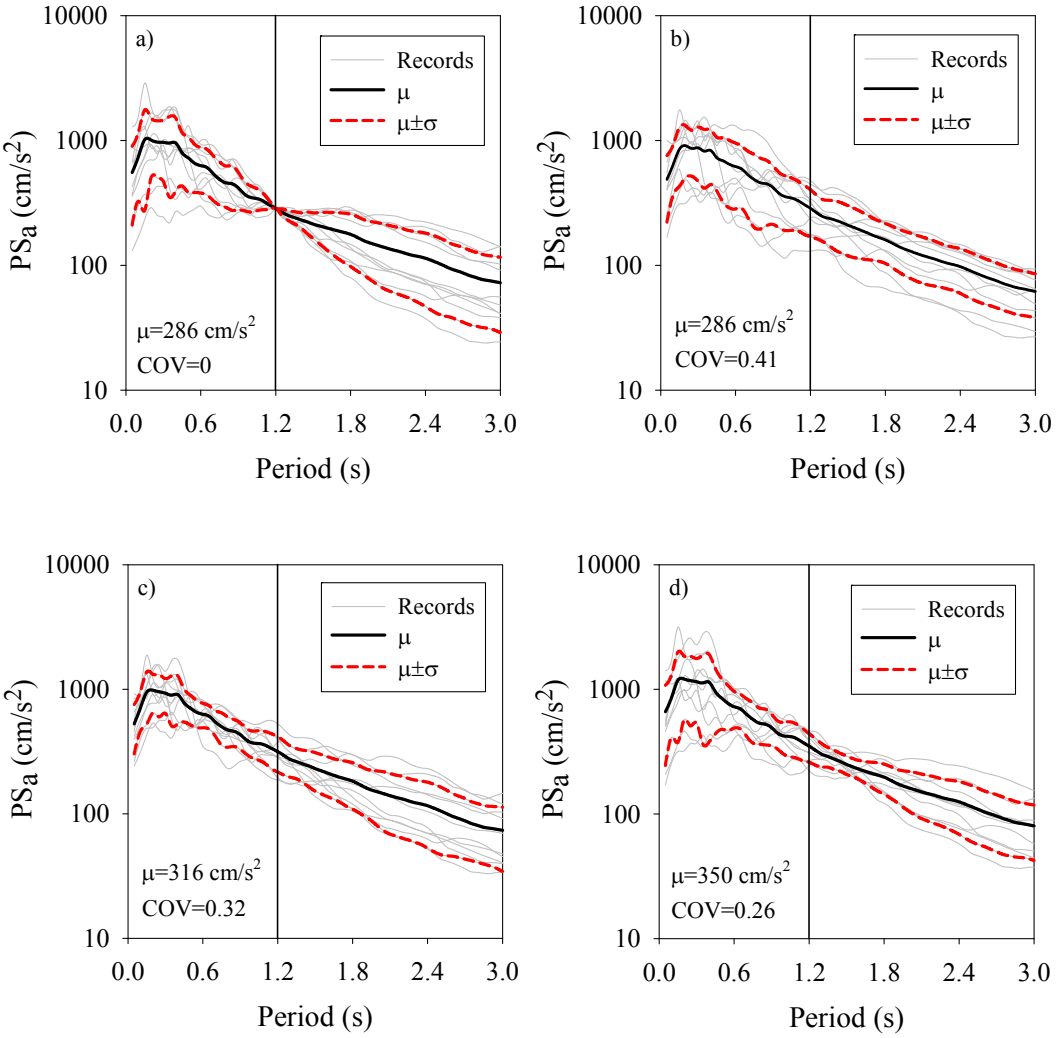

Figure 2.6 The comparison of common scaling methodologies in terms of elastic spectra of scaled ground-motion records, corresponding average, 16 % and 84 % percentile curves. The panels denote a) stripe-scaling, b) cloud-scaling, c) spectrum matching, d) scaling with respect to inelastic target

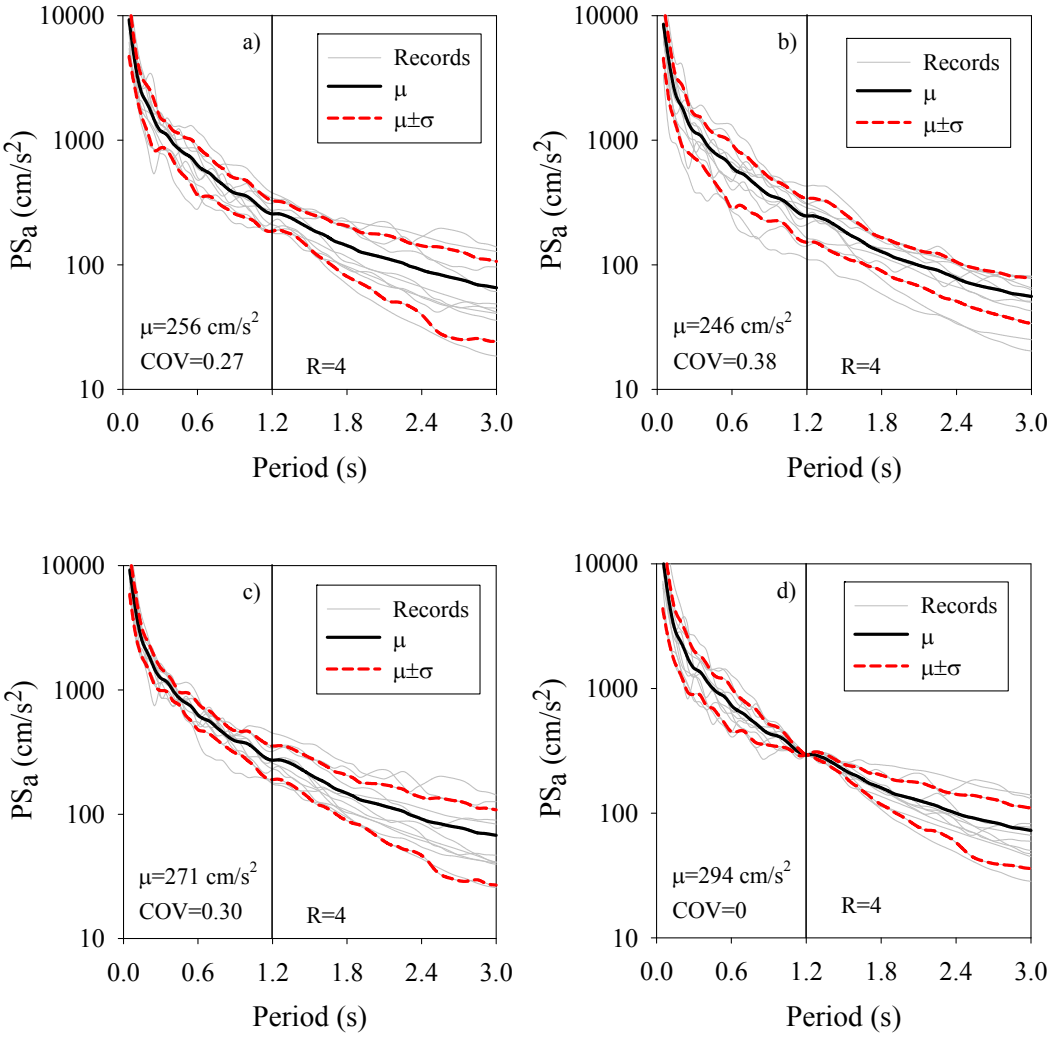

Figure 2.7 The comparison of scaling methodologies in terms of inelastic (R = 4) spectra of scaled ground-motion records, corresponding average, 16 % and 84 % percentile curves. The panels denote a) stripe-scaling, b) cloud-scaling, c) spectrum matching, d) scaling with respect to inelastic target

Figure 2.6 shows that stripe-scaling (upper panel on the left) and cloud-scaling (upper panel on the right) satisfying the target hazard level ($PS_{a,target}$ = 286 cm/s^2). Matching with the target hazard level is advantageous for probabilistic methods that should associate the elastic target hazard with structural response results to compute the probability of exceedance of a damage limit state. Figure 2.6 reveals the fact that spectrum matching (lower panel on the left) and inelastic target scaling (lower panel on the right) may yield larger or smaller average elastic spectral ordinates although these scaling methodologies modifies the identical ground-motion bin according to the same target scenario earthquake. The nonlinear response results compared in Figure 2.7 indicate that stripe-scaling (upper panel on the left), cloud scaling (upper panel on the right) and spectrum matching (lower panel on the left) yield similar dispersion about nonlinear response whereas inelastic target scaling methodology (lower panel on the right) results in zero variance. Similar to the elastic case, almost 20 % difference exists in average nonlinear response results of the compared methodologies.

CHAPTER 3

SELECTION AND SCALING METHODOLOGY FOR LINEAR STRUCTURAL SYSTEMS

3.1 Introduction

The scaling methodology presented in this dissertation linearly scales the accelerograms to ensure a target intensity level by preserving the inherent uncertainty in the scaled recordings. This goal is achieved by constraining the modification of the records to the difference between the actual ground motion and corresponding GMPE estimation.

Consideration of inherent uncertainty in ground-motion records originates from the purpose of obtaining unbiased structural response estimations. In other words, the need of simulating the effects of future scenario earthquakes on structures requires the consideration of record-to-record variability in a reasonable way. Cloud-scaling methodology presented in the previous chapter primarily deals with this objective and modifies the records by preserving the variability among unscaled records in an absolute manner (see Figure 2.4). Although the endeavor of cloud-scaling methodology is crucial for obtaining reliable structural response estimations, the question of "What is preserved?" in terms of record-to-record variability by this procedure is still open for discussion. The cloud-scaling method should clarify whether the scatter in ground-motion amplitudes reflects the inherent uncertainty or it partially originates from the differences between

records having different seismological properties. On the other hand, scaling procedures like stripe-scaling totally eliminate the record-to-record variability about elastic spectral quantities and focus merely on providing low dispersion statistics. The inadequacy of mere consideration of elastic spectral quantity is emphasized in Chapter 2 in terms of inelastic response. Additionally, such a procedure artificially suppresses the record-to-record variability that may result in disregarding the inherent nature of earthquake kinematics. In essence, this dissertation aims at presenting an alternative methodology that provides a theoretically consistent approach in between these two procedures. The seismological features of ground motions that will be scaled are constrained by the chosen GMPE that is suitable for the considered hazard scenario. The scaling does not artificially suppress the aleatoric variability of ground motions to give an overall view of complex earthquake phenomenon. These two points are believed to be different than the scaling concepts of cloud- and stripe-scaling.

3.1.1 Proposed Scaling Methodology

In order to reflect the aleatory (record-to-record) variability inherent in the nature of earthquakes, the proposed procedure constrains the scaling to a parameter ($\varepsilon\sigma$) defined as the logarithmic difference between the observed intensity of the unscaled record and corresponding median estimation obtained from a representative GMPE.

The $\varepsilon\sigma$ concept used in the proposed scaling methodology is analogous to the parameter called “epsilon” (ε) presented by Baker and Cornell (2005; 2006a). In their consecutive studies, Baker and Cornell (2005; 2006a) use ε as a record selection parameter because they have shown that ε is an effective predictor of structural response.

The proposed procedure linearly scales the records in terms of peak ground-motion values or spectral ordinates. Although any spectral value such as PS_a or a peak ground motion value (e.g., PGA, PGV) can be used in the proposed scaling procedure, for illustrative purposes, it will be described by using spectral displacement. Spectral displacement is one of the common ground-motion intensity measures in engineering applications. The nonlinear extension of the proposed methodology is also investigated (see the following chapters) by using the inelastic spectral displacement values of idealized nonlinear SDOF systems. The application of the proposed procedure for peak ground-motion values is very similar and discussed in the latter parts of this chapter.

In most basic terms, $\varepsilon\sigma$ is a measure of logarithmic difference between the observed and the expected ground motion. Equation 3.1 describes the calculation of $\varepsilon\sigma_{Sd}$, which is the logarithmic difference between spectral displacement of an unscaled record, S_d, and corresponding median estimation ($\bar{S}_d$) from a GMPE.

$$\varepsilon\sigma_{Sd} = \ln\left(S_d\right) - \ln\left(\bar{S}_d\right) \tag{3.1}$$

The proposed scaling procedure linearly modifies each accelerogram to its individual target level instead of scaling all records to a common spectral value. To define individual target levels, the procedure makes use of θ; a parameter that is called as scaling origin. This parameter is a reference value, which is employed to make the mean of scaled spectral ordinates exactly matching with the target spectral displacement value ($\bar{S}_{dtarget}$). Given a suite of ground motions, Equation 3.2 shows the general form of θ.

In Equation 3.2, n is the total number of records that are going to be scaled. After determining the parameter θ for a suite of n ground motions, the procedure modifies each individual recording with its own linear scaling factor, γ, which is given in Equation 3.3.

$$\theta = \ln\left(\bar{S}_{dt\,arg\,et}\right) - \ln\left(\frac{\sum_{i=1}^{n} \exp\left(\varepsilon\sigma_{Sd,i}\right)}{n}\right) \tag{3.2}$$

$$\gamma = \frac{S_{dt\,arg\,et}}{S_d} = \frac{\exp\left(\theta + \varepsilon\sigma_{Sd}\right)}{S_d} \tag{3.3}$$

To summarize, the procedure linearly scales the spectral displacement of a record (S_d) to its individual target level ($S_{dtarget}$) so that the average of spectral displacement values of the scaled recordings exactly matches with the target spectral displacement ($\bar{S}_{dtarget}$). This target intensity can be obtained either from a deterministic or probabilistic site-specific hazard study. The major assumption in the proposed scaling procedure is the independence of the standard deviation of GMPE (σ; Strasser et al., 2009), from the record-specific event and target event. Further discussions on how well σ can predict the genuine ground-motion randomness and how much modeling uncertainty it contains (Moss, 2011) are out of scope of this study. Figures 3.1-3.3 illustrate the proposed scaling procedure schematically. Figure 3.1 shows the evaluation of $\varepsilon\sigma_{Sd}$ values of three sample records with different seismological parameters (magnitude, distance, site class, style-of-faulting, etc.). Each panel illustrates the logarithmic difference between the observed (S_d) and predicted spectral displacement ($\bar{S}_d$). Note that $\varepsilon\sigma_{Sd}$ value of the record presented in the top panel has a positive value whereas bottom panels display records having negative $\varepsilon\sigma_{Sd}$ values. Figure 3.2 presents the scaling procedure of the record with a positive $\varepsilon\sigma_{Sd}$ value in detail. The individual target of the subject record is found by using two parameters: $\varepsilon\sigma_{Sd}$ and θ that are defined in the above lines. Figure 3.3 shows scaled records and inherent record-to-record variability among the recordings. Note that proposed scaling method preserves the inherent record-to-record (aleatory) variability. It is believed that this method reflects the scaled ground-motion features in a more realistic way when compared to the scaling of records to a common target spectral ordinate.

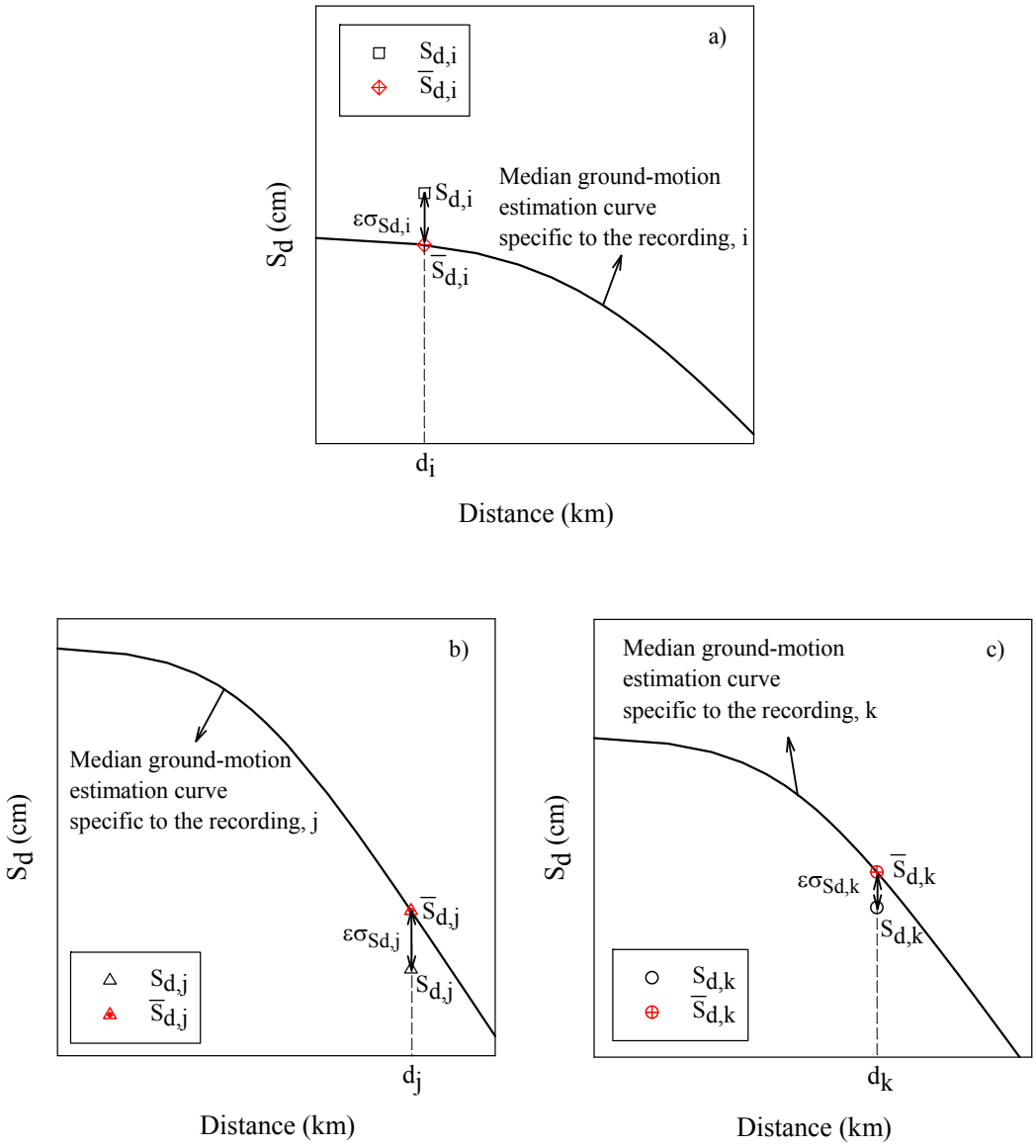

Figure 3.1 Graphical evaluation of $\varepsilon\sigma_{Sd}$ values for three sample records with known seismological parameters

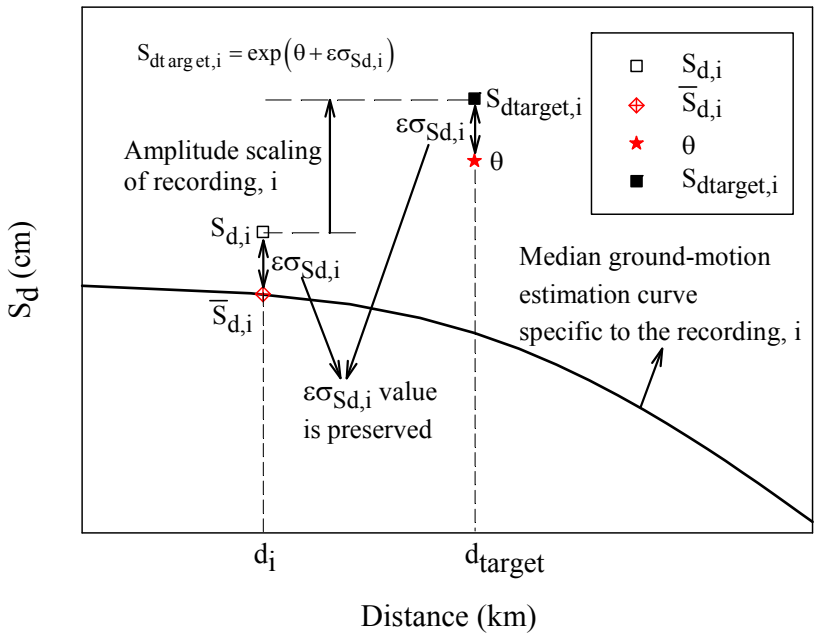

Figure 3.2 Amplitude scaling of the record i with known seismological parameters (magnitude, source-to-site distance, site class, style-of-faulting, etc.) to its individual target spectral level according to the proposed methodology

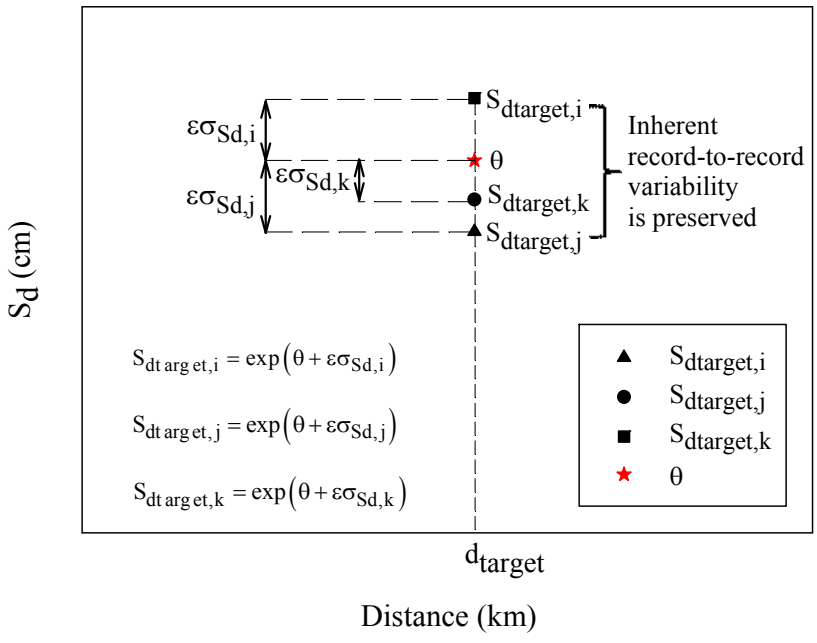

Figure 3.3 Determination of individual target points and record-to-record variability among scaled ground motions

As shown in Equation 3.3, the numerator, $S_{dtarget}$, is a linear function of $\varepsilon\sigma_{Sd}$ and θ terms in logarithmic domain for elastic systems. Thus the scaling procedure described above let the analyst define the distribution of modified ground motions about $\bar{S}_{dtarget}$. By assuming the distribution of spectral response as log-normal, the expected spectral displacement ($\lambda_{S_{dtarget}}$) and standard deviation ($\zeta_{S_{dtarget}}$) of the scaled recordings can be calculated by using Equation 3.4 and Equation 3.5, respectively. In these equations, $\mu_{\varepsilon\sigma}$ is the average of $\varepsilon\sigma_{Sd}$ values of n recordings.

$$\lambda_{S_{dtarget}} = \theta + \frac{\sum_{i=1}^{n} \varepsilon\sigma_{Sd,i}}{n} = \theta + \mu_{\varepsilon\sigma} \tag{3.4}$$

$$\zeta_{S_{dtarget}} = \sqrt{\frac{1}{n-1} \cdot \sum_{i=1}^{n} \left(\varepsilon\sigma_{Sd,i} - \mu_{\varepsilon\sigma}\right)^2} \tag{3.5}$$

3.1.2 Evaluation of the Proposed Scaling Methodology

Dynamic analyses of SDOF systems are conducted to investigate the features and effects of the proposed scaling procedure. SDOF systems are employed in order to scrutinize the results by excluding the variability that can originate from structural modeling uncertainties and higher-mode effects. In the subsequent chapters, the proposed selection and scaling procedure is re-evaluated for multi-degree-of-freedom (MDOF) systems.

A special consideration is given to select ground-motion records having reliable magnitude, source-to-site distance, site class and style-of-faulting information during the evaluation. To obtain generalized results, the ground-motion library

clustered in different magnitude and source-to-site distance intervals is employed (see Chapter 1 for details of compiled ground-motion library).

The discussions in the previous chapter have already shown the importance of style-of-faulting as well as site conditions on ground-motion behavior and amplitude. The value of $\varepsilon\sigma_{Sd}$ implicitly considers these parameters through the median estimation of the used ground-motion prediction model. Consequently, the scaling procedure considers the pertinent soil class of each candidate recording as well as the rupture mechanism while computing $\varepsilon\sigma_{Sd}$. This way, the procedure accounts for the information of style-of-faulting and site conditions even if these seismological parameters are relaxed in the selection stage of the candidate records.

Another important issue is the horizontal component definition used in scaling procedure (see the relevant discussion in Chapter 2). To maintain the consistency in the horizontal component definition, the scaling factor should be applied either to one or both horizontal components of the accelerogram depending on the horizontal component definition of the GMPE employed. Since, the GMPE used in this study (Akkar and Bommer (2010)) predicts for the geometric mean of spectral displacement ordinates, the same scaling factor is applied to both horizontal components simultaneously. Note that such a procedure also lets the analyst conserve the original difference between these components, which is a recommendation of other studies (e.g., Bommer and Acevedo, 2004).

The effects of the proposed scaling procedure are compared with stripe-scaling method since it is the most common procedure employed in engineering applications. Besides, stripe-scaling methodology provides the most efficient results in terms of reduced scatter in elastic spectral response for a given period with respect to the other alternative scaling methodologies (see Figure 2.6). The comparisons are based on the scaling factors implemented and the dispersion statistics (COV statistics). Scaling factors of the compared methods are presented

in terms of their maximum and minimum values. The comparative statistics are described for elastic and inelastic spectral displacements for vibration periods of T = 0.3 s, 0.6 s, 0.9 s, 1.2 s, and 1.5 s. The nonlinear SDOF response is represented by a bilinear hysteretic model with 3 % post-yield stiffness ratio. The inelastic spectral ordinates are computed for constant strength, R. The method is evaluated for nonlinear response to assess its limitations as the entire procedure is based on linear structural behavior. The discussions about nonlinear response will establish basis to fine tune the proposed procedure for record selecting and scaling of nonlinear systems.

The concerns on the level of scaling and possible drawbacks of using high scaling factors have been discussed in Chapter 2. Bearing on these discussions, Figure 3.4 presents the maximum and minimum scaling factors of the proposed procedure and stripe-scaling method for all ground-motion bins and periods considered in this study. The magnitude and source-to-site distance of the target hazard scenario is taken as the median M_w and R_{JB} value of each ground-motion bin, respectively. The soil condition is assumed as NEHRP C site class for the target scenario in this illustrative case study.

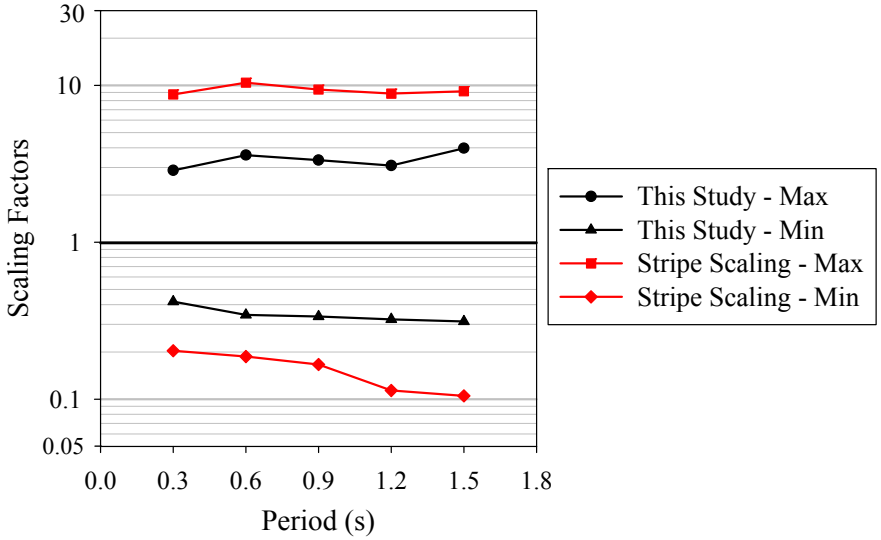

Figure 3.4 Maximum and minimum modification factors computed by alternative scaling procedures

Figure 3.4 clearly shows that scaling factors of stripe-scaling are significantly larger than those of the proposed methodology. While the maximum amplification factors of the proposed scaling procedure vary between 2 and 4, the maximum scaling values of stripe-scaling method are generally above 8 and reach to values more than 10 that would suggest a significant manipulation in the genuine features of the ground motions.

Figure 3.5 compares the COV statistics of proposed scaling procedure (left panel) and stripe-scaling (right panel) for some of the M_w–R_{JB} bins of the ground-motion library (see Chapter 1). The figure depicts that COV statistics are affected by the level of inelasticity (represented by the increase with R values).

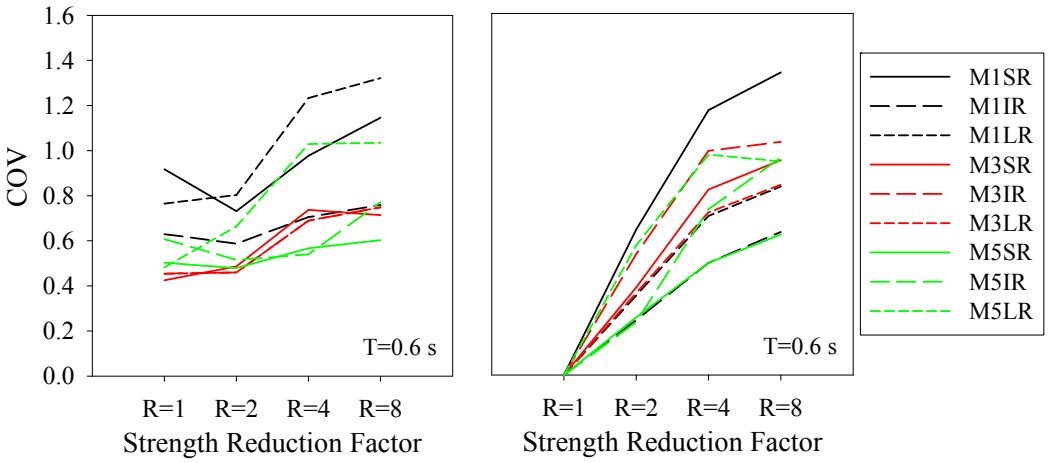

Figure 3.5 COV statistics computed at T = 0.6 s for constant strength values varying between R = 1 (elastic behavior) to R = 8 (highly nonlinear behavior). Each abbreviation in the legend refers a specific M_w-R_{JB} bin compiled from the ground-motion library (see Section 1.4 for the meanings of abbreviations used in the legend).

Ruiz-García and Miranda (2003) indicate that the dispersion about median nonlinear response trends tend to increase with the increasing level of inelasticity. In a similar fashion, other studies (e.g., Akkar and Özen, 2005; Akkar and

Küçükdoğan, 2008) reported an increase on the level of dispersion about median nonlinear structural response upon the increased nonlinearity. Therefore, the increase in COV statistics as given in Figure 3.5 is expected. Nevertheless, an interesting observation to note is that R dependent variation of stripe-scaling displays a more sensitive (continually increasing) trend in COV with respect to the proposed scaling method. Therefore, the uncertainty in nonlinear structural response is influenced less from the variations of inelasticity level in the proposed scaling methodology. Inherent in stripe-scaling strategy, the dispersion is zero for the elastic (R=1) case.

Figure 3.6 compares the COV statistics illustrated in Figure 3.5 in a different way. The period-dependent dispersion statistics of alternative scaling methodologies are compared for two particular R values in this figure. Only M3SR bin (see explanations in Section 1.4 for name convention) results are presented in Figure 3.6 because the other bins display similar results. The panel on the left shows the COV statistics for moderate level of inelasticity (mimicked by R = 4) whereas the right-hand-side panel exhibits the same statistics for R = 8 (high level inelasticity).

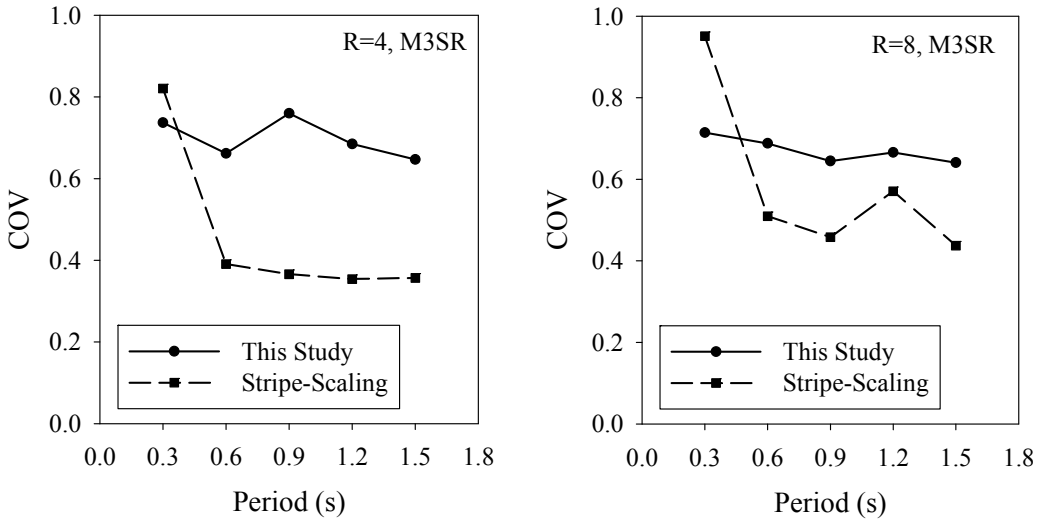

Figure 3.6 COV statistics of SDOF systems as a function of vibration period with different level of inelasticity

The comparative plots in Figure 3.6 show that stripe-scaling results in high dispersion in short period structural response and dispersion increases with increasing level of inelasticity (when strength reduction factor changes from R=4 to R=8). For all other vibration periods, stripe-scaling yields lower dispersion statistics since it scales each record to a common spectral ordinate whereas the proposed methodology preserves the inherent aleatory variability by scaling each record to its individual spectral target. As emphasized previously, the stripe-scaling methodology employs larger scaling factors to scale each record to a common target level (see Figure 3.4) and it restraints the scatter in ground-motion amplitudes for a predetermined vibration period of linear structural systems. Thus the dispersion statistics of stripe-scaling methodology is very sensitive to the changes in nonlinearity level due to the inherent period shift resulting from nonlinear response. Since the period shift is much more pronounced at short-period structural systems, stripe-scaling results in higher dispersion statistics about short-period median structural response when compared to the scaling procedure presented in this study. For long-period structural systems that are subjected to higher nonlinearity, the dispersion of stripe-scaling also increases and attains closer values to the dispersion statistics of the proposed method.

Higher dispersion can be considered as disadvantageous especially for deterministic damage state assessment studies. Nevertheless, preserving the record-to-record variability in a reasonable way is essential for accurate estimation of structural response. It should be noted that at the expense of preserving record-to-record variability, the proposed procedure generally yields higher dispersion with respect to stripe-scaling. However, the pertaining dispersion statistics draw a stable trend and once they can be estimated with a certain confidence, the presented method is believed to reflect more realistic results about structural response under complex earthquake behavior. Estimation of dispersion about the median structural response subjected to records scaled by the method described here will be discussed extensively in various parts of this chapter as well as in the rest of this dissertation.

Since the definition of target intensity measure is an important issue of ground-motion amplitude modification, scaling methodologies which are equally applicable to a variety of intensity measures are advantageous. Thus the proposed procedure is further discussed through its implementation with PGA and PGV intensity measures that can be considered as alternatives to spectral quantities. The only difference while applying the proposed procedure for PGA and PGV is use of GMPEs that can estimate these intensity measures.

Figure 3.7 compares the COV statistics of proposed scaling procedure in terms of PGA, PGV and spectral displacement for M5SR and M5LR bins.

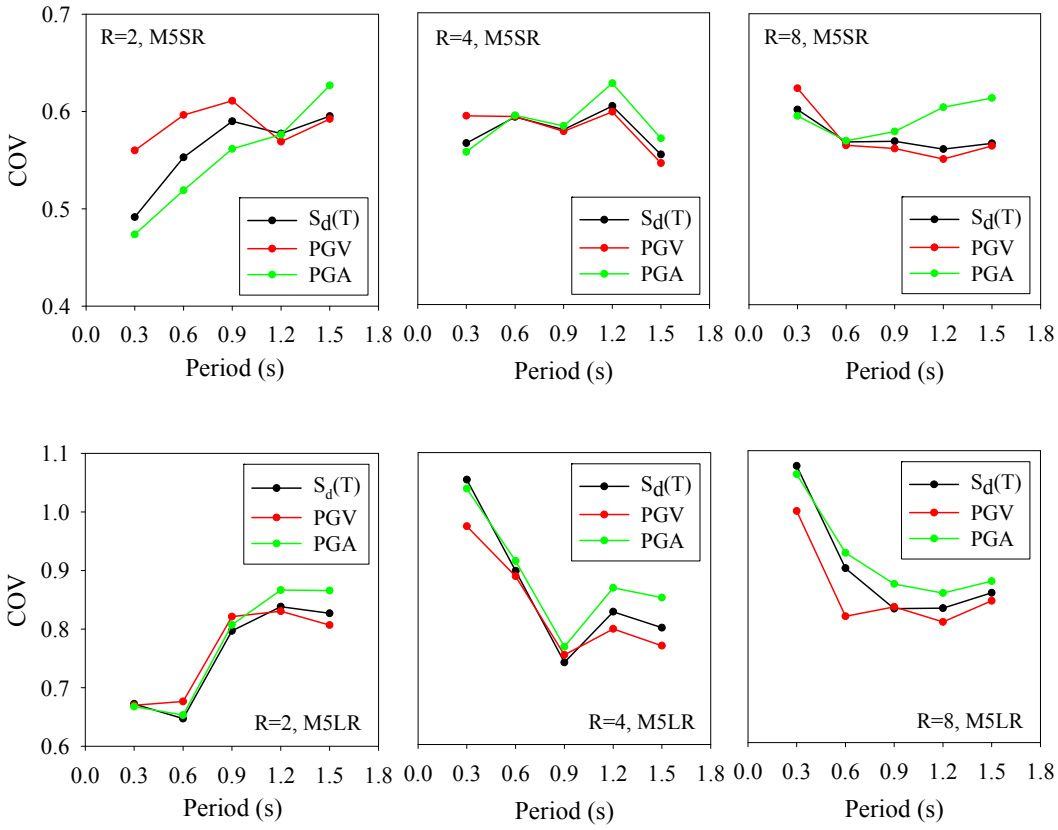

Figure 3.7 Comparison of PGA and PGV with $S_d(T)$ as alternative intensity measures for different inelasticity levels (R = 2, 4 and 8) and periods (T = 0.3 s, 0.6 s, 0.9 s, 1.2 s and 1.5 s)

The figures depict that scaling with respect to PGA results in relatively higher dispersion as inelasticity attains larger levels (described by R = 8; third column). PGA-based scaling also results in higher dispersion for long-period systems. There is almost no difference between alternative intensity measure results at intermediate inelasticity levels for systems having moderate vibration periods. Figure 3.7 also shows that scaling with respect to PGV results in relatively high dispersion at low inelasticity levels whereas the dispersion decreases as structures are exposed to higher inelasticity (increasing R values). Similar results were also obtained by Akkar and Özen (2005) while investigating the effect of PGV on SDOF deformation demands.

The above case study shows that the proposed method is equally applicable to scaling with alternative intensity measures. The comparisons suggest that different intensity measures result in different levels of dispersion about median structural response that seems to be correlated with structural period and level of inelasticity. This observation will be used in the following chapter while adopting the proposed scaling procedure for nonlinear structural response.

3.2 Proposed Selection of Ground-Motion Recordings

This part of the dissertation introduces the record selection strategy that is framed with the presented scaling procedure for elastic systems. This approach is extended further for nonlinear systems in the next chapter. The proposed strategy accomplishes the final selection and scaling of the optimum ground-motion bin by estimating the standard deviation of all combinations resulting from a relatively large candidate accelerogram dataset. It is a nested ground-motion selection and scaling strategy with minimum interference to the inherent ground-motion features. Thus the scaled ground motions in the optimum bin are believed to yield unbiased structural response reflecting the genuine features of target earthquake scenario.

3.2.1 Candidate Ground Motion Selection Strategy

In order to assemble the candidate acceleration bin, this study uses seismological parameters as primary constraints. Some general issues such as reliability and consistency of the records are already mentioned in Chapter 2. Besides, priority of seismological parameters in terms of their influence on structural response is discussed. Keeping these discussions in mind, the proposed record selection strategy gives priority to magnitude and source-to-site distance as the first and second query parameters, respectively. Additional parameters as style-of-faulting and site class are considered as secondary query parameters. The reason of treating style-of-faulting and site class as secondary seismological parameters is discussed in the following paragraphs.

The differences in the ground-motion amplitudes due to style-of-faulting are still a topic of discussion among seismological community. The pre-NGA (Next Generation Attenuation Project; Power et al., 2008) predictive models derived in the US propose values of reverse to strike-slip spectral ratios (RV:SS) ranging between 1.2 and 1.4 at very short periods that diminish towards longer spectral period range. Bommer et al. (2003) indicate that such large ratios can stem from different classification schemes used in determining the rupture mechanism of earthquakes. They also state that the style-of-faulting distribution of the ground-motion dataset as well as the source-to-site distance metric used in the ground-motion model can provoke such high RV:SS ratios. The left panel in Figure 3.8 shows RV:SS spectral ratios of recent NGA GMPEs. The RV:SS ratios do not reveal significantly large differences between reverse and strike-slip spectral ratios (± 20% difference depending on the spectral period range) but they also do not indicate a strong agreement between the NGA model developers in terms of style-of-faulting scaling. The Abrahamson and Silva (2008) model (AS08) suggests larger spectral ordinates for reverse style-of-faulting towards longer vibration periods whereas Idriss (2008) and Chiou and Youngs (2008) GMPEs

(I08 and CY08, respectively) draw an opposite trend. The Campbell and Bozorgnia (2008) GMPE (abbreviated as CB08) considers equal spectral ordinates for both reverse and strike-slip styles-of-faulting. The Boore and Atkinson (2008) model (BA08) follows closely the RV:SS ratios of AS08 at short periods but its RV:SS trend is similar to those of I08 and CY08 at longer periods. In general, it is assumed that the normal style-of-faulting events produce slightly lower ground-motion amplitudes with respect to the strike-slip earthquakes (see detailed discussions in Bommer et al. (2003)). Nevertheless, considering the previous studies in the literature, Bommer et al. (2003) suggest an equivalence of normal and strike-slip spectral ordinates in hazard analysis due to limited availability of normal earthquakes in ground-motion datasets. The points about N:SS made by Bommer et al. (2003) are partially confirmed by some of the NGA model developers. The N:SS ratios of I08, CB08 and AS08 are either 1 or close to 1 as shown in the right panel of Figure 3.8. However, BA08 and CY08 suggest larger differences between the normal and strike-slip spectral ordinates emphasizing once again the likely influence of style-of-faulting distribution in the ground-motion databases as well as differences in style-of-faulting modeling that are used in the derivation of ground-motion models. For example, ruptures emerging at the surface due to different earthquake faulting may result in differences in RV:SS and N:SS ratios. Thus GMPEs that model this effect will certainly impose different RV:SS and N:SS ratios depending on the surface and subsurface rupture conditions.

In their paper Boore and Atkinson (2008) also indicate that the use of style-of-faulting as the estimator parameter in GMPEs does not make a significant impact in reducing the aleatory variability (i.e., standard deviation of GMPE). Controversially, a small change in sigma due to the consideration of style-of-faulting may have an impact for site-specific hazard that in turn can affect the scaling factors of ground-motions.

Based on these discussions and the difficulties experienced while finding the necessary number of strong-motion recordings for selecting and scaling purposes, this study prefers relaxing the constrains on the style-of-faulting while identifying the candidate accelerograms. Nevertheless, during the identification of candidate records it is suggested to give priority to accelerograms that represent the same style-of-faulting feature as of the target hazard scenario. It is also noted that the proposed method preserves the pertinent style-of-faulting feature of each candidate recording in the scaling stage while computing their $\varepsilon\sigma_{Sd}$.

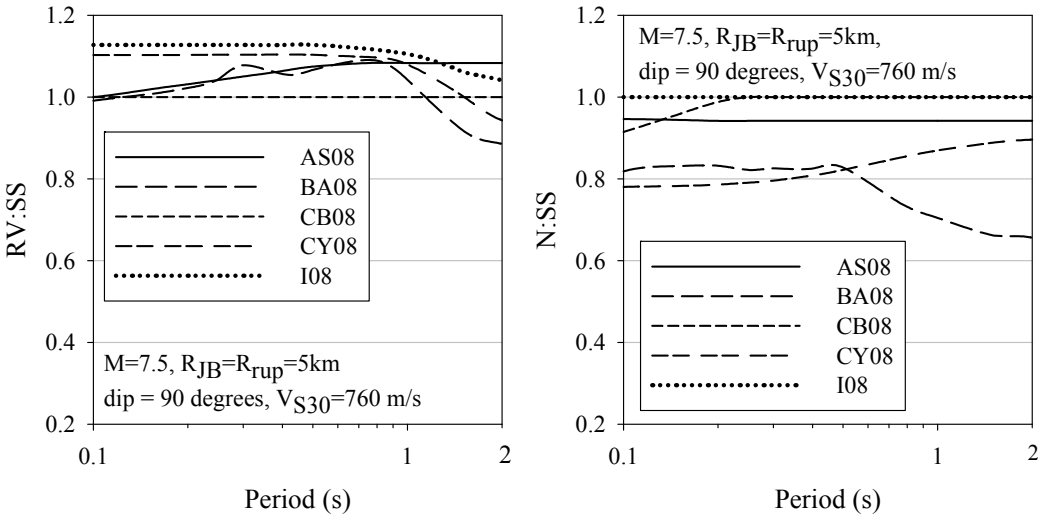

Figure 3.8 The RV:SS and N:SS spectral ordinate ratios inferred from the NGA models

The site conditions impose a much more important influence on the ground-motion amplitudes. In some ground-motion models the soil effects are addressed via dummy site variables by considering a linear soil behavior. The most recent pan-European model (Akkar and Bommer, 2010) indicates that the spectral ordinate ratios of stiff-to-soft soil deposits range between 0.85 and 0.65 for the spectral period range of interest in this study (Figure 3.9).

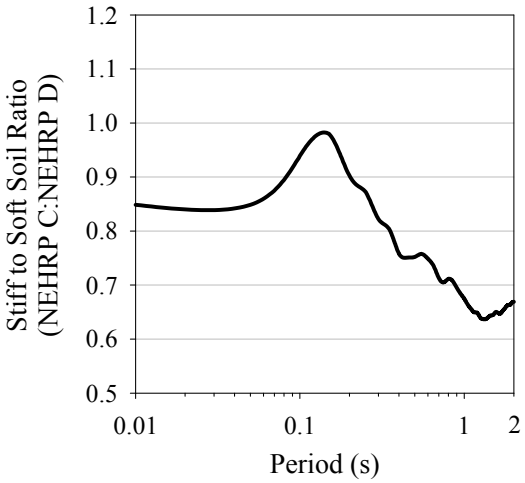

Figure 3.9 Stiff-to-Soft soil spectral ordinate ratios according to Akkar and Bommer (2010) pan-European predictive model that considers linear soil behavior on ground-motion amplitudes

Figure 3.10 shows the distribution of strong-motion recordings in the ground-motion library of this study in terms of V_{S30} (V_{S30} is the average shear-wave velocity measured at the top of 30 m soil profile) intervals. As it can be appreciated from this distribution, 60% of the recordings have V_{S30} values ranging within the 270m/s ≤ V_{S30} < 360m/s and 360m/s ≤ V_{S30} < 450m/s intervals.

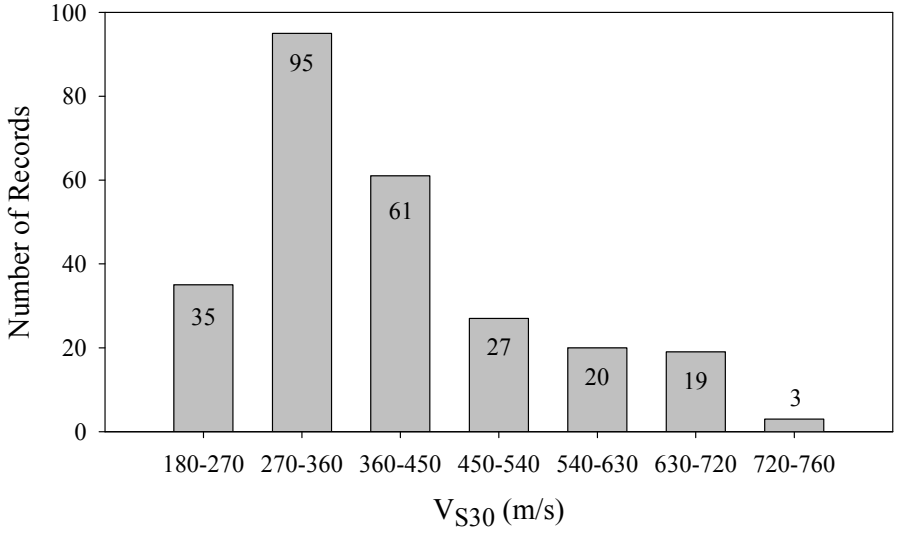

Figure 3.10 V_{S30}-dependent frequency distribution of strong-motion recordings used in this study

Figure 3.11 shows the spectral ordinate ratios of V_{S30} = 400 m/s and V_{S30} = 310 m/s that represent the geometric means of above two intervals. The spectral ratios are computed from the average of NGA GMPEs and they show the period-dependent spectral ratio variations for different magnitude and distance pairs. The ratio plots in Figure 3.11 indicate that the spectral ordinate difference due to different site conditions generally varies in the ± 10% band within the spectral period range of interest in this study. Under these observations, the proposed record selection strategy first gives priority to candidate accelerograms that have the same soil class as of the target hazard scenario. If the chosen accelerograms are not sufficient to assemble the candidate ground-motion bin, the selection methodology allows using other accelerograms that can be proxies to the site conditions dictated by the target hazard scenario. It should be once again emphasized that the scaling method preserves pertinent soil class properties of each candidate recording while computing their $\varepsilon\sigma_{Sd}$.

Following the discussions given above, the candidate record selection strategy is implemented as follows. Records within ±0.25 units of magnitude range according to the target scenario magnitude (M_{target}) are selected while assembling the candidate strong-motion dataset. The candidate ground-motion records are chosen within ± 25 km distance range with respect to the target distance range identified by the target hazard scenario. Finally, recordings either having the same style-of-faulting and site class as of the scenario event or those that are reasonable representatives of the scenario rupture mechanism and site class are preferred. For example, accelerograms from NEHRP C (360m/s < V_{S30} ≤ 760m/s) and NEHRP D (180m/s < V_{S30} ≤ 360m/s) site classes should be selected if the soil conditions of target scenario is either of these two site classes. It is believed that implementation of above strategy would result in a fair amount of records for assembling the candidate ground-motion dataset.

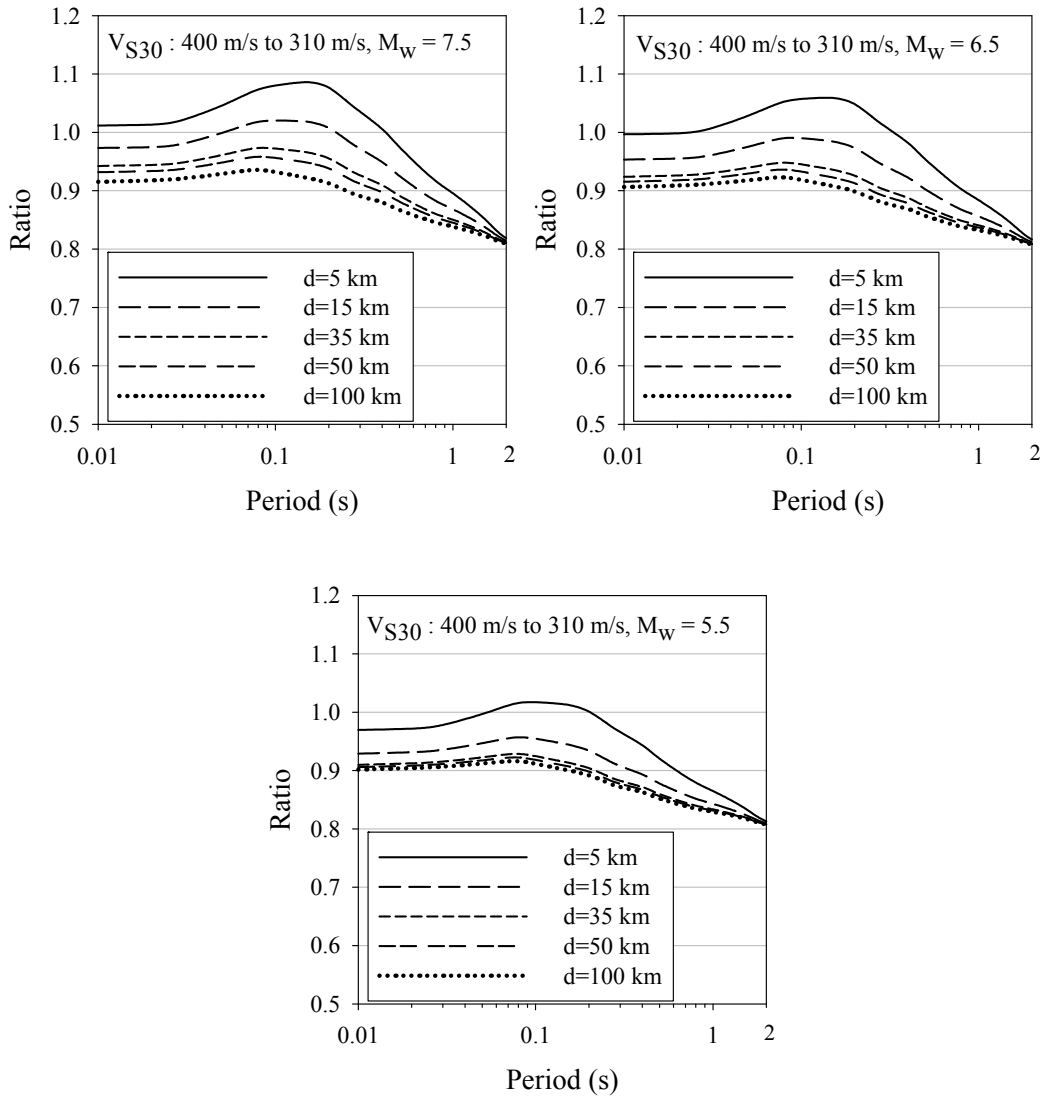

Figure 3.11 Average spectral ordinate ratios of the NGA predictive models for V_{S30} = 400 m/s and V_{S30} = 310 m/s. The upper two panels show the period-dependent spectral ratios for M_w = 7.5 (left) and M_w = 6.5 (right). The lower panel shows the same type of ratios for M_w = 5.5. The chosen source-to-site distances in each panel are 5 km, 15 km, 35 km, 50 km and 100 km. The plots are for a strike-slip fault dipping at 90 degrees.

As indicated in Chapter 2, selection of n records among k candidate accelerograms that are determined according to a scenario event is a combination problem. The number of possible combinations assembled for obtaining the scaled ground-motion bin is equal to C(k,n) that can be calculated by Equation 3.6.

$$C(k,n) = \binom{k}{n} = \frac{k!}{n!(k-n)!} \qquad 0 < n \le k \qquad (3.6)$$

According to the references and ongoing studies presented in Chapter 2, the number of recordings in the scaled ground-motion bin is considered as a subject that needs further refinement and left out of scope of this dissertation. This study will use 10 (n=10) accelerograms for the scaled ground-motion bin as a compromise among various studies in the literature. Nevertheless, any pre-defined quantity of acceleration time-series can be used in the proposed scaling methodology.

The optimum number of recordings in candidate ground-motion dataset is examined by carrying out some simple statistical analysis. The initial statistical study investigates the relationship between the number of candidate recordings and the computation time for selecting and scaling the optimum recording set for elastic structural analysis. As indicated in Equation 3.6, the computation time to select and scale n recordings from k candidate accelerograms depends on the number of possible combinations, C(k,n). Figure 3.12 shows the total elapsed time to select and scale the optimum recordings as a function of C(k,n) when n=10 and k is varied between 14 and 24. When k=14, (C(k,n)=1001), the required time for selecting and scaling the optimum dataset is less than 1 second. If k=22, which is a little bit over k=20 (used in this study), the elapsed time reaches to 820 seconds. Note that when k=20, the computation time is approximately 90 seconds on an ordinary personal computer.

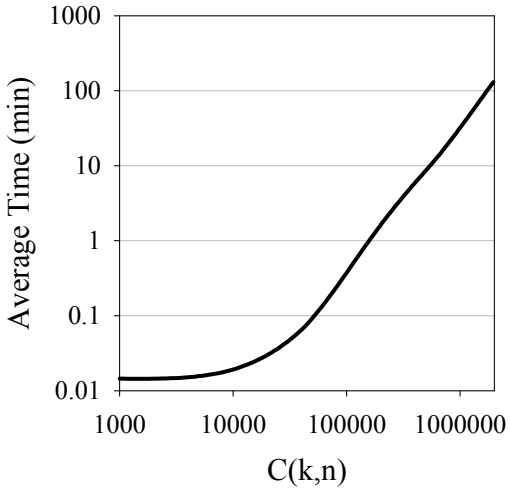

Figure 3.12 The variation of computation time for the proposed procedure as a function of combination number

The number of candidate recordings, k, cannot be decided by the mere consideration of the computation time. The reduction in dispersion about the median target intensity with respect to number of candidate records is the other factor that should be accounted for during this decision process. The left panel in Figure 3.13 shows the variation of dispersion about the median elastic target intensity as a function of k when n = 10. The plot demonstrates that the reduction in dispersion almost flattens when k is 20. The increase in k after this level does not introduce any significant improvement in the reduction of dispersion. Considering the observations on the computation time and the standard deviation in elastic response, choosing k as 20 seems to be the most favorable decision for the efficiency and accuracy of the presented procedure. This decision is re-assessed for nonlinear systems. The right panel of Figure 3.13 presents the variation of standard deviation as a function of k for inelastic spectral ordinates for R = 4. The reduction in the standard deviation becomes stable after k = 16, which advocates that the choice of k = 20 would generally warrant the most efficient scaling results for our procedure.

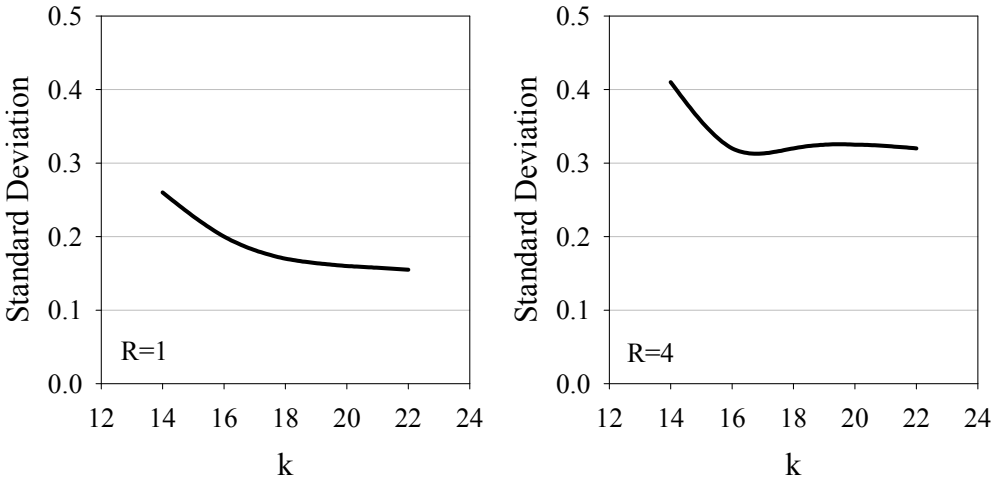

Figure 3.13 Variation of dispersion as a function of k for elastic systems (left panel, R = 1) and inelastic systems (right panel, R = 4)

3.2.2 Determination of the Optimum Recording Set for RHA of Structures

The ground motions scaled according to the proposed procedure preserve the aleatory variability inherent in the nature of earthquakes in order to have accurate structural response estimations. Moreover, the presented procedure conveys information about the median elastic spectral response and corresponding dispersion to the analyst via Equations 3.4 and 3.5, respectively for a given target earthquake scenario. This information can be further utilized in the final selection of the optimum recording set.

Major constraints in ground-motion selection for amplitude modification of records are presented in the previous chapter. In this context, the objectives of RHA are also categorized as accurately estimating the median structural response of interest or determining its distribution for probabilistic damage assessment. These specific objectives will essentially define the optimum ground-motion dataset. The presented ground-motion selection and scaling methodology primarily aims at estimating the median structural response accurately and tries to reduce the dispersion about target response without manipulating the subject

records excessively. Consequently, the method specifies the optimum recording set as the one yielding the least standard deviation about the target hazard. On the other hand the optimum recording set defined in this perspective can also be used for probabilistic damage assessment as it can provide the required probability distribution parameters through Equations 3.4 and 3.5. This feature will be discussed further in Chapter 5.

The proposed methodology calculates the resulting dispersion ($\zeta_{S_{dt\,arg\,et}}$) about target elastic spectral level through Equation 3.5 for each alternative ground-motion bin. Thus among the alternative combinations (total number of alternative bins is equal to C(k,n)), the one that yields the least dispersion about the target hazard level, $\left(\zeta_{S_{dt\,arg\,et}}\right)_{\min}$ is labeled as the optimum recording set. Since Equation 3.5 lets the analyst run the selection and scaling of the records concurrently, this approach significantly speeds up the entire process and gives the optimum scaled recording set to be used in the evaluation of the structure under consideration.

3.3 Application of the Proposed Selection and Scaling Procedure

The selection and scaling procedure developed in this study is illustrated using a case study performed for a target earthquake scenario and a fictitious building with a fundamental period of 0.3 s. (T = 0.3 s). This case study will be employed in the next chapter of this dissertation to describe the nonlinear extensions of the proposed procedure. The target scenario is determined from the deaggregation of a probabilistic site-specific hazard analysis. For the given fictitious reinforced concrete building located on a site classified as NEHRP C, deaggregation results indicate the dominant moment magnitude as 7.15 ($M_{w,target}$ = 7.15). The dominant seismic source is a strike-slip fault that is located 22.5 km from the site (i.e., $R_{JB,target}$ = 22.5 km). The epsilon is calculated as 1.44 from deaggregation for a

return period of 475 years. The Akkar and Bommer (2010) GMPE that is chosen as the representative predictive model according to the seismotectonic settings of the fictitious case yields a target spectral displacement (i.e., $\bar{S}_{dt\arg et}(T)$) of 2.06 cm. A candidate ground-motion dataset of 20 accelerograms is assembled considering the imposed constraints on magnitude, source-to-site distance, style-of-faulting and site class that are previously described within the context of the proposed procedure. The optimum recording set of 10 accelerograms yields a standard deviation of $\left(\zeta_{S_{dt\arg et}}\right)_{\min}$ = 0.111 among 184756 (=C(20,10) alternatives ranging up to 0.651.

Table 3.1 lists the 20 candidate accelerograms with their seismological parameters. The abbreviations, SS, N, and RV indicate strike-slip, normal and reverse faulting mechanisms, respectively. Table 3.1 also lists the observed spectral displacement (S_d) values and corresponding estimations ($\bar{S}_d$) of Akkar and Bommer (2010) model. The ground motions identified in the optimum recording bin are listed in bold letters together with their scaling factors, γ, that are computed in terms of $\varepsilon\sigma_{Sd}$.

Figure 3.14 illustrates some of the specific features of the proposed methodology. The left panel in Figure 3.14 depicts that scaled spectral displacements (i.e., $\ln(S_{dt\arg et}(T))$ are linearly correlated with $\varepsilon\sigma_{Sd}$ values, which is imposed by the scaling factor given in Equation 3.3. The panel on the right shows that the standard deviation ($\zeta_{S_{dt\arg et}}$) computed from Equation 3.5 is exactly the same as the observed values of each alternative ground-motion dataset. Figure 3.15 shows elastic displacement spectra of 20 unscaled candidate records (left panel) and the optimum recording set selected and scaled according to the proposed procedure (right panel). Note that the average of scaled spectral ordinates exactly matches the target spectral intensity level at the fundamental period of the subject building.

Table 3.1 Seismological and ground-motion parameters of the candidate recording set. The records selected and scaled according to the proposed procedure are tabulated in bold characters for a short-period elastic structural system with T = 0.3 s.

Record Name	M_w	R_{JB} (km)	Soil Type	Fault Type	S_d (cm)	$\bar{S}_d$ (cm)	$\varepsilon\sigma_{Sd}$	γ
TGMB1592	**7.1**	**32.1**	**NEHRP D**	**SS**	**0.732**	**0.658**	**0.107**	**2.882**
PEER1794	7.1	31.1	NEHRP C	SS	0.903	0.557	0.483	
PEER1636	7.4	50.0	NEHRP D	SS	1.046	0.506	0.725	
PEER1633	7.4	12.6	NEHRP C	SS	2.807	1.223	0.831	
PEER1144	**7.2**	**43.3**	**NEHRP D**	**SS**	**0.544**	**0.530**	**0.027**	**3.579**
PEER1116	**6.9**	**19.1**	**NEHRP D**	**SS**	**1.042**	**0.945**	**0.098**	**2.007**
PEER1107	6.9	22.5	NEHRP D	SS	1.556	0.823	0.637	
PEER0880	7.3	27.0	NEHRP D	SS	0.624	0.819	-0.271	
PEER0864	**7.3**	**11.0**	**NEHRP C**	**SS**	**1.570**	**1.314**	**0.178**	**1.443**
PEER0848	7.3	19.7	NEHRP D	SS	2.467	1.051	0.853	
PEER0827	7.0	16.0	NEHRP C	RV	0.547	1.157	-0.749	
PEER0826	**7.0**	**40.2**	**NEHRP D**	**RV**	**0.837**	**0.637**	**0.272**	**2.975**
PEER0812	**6.9**	**33.9**	**NEHRP C**	**SS**	**0.446**	**0.470**	**-0.053**	**4.031**
PEER0809	**6.9**	**12.2**	**NEHRP C**	**SS**	**1.041**	**1.112**	**-0.066**	**1.704**
PEER0801	**6.9**	**14.2**	**NEHRP C**	**SS**	**0.953**	**0.990**	**-0.038**	**1.914**
PEER0290	6.9	29.8	NEHRP D	N	0.771	0.565	0.310	
PEER0289	**6.9**	**13.3**	**NEHRP C**	**N**	**0.989**	**0.913**	**0.080**	**2.076**
PEER0288	**6.9**	**22.5**	**NEHRP C**	**N**	**0.704**	**0.594**	**0.169**	**3.190**
PEER0138	7.4	24.1	NEHRP D	RV	0.462	1.137	-0.901	
PEER0015	7.4	38.4	NEHRP C	RV	0.864	0.640	0.300	

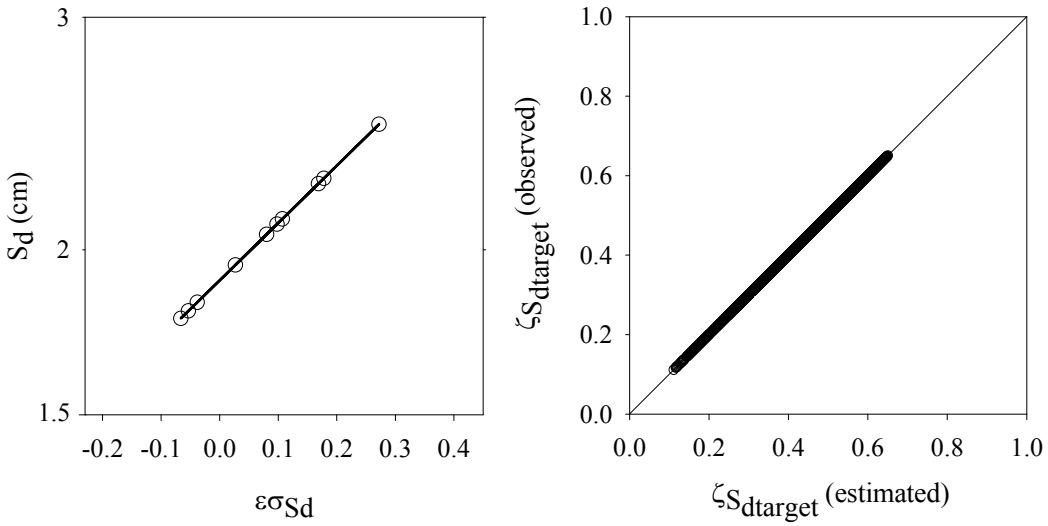

Figure 3.14 Correlation between $\varepsilon\sigma_{Sd}$ and scaled spectral displacement values in logarithmic space (left panel). Standard deviation values calculated from Equation 3.5 and corresponding observations (real) of each alternative ground motion bin (right panel)

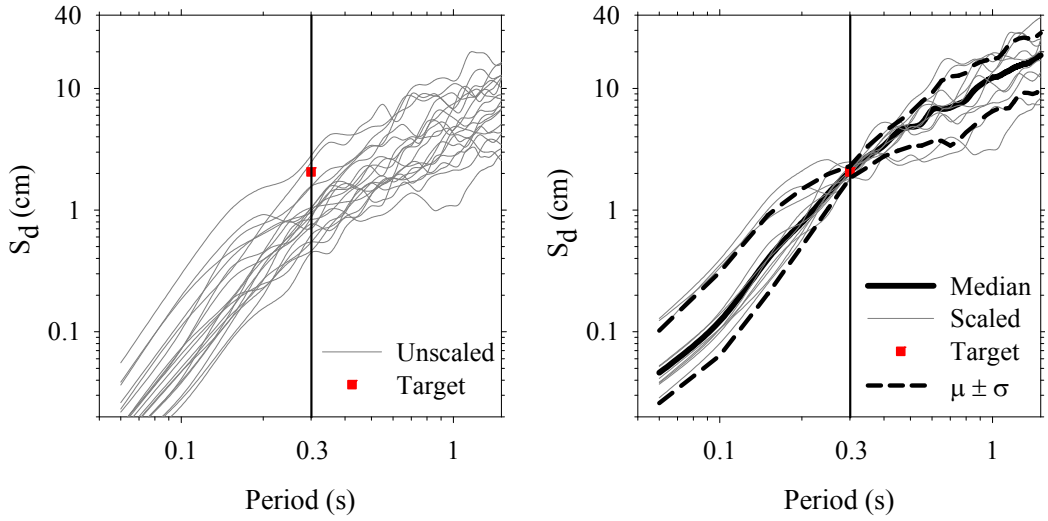

Figure 3.15 Unscaled spectra of candidate records and the target spectral displacement indicated by a square (left panel). Spectra of optimum recording set selected and scaled according to the proposed procedure (right panel). The median of the scaled spectral displacements exactly matches with the target spectral level.

CHAPTER 4

IMPOROVED PROCEDURE FOR NONLINEAR RESPONSE HISTORY ANALYSES

4.1 Introduction

Nonlinear RHA is conducted to obtain seismic deformation demands on a structure imposed by ground-motion records compatible with the hazard analysis. Once the demand statistics are evaluated, seismic performance assessment of the structure can be accomplished for the given hazard level. In Chapter 3, a ground motion scaling and selection procedure is developed in attempts to obtain appropriate records to be used as input for performance verification of linear structural systems. This procedure relies on the established linear relationship between $\varepsilon\sigma$ and intensity parameter used for scaling that essentially leads to optimum recording set. However, the linear relationship among scaled ground-motion intensity (e.g., spectral displacement) and $\varepsilon\sigma$ (e.g., $\varepsilon\sigma_{Sd}$) is valid only for systems behaving in their elastic limits and may fail for inelastic structural response. This chapter presents the modified scaling and selection procedure for RHA of structures that are responding beyond their elastic limit. The modified procedure is entirely based on inelastic spectral displacement. This spectral quantity is the most commonly used parameter by engineers while assessing the seismic performance of structural systems.

4.2 Selection and Scaling for Nonlinear Response of Structural Systems

Improving the selection and scaling procedure for nonlinear structural behavior requires an efficient estimator of inelastic structural response to be employed in the selection algorithm for optimum recording set. Analogous to the linear systems where $\varepsilon\sigma_{Sd}$ parameter becomes a perfect estimator of elastic response through Equation 3.3, the improved approach seeks for an efficient estimator of inelastic response. The perfectly linear correlation between $\varepsilon\sigma_{Sd}$ and scaled spectral displacement in elastic domain (Figure 3.14, left panel) diminishes with the increasing level of inelasticity. This fact is illustrated in Figure 4.1, which demonstrates the Pearson's correlation coefficients (lower right corner in each panel) between $\varepsilon\sigma_{Sd}$ and inelastic spectral displacement ($S_{d,ie}$) of scaled recordings for the optimum recording set identified for the fictitious case presented in Chapter 3. Each panel in Figure 4.1 corresponds to a different level of inelasticity that is described by R (R values increase from R = 2 to R = 8 following a consequential order in this figure. Increase in R value means increasing level of inelasticity). The correlation coefficients (ρ) indicate a significant decrease with respect to the elastic case (presented by solid straight lines showing the relation between $\varepsilon\sigma_{Sd}$ and scaled elastic spectral displacement) conveying the fact that the optimum recording set identified according to the elastic properties of fictitious structural system does not necessarily correspond to the ideal ground-motion bin when the structure starts to respond beyond its elastic limits. In other words, the optimum recording set that yields the minimum dispersion about the elastic response for a given target hazard level may not be the best choice for nonlinear structural systems. According to these discussions, when nonlinear structures are of concern, a new indicator that better correlates with inelastic response is required. Consequently, a new parameter $\varepsilon\sigma_{ISd}$ is proposed to replace $\varepsilon\sigma_{Sd}$. Details for the computation of $\varepsilon\sigma_{ISd}$ are given in the following sections.

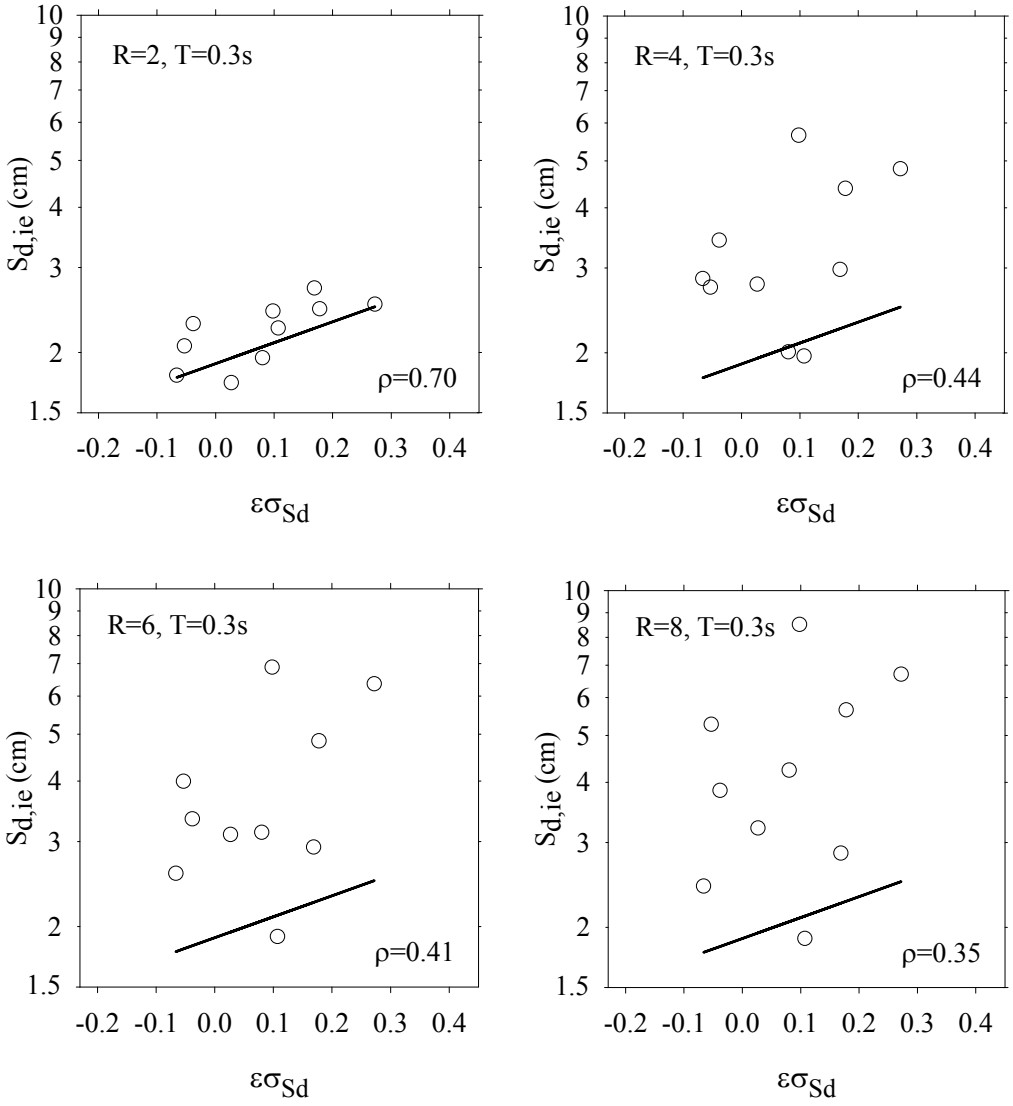

Figure 4.1 Correlation coefficients between $\varepsilon\sigma_{Sd}$ and $S_{d,ie}$ of scaled ground motions with respect to increasing level of inelasticity. The scaled ground motions constitute the optimum recording set that is obtained when the considered structural system behaves elastic. The black solid line shows the linear relationship existing between $\varepsilon\sigma_{Sd}$ and the scaled elastic spectral displacements (that shown in Figure 3.14).

4.2.1 Detailed Description of $\varepsilon\sigma_{ISd}$

An analytical model is established between $\varepsilon\sigma_{Sd}$ and $\varepsilon\sigma_{ISd}$ to estimate the median nonlinear structural response of scaled recordings and corresponding dispersion. For a given level of nonlinearity and vibration period, the proposed empirical model estimates $\varepsilon\sigma_{ISd}$ that is used while selecting the optimum recording set for nonlinear structural response.

To obtain a robust empirical model for cases within the common range of engineering interest, nonlinear spectral analyses of 260 accelerograms (ground-motion library of this dissertation that is described in Chapter 1) are conducted for vibration periods of T = 0.3 s, 0.6 s, 0.9 s, 1.2 s, and 1.5 s. The level of nonlinearity is designated by strength reduction factor, R, ranging from 1 (elastic case) to 8 (maximum nonlinearity). The considered vibration periods are assumed to represent the fundamental periods of low- to mid-rise reinforced concrete (RC) moment resisting frame (MRF) buildings.

In the first stage the records in each M_w–R_{JB} cluster of the ground-motion library are scaled by following the scaling procedure presented in Chapter 3 in order to derive the proposed empirical model for nonlinear response. Thus for each M_w–R_{JB} bin, the values of $\varepsilon\sigma_{Sd}$ (Equation 3.1) and θ (Equation 3.2) are computed for a predetermined discrete period to scale each accelerogram to its target elastic spectral displacement level, $S_{dtarget}(T)$, by using Equation 3.3. The period range of interest is described in the previous paragraph. The target hazard at the considered vibration period, $\bar{S}_{dtarget}(T)$, is established by using the Akkar and Bommer (2010) ground-motion predictive model. The magnitude and distance values of target hazard scenario are assumed to be the median magnitude (M_w) and distance (R_{JB}) values of each ground-motion bin.

The nonlinear response spectrum analyses are conducted to compute the peak deformation demands of scaled accelerograms for the predetermined vibration periods (T = 0.3 s, 0.6 s, 0.9 s, 1.2 s and 1.5 s) and strength reduction factors (R = 2, 4, 6 and 8). These calculations lead to the inelastic spectral displacements, $S_{d,ie}(T)|R$, for the entire ground-motion library for the interested period and strength reduction factor ranges of this study. The nonlinear behavior is represented by a bilinear non-degrading hysteretic model with 3% post-yield stiffness ratio (α) in response spectrum analyses. This simplified model is assumed to simulate the post-elastic behavior of RC MRF buildings. The non-degrading bilinear systems associated with a reasonable post-yield stiffness ratio is one of the common ways of representing actual nonlinear behavior in earthquake engineering studies (e.g., Chopra and Chintanapakdee, 2004; Iervolino and Cornell, 2005). This subject is further discussed and evaluated in subsequent chapters.

The above process not only considers one of the most practical approaches to mimic the nonlinear response of RC structures in engineering practice but also conveys an easy methodology to improve the proposed record selection and scaling procedure for nonlinear structural response. A scaled recording set that is consistent with the target hazard level, which is typically provided in terms of elastic spectral ordinates, and yielding minimum dispersion about median structural response is the ultimate objective of most modern risk assessment studies. For this reason, the records in each ground-motion bin are initially scaled for target elastic response. The analytical expression for $\varepsilon\sigma_{ISd}$ is then obtained through the results of inelastic spectral analysis to improve the selection algorithm for nonlinear dynamic response. This way, the analyst would associate the typically calculated elastic target hazard with RHA results to realistically compute the exceedance probability of a damage limit state.

The relationship between $\varepsilon\sigma_{Sd}$ and $\varepsilon\sigma_{ISd}$ is evaluated while deriving the analytical expression for the latter parameter. Analogous to $\varepsilon\sigma_{Sd}$, the observed values of $\varepsilon\sigma_{ISd}$ are also calculated as the logarithmic difference between θ (the scaling origin) and $S_{d,ie}$. Figure 4.2 shows the correlation between $\varepsilon\sigma_{Sd}$ and $\varepsilon\sigma_{ISd}$ by using the same recording set presented in Figure 4.1. The relationships between $\varepsilon\sigma_{Sd}$ and $\varepsilon\sigma_{ISd}$ are given for two R values (R = 2 and 6) and for two different vibration periods (T = 0.9 s and T = 1.5 s). The plots in this figure indicate that the linear correlation (designated by ρ) between $\varepsilon\sigma_{Sd}$ and $\varepsilon\sigma_{ISd}$ decreases with increasing level of inelasticity (1st and 2nd row plots) and decreasing vibration period (1st and 2nd column plots).

The relationship between $\varepsilon\sigma_{Sd}$ and $\varepsilon\sigma_{ISd}$ that is given for particular cases in Figure 4.2 is generalized in Figure 4.3. The median correlation coefficients between $\varepsilon\sigma_{Sd}$ and $\varepsilon\sigma_{ISd}$ are computed by following the procedure described in the previous paragraphs for the entire ground-motion library (260 accelerograms clustered in pre-defined M_w-R_{JB} bins). The left panel in Figure 4.3 illustrates the median variation of correlation coefficients as a function of T for different R values. The panel on the right shows the same variation as a function of R for different T values. The panels in Figure 4.3 depict that the correlation between $\varepsilon\sigma_{Sd}$ and $\varepsilon\sigma_{ISd}$ is influenced more at short periods (i.e. $T \leq 0.6$ s) as the gradient of ρ is very sensitive to the changes in R within this period range. For long periods, the correlation between $\varepsilon\sigma_{Sd}$ and $\varepsilon\sigma_{ISd}$ is relatively high and its variation is mild. Although these observations would suggest the use of $\varepsilon\sigma_{Sd}$ for record selection and scaling of long-period nonlinear systems, implementation of $\varepsilon\sigma_{ISd}$ seems to be inevitable when the concern is the record selection and scaling of short-period nonlinear structures. This remark is even more prominent when short-period structures are exposed to high levels of nonlinearity (i.e. represented by large R values).

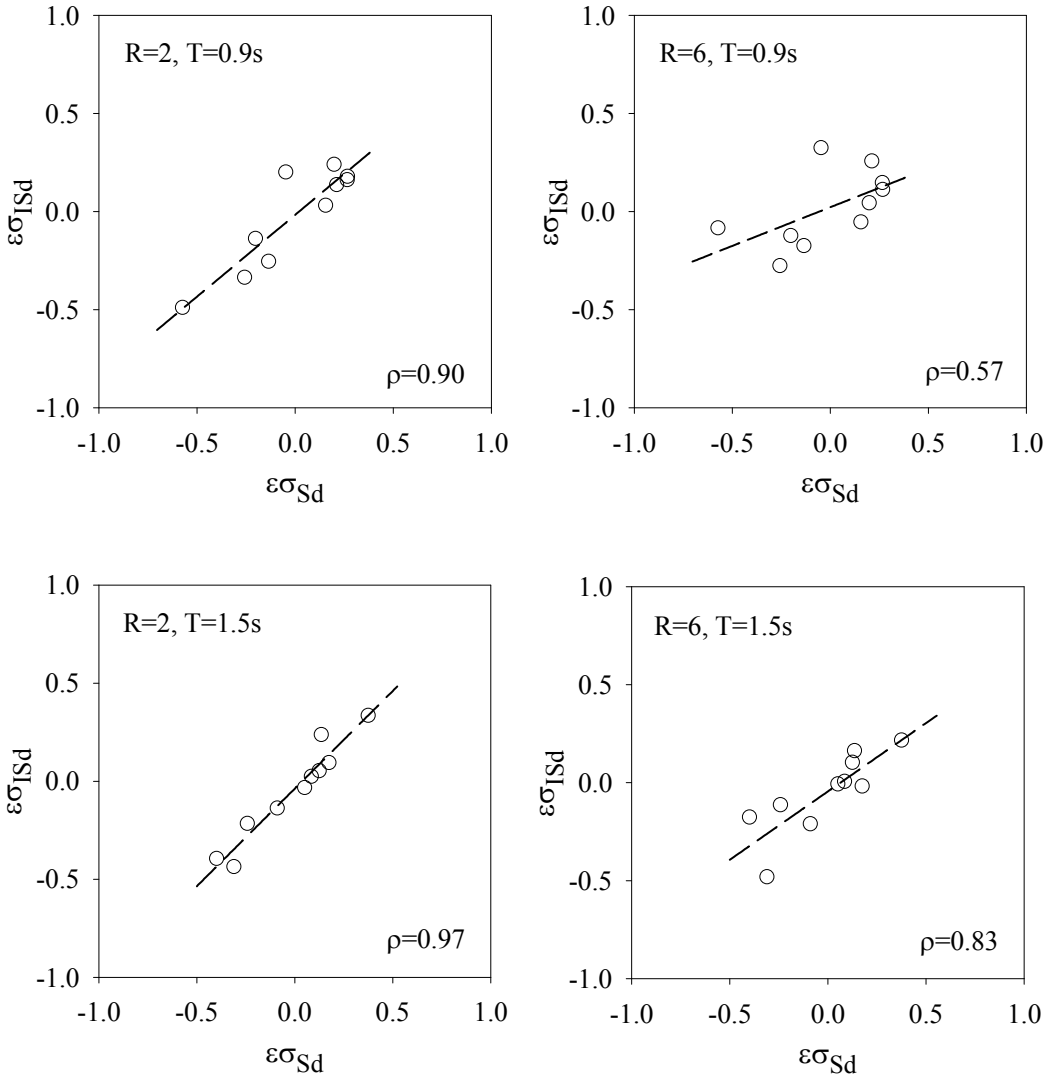

Figure 4.2 Correlation between $\varepsilon\sigma_{Sd}$ and $\varepsilon\sigma_{ISd}$ computed from scaled ground motions for a given elastic target hazard for different R and T combinations. The plots in each row illustrate the variation of correlation with respect to increasing level of inelasticity for T = 0.9 s (1st row) and T = 1.5 s (2nd row). The plots in each column show the same information for increasing vibration period for R = 2 (1st column) and R = 6 (2nd column)

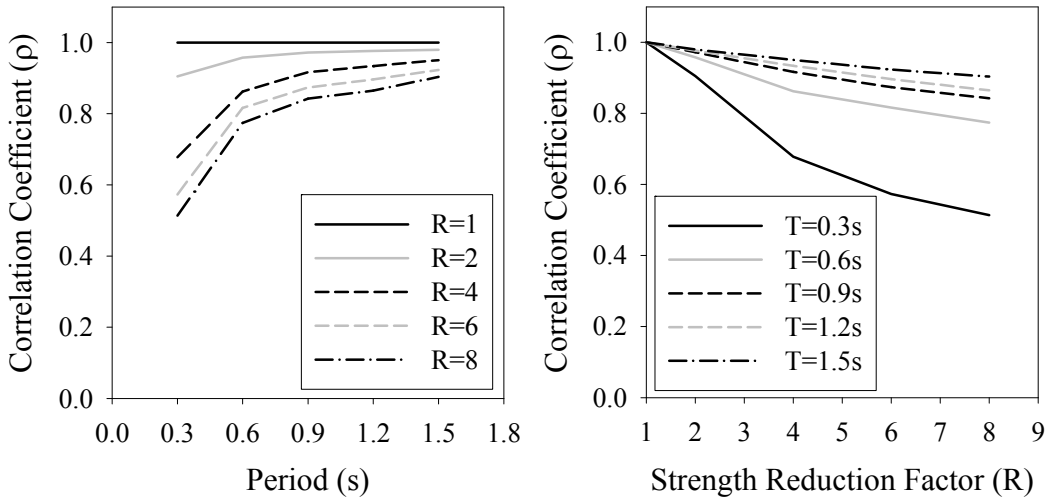

Figure 4.3 Correlation between $\varepsilon\sigma_{Sd}$ and $\varepsilon\sigma_{ISd}$ as a fact of vibration period (left panel) and strength reduction factor (right panel)

As indicated various times in the text $\varepsilon\sigma_{ISd}$ parameter should be employed in selection of optimum ground motion bin for structures responding beyond their elastic limits. According to the observations on the correlation between $\varepsilon\sigma_{Sd}$ and $\varepsilon\sigma_{ISd}$ as presented in previous paragraphs, this study investigated alternative predictors for $\varepsilon\sigma_{ISd}$. The alternative predictors investigated in this context are peak ground acceleration (PGA), peak ground velocity (PGV) and the period-shift due to nonlinear response of SDOF systems (T_{ie}). Of these alternative predictors PGA and PGV are always available from the accelerograms whereas T_{ie} can only be estimated from an empirical formulation. Since PGV is shown as an efficient parameter for describing the nonlinear structural response (e.g., Akkar and Özen, 2005; Akkar et al., 2005), more emphasis is placed on this parameter (rather than PGA and T_{ie}) while describing $\varepsilon\sigma_{ISd}$. While evaluating PGV as an alternative predictor of $\varepsilon\sigma_{ISd}$, $\varepsilon\sigma_{PGV}$ is computed as the logarithmic difference between the observed PGV (from considered accelerogram) and its corresponding estimation from a predictive model. Alternative to PGV, the combination of PGV and elastic spectral ordinate (i.e. $\varepsilon\sigma_{Sd+PGV}$) is also evaluated for describing $\varepsilon\sigma_{ISd}$ as few studies (e.g., Mousavi et al. (2011)) indicated that the

combination of these two predictor parameters can better describe the nonlinear structural response. Figure 4.4 shows the variation of $\varepsilon\sigma_{PGV}$ versus $S_{d,ie}$ (left panel) and $\varepsilon\sigma_{Sd+PGV}$ versus $S_{d,ie}$ (right panel) for the case study given in the upper right panel of Figure 4.1. Similar to other comparative plots given in this chapter the performances of $\varepsilon\sigma_{PGV}$ and $\varepsilon\sigma_{Sd+PGV}$ are measured by the Pearson's linear correlation coefficient, ρ. The computed correlation coefficients for $\varepsilon\sigma_{PGV}$ versus $S_{d,ie}$ and $\varepsilon\sigma_{Sd+PGV}$ versus $S_{d,ie}$ are significantly better than the ρ computed from $\varepsilon\sigma_{Sd}$ versus $S_{d,ie}$ relation (upper right panel in Figure 4.1). Note that $\varepsilon\sigma_{Sd+PGV}$ performs slightly better than $\varepsilon\sigma_{PGV}$ as the correlation coefficient of former is slightly larger than that of latter.

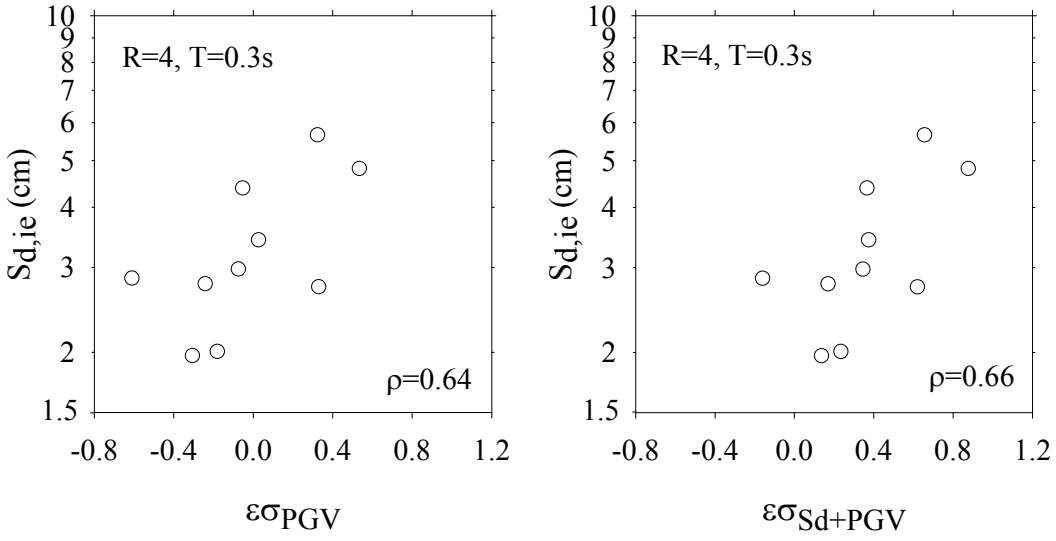

Figure 4.4 Correlation between $S_{d,ie}$ versus $\varepsilon\sigma_{PGV}$ (left panel) and $S_{d,ie}$ versus $\varepsilon\sigma_{Sd+PGV}$ (right panel)

The efficacy of $\varepsilon\sigma_{Sd+PGV}$ is further compared against $\varepsilon\sigma_{Sd}$ and $\varepsilon\sigma_{PGV}$ by computing ρ between $S_{d,ie}$ and each of these variables for the considered period ($0.3\ s \leq T \leq 1.5\ s$) and strength reduction factor ($2 \leq R \leq 8$) ranges of this study. The left panel in Figure 4.5 displays the computed period-dependent median correlation coefficients for $\varepsilon\sigma_{Sd+PGV}$, $\varepsilon\sigma_{PGV}$ and $\varepsilon\sigma_{Sd}$ using the entire ground-motion library for a strength reduction factor of R = 6. The right panel of the

same figure shows similar information for T = 0.3 s as a function of strength reduction factor, R. The plots in this figure indicate higher correlations between $S_{d,ie}$ and $\varepsilon\sigma_{Sd+PGV}$ with respect to those of $\varepsilon\sigma_{Sd}$ and $\varepsilon\sigma_{PGV}$.

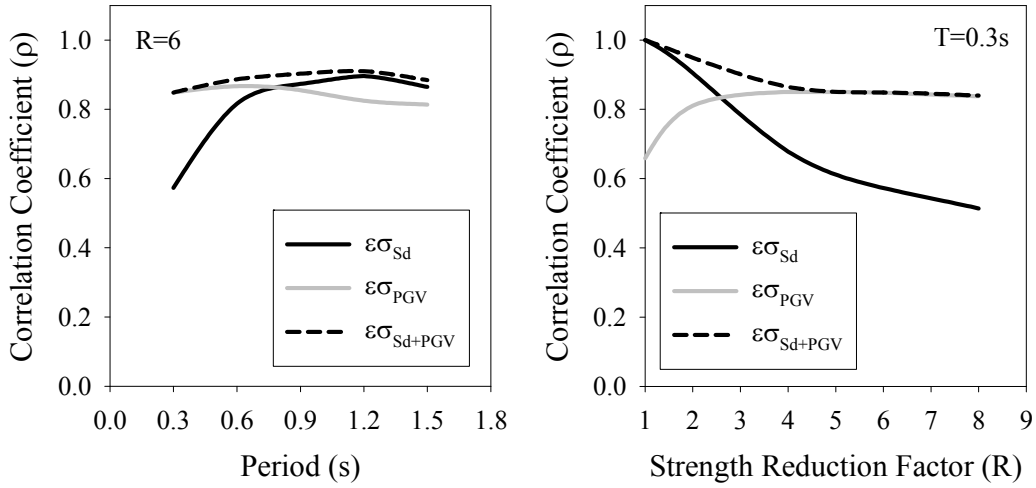

Figure 4.5 Correlation between $\varepsilon\sigma_{ISd}$ versus $\varepsilon\sigma_{Sd}$, $\varepsilon\sigma_{PGV}$, and $\varepsilon\sigma_{Sd+PGV}$

Under the light of above discussions, the empirical expression given in Equations 4.1 is developed to describe $\varepsilon\sigma_{ISd}$ as a linear combination of PGV ($\varepsilon\sigma_{PGV}$) and elastic spectral displacement ($\varepsilon\sigma_{Sd}$). It is noted that Equations 4.1 warrant the equality of $\varepsilon\sigma_{ISd}$ and $\varepsilon\sigma_{Sd}$ for the elastic case (i.e., R=1).

$$\varepsilon\sigma_{ISd} = c_1(R,T)\cdot\varepsilon\sigma_{Sd} + c_2(R,T)\cdot\varepsilon\sigma_{PGV} + c_3(R,T) \quad (4.1a)$$

$$c_1(R,T) = 1 - 0.72\ln(R) + 0.7T\ln(R) - 0.21T^2\ln(R) \quad (4.1b)$$

$$c_2(R,T) = 0.81\ln(R) - 0.78T\ln(R) + 0.23T^2\ln(R) \quad (4.1c)$$

$$c_3(R,T) = 0.22\ln(R) - 0.4T\ln(R) + 0.15T^2\ln(R) \quad (4.1d)$$

The likely bias in the estimation of $\varepsilon\sigma_{ISd}$ with respect to M_w and R_{JB} is investigated through residual analysis. The residuals are computed as the ratios of observed and estimated $\varepsilon\sigma_{ISd}$. Therefore ratios less than 1 would indicate conservative $\varepsilon\sigma_{ISd}$ estimations of Equations 4.1 whereas ratios of unity would

describe the equality of $\varepsilon\sigma_{ISd}$ estimations with the corresponding observed values. The bias in $\varepsilon\sigma_{ISd}$ estimations (with respect to M_w and R_{JB}) from Equations 4.1 are investigated by fitting straight lines to the residuals computed for each T and R pair used in this study. Whenever the slope term of a straight line is significantly different than zero, the $\varepsilon\sigma_{ISd}$ estimations by Equations 4.1 are considered as biased; residuals should not follow a particular trend for the entire range of concerned seismological parameters.

Figure 4.6 and 4.7 show residual plots as a function of M_w and R_{JB}, respectively. The presented scatters constitute a sample case for T = 0.6 s. Each figure consists of 4 panels showing the residual distributions of R = 2, 4, 6 and 8. The rest of residual analysis results are given in Appendix B of this dissertation. The straight line fits attain values close to one indicating that on average, the residuals are distributed around 1. This observation suggests that the estimations of Equations 4.1 are unbiased. The significance of slope term in each fitted straight line is assessed by applying t-statistics to test the null hypothesis: the slope term is zero. The significance level (P-value) provided by t-statistics is used for rejecting or fail-to-rejecting the null hypothesis. A P-value that is well above 0.05 is generally accepted as sufficient for fail-to-rejecting the null hypothesis.

The P-values given in Figures 4.6 and 4.7 are considerably larger than 0.05 indicating that the slope term is not significantly different than zero. The P-value statistics for the entire set of residual analysis are provided in Table 4.1. The bold P-values show the cases where the t-test results reject the null hypothesis (i.e., slope terms cannot be disregarded). Except for a few cases, where residuals do show a trend due to significant slope terms of fitted straight lines, the rest of the analyses advocate the fairly good performance of analytical expressions presented in Equations 4.1. Thus these equations are used while improving the proposed procedure for selecting and scaling of accelerograms for nonlinear structural systems.

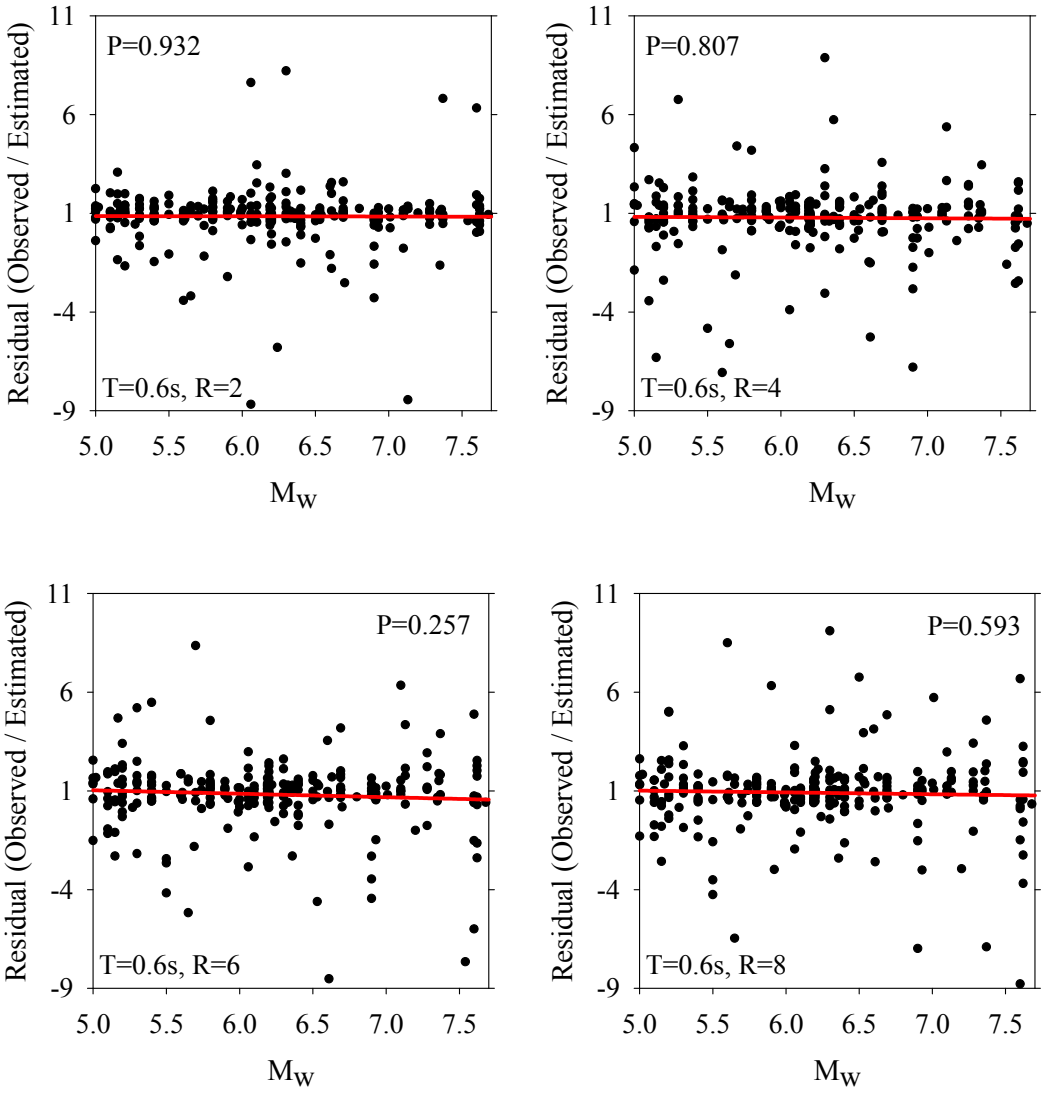

Figure 4.6 Residual scatters as a function of M_w for T = 0.6 s

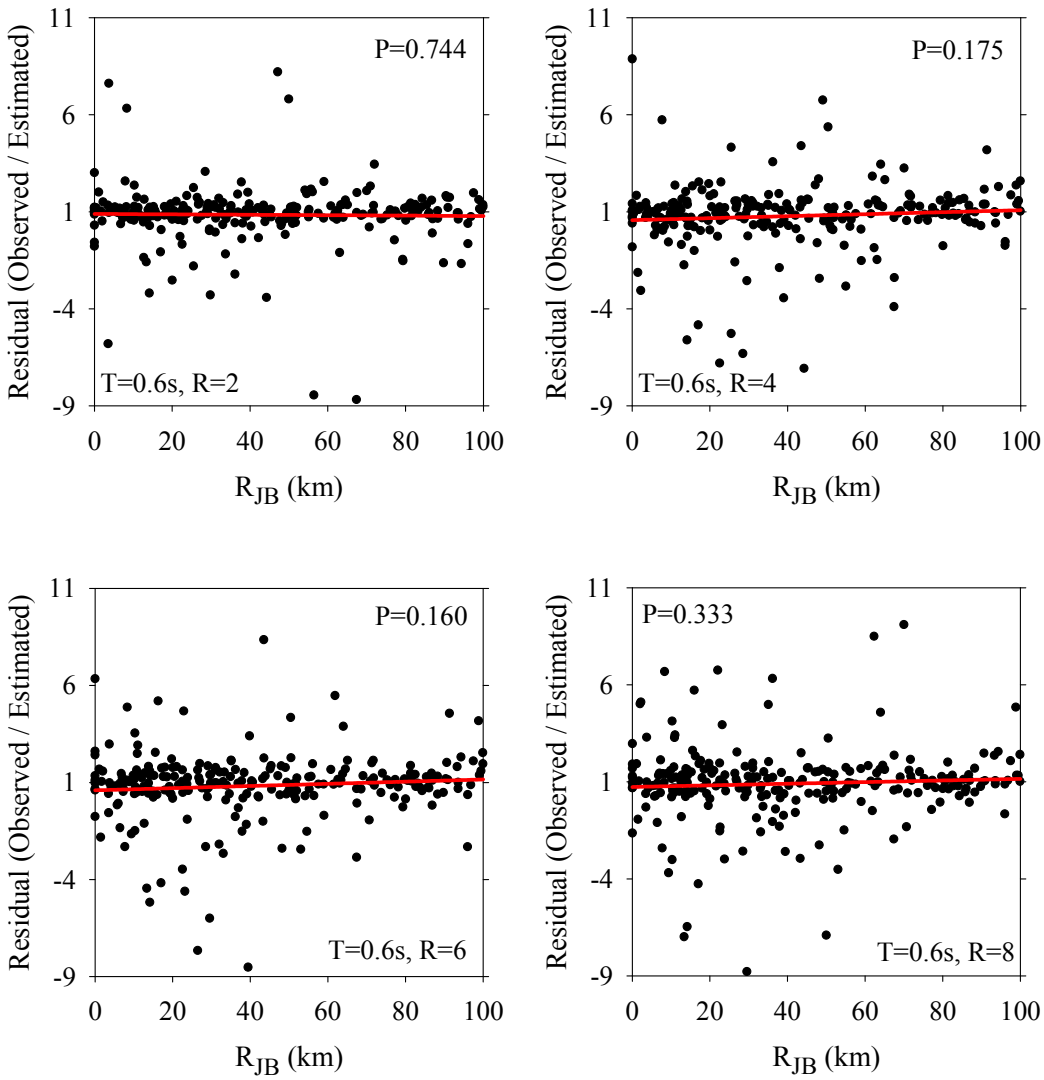

Figure 4.7 Residual scatters as a function of R_{JB} for T = 0.6 s

Table 4.1 P-values computed from the residual analysis with respect to M_w and R_{JB}

P-value		T = 0.3 s	T = 0.6 s	T = 0.9 s	T = 1.2 s	T = 1.5 s
M_w	R = 2	0.477	0.932	0.776	0.729	0.590
	R = 4	**0.023**	0.807	**0.023**	0.069	0.334
	R = 6	**0.003**	0.257	0.126	0.317	0.941
	R = 8	**0.047**	0.593	**0.002**	0.053	0.809
R_{JB}	R = 2	0.345	0.744	0.115	0.345	**0.036**
	R = 4	**0.019**	0.175	0.459	0.300	0.858
	R = 6	0.126	0.160	0.220	0.217	0.230
	R = 8	0.299	0.333	0.167	0.005	0.053

In essence, the parameter $\varepsilon\sigma_{ISd}$ computed from the functional forms given in Equation 4.1 should be employed in the median structural response and dispersion estimations while running the improved selection and scaling procedure for nonlinear structural systems. Equation 4.2 and Equation 4.3 define the median structural response and corresponding dispersion estimations that should be used together with Equations 4.1 for the selection and scaling procedure of structures responding beyond their elastic limits. Note that Equations 4.2 and 4.3 are modified versions of Equations 3.4 and 3.5 that are derived in the previous chapter assuming that the structures would respond in their elastic limits.

$$\lambda_{S_{dt\,arg\,et}} = \theta + \frac{\sum_{i=1}^{n} \varepsilon\sigma_{ISd,i}}{n} = \theta + \mu_{\varepsilon\sigma} \tag{4.2}$$

$$\zeta_{S_{dt\,arg\,et}} = \sqrt{\frac{1}{n-1} \cdot \sum_{i=1}^{n} \left(\varepsilon\sigma_{ISd,i} - \mu_{\varepsilon\sigma}\right)^2} \tag{4.3}$$

The parameter $\mu_{\varepsilon\sigma}$ in Equations 4.2 and 4.3 describes the average of $\varepsilon\sigma_{ISd}$ computed from n recordings. Equation 4.3 should be used while selecting the optimum recording bin populated from a ground-motion dataset of k recording. Note that these two equations can also be useful while assessing the seismic performance of buildings. This particular feature of the proposed procedure is further discussed in the following chapters.

4.3 Comparisons with Other Methodologies

The improved proposed selection and scaling procedure is tested for nonlinear structures by comparing its performance with other selection and scaling procedures. The comparisons are presented by using the previous case study discussed in Chapter 3 assuming that the fictitious structure deforms beyond its elastic capacity for a given R.

The selection and scaling methodologies proposed by Shome et al. (1998) and Baker (2011) are employed in the comparisons. These methodologies rely on stripe-scaling (see Chapter 2 for definition) to modify the records to the target spectral ordinate. Baker (2011) recommends stripe-scaling but he also mentions an alternative procedure that scales each individual record by the ratio of average spectral ordinates of individual and target spectra within the pre-defined period range (see Equation 2.4). The target spectrum in Baker (2011) is CMS and scaling is done over a period interval of interest. Following his conclusion about the simplicity and better performance of stripe-scaling with respect to its alternative, this study employs stripe-scaling while implementing Baker's selection and scaling methodology. It should be noted that the procedures of Shome et al. (1998) and Baker (2011) promote stripe-scaling as the scaling methodology. However these two studies differ in the ground-motion selection strategy. Shome et al. (1998) suggest using ground motions having magnitudes similar to the target hazard scenario whereas Baker (2011) brings forward the

significance of matching with CMS. Baker (2011) uses deaggregation results of PSHA to determine the target scenario in terms of magnitude and source-to-site distance associated with an epsilon value. Among the scaled candidate records that are compatible with the target scenario earthquake, he selects records having similar elastic spectral shape with CMS for a given period band to reduce the dispersion about nonlinear median response. Baker (2011) defines this period interval as $0.2\ T_1 \leq T_1 \leq 2.0\ T_1$ where T_1 is the fundamental period of investigated structure. Baker (2011) sets a statistical measure (sum of squared errors, SSE) to quantify the match between the spectrum of each candidate record and CMS (target spectrum) over the pre-defined period range. In his selection methodology, the candidate accelerograms are ranked in increasing order using their SSE scores. The first n records that constitute the lowest SSE scores are selected for seismic performance assessment.

As discussed in Chapter 3, the deaggregation of fictitious site-specific scenario yields $M_{w,target} = 7.15$, $R_{JB,target} = 22.5$ km and an epsilon value of 1.44 that results in an elastic spectral displacement of 2.06 cm at $T_1 = 0.3$ s. The predictive model to estimate target hazard level is developed by Akkar and Bommer (2010). The candidate recording set that contains 20 accelerograms is already given in Table 3.1 (see Chapter 3). Among these accelerograms, recordings are assembled and scaled according to the selection and scaling procedures described above. There is no bias in the implementation of these selection procedures because all three methods use the same candidate ground-motion dataset that is composed of accelerograms having comparable seismological features with the target hazard scenario. Table 4.2 lists the accelerograms selected by each methodology from the candidate ground-motion dataset. Note that the selection and scaling methodology proposed in this study identifies different records for assembling the optimum ground-motion bin for linear and nonlinear structural response as the procedure employs $\varepsilon\sigma_{Sd}$ and $\varepsilon\sigma_{ISd}$, respectively for these different behaviors.

Table 4.2 Recordings that are selected by the procedures compared in this study

Record name	This Study R=1 (Elastic)	This Study R=6	CMS Baker (2011)	Shome et al. (1998)
TGMB1592	X			X
PEER1794			X	X
PEER1636		X		
PEER1633				X
PEER1144	X	X	X	X
PEER1116	X			
PEER1107		X	X	
PEER0880				X
PEER0864	X	X	X	X
PEER0848		X	X	X
PEER0827		X	X	X
PEER0826	X		X	
PEER0812	X			
PEER0809	X			X
PEER0801	X	X		
PEER0290			X	
PEER0289	X	X	X	
PEER0288	X	X		
PEER0138				X
PEER0015		X	X	

Figures 4.8-4.10 show displacement spectra of 10 optimum records selected and scaled by each procedure for linear and nonlinear response. The spectral ordinates are presented for a period interval of 0.06 s to 2.0 s to compare the performance of the methods in a complete manner. The left hand side panels in each figure display the elastic displacement spectra, their median and corresponding dispersion whereas panels on the right show the variation of spectral ordinates for nonlinear structural response represented by a bilinear non-degrading hysteretic model with 3% post-yield stiffness ratio for R=6. Figure 4.8 displays the results obtained by the selection and scaling procedure proposed by Shome et al. (1998) whereas Figures 4.9 and 4.10 give the same information for Baker (2011) and the proposed procedure, respectively.

As indicated, Figures 4.8-4.10 compare the period-dependent variation of dispersion about median spectrum of scaled records to test the success of each investigated selection and scaling procedure for linear and nonlinear structural response. The left panel of Figure 4.9 displays the scenario-specific CMS that is used in Baker (2011) to constrain the selection and scaling of records. In a similar manner, the linear response plots of Shome et al. (1998) and this study includes median spectrum predictions of Akkar and Bommer (2010) for the target earthquake scenario. The left panel of Figure 4.9 reveals a good match between the median elastic spectrum and CMS. Shome et al. (1998) and this study also yield fairly similar median trends with the predictions of Akkar and Bommer (2010) although none of these methods explicitly consider a spectrum match for a predetermined period interval. Inherent in stripe-scaling methodology employed by Shome et al. (1998) and Baker (2011), linear spectral ordinates of selected and scaled records result in zero dispersion about $S_{dtarget}$ at T_1. The proposed procedure results in a standard deviation value of 0.111 about the same target hazard level (also discussed in Chapter 3) because the major objective of the proposed methodology is to provide accurate median response estimations by preserving the inherent record-to-record variability in the selected and scaled ground motions.

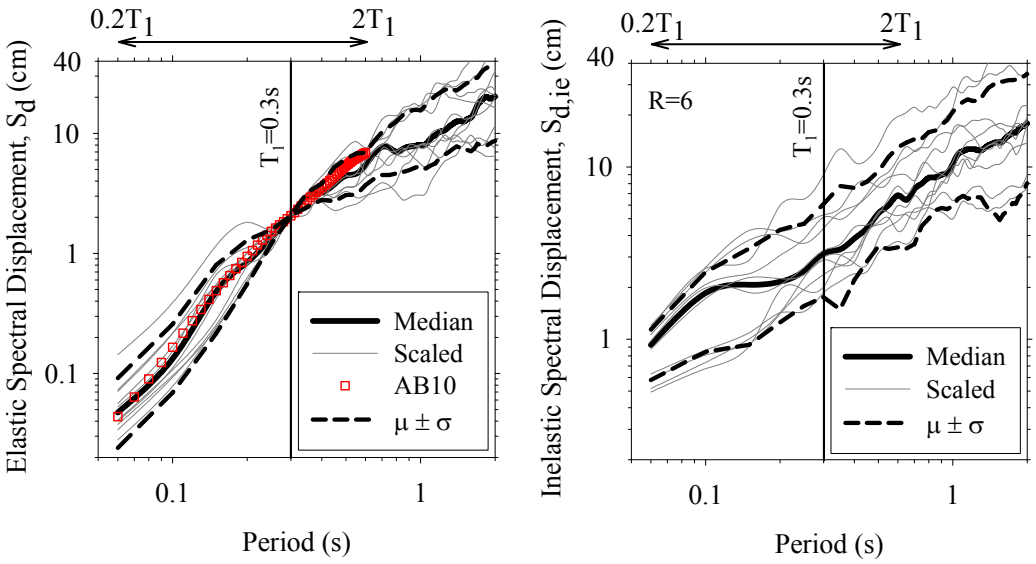

Figure 4.8 Linear (left panel) and nonlinear (right panel) response spectra of records selected and scaled by Shome et al. (1998)

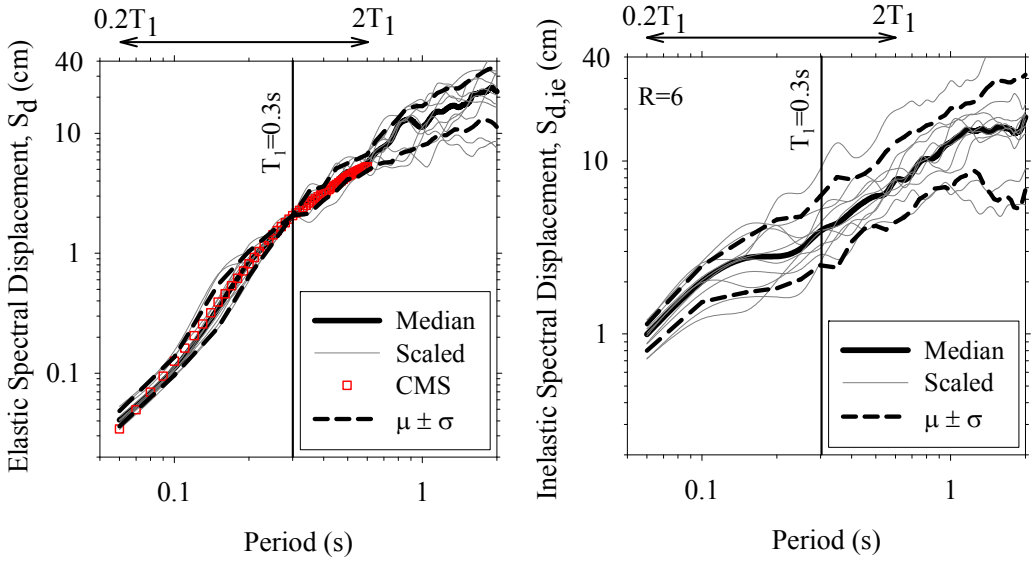

Figure 4.9 Linear (left panel) and nonlinear (right panel) response spectra of records selected and scaled by Baker (2011)

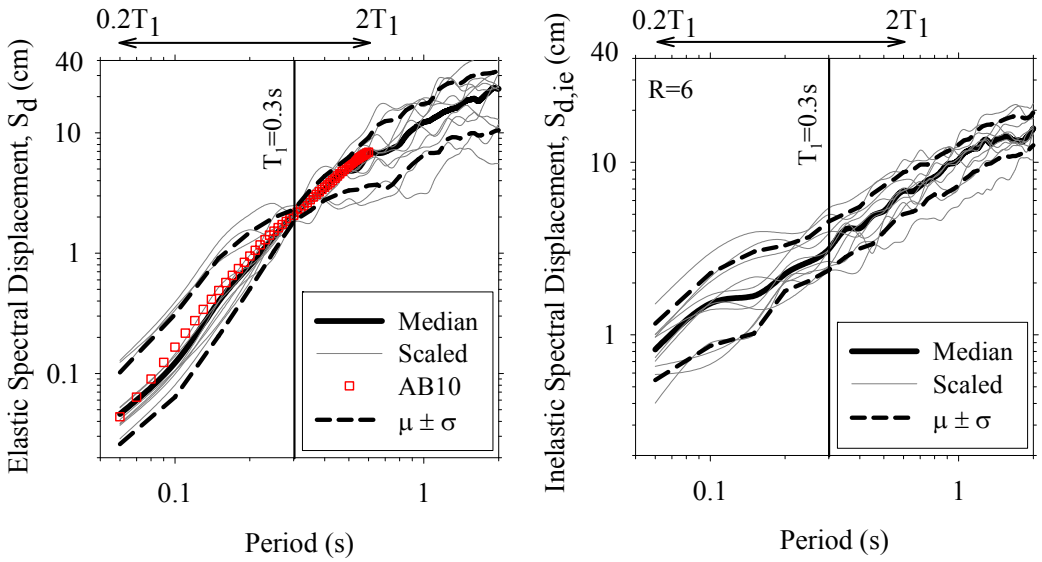

Figure 4.10 Spectral ordinates of optimum recording set selected and scaled by this study for linear (left panel) and nonlinear structural response (right panel)

The period dependent dispersion statistics of Baker (2011) show the advantage of spectrum matching when the elastic response is of concern for the given period interval, because the scaled spectra have less variation about target elastic response compared with other alternatives. However, when the nonlinear response is considered, the proposed procedure results in relatively smaller uncertainty with respect to other two methodologies investigated here.

Figure 4.11 gives the dispersion statistics shown in Figures 4.8–4.10 in a generalized frame to compare the performance of proposed methodology with other two procedures for different levels of nonlinearity. The resulting dispersion (represented by standard deviation) in scaled ground motions for different R values is calculated for the same fictitious building and target hazard scenario. The comparisons show that the procedure proposed in this study yields smaller standard deviations for response estimation of this structural system with respect to its alternatives. This plot advocates that the proposed methodology results in lesser uncertainty for almost all levels of inelasticity for this specific case. Note

that the observations made in Figure 3.5 concerning the variation of dispersion with respect to increasing inelasticity level also confirmed in Figure 4.11. The dispersion is continuously increases with increasing R for all three methods; an observation that is discussed in other studies (e.g., Akkar and Özen, 2005; Akkar and Küçükdoğan, 2008). However, the standard deviation of Shome et al. (1998) is more sensitive to variations in R that may advocate its shortcoming with respect to other two methods.

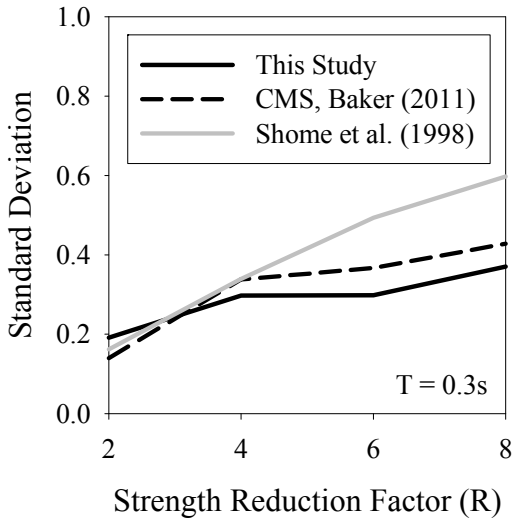

Figure 4.11 Observed standard deviation of nonlinear spectral response obtained from recordings selected and scaled by three methods compared in this study

CHAPTER 5

EVALUATION OF PROPOSED SELECTION AND SCALING PROCEDURE FOR MULTI-DEGREE-OF-FREEDOM SYSTEMS

5.1 Introduction

Estimating seismic induced risk is a challenging subject as it has to consider both structural and ground motion uncertainties. The reason for this assertion is the random nature of earthquake phenomena and variability in structural properties that complicate the reliability of seismic performance assessment studies. In this chapter, the limitations of the proposed selection and scaling procedure are investigated by verifying the seismic response of structural models that are developed from a statistical study that compiled the general characteristics of Turkish reinforced concrete (RC) building stock. Structural response statistics obtained from the accelerograms selected and scaled according to the proposed methodology are compared with the results of two recently proposed ground motion selection and scaling procedures (i.e., Baker, 2011 and Kalkan and Chopra, 2011) to evaluate the efficiency of the presented method in this dissertation.

The first part of this chapter presents a brief discussion on the statistical features of the Turkish building stock that fairly reflects the daily construction practice in Turkey. The first part also discusses the analytical building models that reflect the observed characteristics of the examined building stock. The target hazard scenario used for the verification of subject structural systems is the last topic

considered in this part. Evaluation of the proposed methodology for MDOF systems and comparisons of alternative procedures are discussed in the second half of the chapter. The limitations of the procedure as a tool for probabilistic vulnerability assessment studies are given as the final point in Chapter 5.

5.2 Study on Geometrical Properties of the Turkish RC Building Stock

General structural properties of the Turkish RC building stock are examined through a statistical study that compiles the major structural attributes of building inventories in the city of Düzce as well as Zeytinburnu, Küçükçekmece, and Bakırköy districts in İstanbul. The total number of 3- to 9-story RC buildings compiled in this statistical study is 33773. The majority of the building data is from the Küçükçekmece (29945 buildings) and Zeytinburnu (3034 buildings) building inventories. The most detailed building database comes from the Bakırköy district in İstanbul. The Bakırköy building inventory consists of 333 RC buildings with blue prints, building pictures and structural reports (courtesy of PROTA Engineering and Consultancy Inc.). The geometrical properties studied in the building databases are story height, floor plan dimensions, number of continuous frames, span lengths, dimension and orientation of columns. These major statistical descriptors are presented consecutively in this section. Table 5.1 lists the investigated geometrical properties and building inventories that provide the statistical data whereas Figure 5.1 illustrates some of the investigated properties in a sample floor plan.

Table 5.1 Investigated building properties and corresponding database

	Düzce	Küçükçekmece	Zeytinburnu	Bakırköy
Story height	X		X	X
Floor plan dimension		X	X	X
Number of continuous frames	X		X	X
Span length				X
Dimension and orientation of columns				X

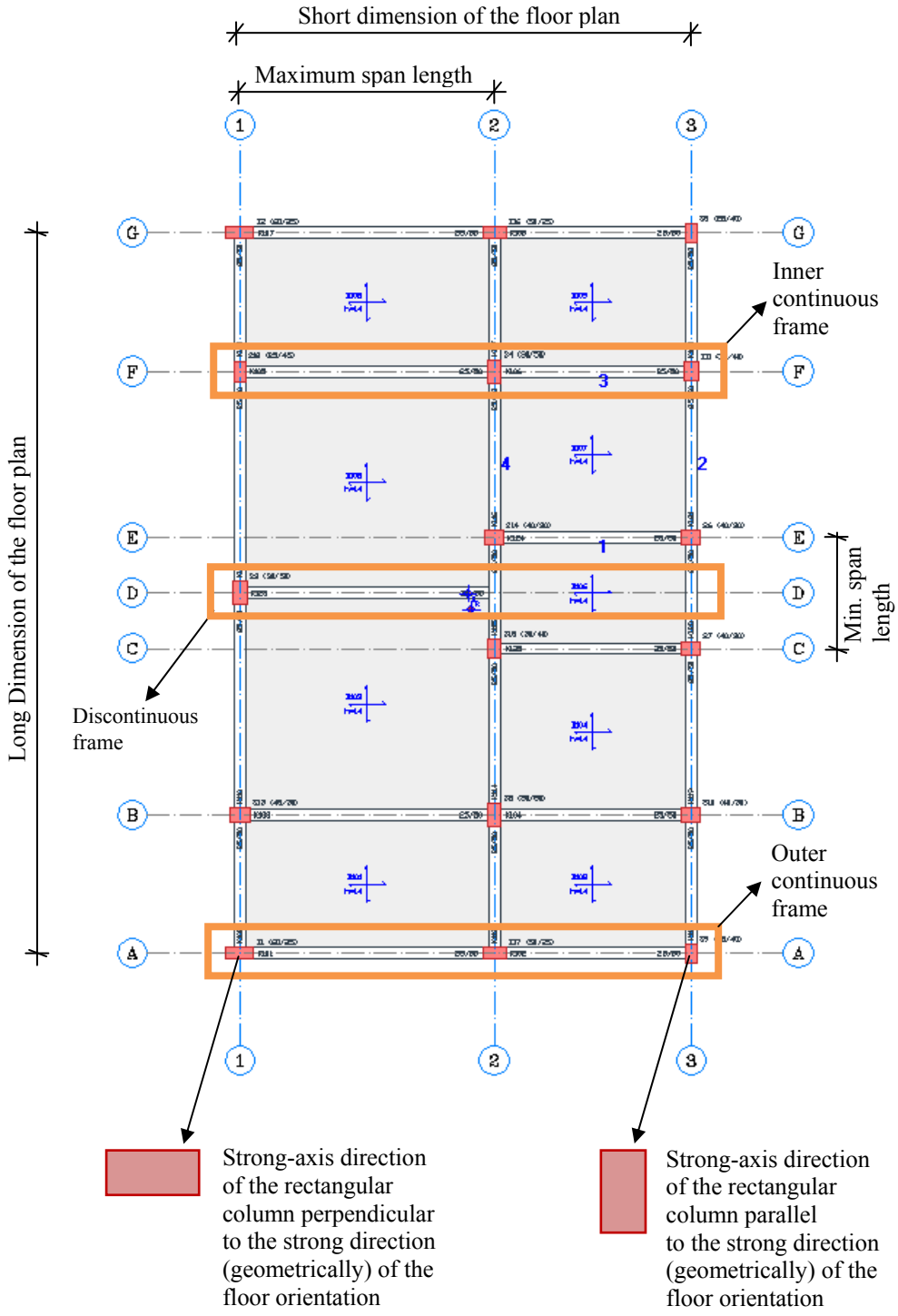

Figure 5.1 The geometrical floor properties studied in the building databases

i. Story Height

The story height data are investigated as the ground-story and upper story height statistics. The results indicate that the average ground-story height is 3.01 m with a standard deviation of 0.39 m. The average upper story height is determined as 2.71 m with a standard deviation of 0.20 m. Ground stories are generally used for commercial purposes in Turkey even if the buildings are residential. This is the major reason for ground stories being higher than the other story heights in the Turkish building stock. This reality is reflected to the statistics presented in this study. It should be noted that the values presented here are very similar to those indicated in Bal et al. (2007). The aforementioned study also investigated the Turkish RC building stock in a detailed manner. The findings of Bal et al. (2007) show a mean ground-story height of 3.23 m with a COV value of 0.15. The same study also reveals that the average upper story heights and corresponding COV value for ordinary RC buildings are 2.84 m and 0.08, respectively.

ii. Plan Dimension

The buildings in the inventory are also investigated for floor plan geometry and dimensions. Most of the sample buildings have a rectangular floor plan. The plan dimensions are described by considering the lengths of short- and long-plan dimensions as well as their ratios. The plan area and dimensions are examined with respect to the number of stories as well. Accordingly, for low-rise buildings (3-, 4- and 5-story), the average length of shorter and longer dimensions are 9.20 m and 13.24 m, respectively. Standard deviation of the shorter dimension length is 3.73 m whereas the standard deviation value of longer dimension length is observed as 8.28 m. For mid-rise buildings (6- to 9-story), the average length of shorter dimension and corresponding standard deviation are 10.30 m and 4.01 m, respectively. The observed average value for the length of longer dimension and corresponding standard deviation are 15.42 m and 7.15 m, respectively. When the building height is disregarded the average ratio of short to long plan dimensions is found as 0.73 with a standard deviation value of 0.18.

iii. Number of Continuous Frames

One of the specific characteristics of the Turkish building stock is the presence of discontinuous frames that yield deficiencies in the lateral load transfer mechanism. Thus the number of continuous and discontinuous frames along short and long dimensions of buildings is also investigated to reflect one of the other general features of the Turkish building stock. The observations indicate that generally 2 or 3 continuous frames exist along each one of the two perpendicular floor plan directions. 40 % of the investigated frames are tagged as continuous whereas 60 % are accepted as discontinuous. The location of continuous frames in floor plan area is also observed. The observations show that 40 % of the continuous frames are distributed as inner frames. 30 % of continuous frames are along the long side of the floor plan as outer frame whereas the 30 % of the continuous frames are located at the perpendicular direction of the floor plan as outer frame.

iv. Span Length

The mean value of span length and corresponding standard deviation are 3.51 m and 0.74 m, respectively for continuous frames along short direction. The mean value of span length is 3.59 m with a standard deviation value of 0.61 m, if continuous frames along long direction are of concern. When orientation is disregarded the average span length is found as 3.55 m with a standard deviation value of 0.68 m. These statistics are almost the same in the study conducted by Bal et al. (2007). The findings of Bal et al. (2007) indicated a mean span length of 3.37 m with a COV value of 0.38 when beam orientation is not of concern.

v. Geometry and Orientation of Columns

The common column geometry, corresponding dimensions and their strong-axis direction with respect to floor plan orientation are investigated from the Bakırköy building inventory. The observations indicate that almost all columns have rectangular geometry (95.73 %). This geometrical shape is followed by square columns (4.05 %). The number of circular columns is negligible and they

constitute 0.22% of the entire data. The strong-axis direction of rectangular columns with respect to floor plan orientation is examined to give an overall idea about the lateral deformation capacity of Turkish building stock. These statistics show that the strong-axis directions of rectangular columns are distributed evenly along the two perpendicular directions of the floor plan.

Column depth statistics are investigated for buildings with different number of stories to obtain a relationship between these two variables. Besides, the ratio of column depth to column width is examined. The column depth and ratio statistics are given in Figure 5.2. This figure shows that as the story number increases, the column depth also increases (left panel of Figure 5.2). However, the column width does not change significantly with increasing story number as given in the column-depth to column-width ratio statistics (right panel of Figure 5.2). Another important characteristic of the Turkish building stock is the variation of column area along the building height. The statistical survey on the variation of column area with respect to increasing story number shows a decrease in column area towards upper stories.

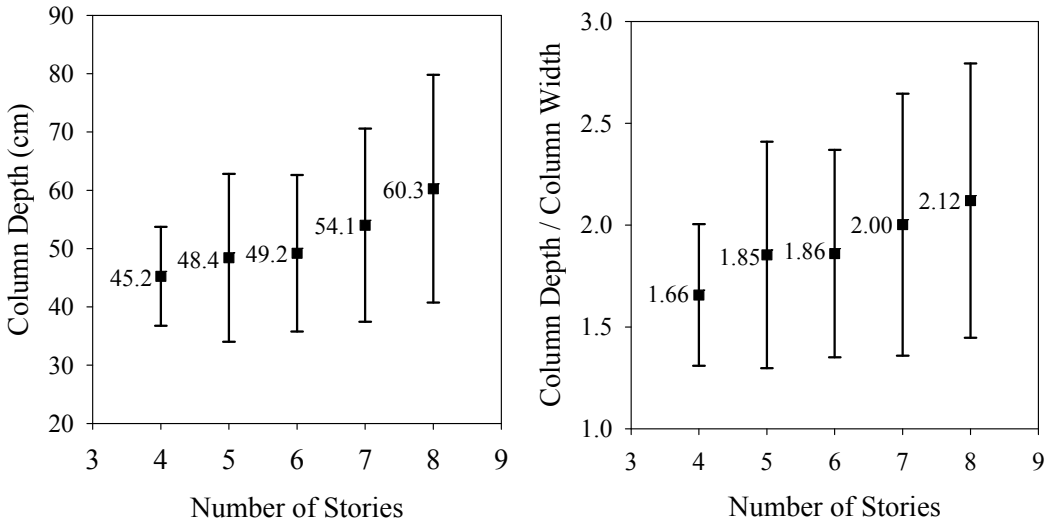

Figure 5.2 Column dimensions with respect to number of stories

Tables 5.2 and 5.3 give the major geometrical properties of the Turkish RC building stock obtained from this statistical study.

Table 5.2 Statistics for geometrical properties of Turkish RC building stock

	Mean	Standard Deviation
Ground-story height (m)	3.01	0.39
Upper-story height (m)	2.71	0.20
Ratio of short to long building plan dimension	0.73	0.18
Number of continuous frames along short direction	2.68	1.30
Number of continuous frames along long direction	2.70	1.17
Average span length (if orientation is disregarded) (m)	3.55	0.68

Table 5.3 Statistics for column dimension properties

Number of Stories	Col. Depth/Col. Width		Ground-story column depth (cm)		Column area decreasing from ground-story to top-story (%)	
	Mean	Std. Dev.	Mean	Std. Dev.	Mean	Std. Dev.
4	1.66	0.35	45.2	8.48	19.0	12.26
5	1.85	0.56	48.4	14.39	24.0	17.85
6	1.86	0.51	49.2	13.42	24.7	18.41
7	2.00	0.64	54.1	16.57	24.4	16.68
8	2.12	0.67	60.3	19.52	30.7	15.15

5.3 Structural Models

Three-dimensional models reflecting general characteristics of Turkish building stock are generated by selecting building floor plans that are compatible with the building statistics discussed in Section 5.2 (modifications are made in original structural geometry in accordance with the statistical study presented in previous paragraphs). For instance, Figure 5.3 displays the original ground-story floor plan of a building from the Bakırköy database, whereas Figure 5.4 shows the modified version of this original plan that is used in three-dimensional models. In essence this approach enables this study to mimic the common geometrical properties of the Turkish building stock in the generated analytical models.

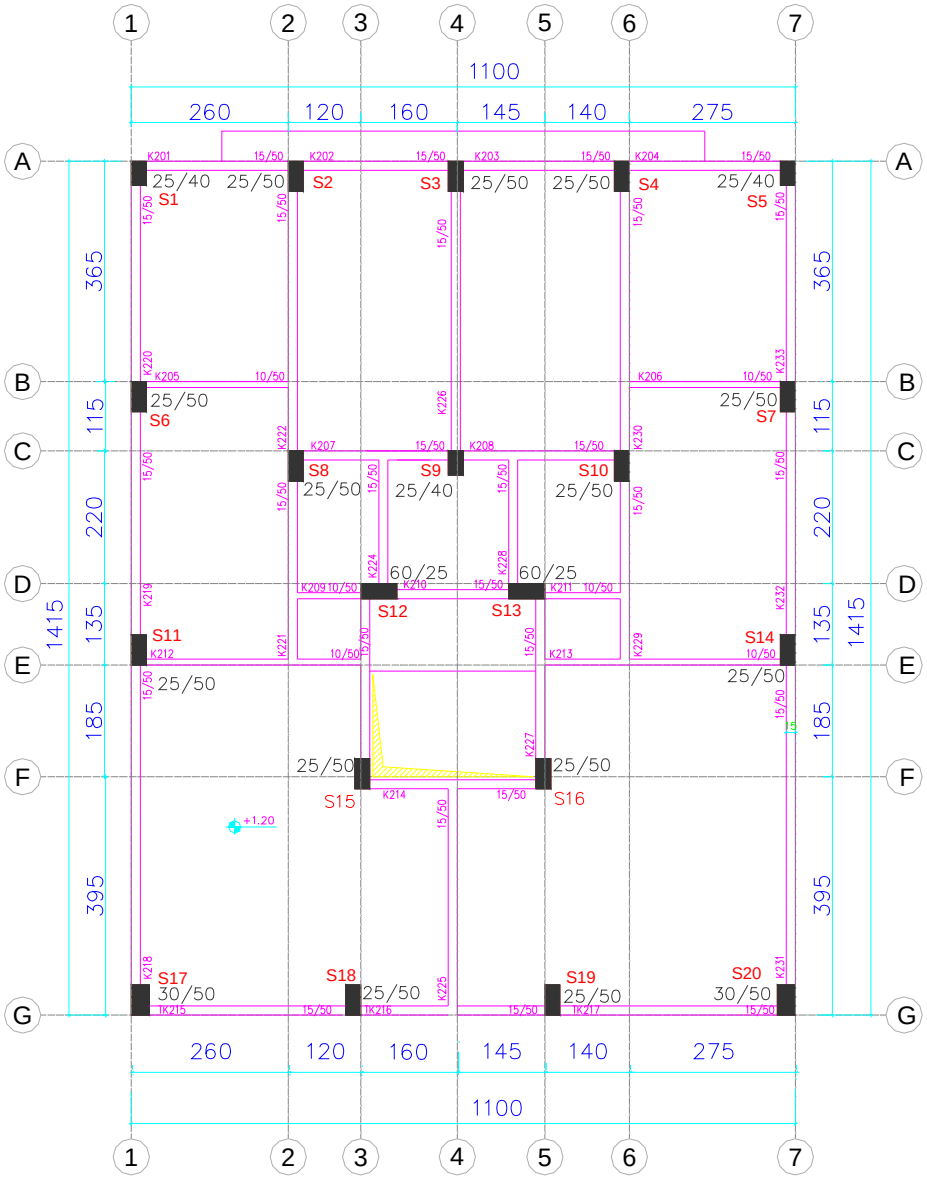

Figure 5.3 Original ground-story floor plan of a building located in Bakırköy, İstanbul

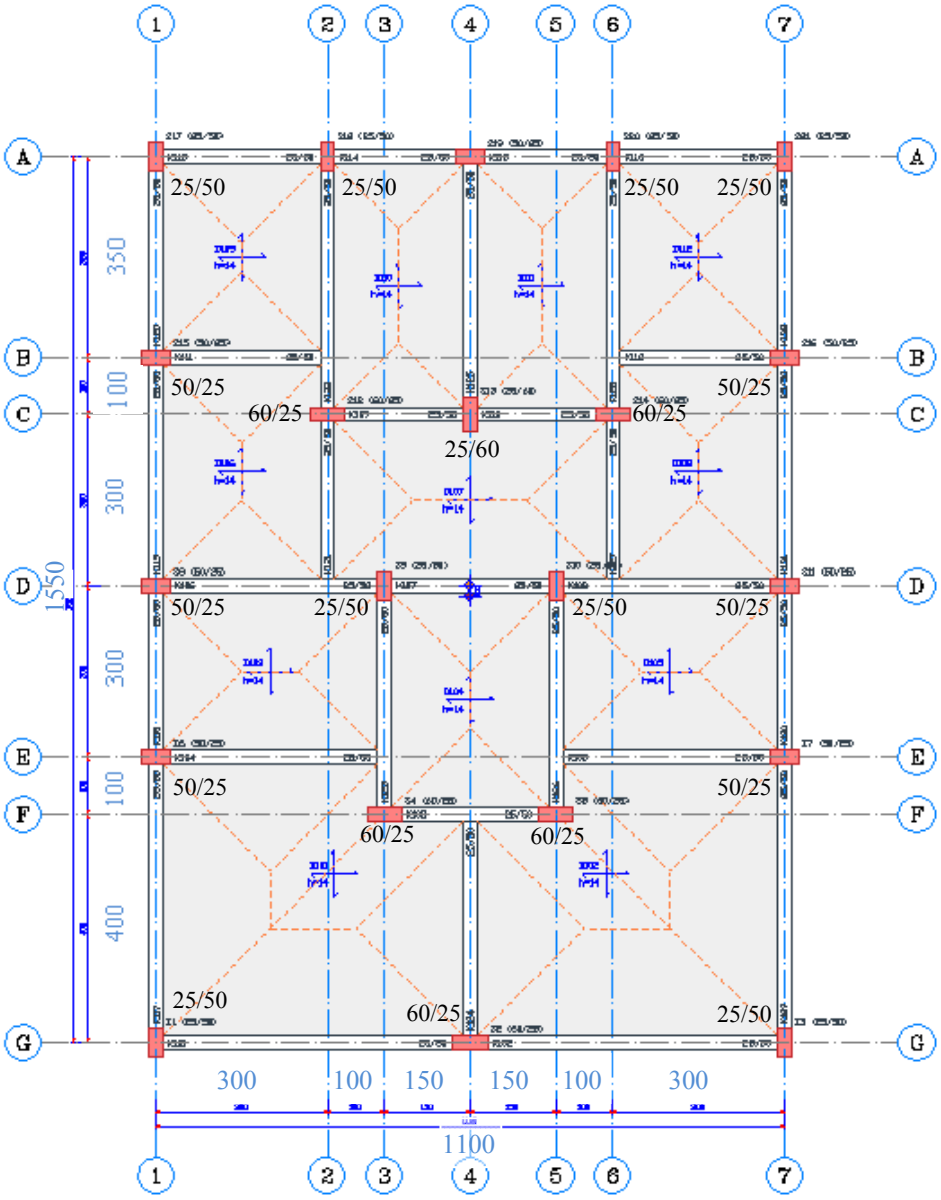

Figure 5.4 Adopted ground-story floor plan of the same building mentioned in Figure 5.3. This modified floor plan is used while modeling the 4-story building in this study.

According to the descriptions given in the previous paragraph, the reinforced concrete design of three MRF building models (3-, 4- and 8-story) is conducted by using the Probina Orion (Prota, 2011) software (version 16.0). The concrete and steel grades used in these models are C20 and S420, respectively. This way, the requirements of current national codes (i.e., TS 500-2000 (Turkish Standards Institute, 2000), TS 498 (Turkish Standards Institute, 1997) and Turkish Earthquake Code (TEC, 2007)) are satisfied for these buildings. It is assumed that these buildings are located in a site that falls into Seismic Zone 1 (The most seismic prone region according to the Turkish Earthquake Code (TEC, 2007)). The site is categorized as Z3 (soft site) in design. The evaluations and investigations presented in this chapter are limited to the analyses of code complying buildings that have invariant material properties.

Three-dimensional models generated to represent the 3-, 4- and 8-story buildings and corresponding ground-story floor plans are given in Figures C1-C6, in Appendix C. From each analytical model, a representative two-dimensional frame is selected and it is used in structural analysis. The selected frames for each model are indicated by rectangular boxes in Figures C2, C4 and C6. Each of these two-dimensional frames is designated with a code that represents the number of story of the building and the label of frame axis (i.e., 4MRF-DD).

Figure 5.5 shows the geometry of 3-story planar frame, whereas Figures 5.6 and 5.7 illustrate the two-dimensional analytical models of 4-story and 8-story frames, respectively. The story heights and span lengths of each model are given on these figures as well. Figures 5.5-5.7 also show the cross-sectional dimensions of the column and beam members in the models. Note that the column cross-sectional area is reduced towards upper stories according to the observations in Turkish construction characteristics.

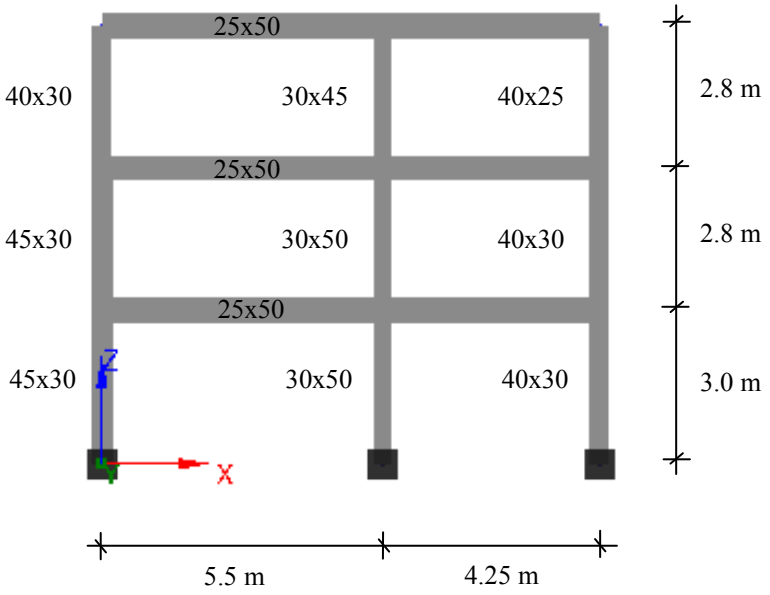

Figure 5.5 3MRF-BB model and member dimensions

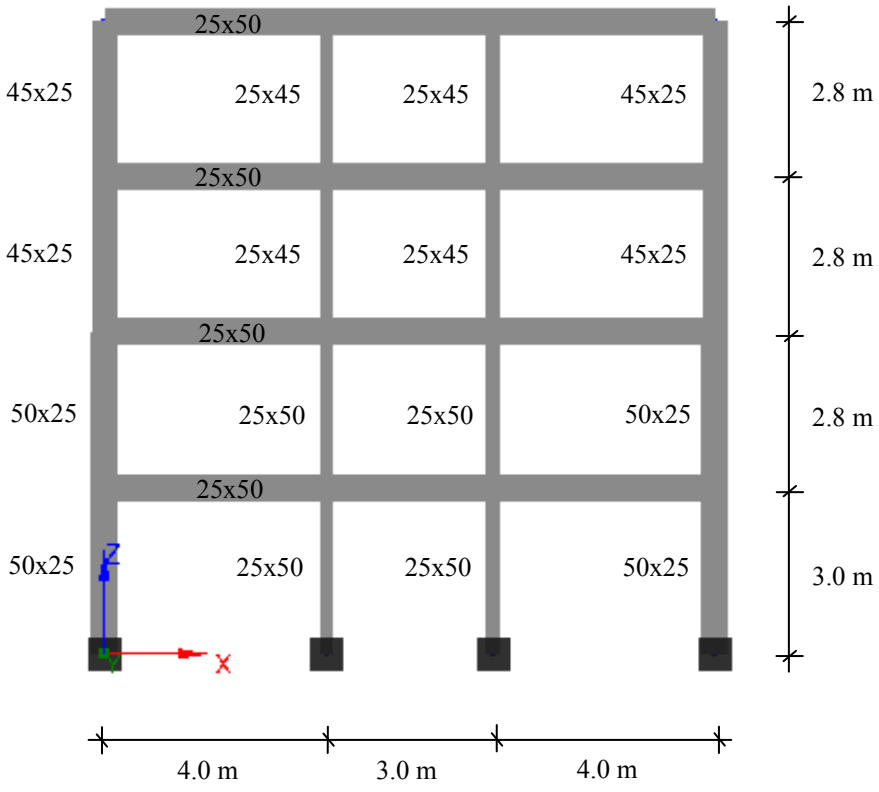

Figure 5.6 4MRF-DD model and member dimensions

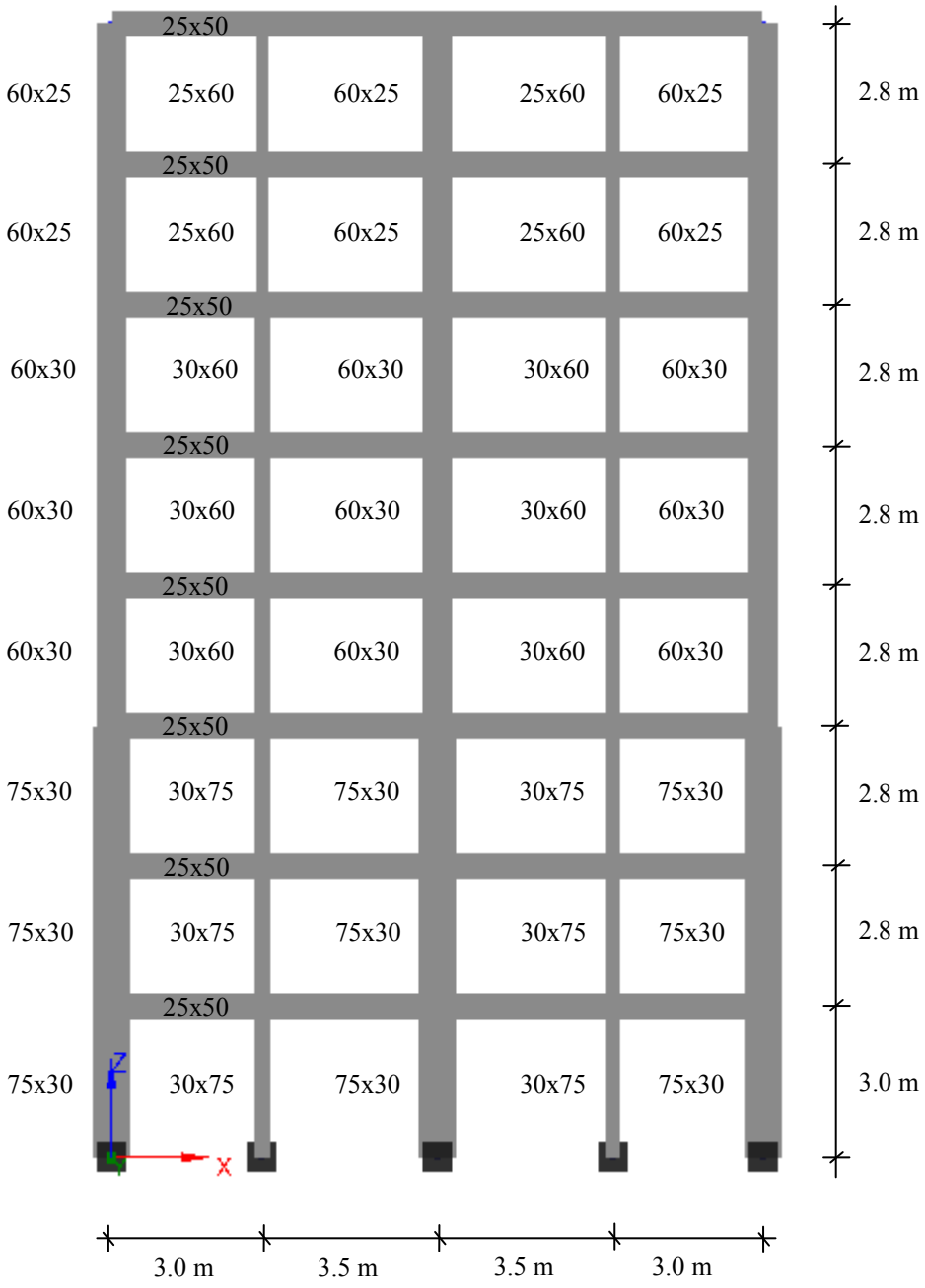

Figure 5.7 8MRF-FF model and member dimensions

5.4 Structural Analyses

The structural analyses of analytical models are conducted by using SeismoStruct (Seismosoft, 2010) platform (version 5.2.2). The software employs Hilber-Hughes-Taylor integration method (Hilber et al., 1977) while performing nonlinear RHA. Eigenvalue analysis, nonlinear static pushover analysis and nonlinear dynamic response history analyses are performed for each analytical model. The frame members are modeled as inelastic force-based fiber elements (Spacone et al., 1996). Nonlinear concrete model of Mander et al. (1988) and bilinear steel model are used to represent material nonlinearity.

Modal parameters of the frames are determined by eigenvalue analysis. Then, nonlinear static pushover analyses are performed to obtain the capacity curves of these frames. An invariant lateral load pattern corresponding to the first-mode shape is used in the pushover analysis (Chopra and Goel, 2002). Roof displacement versus base shear relationship is idealized as a bilinear force-deformation curve according to the ATC-40 (ATC, 1996) procedure. The acceleration versus displacement response spectra (ADRS, Mahaney et al., 1993) of each frame is obtained by using idealized bilinear capacity curves and the modal parameters. This way, the MDOF frame models are idealized as SDOF systems defined with initial period, T_1, yield spectral displacement (elastic limit), $S_{d,y}$, and post-yield stiffness ratio, α.

Inelastic spectral analyses of idealized SDOF systems and the nonlinear RHA of the MDOF systems are done by using the records selected and scaled according to the compared methodologies. Maximum roof drift ratio (MRDR, which is calculated by normalizing the maximum roof displacement with the building height) is used as the global deformation parameter. The median response and corresponding dispersion statistics are investigated in order to compare the alternative selection and scaling methodologies. The subsequent section

summarizes the results of eigenvalue and pushover analyses of the generated building models.

5.4.1 3-Story MRF Building

The eigenvalue analysis of 3MRF-BB frame yields the first and second mode periods as 0.50 seconds and 0.16 seconds, respectively. The first mode modal mass participation is found as 0.87. The eigenvalue analysis indicates a first-mode dominant behavior of 3MRF-BB frame. The left panel of Figure 5.8 shows the pushover curve (base shear versus roof displacement) of the 3MRF-BB frame and corresponding bilinear idealization. The idealized pushover curve results in a post-yield stiffness ratio of 2.10 %. The base shear coefficient, η (the ratio of the yield base shear (V_y) to the building weight (W)) is found as 0.39. The right panel of Figure 5.8 displays the idealized ADRS of the 3MRF-BB frame. According to the idealized capacity spectrum, the yield pseudo-spectral acceleration ($PS_{a,y}$) value of the system is found as 445 cm/s^2, which corresponds to a spectral displacement ($S_{d,y}$) value of 2.85 cm.

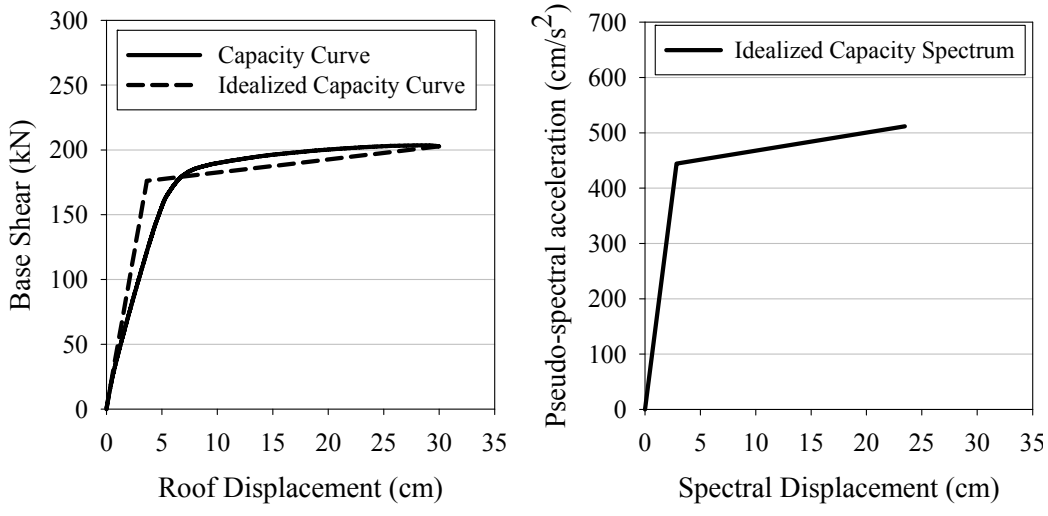

Figure 5.8 Capacity curve (pushover curve), corresponding bilinear idealization (left panel) and capacity spectrum (right panel) of 3MRF-BB frame

5.4.2 4-Story MRF Building

The first and second mode periods of the 4MRF-DD frame are found as 0.61 seconds and 0.20 seconds, respectively. The translational effective modal mass participation of the first mode is found as 0.84. According to the eigenvalue analysis results, the structure predominantly behaves in the first mode. The base shear coefficient, $\eta=V_y/W$, is found as 0.30. Figure 5.9 shows the capacity curve and its ADRS format for this frame. The idealized pushover curve (left panel of Figure 5.9) results in a post-yield stiffness ratio value of 3.03 %. The $PS_{a,y}$ value of the idealized bilinear system (right panel of Figure 5.9) is 354 cm/s^2 whereas $S_{d,y}$ equals to 3.38 cm.

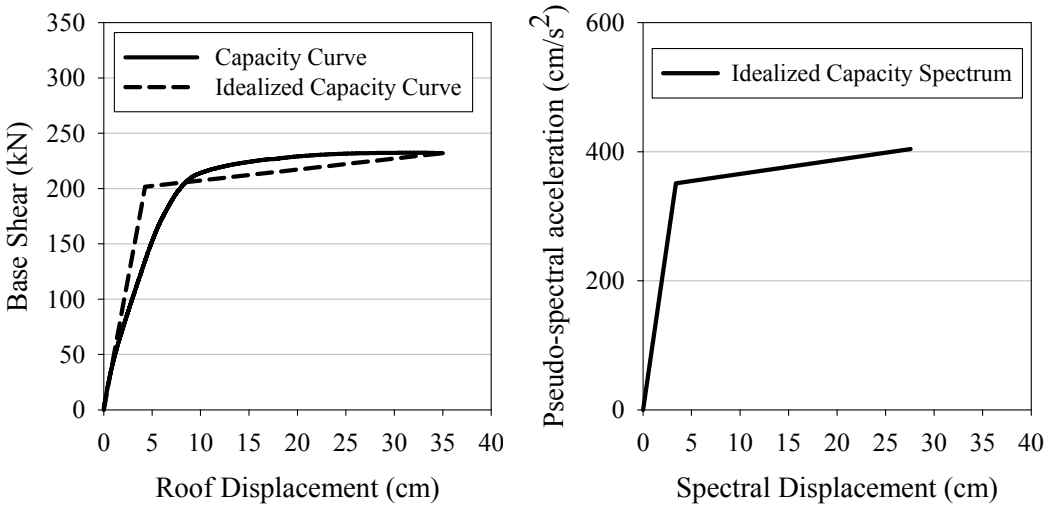

Figure 5.9 Capacity curve, corresponding bilinear idealization (left panel) and capacity spectrum (right panel) of 4MRF-DD frame

5.4.3 8-Story MRF Building

For 8MRF-FF frame, the first mode period and corresponding modal mass participation is 1.12 seconds and 0.78, respectively. The second mode period of this frame is found as 0.39 seconds. The eigenvalue analysis indicates a first-

mode dominant behavior with noticeable higher mode contribution. The left panel of Figure 5.10 shows the capacity curve of the 8MRF-FF frame and corresponding bilinear idealization. The base shear coefficient, $\eta=V_y/W$, of the 8MRF-FF frame is found as 0.16. According to the idealized capacity curve, the post-yield stiffness ratio is found as 0.7 %. The right panel of Figure 5.10 displays the idealized capacity spectrum of the 8MRF-FF frame, which results in a $PS_{a,y}$ value of 205 cm/s^2 and corresponding $S_{d,y}$ value of 6.48 cm.

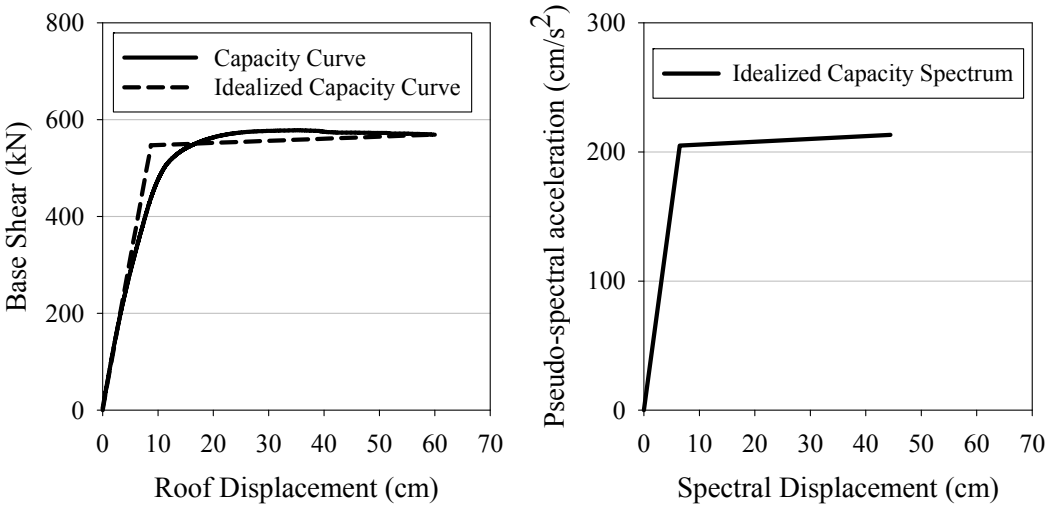

Figure 5.10 Capacity curve, corresponding bilinear idealization (left panel) and capacity spectrum (right panel) of 8MRF-FF frame

The fundamental period (T_1), corresponding modal mass participation, post-yield stiffness ratio (α), yield spectral ordinates ($S_{d,y}$, $PS_{a,y}$) and η of idealized equivalent SDOF systems of 3-, 4- and 8-story frames are listed in Table 5.4.

Table 5.4 Idealized SDOF system properties of frame models

	3MRF-BB	4MRF-DD	8MRF-FF
T_1 (sec)	0.50	0.61	1.12
Modal mass participation of first mode	0.87	0.84	0.78
α (%)	2.10	3.03	0.70
$S_{d,y}$ (cm)	2.85	3.38	6.48
$PS_{a,y}$ (g)	0.45	0.36	0.21
η	0.39	0.30	0.16

5.5 Probabilistic Seismic Hazard Analysis and Target Earthquake Scenario

The comparisons between alternative procedures are made by selecting and scaling ground-motion records for a given target earthquake scenario. Assuming that the sample buildings are located near Erzurum on a soft soil site (NEHRP D), the expected seismic hazard for a return period of 2475 years (T_R = 2475 years) is computed by a specific PSHA study. The spectral ordinates of this return period are assumed to be generated by the maximum credible earthquake (MCE) of the considered region.

Seismic sources are characterized to estimate the target ground-motion intensity and the earthquake scenario (M_w-R_{JB}-ε pair) that contribute mostly to the target intensity level. The characteristics of the seismic sources are determined by investigating the literature describing historical earthquakes and seismic catalogues that yield the information about active faults and background seismicity. North Anatolian Fault, East Anatolian Fault and Erzurum Fault that are likely to produce future earthquakes in the area of interest are assumed as the fault seismic sources. The mechanism of these fault sources are assumed as strike-slip. Among these, Erzurum Fault of 80 km length that is located approximately 3 km from the southern part of the site is assumed as the main fault source that dominates the seismicity of the area of interest.

The deaggregation of the PSHA study yields the target scenarios that are extracted by considering the fundamental period of each model building. The deaggregation results for each building model for a return period of T_R = 2475 years are given in Figure 5.11. Table 5.5 summarizes the target moment magnitude, R_{JB} distance and epsilon values obtained from the deaggregation results that are illustrated in Figure 5.11. Corresponding target hazard levels ($S_{dtarget}$) that are obtained from the Akkar and Bommer (2010) predictive model are also given in Table 5.5. This GMPE is used for the entire hazard study.

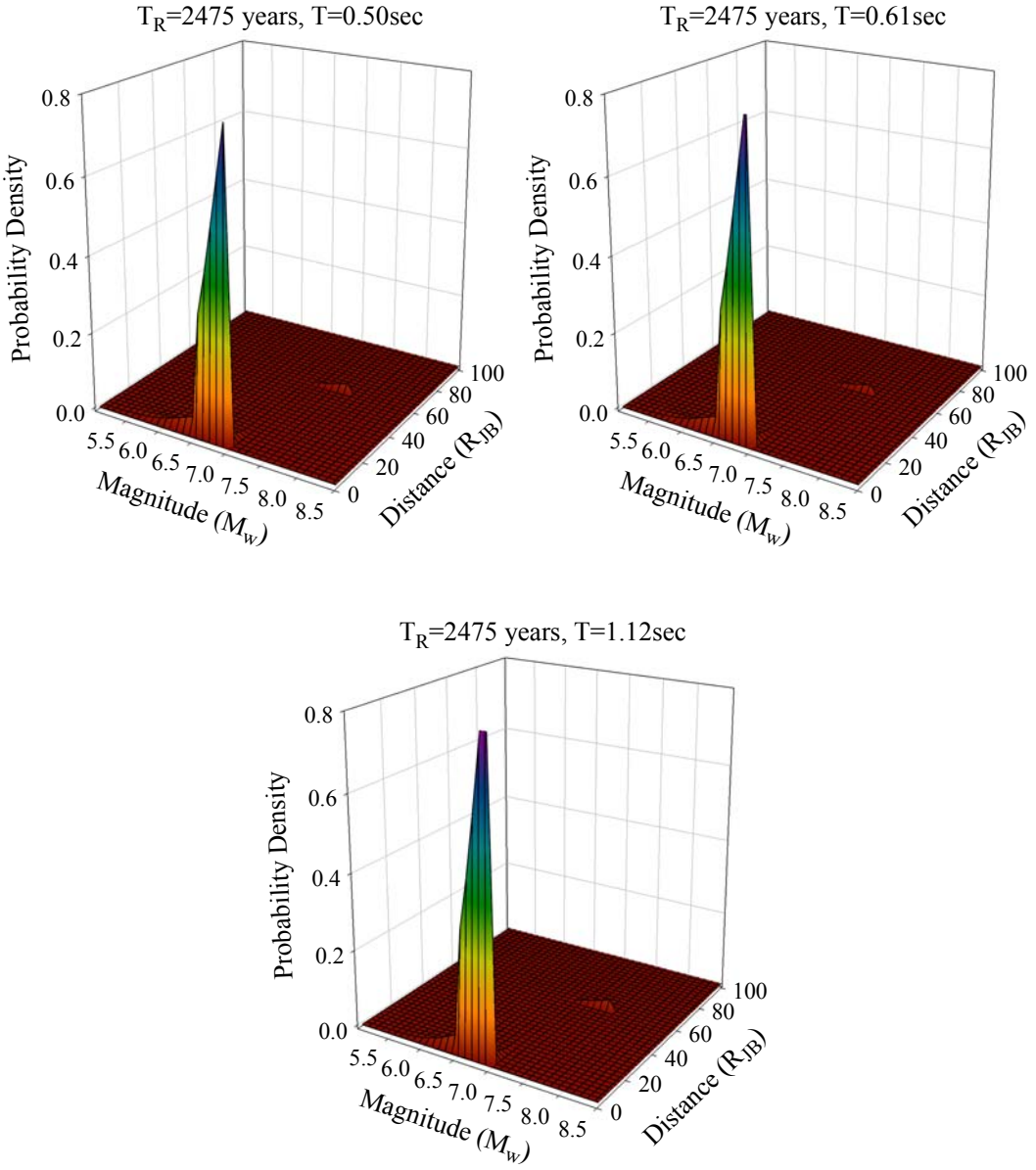

Figure 5.11 PSHA deaggregation for the given exceedance of PS_a values with a return period of 2475 years at T = 0.50 seconds (1st row left panel), at T = 0.61 seconds (1st row right panel) and at T = 1.12 seconds (2nd row)

Table 5.5 Target earthquake scenario and corresponding spectral displacement

	3MRF-BB	4MRF-DD	8MRF-FF
$M_{w,\ target}$	6.95	6.95	6.95
$R_{JB,target}$ (km)	3.75	3.75	3.75
$\varepsilon_{,target}$	0.94	0.89	0.80
$S_{dtarget}(T_1)$ (cm)	12.38	17.01	34.33

5.6 Comparison of Alternative Selection and Scaling Procedures

The performance of the proposed procedure for MDOF response is investigated by comparing MRDR statistics obtained from the methodologies proposed by Baker (2011) and Kalkan and Chopra (2011).

5.6.1 Assembling of Candidate Ground-Motion Dataset

20 candidate accelerograms are assembled according to the target earthquake scenarios presented in the previous section. Ground-motion recordings from soft and stiff sites with a moment magnitude range of $6.7 \leq M_w \leq 7.2$ are selected. The source-to-site distance range of the candidate accelerograms varies between $0\ km \leq R_{JB} \leq 50\ km$ (The accelerograms are selected from a relatively wide distance interval in order to assemble sufficient number of candidate ground-motion recordings). The overall characteristics of candidate accelerograms are listed in Table 5.6. Among these candidate ground-motion recordings, 10 accelerograms are selected and scaled according to the compared procedures. As the candidate accelerograms are the same for all procedures, their performances are objectively evaluated.

Table 5.6 Major Seismological parameters of the candidate recording set

Record Name	M_w	R_{JB} (km)	Soil Type*	Fault Type**
PEER0289	6.9	13.3	NEHRP C	N
PEER0290	6.9	29.8	NEHRP D	N
PEER0764	6.9	10.3	NEHRP D	SS
PEER0801	6.9	14.2	NEHRP C	SS
PEER0809	6.9	12.2	NEHRP C	SS
PEER0968	6.7	43.2	NEHRP D	RV
PEER0971	6.7	36.2	NEHRP D	RV
PEER1005	6.7	28.8	NEHRP C	RV
PEER1042	6.7	7.9	NEHRP C	RV
PEER1052	6.7	5.3	NEHRP C	RV
PEER1078	6.7	1.7	NEHRP C	RV
PEER1116	6.9	19.1	NEHRP D	SS
PEER1144	7.2	43.3	NEHRP D	SS
PEER1776	7.1	40.4	NEHRP C	SS
PEER1794	7.1	31.1	NEHRP C	SS
PEER1795	7.1	50.0	NEHRP C	SS
TGMB1584	7.1	3.7	NEHRP D	SS
TGMB1585	7.1	0.0	NEHRP C	SS
TGMB1591	7.1	6.1	NEHRP C	SS
TGMB1594	7.1	0.0	NEHRP C	SS

*NEHRP C refers to stiff site (Z2 in Turkish Earthquake Code (TEC, 2007)) whereas NEHRP D refers to soft site (Z3 in Turkish Earthquake Code (TEC, 2007))

**N is normal faulting, RV is reverse faulting and SS is strike-slip faulting

5.6.2 Final Selection and Scaling of Ground Motions

First-mode dominant, regular, low- to mid-rise MRF building structures presented in Section 5.4 are employed to obtain compared MRDR statistics. In the subsequent sections, the proposed procedure is compared with the methodologies proposed by Baker (2011) and Kalkan and Chopra (2011) and its limitations are investigated. The details of the selection and scaling procedure proposed by Baker (2011) are already presented in Chapter 4. Similarly, the fundamental assumptions of the methodology presented by Kalkan and Chopra (2011) are discussed in Chapter 2.

The proposed selection and scaling methodology identifies the records in the optimum ground-motion bin by considering their $\varepsilon\sigma_{ISd}$ value which is a function of R and T_1. The method proposed by Kalkan and Chopra (2011) also requires the estimation of strength reduction factor, R, to scale each record to the target inelastic ordinate in an iterative manner. The strength reduction factors are calculated by normalizing the target elastic spectral ordinate with yield spectral ordinate and they are found from the idealized capacity spectrum. The yield spectral displacement ($S_{d,y}$) and target elastic spectral displacement ($S_{dtarget}(T_1)$) values for each frame are given in Tables 5.4 and 5.5, respectively. Note that the strength reduction factor is 4.4 for 3MRF-BB frame ($R=S_{dtarget}/S_{d,y}$), whereas for 4MRF-DD and 8 MRF-FF frames, the strength reduction factor is 5.1 and 5.3, respectively.

Among 20 candidate ground-motion recordings 10 accelerograms are selected and scaled to the target hazard level. Table 5.7 lists the candidate ground-motion dataset and the recordings selected by each methodology from this candidate ground-motion dataset. The columns labeled as AA show the records selected and scaled by the proposed procedure whereas the columns labeled as B11 and KC11 display the records of Baker (2011) and Kalkan and Chopra (2011), respectively.

Table 5.7 Optimum ground-motion records identified by the selection and scaling procedures compared in this study

	3MRF-BB			4MRF-DD			8MRF-FF		
Record name	AA	B11	KC11	AA	B11	KC11	AA	B11	KC11
PEER0289	X	X	X	X		X	X	X	X
PEER0290	X		X	X	X		X		
PEER0764	X	X	X	X	X	X	X	X	X
PEER0801	X	X		X	X		X		
PEER0809									
PEER0968						X	X		
PEER0971	X	X	X	X			X		
PEER1005		X			X	X		X	X
PEER1042	X			X	X	X	X	X	X
PEER1052	X	X	X	X	X	X	X	X	X
PEER1078								X	
PEER1116		X	X		X	X		X	X
PEER1144	X	X	X	X	X	X			X
PEER1776	X	X	X	X	X	X	X	X	X
PEER1794		X	X		X	X		X	X
PEER1795	X			X			X		X
TGMB1584			X						
TGMB1585									
TGMB1591								X	
TGMB1594									

5.6.3 Comparisons of Results

Nonlinear SDOF analyses and MDOF RHA are performed by using the optimum ground-motion records selected and scaled according to the compared methodologies. Figure 5.12 summarizes the results of these analyses. The first column panels describe the elastic median and dispersion statistics computed from SDOF analyses as well as the target elastic hazard. Although the elastic response is not the real focus of the case studies presented here, the first column panels serve for giving a complete picture about the performance of each model in a broader sense. As noted previously the state-of-the-art hazard analysis almost always tends to give the elastic target hazard for ground-motion scaling purposes.

The second column panels of Figure 5.12 show the median spectral displacement values and corresponding dispersion computed from the nonlinear SDOF response analyses of the idealized structural systems (see Figure 5.8, 5.9 and 5.10 about the idealized SDOF behavior of each model). The third column panels of the same figure display the maximum roof drift ratio statistics computed from the nonlinear RHA of the subject model buildings. The solid squares in Figure 5.12 indicate the median response whereas the error bars show the ± one standard deviation about the median. The gray crosses show the structural response subjected to each scaled record. Although the proposed procedure can also estimate the median and standard deviation for each case (Equations 4.2 and 4.3), these values are not given on the plots as the compared methods do not have such a feature. The advantage of estimating the median and standard deviation of scaled ground motions by the proposed procedure is discussed in the next section.

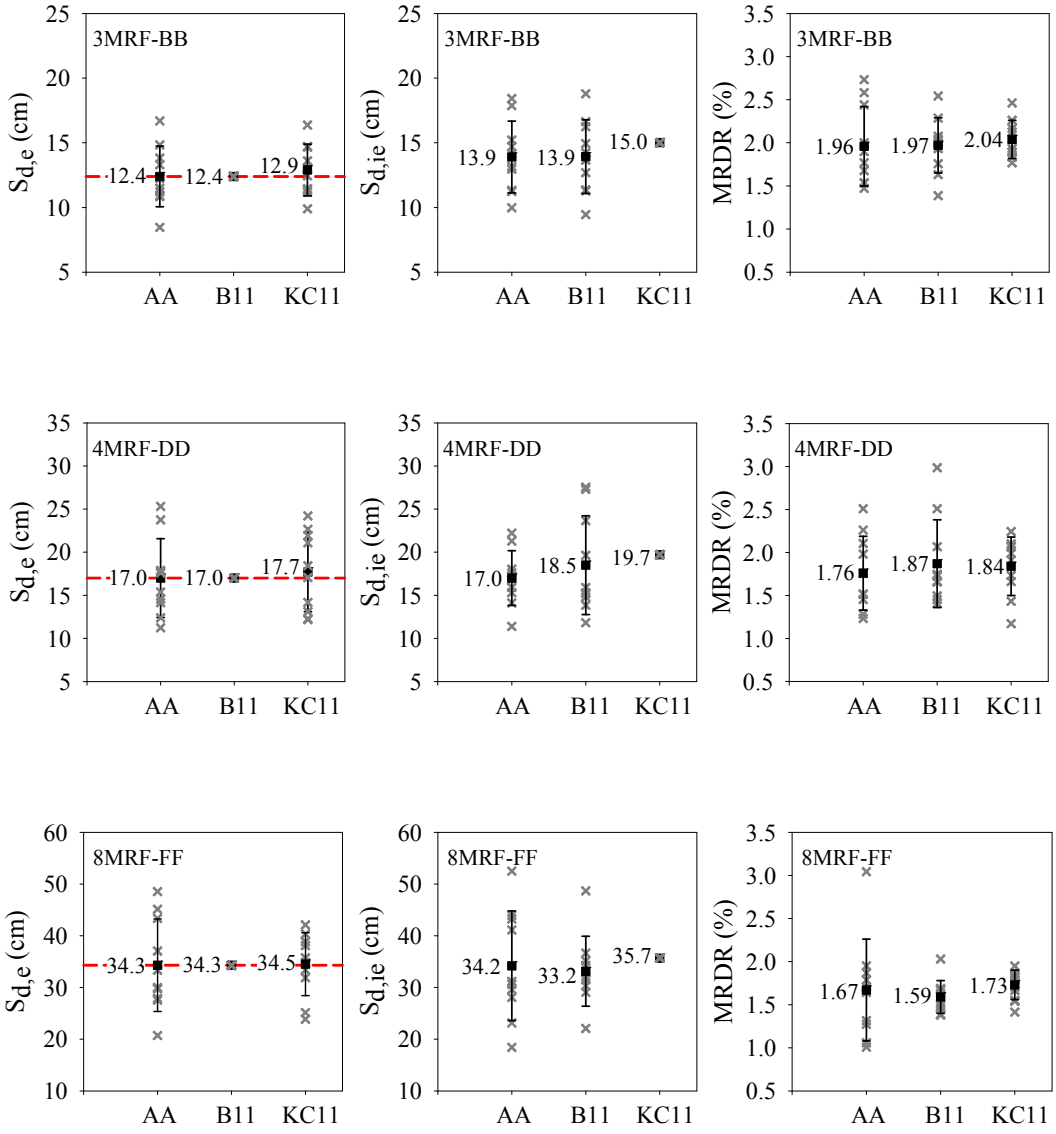

Figure 5.12 Comparisons of linear (first column), nonlinear (second column) SDOF response and MDOF RHA (third column) results obtained from alternative record selection and scaling procedures

The nonlinear SDOF response results presented in the second column panels of Figure 5.12 show that in terms of median nonlinear spectral response, all three selection and scaling procedures yield fairly similar results. Among these, Kalkan and Chopra (2011) (KC11) results in slightly larger median structural response. Note that the procedure presented in this study (AA) and the method proposed by Baker (2011) (B11) scale the records such that the average elastic spectral ordinates of the modified records exactly match with the target elastic spectral level (see first column panels of Figure 5.12). KC11 iteratively scales the records to the inelastic target found by modifying the elastic target ordinate with an empirical equation for a given strength reduction factor and hysteretic model. Thus the average elastic spectral response of the records selected and scaled according to the KC11 method does not necessarily match with the target elastic spectral ordinate (see first column panels of Figure 5.12), which brings forward the significance of the empirical prediction equation used to obtain the inelastic target level. In this study, the empirical equation proposed by Chopra and Chintanapakdee (2004) is used to obtain the target inelastic spectral displacement. In their report, Kalkan and Chopra (2010) quantify the overestimation of inelastic SDOF response through the use of the empirical equation proposed by Chopra and Chintanapakdee (2004) as 1%-8% for building structures and 12%-14% for bridges. The empirical equation proposed by Chopra and Chintanapakdee (2004) (CC04 hereafter) is already presented in Chapter 2. In subsequent paragraphs, the KC11 method is re-evaluated by using alternative empirical equations of elastic-to-inelastic SDOF behavior.

In terms of dispersion about the median nonlinear SDOF response, the presented procedure yields slightly smaller standard deviation statistics with respect to B11 for relatively smaller vibration periods ($T_1 < 0.9$ s). As the period increases ($T_1 \geq 0.9$ s), the efficiency of $\varepsilon\sigma_{lnSd}$ reduces and the proposed method yields higher dispersion statistics with respect to B11. Due to its underlying theory, the dispersion is zero in KC11 for nonlinear spectral response because it scales the

accelerograms to yield the same inelastic target response displacement (i.e., zero dispersion).

The RHA results presented on the third column panels of Figure 5.12 follow similar trends as of nonlinear SDOF response statistics. The RHA results indicate that the compared selection and scaling methodologies result in similar median MRDR values. Among the compared methodologies, the minimum dispersion is achieved by the KC11 method for all three buildings. Thus the dispersion about median structural response statistics presented in Figure 5.12 may suggest the superiority of the KC11 method with respect to the others. However, the dependency of the KC11 procedure on the used empirical equation for relating the elastic target spectrum to the inelastic target can be a shortcoming of this methodology. This intermediate step can introduce an additional uncertainty to the structural response statistics that is associated with the estimation of inelastic target spectral response. Moreover, KC11 selects the scaled records of which elastic spectral response best match with the target spectrum at the second mode period of the structural system (see Chapter 2 for details of KC11 method). Consequently, the elastic second-mode response that is one of the major assumptions of this approach can also reduce its efficiency for structural systems dominated by higher mode effects.

The possible shortcoming of KC11 on the use of alternative empirical elastic-to-inelastic spectral displacement conversion equations is investigated further. Two alternative equations for such conversions proposed by Ruiz-García and Miranda (2003 and 2007) are used to see the sensitivity of the obtained SDOF and MDOF response results upon the implementation of KC11. Table 5.8 lists the target inelastic spectral displacement ($S_{d,ie\ target}$) of the 3-, 4- and 8-story frame models for the given elastic target spectral displacement ($S_{dtarget}$) and strength reduction factor.

Table 5.8 Target elastic spectral displacement ($S_{d,target}$) and corresponding inelastic target spectral displacement ($S_{d,ie\ target}$) of alternative empirical equations

	3MRF-BB	4MRF-DD	8MRF-FF
$S_{dtarget}(T_1)$	12.4 cm	17.0 cm	34.3 cm
$S_{d,ie\ target}(T_1)$ according to Chopra and Chintanapakdee (2004)	15.0 cm	19.7 cm	35.7 cm
$S_{d,ie\ target}(T_1)$ according to Ruiz-García and Miranda (2003)	14.6 cm	19.2 cm	34.2 cm
$S_{d,ie\ target}(T_1)$ according to Ruiz-García and Miranda (2007)	15.5 cm	20.6 cm	36.8 cm

Figure 5.13 presents the median MRDR values and corresponding dispersions computed from the nonlinear RHA by using scaled accelerograms according to the AA method, B11 and KC11 associated with three alternative empirical equations. The abbreviations RM03 and RM07 that are used together with KC11 denote the empirical elastic-to-inelastic spectral conversion equations of Ruiz-García and Miranda (2003 and 2007), respectively.

Figure 5.13 depicts that the median response and corresponding dispersion obtained by the records selected and scaled according to the KC11 method is sensitive to the selected empirical elastic-to-inelastic conversion equation. The differences between median nonlinear structural responses obtained by the use of three alternative empirical conversion equations are about 8%. This observation may indicate that the accuracy of KC11 scaling method is limited to the performance of this intermediate tool that is used to obtain the inelastic target from elastic target. This is partially addressed by Kalkan and Chopra (2010) as indicated in the previous paragraphs. Essentially, although KC11 yields relatively smaller dispersion with respect to the other selection and scaling procedures (i.e., AA and B11 in Figure 5.13), the choice of the empirical conversion equation (CC04, RM03 or RM07) introduces an additional uncertainty to the response, which affects the results of this procedure.

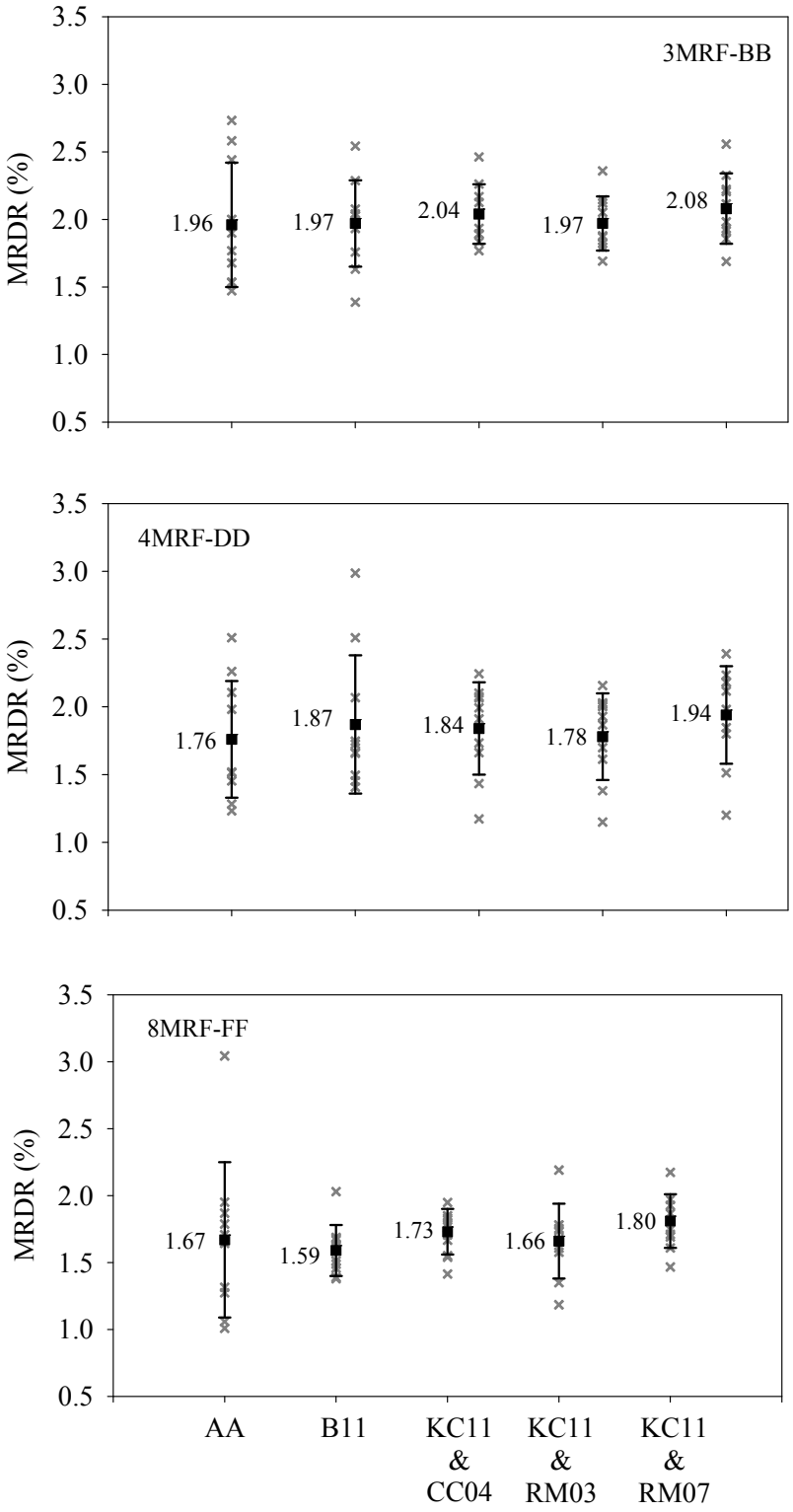

Figure 5.13 Nonlinear RHA results obtained from the compared scaling procedures and alternative empirical inelastic to elastic spectral displacement ratios

In summary, the presented dispersion statistics obtained by the proposed procedure (AA) and B11 method are fairly similar for 3MRF-BB and 4MRF-DD frames. Thus the performance of the proposed methodology suggests an acceptable level of accuracy in RHA results of first-mode dominant MDOF systems. As the fundamental period of the structure increases, the proposed procedure results in relatively higher dispersion about median. It should be noted that the resulting scatter mainly originates from the inherent record-to-record variability that is intentionally preserved by the proposed procedure. This dispersion is approximately parameterized by the proposed procedure, which is useful for probabilistic structural performance assessment (discussed in the following section). The other methodologies compared in this study artificially eliminate the dispersion about median structural response by scaling each record to a common spectral ordinate either in elastic domain (B11) or inelastic domain (KC11). Note that for structural periods where equal displacement rule applies (Veletsos and Newmark, 1960) the selection and scaling procedure of B11 would yield almost zero dispersion for nonlinear SDOF response as target elastic and inelastic spectral ordinates will approximately the same.

5.7 Vulnerability Assessment for a Given Target Scenario

The selection and scaling methodology proposed in this study can estimate the distribution of structural response parameters of interest through the expressions given in Equation 4.2 and Equation 4.3, respectively. This section investigates the practicality of these estimations that convey useful information for probability-based rapid seismic performance assessment. The already presented structural models, target earthquake scenarios and RHA results of MDOF systems are employed to derive the damage probabilities obtained from the probability distribution parameters computed from Equations 4.2 and 4.3 (proposed procedure). These damage probabilities are then compared with those obtained through the use of the actual variation of response statistics (The actual variation

of response statistics are computed from the alternative selection and scaling methods as well as the proposed procedure. The alternative methods are B11 and KC11).

5.7.1 Assigning the Limit States

Given a target intensity measure (e.g., $S_{dtarget}$ as in this study) the damage probability assessment studies require the determination of the exceedance probability of a structural response measure (e.g., MRDR as in this study) at a certain limit state (LS). Exceedance probabilities for different target hazard levels result in fragility functions (Equation 5.1) that can be used in probabilistic loss models.

$$\text{Fragility} = P\left(\text{MRDR} \geq \text{LS} \middle| S_{dt\,\arg et}\right) \tag{5.1}$$

In order to see the performance of the proposed procedure as a tool in damage probability assessment three limit state definitions for RC MRF models are used. The limit states are defined as immediate occupancy (IO), life safety (LS), and collapse prevention (CP). It is assumed that structures having no or slight damage perform at IO limit state whereas structures at LS and CP limit states are assumed to sustain significant and severe damage, respectively. The structures are assumed to collapse beyond CP limit state. In essence, four damage states can be defined as no or slight damage (DS1), significant damage (DS2), severe damage (DS3), and collapse (DS4). Figure 5.14 is an example plot that displays the limit states and corresponding damage levels on the pushover curve of 4MRF-DD model.

The limit state values of RC MRF structures are investigated previously by several publications. These studies reveal that the limit state determination for RC MRF buildings involves a significant uncertainty (Ay and Erberik, 2008).

Following the recommendations of Ay and Erberik (2008), three criteria are employed to specify the structural performance levels. These are the accumulation of damage in structural members, the softening index (SI) which is introduced by Dispasquale and Çakmak (1987) and the ductility level (Calvi, 1999) of the structure. Detailed information about the criteria employed in the specification of limit states can be found in Ay and Erberik (2008).

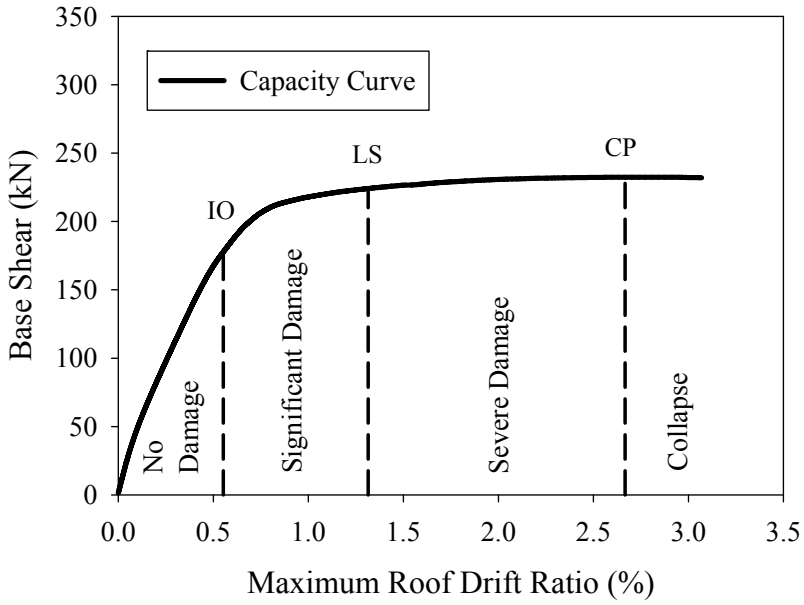

Figure 5.14 Limit states and corresponding damage level definitions

The performance limits are specified in accordance with the criteria stated in previous paragraph and then they are converted to the MRDR values (in %) for each limit state. The details of these calculations are not given in this dissertation as the actual focus is to evaluate the performance of the proposed selection and scaling procedure as a tool for probabilistic damage assessment. Table 5.9 lists the MRDR values (in %) associated with the immediate occupancy (IO), life safety (LS) and collapse prevention (CP) performance levels for 3MRF-BB, 4MRF-DD and 8MRF-FF frame model analyzed in this study. Note that Figure 5.14 shows the MRDR (%) values assigned to the limit states specific to 4MRF-DD.

Table 5.9 Maximum Roof Drift Ratios (%) to describe IO, LS and CP structural limit states

Model Frame Name	Maximum Roof Drift Ratio (%)		
	Immediate Occupancy	Life Safety	Collapse Prevention
3MRF-BB	0.62	1.47	2.87
4MRF-DD	0.55	1.32	2.82
8MRF-FF	0.45	0.96	2.02

5.7.2 Comparisons of Results

RHA results of frame models with the records selected and scaled according to the compared methodologies are presented in previous section. One of the major advantages of the proposed methodology (as a candidate tool for probabilistic damage assessment) is its ability to estimate the distribution parameters of the nonlinear structural response without performing detailed nonlinear RHA of MDOF systems. Assuming the structural response (chosen as MRDR in this study) distribution is log-normal, the distribution parameters (median and logarithmic standard deviation) can be estimated for the given target spectral displacement value from Equations 4.2 and 4.3. This information can be employed to calculate the damage state probabilities (vulnerability data) through Equations 5.2-5.5. The computed results from these equations are used to test the performance of this ability in the proposed procedure.

$$DS1 = P\left(MRDR \le IO \middle| S_{dt\,arg\,et}\right) \tag{5.2}$$

$$DS2 = P\left(IO \le MRDR \le LS \middle| S_{dt\,arg\,et}\right) \tag{5.3}$$

$$DS3 = P\left(LS \le MRDR \le CP \middle| S_{dt\,arg\,et}\right) \tag{5.4}$$

$$DS4 = P\left(CP \le MRDR \middle| S_{dt\,arg\,et}\right) \tag{5.5}$$

Note that Equations 4.2 and 4.3 compute the median and logarithmic standard deviation of scaled inelastic spectral displacements for obtaining their probability distributions at a certain elastic target hazard level. Thus an intermediate step is required to adjust the SDOF information (inelastic spectral displacement distribution) to MDOF response (MRDR distribution).

The ADRS (Mahaney et al., 1993) constitutes the backbone of the intermediate step. The limit states defined in Table 5.9 are modified to SDOF response quantities through ADRS and they are used together with the computed median and logarithmic standard deviation values (i.e., probability distributions per Equations 4.2 and 4.3) to estimate the damage state probabilities. Figure 5.15 compares the damage state probabilities estimated from the proposed procedure (following the above scheme) and those computed from the MDOF RHA results of the other two selection and scaling procedures (B11 and KC11). The figure above presents the nonlinear RHA-based damage state probabilities of the proposed procedure for completeness.

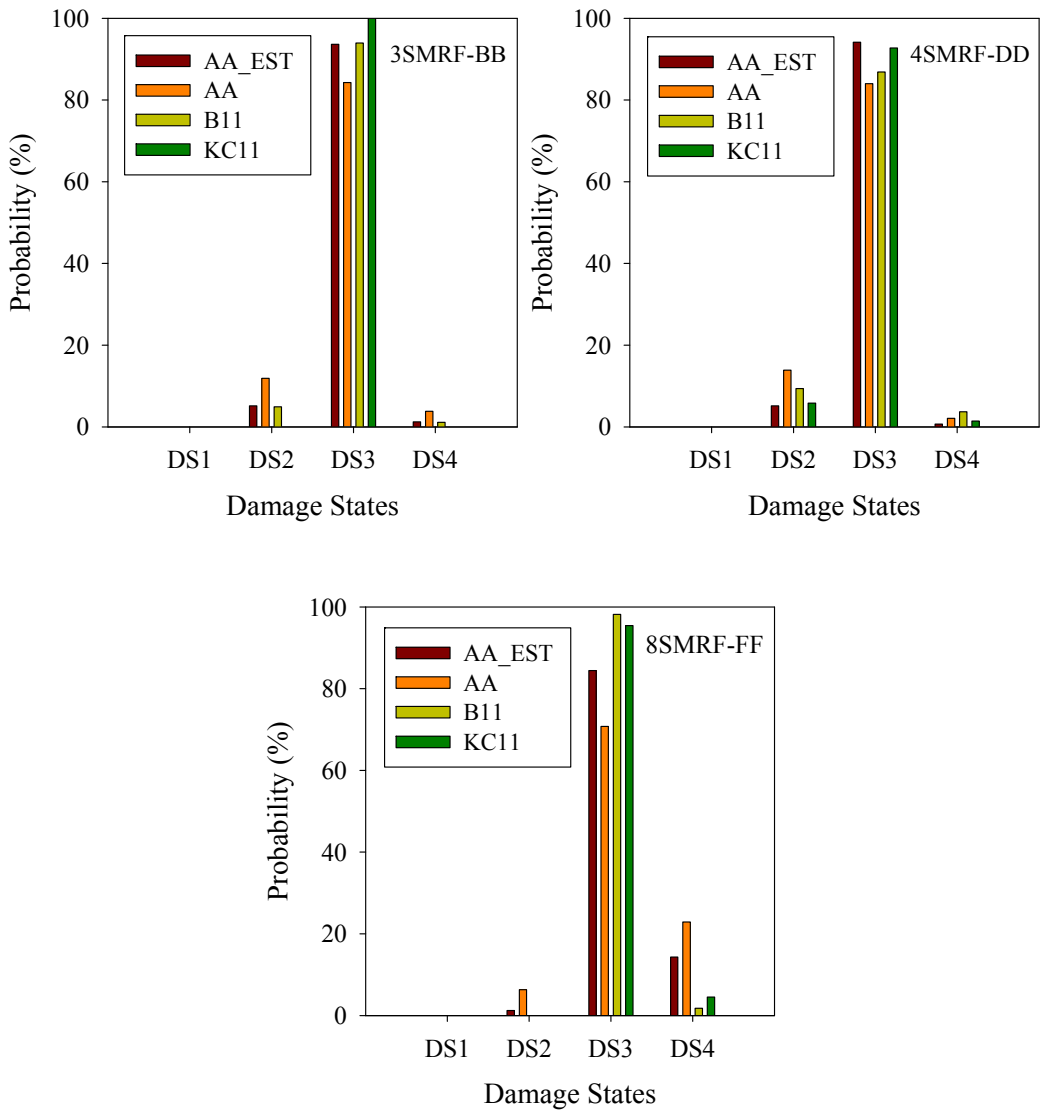

Figure 5.15 Damage state probabilities obtained by the compared methodologies. AA_EST is the approximation from Equations 4.2 and 4.3 by following the procedure described in page 118. AA refers to the damage probabilities obtained from the nonlinear MDOF RHA of the scaled ground motions using the proposed record selection and scaling method. B11 and KC11 represent the probabilities computed form the nonlinear MDOF RHA results of the scaled records that are determined from the other two selection and scaling procedures.

The results presented in Figure 5.15 show that the maximum difference between damage state probabilities obtained by the estimations of the proposed procedure and the observed data is less than 10 % for almost all cases. Only for 8MRF-FF structure, the difference in damage probabilities reaches to a value of 13 %. Considering the computation time and uncertainties involved in the nonlinear RHA of structures, these differences can be accepted as tolerable. Moreover, the estimated damage state probabilities (AA_EST) are calculated from the approximate distributions that are provided to the analyst through simple calculations (Equations 4.2 and 4.3) and manipulations (ADRS conversion) under a given elastic spectral target value, fundamental period and the strength reduction factor. For other cases (AA, B11 and KC11), the damage state probabilities can only be calculated by response distribution parameters that are found by running nonlinear RHA of the frame models. This eventually means a significant computational effort. The other important remark from these comparative plots is the closeness of AA and AA_EST damage probabilities indicating the success of Equations 4.2 and 4.3 in imitating the actual response distribution of scaled ground motions from the proposed procedure. These observations advocate that the performance of the proposed procedure is fairly sufficient for rapid probabilistic building performance assessment and loss studies.

CHAPTER 6

SELECTING AND SCALING GROUND MOTIONS FOR A TARGET RESPONSE SPECTRUM AND VARIANCE

6.1 Introduction

A ground-motion recording set selected and scaled to match a pre-defined target response spectrum and variance within a period interval may be required in some performance-based earthquake engineering applications. Besides structure-specific ground-motion record selection and scaling procedures may not be proper for loss assessment studies conducted for large building stocks that are distributed over a broad region. In such large scale studies, the constraints can force the analyst to select and scale a ground-motion recording set without having specific information about particular features of each building or even a site-specific hazard.

There are various studies that recommend ground-motion record selection and scaling methodologies for matching either only with a target response spectrum or with the target response spectrum and its associated variance (e.g., Kottke and Rathje, 2008; Baker et al., 2011; Jayaram et al., 2011). The major aim of these studies is to develop an efficient and accurate ground-motion record selection algorithm. The objective of this chapter is not to introduce an alternative selection algorithm. This chapter aims to investigate the applicability of the proposed selection and scaling procedure for matching with a target median response spectrum and corresponding variance.

The selection and scaling procedure presented in Chapter 3 (and its improved version for nonlinear response in Chapter 4) ensures the match between average spectral ordinate of scaled accelerograms and target intensity level at the predefined period value. However, it does not guarantee a close match with the median target spectrum or its associated variance in the period range of interest. This chapter first illustrates the cases in which the direct record scaling to match the target response spectrum would be irrational. The latter parts of the chapter introduce a new parameter to be used in the proposed selection and scaling procedure for cases where target response spectrum and variance matching is desired over the pre-defined period range. At the end of this chapter, the performance of this new procedure is investigated and corresponding limitations are discussed.

6.2 A Discussion on the Target Spectrum and its Variance

The verification of seismic performance of structural systems under a set of ground-motion records that are scaled for a target response spectrum has become common in many earthquake codes. In general, the target spectrum is described either as the uniform hazard spectrum (UHS), the smoothed envelope of uniform hazard spectrum or structure-specific target spectrum derived from the deaggregation of UHS. As stated in various parts of this dissertation (e.g., Section 2.2.2), Baker (2011) suggested using the conditional mean spectrum (CMS) instead of UHS for the scaling of ground motions for a given target earthquake scenario. The major reason behind this recommendation is the unrealistic representation of earthquake demands by UHS for the particular structural system being verified under the target earthquake scenario. CMS simply considers the effects of epsilon (logarithmic deviation from the expected spectral ordinate) on the target response spectral shape (Gülerce and Abrahamson, 2011). Figure 6.1 compares the UHS computed for a return period

of T_R=2475 years (i.e., 2% probability of exceedance in 50 years exposure time) and corresponding CMS derived for a fundamental period of T_1=0.61 seconds. This case refers to the 4MRF-DD model that is discussed in the previous chapter.

It should also be noted that several other studies (e.g., Bommer et al., 2000; Naeim and Lew, 1995) did not favor the match of ground-motion records with the UHS to verify the seismic performance of a specific structure. Their major assertion against UHS is the inherent pooling of large and small size earthquakes by UHS within different period ranges of the entire spectral band that may be unsuitable to describe the genuine seismic demands for the structural system under consideration. This reasoning is similar, in some perspective, to the one put forward by Baker (2011) while proposing CMS instead of UHS. Essentially, such previous studies recommended the ground-motion scaling through the use of target spectrum derived from the deaggregation of UHS that accounts for the particular features of the considered structural system.

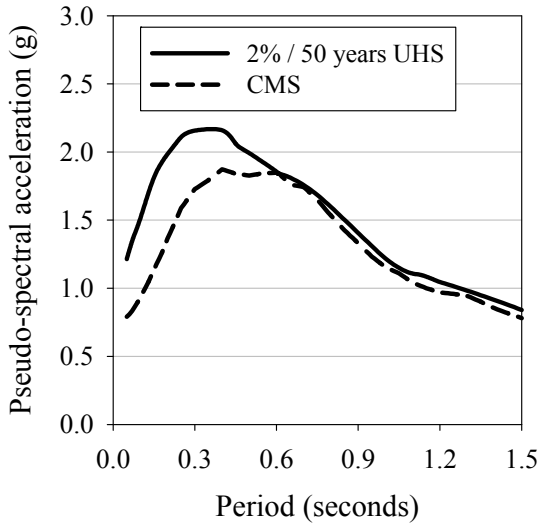

Figure 6.1 The 2475 years UHS and CMS (Baker, 2011) for a given fundamental period value of 0.61 seconds

Whether the analyst considers CMS or the target spectrum after deaggregation, these spectra associate non-zero variance for the spectral period band of interest. Jayaram et al. (2011) indicated that the response statistics of the considered structure will not represent its realistic probabilistic behavior if the analyst uses ground motions that are scaled to such target spectra without considering their associated variance. Figure 6.2 illustrates this fact by a simple example. The black curves on this figure describe the target CMS and corresponding conditional standard deviation for a period interval of $0.2\ T_1 \leq T \leq 2.0\ T_1$. The red solid line represents the observed average spectrum of records selected and scaled by considering only the target CMS (black solid curve). Consequently, the suppressed standard deviation (represented by dotted red lines) of scaled ground-motion set is smaller than the essential standard deviation associated with the target CMS (dotted black lines).

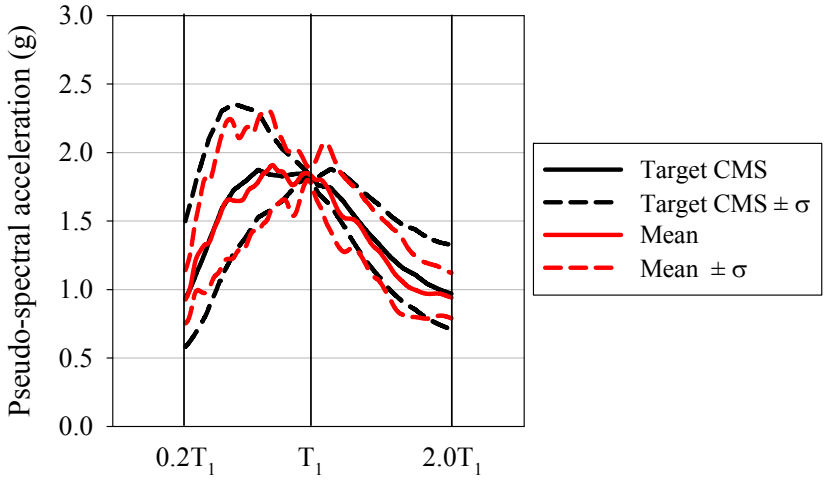

Figure 6.2 Target CMS, associated standard deviation, observed mean and observed standard deviation of the records selected and scaled to match the CMS

For a given period interval from T_i to T_n, the target CMS and corresponding standard deviation can be found by using Equation 6.1 and Equation 6.2, respectively. In these equations, T_1 is the fundamental period of the investigated structure, $\ln \overline{S_d}$ and $\sigma_{\ln \overline{S_d}}$ are the logarithmic spectral displacement prediction

and corresponding standard deviation of the GMPE. $\rho(T_i,T_1)$ is the correlation coefficient that can be given together with the used GMPE or found through empirical equations given in literature (e.g., Baker and Cornell, 2006b).

$$\mu_{target} = \begin{bmatrix} \ln \overline{S_d}(T_i) + \rho(T_i, T_1)\varepsilon(T_1)\sigma_{\ln \overline{S_d}(T_i)} \\ \ln \overline{S_d}(T_{i+1}) + \rho(T_{i+1}, T_1)\varepsilon(T_1)\sigma_{\ln \overline{S_d}(T_{i+1})} \\ \vdots \\ \ln \overline{S_d}(T_n) + \rho(T_n, T_1)\varepsilon(T_1)\sigma_{\ln \overline{S_d}(T_n)} \end{bmatrix} \quad (6.1)$$

$$\sigma_{target} = \begin{bmatrix} \sigma_{\ln \overline{S_d}(T_i)}\sqrt{1-\rho(T_i, T_1)} \\ \sigma_{\ln \overline{S_d}(T_{i+1})}\sqrt{1-\rho(T_{i+1}, T_1)} \\ \vdots \\ \sigma_{\ln \overline{S_d}(T_n)}\sqrt{1-\rho(T_n, T_1)} \end{bmatrix} \quad (6.2)$$

Another particular case that requires the scaling of ground-motions to match with a non-zero variance target spectrum is the damage assessment or loss estimation studies of building stocks (not a specific structure) located in large urban districts. For such projects, a generalized response spectrum and its associated variance should be utilized in order to define the genuine structural response statistics of the concerned building stock due to ground-motion variability. Such a generalized target response spectrum can be derived from a generic earthquake scenario (Jayaram and Baker, 2010). For example, Yakut et al. (2012) perform a seismic risk prioritization study for buildings located in İstanbul by considering a deterministic future earthquake scenario. The deterministic scenario is based on the unruptured Marmara segment of the strike-slip North Anatolian Fault that is located approximately 15 km from the southern part of İstanbul. The magnitude of the deterministic earthquake is taken as M_w=7.5.

Inspiring from the context of the Yakut et al. (2012) study, but making some simplifications, the deterministic earthquake scenario presented above (i.e., M_w=7.5, R_{JB}=15 km, style-of-faulting: strike-slip) is used to illustrate the development of a generalized target response spectrum and corresponding variance. The majority of buildings are assumed to be located on soft soil sites (180 m/s < V_{S30} ≤ 360 m/s, NEHRP D). The sample building class is selected as low-rise RC MRF structures (3-5 story buildings) with a variation of their fundamental periods between 0.3 s ≤ T_1 ≤ 0.7 s. The variation of fundamental period is computed from the empirical relationships of Goel and Chopra (1997) that are functions of total building height. These relationships are derived from the buildings located in California and may not be 100 % applicable to the buildings in Turkey. However, they are sufficient for the discussions presented in this section. Considering the contribution of higher-modes and period elongation in nonlinear response, a target response spectrum defined within a period interval of 0.1 seconds to 1.2 seconds is assumed to be suitable for the verification of low-rise buildings. The seismological parameters of the deterministic scenario earthquake and Akkar and Bommer (2010) GMPE, that is a representative model of the seismicity in the region, are employed to obtain the generalized target response spectrum and variance. Equation 6.3 should be utilized to calculate the target mean logarithmic response spectrum vector whereas the corresponding covariance matrix can be found by using Equation 6.4. The required parameters for constructing the covariance matrix is the correlation coefficient, $\rho(T_i,T_1)$ and the standard deviation of the predictions, $\sigma_{\ln S_d}$. Akkar and Bommer (2010) GMPE provides only the latter parameter. Thus $\rho(T_i,T_1)$ is established by using the empirical equation given in Baker and Cornell (2006b). Further details of the parameterization of target response spectrum distribution can be found in Jayaram and Baker (2010).

$$\mu_{target} = \begin{bmatrix} \ln \overline{S_d}(T_i) \\ \ln \overline{S_d}(T_{i+1}) \\ \vdots \\ \ln \overline{S_d}(T_n) \end{bmatrix} \tag{6.3}$$

$$\Sigma = \begin{bmatrix} \sigma(T_i)^2 & \rho(T_i, T_{i+1})\sigma(T_i)\sigma(T_{i+1}) & \cdots & \rho(T_i, T_n)\sigma(T_i)\sigma(T_n) \\ \rho(T_{i+1}, T_i)\sigma(T_{i+1})\sigma(T_i) & \sigma(T_{i+1})^2 & \cdots & \rho(T_{i+1}, T_n)\sigma(T_{i+1})\sigma(T_n) \\ \vdots & \vdots & \vdots & \vdots \\ \rho(T_n, T_i)\sigma(T_n)\sigma(T_i) & \rho(T_n, T_{i+1})\sigma(T_n)\sigma(T_{i+1}) & \cdots & \sigma(T_n)^2 \end{bmatrix} \tag{6.4}$$

Figure 6.3 displays the target displacement spectrum and corresponding standard deviation for a period interval from 0.1 seconds to 1.2 seconds. Scaling of ground motions by considering this non-zero variance spectrum would reflect the actual variation of building response due to the ground motion variability of the scenario earthquake.

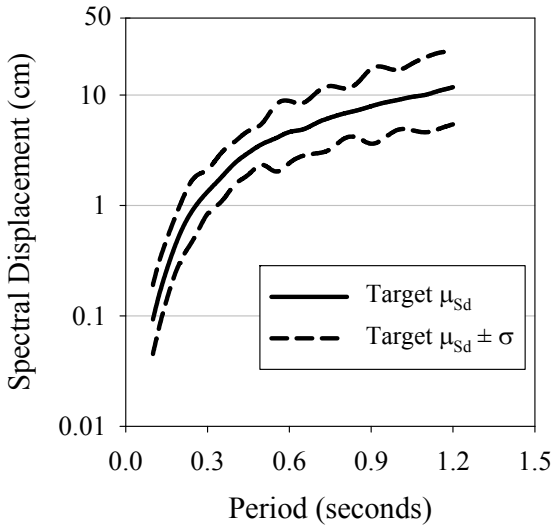

Figure 6.3 Target median displacement spectrum and corresponding variance that are associated with the deterministic earthquake scenario

It should be noted that for cases where UHS, an example of zero-variance spectrum, is employed as the target, ground-motion records should be selected and scaled by considering only the target mean which, inherently, accounts for the variability in spectral ordinates.

Proposing a proper target response spectrum (e.g., CMS) and corresponding variance that are suitable for verification of structural systems is out of scope of this dissertation. This chapter merely investigates the applicability of the proposed selection and scaling procedure to match a target elastic response spectrum and its associated variance. The subsequent parts of this chapter initially introduce the improved selection and scaling procedure for matching a target spectrum and then investigate its performance to achieve a satisfactory fit.

6.3 Selection and Scaling for Matching a Target Response Spectrum

Chapter 3 presents the record scaling procedure for linear systems that constraints the modification of the records to the estimations of a predictive model for a spectral value at a given vibration period. The same chapter also describes the selection of the optimum ground motion bin that yields the minimum dispersion about this median elastic spectral ordinate. This chapter modifies this selection and scaling procedure by introducing a new parameter, Γ, for matching the median response spectrum of scaled records to a pre-defined target response spectrum. The parameter Γ is analogous with $\varepsilon\sigma$ that is defined as the logarithmic difference between the observed spectral ordinate of the unscaled record and corresponding median estimation obtained from a representative GMPE at the fundamental period of structure (see Equation 3.1). The major difference between $\varepsilon\sigma$ and the new parameter Γ is that $\varepsilon\sigma$ is defined for a certain vibration period, whereas Γ is defined for a predetermined period interval. Equation 6.5 describes the calculation of Γ_{Sd} for a given period range. In Equation 6.5, $S_d(T)$ is the

spectral displacement of an unscaled record and ($\bar{S}_d(T^*)$) is the corresponding median estimation from a representative GMPE at the given period value of T*. The period T* should be taken as the fundamental period if a specific structure is of concern or it is the median value of the predetermined period interval if a ground motion bin that is compatible with a generalized target response spectrum is desired.

$$\Gamma_{Sd}(T) = \ln\left(S_d(T)\right) - \ln\left(\bar{S}_d(T^*)\right) \tag{6.5}$$

The new selection and scaling approach specifically replaces the parameter $\varepsilon\sigma_{Sd}$ with the new parameter Γ_{Sd}. The scaling origin and scaling factor for each record is computed by using Equation 6.6 and Equation 6.7, respectively. For a given target response spectrum, $\bar{S}_{dtarget}(T^*)$ is the corresponding spectral displacement at the period value of T*.

$$\theta = \ln\left(\bar{S}_{dt\,arg\,et}(T^*)\right) - \ln\left(\frac{\sum_{i=1}^{n} \exp\left(\Gamma_{Sd,i}(T^*)\right)}{n}\right) \tag{6.6}$$

$$\gamma = \frac{\exp\left(\theta + \Gamma_{Sd}(T^*)\right)}{S_d(T^*)} \tag{6.7}$$

Assuming that the structural response is log-normally distributed, Equation 6.8 and Equation 6.9 give the median logarithmic spectral displacement of scaled records and corresponding standard deviation, respectively. More specifically, these equations prescribe the parameters of the target response spectrum distribution of scaled records. This information can be employed to quantify the match between target response spectrum and corresponding variance.

$$\mu_{\ln S_d}(T) = \theta + \frac{\sum_{i=1}^{n} \Gamma_{Sd,i}(T)}{n} = \theta + \mu_{\Gamma_{Sd}(T)} \tag{6.8}$$

$$\sigma_{\ln S_d}(T) = \sqrt{\frac{1}{n-1} \cdot \sum_{i=1}^{n} \left(\Gamma_{Sd,i}(T) - \mu_{\Gamma_{Sd}(T)} \right)^2} \tag{6.9}$$

The goodness of fit between observed scaled spectrum and target response spectrum can be measured by using sum-of-squared errors (SSE) or root-mean-square difference (RMSD). In this study, SSE is used to quantify the match between the target and observed spectra. Equation 6.10 measures the match between target and observed response spectra whereas Equation 6.11 calculates the goodness of fit with a target response spectrum and corresponding variance. In Equation 6.11, the parameter w is used to adjust the relative importance of the difference in the observed and target mean and standard deviation values (Jayaram et al., 2011). A larger value assigned to w brings forward the significance of standard deviation during the selection and scaling of ground motions.

$$SSE_{\mu} = \sum_{i=1}^{n} \left(\mu_{\ln S_d(T_i)} - \mu_{target} \right)^2 \tag{6.10}$$

$$SSE_{\mu,\sigma} = \sum_{i=1}^{n} \left[\left(\mu_{\ln S_d(T_i)} - \mu_{target} \right)^2 + w \left(\sigma_{\ln S_d(T_i)} - \sigma_{target} \right)^2 \right] \tag{6.11}$$

The ground motion set that yields the minimum SSE score among alternative recording bins is selected as the optimum ground-motion recording bin. Note that $\mu_{\ln S_d(T_i)}$ and $\sigma_{\ln S_d(T_i)}$ are prescribed by the proposed procedure through theoretical expressions which significantly increases the computational efficiency of the overall procedure.

6.4 Evaluation of the Target Response Spectrum Matching Procedure

The background theory of the proposed procedure to match the median spectral response and corresponding standard deviation for a given period interval is formulated in the previous paragraphs. This section evaluates the proposed selection and scaling procedure by observing its limitations in matching a target displacement spectrum and variance.

The generalized displacement spectrum presented in Figure 6.3 is used to test the performance of the proposed selection and scaling procedure. According to the deterministic earthquake scenario described in the previous section, candidate ground-motion recordings from soft and stiff sites with a moment magnitude range of 7.1 to 7.6 are selected. The seismological parameters of the candidate records are tabulated in Table 6.1.

Two different sets of records are selected and scaled in order to match either only with the target response spectrum (μ-Fit) or with the target response spectrum and corresponding variance together (μ±σ-Fit). The match between the target and observed ground motions is compared for a period interval from T = 0.1 seconds to T = 1.2 seconds. The scaling factors of each selected record in ground-motion recording bin are listed in the last two columns of Table 6.1 after applying Equations 6.5 to 6.7.

Table 6.1 Seismological parameters of the candidate recording set. The scaling factors of the selected records to achieve either μ-Fit or μ±σ-Fit are tabulated in last two columns of the table, respectively.

Record Name	M_w	R_{JB} (km)	Soil Type	Fault Type	γ_i μ-Fit	γ_i μ±σ-Fit
PEER0014	7.4	81.3	NEHRP C	RV		5.500
PEER0015	7.4	38.4	NEHRP C	RV		
PEER0138	7.4	24.1	NEHRP D	RV	1.978	
PEER0139	7.4	0.0	NEHRP C	RV	0.719	0.556
PEER0140	7.4	89.8	NEHRP D	RV		
PEER0848	7.3	19.7	NEHRP D	SS		
PEER0855	7.3	63.0	NEHRP D	SS		
PEER0864	7.3	11.0	NEHRP C	SS		
PEER0880	7.3	27.0	NEHRP D	SS		
PEER1196	7.6	42.0	NEHRP D	RV	2.903	2.244
PEER1532	7.6	17.2	NEHRP C	RV	1.972	
PEER1578	7.6	67.4	NEHRP C	RV	5.765	4.456
PEER1628	7.5	26.5	NEHRP D	RV	2.041	1.577
PEER1633	7.4	12.6	NEHRP C	SS		
PEER1636	7.4	50.0	NEHRP D	SS	3.933	3.040
PEER1640	7.4	93.3	NEHRP D	SS		
PEER1783	7.1	65.0	NEHRP D	SS		4.328
TGMB1102	7.6	54.6	NEHRP C	SS	5.473	4.231
TGMB1106	7.6	10.1	NEHRP C	SS	1.536	1.187
TGMB1108	7.6	49.3	NEHRP C	SS	5.045	3.900

Figure 6.4 compares the target displacement spectrum with the observed median displacement spectrum of selected and scaled records according to the proposed procedure.

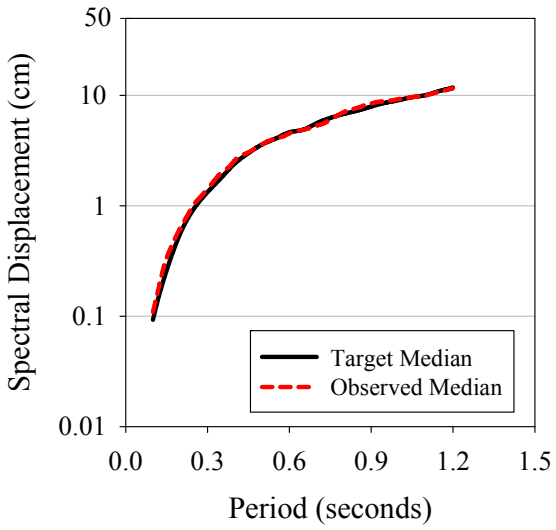

Figure 6.4 Target median displacement spectrum and observed median displacement spectrum of the ground motion bin selected and scaled according to the proposed procedure

The SSE_{μ} measure given in Equation 6.10 is used to quantify the match between the observed and target response spectrum. Similarly, the ability of the proposed procedure to match the target response spectrum and its variance is tested by measuring the $SSE_{\mu,\sigma}$ parameter that is given in Equation 6.11. In this specific case, w is assumed as 2 to increase the goodness of fit with target standard deviation. Figure 6.5 compares the target and observed response spectrum and corresponding variance. As briefed in Section 6.2, the generalized response spectrum and corresponding variance presented in this figure is determined by using the procedure presented in Jayaram and Baker (2010). The predictive model proposed by Akkar and Bommer (2010) is employed in determination of the target median displacement spectrum and standard deviation.

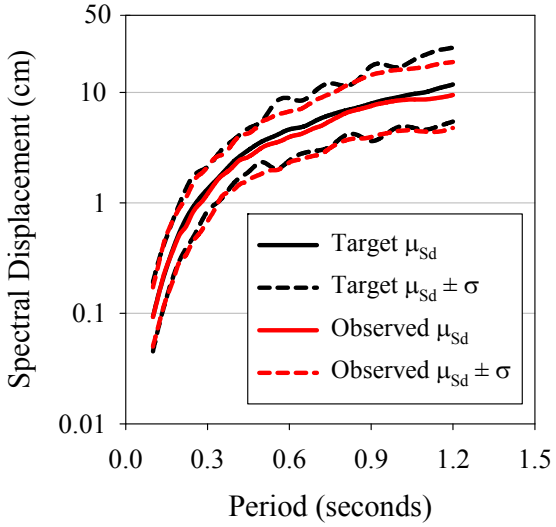

Figure 6.5 Comparison of target response spectrum and its variance with observed data obtained from the optimum ground motion bin

Figure 6.4 and Figure 6.5 show that the achieved match between the target and observed response spectrum are fairly acceptable. Apparently the fit is much better for cases where the matching with the logarithmic standard deviation is not considered as the target constraint (Figure 6.4). The observations from Figure 6.5 support this point clearly. The plots on this figure convey the fact that the goodness of fit between the target and observed logarithmic standard deviation is relatively less when compared to the matching that only considers the median target response spectrum (Figure 6.4). Figure 6.6 is the close-up view of the comparison between target and observed logarithmic standard deviation of the optimum ground motion bin.

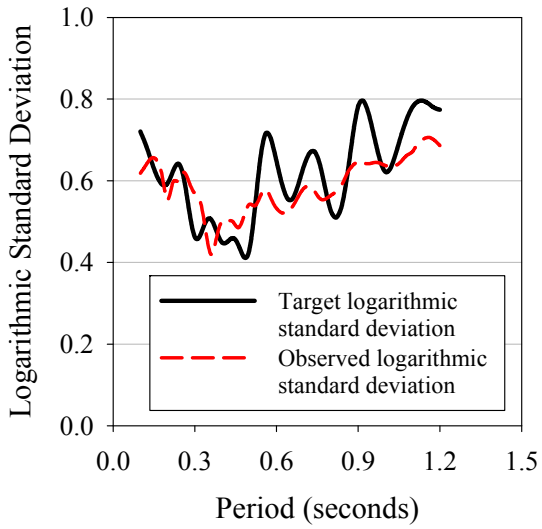

Figure 6.6 Comparison of target and observed logarithmic standard deviation

The target and observed logarithmic standard deviation trends in Figure 6.6 are fairly comparable. However, for some period values there is almost 30 % difference between the target and observed logarithmic standard deviation values. Increasing the number of candidate accelerograms would probably improve the goodness of fit. The possible limitations to this solution will be the number of available ground-motion records compatible with the earthquake scenario and the computation time required to complete the selection process. The concerns raised about the constraints on the seismological properties of candidate records are already discussed in Chapter 2. Nevertheless, relaxing the constraints related with magnitude and distance seems to be the easiest way to increase the number of candidate records. For instance Jayaram et al. (2011) selects 10 records within 7102 ground motions without having any constraint on magnitude and distance.

Another concern about increasing the number of candidate records is the excessive computational demand. This issue can be addressed by utilizing more complex software (e.g., REXEL: computer aided record selection for code-based seismic structural analysis (Iervolino et al., 2010)) and powerful computers or by employing additional post-processors (e.g., the greedy optimization technique

presented in Jayaram et al. (2011)). However, such complexities would reduce the practicality of the overall procedure. As a matter of fact, the proposed procedure is capable of selecting and scaling the optimum recording bin from a larger candidate ground motion dataset. For cases where larger candidate ground motion dataset is required, the efficiency of the selection procedure can be improved further by advanced selection algorithms. Considering the processing abilities of usual desktop computers and widely available software (e.g., *MATLAB*, *Microsoft Excel*), the current performance of the proposed selection algorithm can be accepted as fairly optimum.

The ability of the proposed selection and scaling procedure to match for a target response spectrum and variance derived for a specific structure is also investigated. The CMS and corresponding variance given in Figure 6.2 are employed as target values to achieve this objective. For this illustrative case study, an alternative candidate ground motion set is assembled to improve the match between target and observed data further. The new candidate ground-motion dataset is obtained by extending the magnitude range and relaxing the distance parameter. Thus ground motions with a moment magnitude range of $6.5 \leq M_w \leq 7.4$ (which was $6.7 \leq M_w \leq 7.2$ in the original bin) are selected. A total of 71 records satisfy the relaxed magnitude criterion in the compiled ground-motion library. During the course of this case study, the number of candidate records or simply the processing demand is limited by using the constraint of epsilon (ε) which is presented as an efficient indicator of spectral shape by Baker (2006a). Consequently, candidate records are selected from a pre-defined narrow epsilon range ($0.35 \leq \varepsilon \leq 1.35$). Table 6.2 lists the seismological parameters and epsilon values of the 20 candidate records. The comparative plots between target and observed data are presented in Figure 6.7. The comparison between target and observed median displacement response indicate a good match whereas the fit to target logarithmic standard deviation is reasonably acceptable considering the limited number of candidate records.

Table 6.2 Seismological parameters and epsilon values of the alternative candidate recording set

Record name	M_w	R_{JB} (km)	Soil Type	Fault Type	S_d (cm) (T=0.61sec)	ε (T=0.61sec)
PEER0855	7.3	63.0	NEHRP D	SS	1.828	0.386
PEER1052	6.7	5.3	NEHRP C	RV	8.418	0.485
PEER1107	6.9	22.5	NEHRP D	SS	3.916	0.460
PEER0801	6.9	14.2	NEHRP C	SS	4.673	0.568
PEER1633	7.4	12.6	NEHRP C	SS	6.136	0.583
PEER0848	7.3	19.7	NEHRP D	SS	5.493	0.535
PEER1794	7.1	31.1	NEHRP C	SS	2.645	0.561
PEER0015	7.4	38.4	NEHRP C	RV	3.027	0.650
PEER0164	6.5	15.2	NEHRP C	SS	3.893	0.746
PEER0729	6.5	23.9	NEHRP D	SS	3.451	0.735
PEER1005	6.7	28.8	NEHRP C	RV	2.815	0.699
PEER0968	6.7	43.2	NEHRP D	RV	2.842	0.821
PEER1116	6.9	19.1	NEHRP D	SS	6.236	0.884
PEER1112	6.9	86.9	NEHRP C	SS	1.024	0.698
PEER0014	7.4	81.3	NEHRP C	RV	1.974	0.928
PEER0125	6.5	15.0	NEHRP C	RV	5.496	1.005
PEER0888	7.3	79.8	NEHRP D	SS	2.577	1.101
TGMB3011	6.5	51.7	NEHRP D	N	1.996	1.098
PEER1109	6.9	69.0	NEHRP C	SS	1.812	1.163
PEER1640	7.4	93.3	NEHRP D	SS	2.540	1.201

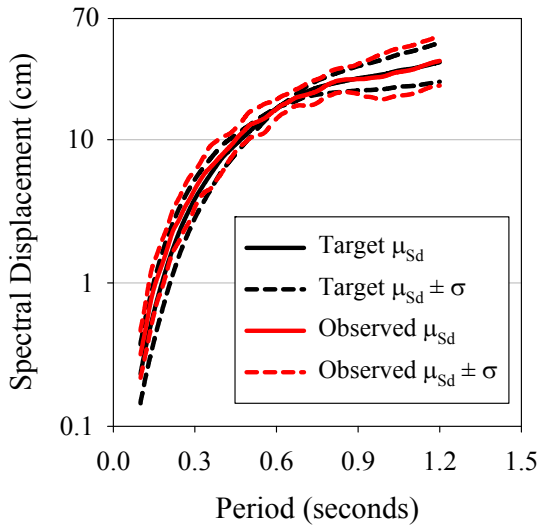

Figure 6.7 Comparison of CMS and corresponding variance with observed data obtained from the recording set selected and scaled according to the proposed procedure

CHAPTER 7

SUMMARY AND CONCLUSIONS

7.1 Summary

This dissertation proposed a record selection and scaling methodology with the aim of obtaining a target-hazard compatible ground-motion recording set to be used in the performance verification of structural systems. Under this objective, assembling a candidate ground-motion bin, selection of the most suitable records from this bin and their proper scaling to the target hazard level are presented. A total of 260 accelerograms from 113 events recorded on NEHRP C and NEHRP D type soil conditions are compiled as a ground-motion library to derive some of the important components of the proposed model. The ground-motion library is also used for the evaluation of the proposed procedure. The records in the ground-motion library cover a moment magnitude range of $5.0 \leq M_w \leq 7.7$ and a distance interval of 0 km $\leq R_{JB} \leq$ 100 km. The study used many sets of ground-motion combinations in the derivation and implementation of the proposed procedure. These combinations are selected from the magnitude and distance ranges of the ground-motion library that are particularly of engineering interest. Thus, the abilities as well as the limitations of the proposed selection and scaling methodology presented throughout the dissertation draw a realistic framework.

The proposed procedure linearly scales each ground-motion record to its target level depending on the difference between the observed intensity of the unscaled record and corresponding median estimation obtained from a representative predictive model. This approach results in preserving the inherent record-to-record variability of the scaled ground motions. Thus, the methodology does not artificially manipulate the selected records during the scaling stage. The predictive ground-motion model proposed by Akkar and Bommer (2010) is employed throughout this study to show the implementation of the procedure. On the other hand, any other GMPE that properly reflects the seismotectonic features of the region of concern can be used without any limitation with the presented methodology. The final set of ground motions selected and scaled from the candidate recording set is the optimum one that can convey reasonably accurate information about the dynamic response of the structure under the target earthquake scenario.

The proposed selection and scaling procedure is initially introduced for linear structural systems. The records are scaled such that the average of the modified ground motions at the period of interest (usually the fundamental period of the structure) is equal to the target spectral ordinate. The methodology is capable of computing the logarithmic standard deviations of the scaled ground-motion bins about target hazard level. The final selection of records is accomplished by calculating the standard deviation of alternative ground-motion bins populated from a relatively large candidate ground-motion dataset. Bearing on the theoretical and practical constraints of ground-motion record selection and scaling, the scaled recording set that is compatible with the major seismological features of the target hazard scenario with the smallest standard deviation about target hazard level is considered as the optimum ground-motion bin in this method. The proposed procedure is evaluated in terms of level of modifications in the scaled ground motions (i.e., the amplitudes of scaling factors) through comparisons with stripe-scaling methodology. The proposed procedure is also used to evaluate the performance of alternative ground-motion intensity measures

(i.e., ground-motion parameters other than elastic spectral ordinates) to test their level of success for relating the ground-motion demand and target structural response.

The selection and scaling methodology presented for linear systems is extended for structures responding beyond their elastic limits in the latter parts of the dissertation. This modification was necessary as the selection parameter for linear structural response ($\varepsilon\sigma_{Sd}$) may not be self-sufficient for identifying the most suitable recordings that would yield the minimum dispersion in structural response when structures respond in the nonlinear range. The ground-motion library is divided into different sets having pre-determined magnitude and distance intervals. The accelerograms falling into these bins are scaled to the central magnitude and distance values of each bin for spectral periods of T = 0.3 s, 0.6 s, 0.9 s, 1.2 s and 1.5 s. The central magnitude and distances are assumed to represent the target hazard at this stage of the study. The nonlinear RHA of the scaled ground motions in each bin are investigated for the most efficient ground-motion selection parameter that would yield the minimum dispersion about the nonlinear structural response by simplifying the structures as SDOF systems (a common intermediate step in engineering practice realized through pushover analysis). The nonlinear RHA are computed for R = 2, 4, 6 and 8 and the nonlinear behavior is mimicked by the non-degrading bilinear hysteretic model with 3% post-yield stiffness ratio. The selected hysteretic behavior can represent code-complying RC frames. These analyses lead to the identification of $\varepsilon\sigma_{ISd}$ (linear combination of PGV and elastic spectral ordinate; $\varepsilon\sigma_{Sd+PGV}$) as the most efficient record selection parameter for the selection and scaling of records for nonlinear structures. Empirical relationships are derived to estimate the standard deviation of the nonlinear structural response from the scaled ground motions. These empirical expressions use $\varepsilon\sigma_{Sd}$, $\varepsilon\sigma_{PGV}$, T (fundamental structural period) and R as the independent parameters. The performance of the modified scaling and selection procedure for nonlinear

structures is evaluated through conventional residual analyses. The observations on residual analyses suggest the acceptable performance of the procedure.

The selection and scaling procedure modified for nonlinear structural response is verified using code complying buildings of 3-, 4- and 8-story RC MRF structures. The selected models represent the general characteristics of the Turkish building stock and are employed to see the performance of the proposed procedure for nonlinear MDOF response. This was a necessary step as the proposed procedure is developed using the results of SDOF systems. Structural response statistics obtained by the records selected and scaled according to the proposed procedure are compared with the results of two alterative procedures proposed by Baker (2011) and Kalkan and Chopra (2011). A simple damage assessment study is also conducted by using the observed response statistics from nonlinear RHA and estimations of the likely distributions of response provided by the proposed methodology. These limited studies show the capacity of the proposed methodology as an auxiliary tool for damage assessment of building systems.

Finally, the proposed selection and scaling methodology is modified once again to match a target response spectrum and its pre-defined variance. This type of selection and scaling methodology is necessary for a target response spectrum such as CMS (Baker, 2011) that implicitly disregards the variance except for the specific fundamental vibration period of the structure. Such a record selection and scaling methodology is also necessary for the loss assessment studies of large building stocks that require a target response spectrum associated with a variance for a pre-defined period interval. To this end a new parameter is introduced to the modified procedure for record selection and scaling of above cases. The limitations of this new methodology are investigated via goodness of fit statistics by comparing the match between the scaled accelerograms through this new method and the target elastic spectral shapes together with their variances.

7.2 Conclusions

The main conclusions derived from this dissertation are given below.

i. In general, it is difficult to obtain a sufficient number of ground-motion records that fully comply with the fundamental seismological and geological constraints (e.g., magnitude, source-to-site distance, style-of-faulting, site class) of the target earthquake scenario and its corresponding target hazard level. This issue becomes more critical especially for cases where the distribution of available recordings is sparse (e.g., large-magnitude and close-distance ground motions) as the structural response can be sensitive to these ground-motion characteristics. The proposed methodology inherently accounts for the seismological and geological limitations of the candidate accelerograms by using GMPEs. It considers the difference between the observed intensity of the unscaled accelerograms and the corresponding median estimation of the GMPE to tailor the unsupported seismological and geological target-hazard driven constraints by the candidate accelerograms. This property can let the analyst relax the imposed seismological and geological constraints by the target hazard scenario while gathering the candidate accelerograms.

ii. Probabilistic performance assessment of buildings requires accurate estimation of structural response parameters for a given target hazard level. Consequently, scaling methods that ensure the match between the average intensity of the scaled accelerograms and target hazard level are advantageous. Otherwise, intermediate steps are required to relate the target hazard level and its corresponding exceedance probability. Scaling procedures which are equally applicable to a variety of intensity measures and horizontal component definitions that

are of common use in GMPEs are also more useful. Case studies in this dissertation show that the proposed procedure is capable of scaling ground motions with alternative intensity measures (e.g., PGA and PGV) and it is equally applicable to state-of-art GMPEs that increase its implementation to many fields of engineering interest.

iii. The comparisons between alternative scaling procedures reveal the fact that some methodologies (e.g., spectrum matching and inelastic target scaling) may yield over- or under-estimation of structural response although these scaling methods modify the identical ground-motion bin for the same target scenario earthquake. The observations from the case study presented in Chapter 2 (see Figure 2.6) indicate that there can be 20% difference in the average spectral response between the compared scaling methodologies.

iv. The optimum number of recordings in the candidate ground-motion dataset is suggested to be 20 by considering the observations on the computation time and the standard deviation of elastic simplified structural response. The proposed optimum number for the candidate ground-motion data size fairly ensures the efficiency and accuracy of the proposed procedure.

v. Stripe-scaling artificially suppresses the scatter in elastic spectral response whereas the proposed scaling procedure (as a trade-off approach between stripe- and cloud-scaling) preserves the inherent record-to-record variability. It is believed that this specific feature of the proposed methodology reflects the inherent randomness in future seismic actions. The resulting structural response can be evaluated in a more realistic way against the future seismic action when compared to the accelerograms that are scaled to one common spectral ordinate

(stripe-scaling). The observations also show that the R-dependent dispersion (structural response scatter of nonlinear systems) in the proposed scaling procedure displays a more stable trend when compared to the stripe-scaling results.

vi. The observations on the scatter of structural response suggest that scaling with respect to different intensity measures result in different levels of dispersion about median structural response. PGV-based scaling results in relatively lower levels of dispersion when the response of structures are significantly beyond the elastic limits. This type of observation is previously done by other studies (e.g., Akkar and Özen, 2005). Scaling of accelerograms through PGA seems to be reasonable for short-period systems that respond in the vicinity of their elastic capacity.

vii. The comparisons based on the level of amplitude modification show that scaling factors of stripe-scaling are larger than those of the proposed methodology for the entire set of M_w-R_{JB} clusters and for all periods considered in this study. This observation can be interpreted as the significant manipulation of accelerograms by stripe-scaling that may distort their genuine features. Contrary to the use of large scaling factors, applying smaller scaling factors, as in the case of proposed procedure, would result in more realistic assessment of structural response statistics.

viii. The linear relationship established through the proposed scaling procedure among scaled records and $\varepsilon\sigma_{Sd}$ constitutes the basis of selecting the optimum ground-motion bin. However, this correlation is valid only for elastic systems (or buildings responding in the vicinity of their elastic capacity) and may not be sufficient for significant

nonlinear response. Thus, this study introduced an alternative predictor for the nonlinear response. The observations indicated that the combination of elastic spectral ordinate and PGV (i.e., $\varepsilon\sigma_{Sd+PGV}$) yields higher correlations with inelastic spectral response when compared to $\varepsilon\sigma_{Sd}$ and $\varepsilon\sigma_{PGV}$ separately.

ix. The bias in $\varepsilon\sigma_{ISd}$ estimations with respect to M_w and R_{JB} is investigated by residual analyses. Straight lines are fitted to the residual scatters to investigate the significance of the slope terms in straight lines for each T and R pair used in this study. The residual analyses and p-value statistics about the significance of slope terms show that, except for a few cases, the analytical expressions derived for $\varepsilon\sigma_{ISd}$ are unbiased. This observation advocates a fairly good performance of the proposed method for the record selection and scaling of structures responding in the nonlinear range.

x. Comparisons between the proposed selection and scaling methodology with the procedure proposed by Baker (2011) show that the proposed procedure yields slightly smaller dispersion for relatively small vibration periods ($T_1 < 0.9$ s). As the period increases ($T_1 \geq 0.9$ s), the efficiency of the proposed procedure reduces and yields higher standard deviation values with respect to Baker (2011). This scatter mainly originates from the inherent record-to-record variability that is intentionally preserved by the proposed procedure.

xi. The observations on the inelastic scaling methodology proposed by Kalkan and Chopra (2011) reveal that the structural response statistics are sensitive to the selected empirical elastic-to-inelastic spectrum conversion relations (e.g., the expressions proposed by Chopra and Chintanapakdee (2004) vs. Ruiz-García and Miranda (2003 and 2007)).

Therefore the accuracy of such scaling methodologies is limited to the performance of the inelastic target spectral ordinate estimations. The case studies in this dissertation concluded that although the methodology proposed by Kalkan and Chopra (2011) yields relatively smaller dispersion statistics about nonlinear structural response, the method introduces an additional uncertainty to the results stemming from the use of empirical elastic-to-inelastic spectrum conversion equations.

xii. The proposed methodology can give a rough estimation on the response distribution of structures when they are subjected to the optimally selected and scaled ground-motion bin. This feature conveys useful information for probabilistic damage assessment studies. The limitations and practicality of these estimations are investigated throughout the dissertation. The observations suggest a fairly good performance of the proposed procedure as a useful tool for rapid probabilistic building performance assessment and loss studies. The comparisons from the limited case studies show that the maximum difference between the damage state probabilities obtained from the estimations of the proposed procedure and the observed data is about 10% in almost all cases. Considering the computation time and uncertainties involved in the nonlinear RHA of structures, these differences are accepted as tolerable.

xiii. The case studies show that the performance of the modified selection and scaling procedure to match a median spectrum and its specified variance for a pre-determined period interval is fairly acceptable when the limitations on the candidate accelerograms are considered. The fit is better for cases where matching with the median spectrum is the only constraint.

7.3 Limitations and Future Work

The evaluations of the proposed selection and scaling procedure are based on the use of maximum roof displacement as the structural response measure. Although this parameter is proven to be a good indicator of seismic demand on first-mode dominant regular structures, other damage measures (e.g., maximum interstory drift ratio, floor accelerations, etc.) might be required for the verification of structures having irregularities or dominated by higher mode contributions. The proposed procedure and alternative methodologies are investigated by using 10 (n=10) accelerograms in the optimum ground-motion bin as a compromise among various studies in the literature. Sensitivity analysis on structural response estimations with respect to different numbers of scaled accelerograms as inputs to RHA can be performed as a future research. The empirical equation for $\varepsilon\sigma_{lSd}$ derived in this study relies on nonlinear SDOF response represented by a non-degrading bilinear hysteretic model. The efficacy and accuracy of this expression can be further improved by employing alternative hysteretic models to simulate a wider range of structural systems. The proposed procedure can be improved by introducing advanced selection algorithms for cases where larger candidate ground-motion datasets are required. The performance of the proposed procedure can be tested for the selection and scaling of vertical accelerograms as they can be important for the risk and damage assessment of short period buildings.

REFERENCES

Abrahamson, N.A., and Silva, W.J., (2008). Summary of the Abrahamson & Silva NGA Ground-Motion Relations, *Earthquake Spectra*, Vol. 24 (1), 67–97.

Akkar, S. and Bommer, J.J., (2010). Empirical equations for the prediction of PGA, PGV, and spectral accelerations in Europe, the Mediterranean Region, and the Middle East. *Seismological Research Letters*, Vol. 81 (2), 195–206.

Akkar, S., Douglas, J., Di Alessandro, C., Campbell, K., Somerville, P., Cotton, F., Silva, W. and Baker, J., (2012). Defining a consistent strategy to model ground-motion parameters for the GEM-PEER Global GMPEs Project. *15th World Conference on Earthquake Engineering*, Lisbon, Portugal.

Akkar, S. and Küçükdoğan, B., (2008). Direct use of PGV for estimating peak nonlinear oscillator displacements. *Earthquake Engineering and Structural Dynamics*, Vol. 37 (12), 1411–1433.

Akkar, S. and Özen, Ö., (2005). Effect of peak ground velocity on deformation demands for SDOF systems. *Earthquake Engineering and Structural Dynamics*, Vol. 34 (13), 1551–1571.

Akkar, S., Sucuoğlu, H. and Yakut, A., (2005). Displacement-Based Fragility Functions for Low- and Mid-rise Ordinary Concrete Buildings. *Earthquake Spectra*, Vol. 21 (4), 901–927.

American Society of Civil Engineers (ASCE), (2006). ASCE 7–05, Minimum design loads for buildings and other structures, Reston, VA, 388 pp.

Applied Technology Council (ATC), (1996). ATC-40, Seismic evaluation and retrofit of concrete buildings, Report No: SSC 96-01, Redwood City, CA.

Applied Technology Council (ATC), (2007). ATC-58 35% Draft, Guidelines for seismic performance assessment of buildings, Redwood City, CA.

Applied Technology Council (ATC), (2009). ATC-58 50% Draft, Guidelines for seismic performance assessment of buildings, Redwood City, CA.

Applied Technology Council (ATC), (2011). ATC-58-1 75% Draft, Seismic performance assessment of buildings, Redwood City, CA.

Arias, A., (1970). A measure of earthquake intensity, *Seismic Design for Nuclear Power Plants*, R.J. Hansen (ed.). Massachusetts Institute of Technology Press, Cambridge, MA, 438–483.

Atkinson, G.M. and Boore, D.M., (2003). Empirical ground-motion relations for subduction zone earthquakes and their application to Cascadia and other regions, *Bulletin of the Seismological Society of America*, Vol. 93 (4), 1703-1729.

Ay, B.Ö. and Erberik, M.A., (2008). Vulnerability of Turkish Low-Rise and Mid-Rise Reinforced Concrete Frame Structures, *Journal of Earthquake Engineering*, Vol. 12 (S2), 2–11.

Baker, J.W. and Cornell, C.A., (2005). A vector-valued ground motion intensity measure consisting of spectral acceleration and epsilon. *Earthquake Engineering and Structural Dynamics*, Vol. 34 (10), 1193–1217.

Baker, J.W. and Cornell, C.A., (2006a). Spectral shape, epsilon and record selection, *Earthquake Engineering and Structural Dynamics*, Vol. 35 (9), 1077–1095.

Baker, J.W. and Cornell, C.A., (2006b). Correlation of Response Spectral Values for Multicomponent Ground Motions, *Bulletin of the Seismological Society of America*, Vol. 96 (1), 215–227.

Baker, J.W., Lin, T., Shahi, S.K., and Jayaram, N., (2011). New Ground Motion Selection Procedures and Selected Motions for the PEER Transportation Research Program, *PEER Technical Report 2011/03*, Pacific Earthquake Engineering Research Center, University of California, Berkeley, 106 pp.

Baker, J.W., (2011). Conditional Mean Spectrum: Tool for ground-motion selection, *Journal of Structural Engineering (ASCE)* Vol. 137 (3), 322–331.

Bal, E.İ., Crowley, H., Pinho, R. and Gülay, F.G., (2007). Structural Characteristics of Turkish RC Building Stock in Northern Marmara Region for Loss Assessment Applications, IUSS Press, Pavia, Italy, 107 pp.

Beyer, K. and Bommer, J.J., (2006). Relationships between median values and between aleatory variabilities for different definitions of the horizontal component of motion, *Bulletin of the Seismological Society of America*, Vol. 96 (4A), 1512–1522.

Beyer, K and Bommer, J.J. (2007). Selection and Scaling of Real Accelerograms for Bi-Directional Loading: A Review of Current Practice and Code Provisions, *Journal of Earthquake Engineering*, Vol. 11, 13–45.

Bindi, D., Luzi, L., Massa, M. and Pacor, F., (2010). Horizontal and vertical ground motion prediction equations derived from the Italian Accelerometric Archive (ITACA), *Bulletin of Earthquake Engineering*, Vol. 8 (5), 1209–1230.

Bommer, J.J. and Acevedo, A.B., (2004). The use of real earthquake accelerograms as input to dynamic analysis, *Journal of Earthquake Engineering*, Vol. 8 (Special Issue 1), 43–91.

Bommer, J.J., Douglas, J. and Strasser, F.O., (2003). Style-of-faulting in ground-motion prediction equations, *Bulletin of Earthquake Engineering*, Vol. 1 (2), 171–203.

Bommer, J.J., Scott, S.G. and Sarma, S.K., (2000). Hazard-consistent earthquake scenarios, *Soil Dynamics and Earthquake Engineering*, Vol. 19 (4), 219–231.

Boore, D.M. and Atkinson, G.M., (2008). Ground-motion prediction equations for the average horizontal component of PGA, PGV, and 5%-damped PSA at spectral periods between 0.01 s and 10.0 s, *Earthquake Spectra*, Vol. 24 (1), 99–138.

Bradie, B., (2005). A Friendly Introduction to Numerical Analysis, 1st Edition, Pearson, ISBN-10: 0130130540, ISBN-13: 978-0130130549, 976 pp.

Building Seismic Safety Council (BSSC), (2009). FEMA P-750, NEHRP recommended provisions for seismic regulations for new buildings and other structures, Washington, DC.

Buratti, N., Stafford, P.J. and Bommer, J.J., (2011). Earthquake accelerogram selection and scaling procedures for estimating the distribution of drift response, *Journal of Structural Engineering (ASCE)*, Vol. 137 (3), 345-357.

Campbell, K.W. and Bozorgnia, Y. (2008). NGA ground motion model for the geometric mean horizontal component of PGA, PGV, PGD and 5% damped linear elastic response spectra for periods ranging from 0.01 to 10 s, *Earthquake Spectra*, Vol. 24 (1), 139–171.

Calvi, G.M., (1999). A displacement–based approach for vulnerability evaluation of classes of buildings, *Journal of Earthquake Engineering*, Vol. 3 (3), 411–438.

Chiou, B.S.-J. and Youngs, R.R., (2008). An NGA Model for the Average Horizontal Component of Peak Ground Motion and Response Spectra, *Earthquake Spectra*, Vol. 24 (1), 173–215.

Chopra, A.K. and Chinatanapakdee, C., (2004). Inelastic deformation ratios for design and evaluation of structures: Single-degree-of-freedom bilinear systems, *Journal of Structural Engineering (ASCE)*, Vol. 130 (9), 1309–1319.

Chopra, A.K. and Goel, R.K., (2002). A modal pushover analysis procedure for estimating seismic demands for buildings, *Earthquake Engineering and Structural Dynamics*, Vol. 31 (3), 561–582.

Cimellaro, G.P., Reinhorn, A.M., D'Ambrisi, A. and De Stefano, M., (2011). Fragility analysis and seismic record selection, *Journal of Structural Engineering (ASCE)*, Vol. 137 (3), 379–390.

Cordova, P.P., Deierlein, G.G., Mehanny, S.S.F. and Cornell, CA., (2000). Development of a two-parameter seismic intensity measure and probabilistic assessment procedure, *The Second U.S.-Japan Workshop on Performance-Based Earthquake Engineering Methodology for Reinforced Concrete Building Structures*, Sapporo, Hokkaido, Japan.

DiPasquale, E. and Çakmak, A.S., (1987). Detection and assessment of seismic structural damage. *Technical Report NCEER–87–0015*, State University of New York, Buffalo, NY.

European Committee for Standardization (CEN), (2004). Eurocode 8: Design of structures for earthquake resistance-Part 1: General rules, seismic actions and rules for buildings, EN1998-1, Brussels.

Giovenale, P., Cornell, C.A. and Esteva, L., (2004). Comparing the adequacy of alternative ground motion intensity measures for the estimation of structural responses, *Earthquake Engineering and Structural Dynamics*, Vol. 33, 951–975.

Goel, R.K. and Chopra, A.K., (1997). Period formulas for moment resisting frame buildings, *Journal of Structural Engineering (ASCE)*, Vol. 123 (11), 1454–1461.

Gülerce, Z. and Abrahamson, N.A., (2011). Site-Specific Design Spectra for Vertical Ground Motion, *Earthquake Spectra*, Vol. 27 (4), 1023–1047.

Hancock, J., Bommer, J.J. and Stafford, P.J., (2008). Numbers of scaled and matched accelerograms required for inelastic dynamic analyses, *Earthquake Engineering and Structural Dynamics*, Vol. 37 (14), 1585–1607.

Haselton, C.B., (2009). Evaluation of ground motion selection and modification methods: Predicting median interstory drift response of buildings, *PEER Report 2009/01*, Pacific Earthquake Engineering Research Center, University of California, Berkeley, 288pp.

Hilber, H.M., Hughes, T.J.R. and Taylor, R.L., (1977). Improved numerical dissipation for time integration algorithms in structural dynamics, *Earthquake Engineering and Structural Dynamics*, Vol. 5 (3), 283–292.

Housner, G.W., (1952). Spectrum Intensity of Strong-Motion Earthquakes, *Proceedings of the Symposium on Earthquakes and Blast Effects on Structures*, Earthquake Engineering Research Institute, Los Angeles, CA, 20–36.

Huang, Y., Whittaker, A.S., Luco, N. and Hamburger, R.O., (2011). Scaling Earthquake Ground Motions for Performance-Based Assessment of Buildings, *Journal of Structural Engineering (ASCE)*, Vol. 137 (3), 311–321.

Iervolino, I. and Cornell, C.A., (2005). Record selection for nonlinear seismic analysis of structures, *Earthquake Spectra*, Vol. 21 (3), 685–713.

Iervolino, I., Galasso, C. and Cosenza, E., (2010). REXEL: computer aided record selection for code-based seismic structural analysis, *Bulletin of Earthquake Engineering*, Vol. 8, 339–362.

Idriss, I.M., (2008). An NGA empirical model for estimating the horizontal spectral values generated by shallow crustal earthquakes, *Earthquake Spectra*, Vol. 24 (1), 217–242.

Jalayer, F., Franchin, P. and Pinto, P.E., (2007). A scalar damage measure for seismic reliability analysis of RC frames, *Earthquake Engineering and Structural Dynamics*, Vol. 36 (13), 2059–2079.

Jayaram, N. and Baker, J.W., (2010). Ground-motion selection for PEER Transportation Systems Research Program, *Proceedings of the 7th CUEE and 5th ICEE Joint Conference*, Tokyo Institute of Technology, Tokyo, Japan.

Jayaram, N., Lin, T. and Baker, J.W., (2011). A Computationally Efficient Ground-Motion Selection Algorithm for Matching a Target Response Spectrum Mean and Variance, *Earthquake Spectra*, Vol. 27, 797–815.

Joyner, W.B. and Boore, D.M., (1981). Peak horizontal acceleration and velocity from strong-motion records including records from the 1979 Imperial Valley, California, Earthquake, *Bulletin of the Seismological Society of America*, Vol. 71 (6), 2011–2038.

Kadaş, K., Yakut, A. and Kazaz, İ., (2011). Spectral Ground Motion Intensity Based on Capacity and Period Elongation, *Journal of Structural Engineering, ASCE*, Vol. 137 (3), 401–409.

Kalkan, E., and Chopra, A.K., (2010). Practical guidelines to select and scale earthquake records for nonlinear response history analysis of structures, *USGS Open-File Report 2010-1068*, U.S. Geological Survey, Reston, Virginia, 126pp.

Kalkan, E. and Chopra, A.K., (2011). Modal-Pushover-based Ground Motion Scaling Procedure, *Journal of Structural Engineering (ASCE)*, Vol. 137 (3), 298–310.

Kappos, A.J. and Kyriakakis, P., (2000). A re-evaluation of scaling techniques for natural records, *Soil Dynamics and Earthquake Engineering*, Vol. 20, 111–123.

Kottke, A. and Rathje, E.M., (2008). A semi-automated procedure for selecting and scaling recorded earthquake motions for dynamic analysis, *Earthquake Spectra*, Vol. 24 (4), 911–932.

Krawinkler, H., Medina, R., and Alavi, B., (2003). Seismic drift and ductility demands and their dependence on ground motions, *Engineering Structures*, Vol. 25, 637–653.

Luco, N., (2002). Probabilistic Seismic Demand Analysis: SMRF Connection Fractures, and Near-Source Effects, Ph.D. Dissertation, Department of Civil and Environmental Engineering, June 2002, Stanford University, Stanford, CA.

Luco, N. and Bazzurro, P., (2007). Does amplitude scaling of ground motion records result in biased nonlinear structural drift responses?, *Earthquake Engineering and Structural Dynamics*, Vol. 36 (13), 1813–1835.

Luco, N. and Cornell, C.A., (2007). Structure-specific scalar intensity measures for near-source and ordinary earthquake ground motions, *Earthquake Spectra*, Vol. 23 (2), 357–392.

Mahaney, J.A., Paret, T.F., Kehoe, B.E. and Freeman, S.A, (1993). The Capacity Spectrum Method for Evaluating Structural Response During the Lorna Prieta Earthquake, 1993 National Earthquake Conference, Memphis.

Mander, J.B., Priestley, M.J.N., Park, R., (1988). Theoretical stress-strain model for confined concrete, *Journal of Structural Engineering*, Vol. 114 (8), 1804–1826.

Martinez-Rueda, J.E., (1996). Application of passive devices for the retrofitting of reinforced concrete structures, *Proceedings of 11th WCEE*, Acapulco, México.

Martinez-Rueda, J.E., (1998). Scaling procedure for natural accelerograms based on a system of spectrum intensity scales, *Earthquake Spectra*, Vol. 14 (1), 135–152.

Matsumura, K., (1992). On the intensity measure of strong motions related to structural failures, *Proceedings of 10th WCEE*, Madrid, Spain, 375-380.

Moss, R.E.S., (2011). Reduced Sigma of Ground-Motion Prediction Equations through Uncertainty Propagation, *Bulletin of the Seismological Society of America*, Vol. 101 (1), 250–257.

Mousavi, M., Ghafory-Ashtiany, M. and Azarbakht, A., (2011). A new indicator of elastic spectral shape for the reliable selection of ground motion records, *Earthquake Engineering and Structural Dynamics*, Vol. 40 (7), 1403–1416.

Naeim, F., Alimoradi, A. and Pezeshk, S., (2004). Selection and scaling of ground motion time histories for structural design using genetic algorithms, *Earthquake Spectra*, Vol. 20 (2), 413–426.

Naeim, F. and Lew, M., (1995). On the use of design spectrum compatible time histories, *Earthquake Spectra*, Vol. 11 (1), 111–127.

Nau, J.M. and Hall, W.J., (1984). Scaling methods for earthquake response spectra, *Journal of Structural Engineering (ASCE)*, Vol. 110 (7), 1533–1548.

Power, M., Chiou, B., Abrahamson, N., Bozorgnia, Y., Shantz, T. and Roblee, C., (2008). An overview of the NGA project, *Earthquake Spectra*, Vol. 24 (1), 3–21.

Prota, (2011). Probina Orion – Bina Tasarım Sistemi 2011, Teknik Özellikler, Ankara, Turkey.

Reyes, J.C. and Kalkan, E., (2011). How many records should be used in ASCE/SEI-7 ground motion scaling procedure, *Earthquake Spectra*, Vol. 28 (3), 1223–1242.

Ruiz-García, J. and Miranda, E., (2003). Inelastic displacement ratios for evaluation of existing structures, *Earthquake Engineering and Structural Dynamics*, Vol. 32 (8), 1237–1258.

Ruiz-García, J. and Miranda, E., (2007). Probabilistic estimation of maximum inelastic displacement demands for performance-based design, *Earthquake Engineering and Structural Dynamics*, Vol. 36, 1235–1254.

Seismosoft, (2010). SeismoStruct – A computer program for static and dynamic nonlinear analysis of framed structures, Version 5.2.2, Available from URL: http://www.seismosoft.com/ (accessed 06.02.2012).

Shome, N., Cornell, C.A., Bazzurro, P. and Carballo, J.E., (1998). Earthquakes, records, and nonlinear responses, *Earthquake Spectra*, Vol. 14 (3), 469–500.

Shome, N., (1999). Probabilistic Seismic Demand Analysis of Nonlinear Structures, PhD Thesis, Department of Civil and Environmental Engineering, March 1999, Stanford University, Stanford, CA.

Spacone, E., Ciampi, V. and Filippou, F.C., (1996). Mixed formulation of nonlinear beam finite element, *Computers & Structures*, Vol. 58 (1), 71–83.

Stewart, J.P., Chiou, S.J., Bray, J.D., Graves, R.W., Somerville, P.G. and Abrahamson, N.A., (2001). Ground motion evaluation procedures for performance-based design, *PEER Report 2001/09*, Pacific Earthquake Engineering Research Center, University of California, Berkeley, 229 pp.

Strasser, F.O., Abrahamson, N.A. and Bommer, J.J., (2009). Sigma: Issues, insights, and challenges, *Seismological Research Letters*, Vol. 80 (1), 40–56.

Turkish Standards Institute, (2000). TS 500-2000 Requirements for Design and Construction of Reinforced Concrete Structures, Ankara, Turkey.

Turkish Standards Institute, (1997). TS 498, Design loads for buildings, Ankara, Turkey.

TEC, (2007). TEC-07 Specification for buildings to be built in seismic zones, Ministry of Public Works and Settlement, Government of Republic of Turkey, Ankara, Turkey.

Tothong, P. and Cornell, C.A., (2008). Structural performance assessment under near-source pulse-like ground motions using advanced ground motion intensity measures, *Earthquake Engineering and Structural Dynamics*, Vol. 37 (7), 1013–1037.

Vamvatsikos, D. and Cornell, C.A., (2005). Developing efficient scalar and vector intensity measures for IDA capacity estimation by incorporating elastic spectral shape information, *Earthquake Engineering and Structural Dynamics*, Vol. 34 (13), 1573–1600.

Veletsos, A.S. and Newmark, N.M., (1960). Effect of inelastic behavior on the response of simple systems to earthquake motions, *Proceedings of 2nd World Conference on Earthquake Engineering*, Vol. 2, Tokyo, Japan, 895–912.

Watson-Lamprey, J. and Abrahamson, N., (2006). Selection of ground motion time series and limits on scaling, *Soil Dynamics and Earthquake Engineering*, Vol. 26, 477–482.

Yakut, A., Sucuoğlu, H. and Akkar, S., (2012). Seismic risk prioritization of residential buildings in Istanbul, *Earthquake Engineering and Structural Dynamics*, Vol. 41, 1533–1547.

Yang, D., Pan, J. and Li, G., (2009). Non-structure-specific intensity measure parameters and characteristic period of near-fault ground motions, *Earthquake Engineering and Structural Dynamics*, Vol. 38 (11), 1257–1280.

APPENDIX A

GROUND-MOTION RECORDS

Table A1.1 M1SR

Record Name	M_w	R_{JB} (km)	Soil Type	Fault Type	PGA (cm/s^2)	PGV (cm/s)	S_d (5%, 0.3s) (cm)	S_d (5%, 0.6s) (cm)	S_d (5%, 0.9s) (cm)	S_d (5%, 1.2s) (cm)	S_d (5%, 1.5s) (cm)
TGMB1827	5.0	0.0	NEHRP C	N	51.7	2.1	0.20	0.17	0.17	0.25	0.34
TGMB0544	5.2	2.0	NEHRP D	N	131.7	8.8	0.60	2.39	3.16	2.42	2.94
TGMB4104	5.2	7.3	NEHRP D	N	190.0	9.4	0.85	1.42	1.70	1.75	1.71
TGMB1831	5.0	10.4	NEHRP C	N	183.3	6.4	1.10	0.88	0.53	0.49	0.48
TGMB1829	5.0	10.7	NEHRP C	N	44.8	1.5	0.20	0.23	0.15	0.14	0.13
TGMB4103	5.2	10.7	NEHRP D	N	169.1	6.6	0.63	1.04	1.02	0.88	0.85
TGMB3432	5.3	10.9	NEHRP D	N	105.3	4.9	0.19	0.55	1.53	1.73	1.78
TGMB3455	5.4	11.2	NEHRP D	N	114.5	4.7	0.35	0.67	1.33	2.06	2.27
TGMB4106	5.2	12.7	NEHRP D	N	78.9	4.1	0.43	0.68	1.50	1.84	1.17
TGMB4105	5.2	13.7	NEHRP C	N	83.1	4.5	0.45	0.98	0.73	0.63	0.50
TGMB2610	5.3	14.2	NEHRP D	SS	87.4	17.6	0.32	1.81	4.34	7.20	8.92
ECDE6167	5.1	15.0	NEHRP C	SS	95.0	4.3	0.49	0.80	0.88	0.98	1.07
TGMB1828	5.0	15.6	NEHRP D	N	44.2	1.5	0.27	0.24	0.15	0.14	0.15
TGMB3717	5.3	16.2	NEHRP C	N	32.4	1.9	0.27	0.59	0.50	0.46	0.41
ECDE1808	5.1	18.0	NEHRP D	SS	88.5	4.6	0.72	0.76	1.26	1.34	1.07
ECDE0192	5.4	18.0	NEHRP C	RV	68.8	3.9	0.38	0.66	1.22	1.20	1.13
TGMB0073	5.2	19.6	NEHRP D	SS	46.3	2.9	0.25	0.75	1.02	0.64	0.97

Table A1.2 M1IR

Record Name	M_w	R_{JB} (km)	Soil Type	Fault Type	PGA (cm/s^2)	PGV (cm/s)	S_d (5%, 0.3s) (cm)	S_d (5%, 0.6s) (cm)	S_d (5%, 0.9s) (cm)	S_d (5%, 1.2s) (cm)	S_d (5%, 1.5s) (cm)
TGMB2209	5.4	22.6	NEHRP D	N	22.0	2.4	0.11	0.33	0.72	1.14	1.42
TGMB2952	5.2	22.8	NEHRP D	SS	156.7	2.5	0.10	0.08	0.07	0.08	0.08
TGMB3738	5.0	25.5	NEHRP C	N	16.4	0.8	0.11	0.15	0.13	0.09	0.09
TGMB4101	5.2	27.0	NEHRP C	N	32.1	1.0	0.17	0.12	0.13	0.19	0.23
TGMB4109	5.2	28.5	NEHRP D	N	31.1	1.6	0.30	0.23	0.21	0.21	0.17
TGMB2614	5.3	29.8	NEHRP C	SS	22.2	0.8	0.07	0.09	0.14	0.22	0.25
TGMB2917	5.4	31.2	NEHRP C	SS	20.7	2.2	0.10	0.53	0.70	0.74	0.70
ECDE6087	5.3	32.0	NEHRP C	N	33.4	1.3	0.15	0.18	0.27	0.24	0.22
TGMB1088	5.2	35.1	NEHRP C	SS	13.6	1.0	0.08	0.08	0.21	0.23	0.17
TGMB0555	5.2	36.9	NEHRP C	SS	12.9	0.9	0.04	0.09	0.29	0.28	0.32
TGMB1079	5.0	37.9	NEHRP C	SS	12.0	0.9	0.11	0.12	0.08	0.12	0.12
ECDE7343	5.1	39.0	NEHRP D	SS	26.0	1.2	0.19	0.15	0.14	0.12	0.14
TGMB0364	5.2	39.8	NEHRP C	SS	21.4	0.9	0.09	0.07	0.14	0.15	0.10
TGMB2902	5.4	40.6	NEHRP C	N	6.6	0.3	0.02	0.05	0.06	0.13	0.10
TGMB1176	5.1	48.0	NEHRP C	N	6.5	0.4	0.02	0.07	0.11	0.16	0.26
TGMB3758	5.3	49.1	NEHRP D	SS	9.6	1.1	0.08	0.17	0.37	0.61	0.51
TGMB3459	5.4	49.9	NEHRP D	N	27.0	1.6	0.12	0.52	0.41	0.53	0.53

Table A1.3 M1LR

Record Name	M_w	R_{JB} (km)	Soil Type	Fault Type	PGA (cm/s^2)	PGV (cm/s)	S_d (5%, 0.3s) (cm)	S_d (5%, 0.6s) (cm)	S_d (5%, 0.9s) (cm)	S_d (5%, 1.2s) (cm)	S_d (5%, 1.5s) (cm)
TGMB2153	5.3	51.7	NEHRP D	SS	33.3	1.8	0.28	0.26	0.37	0.25	0.19
TGMB3901	5.1	56.1	NEHRP C	N	6.4	0.3	0.04	0.06	0.11	0.08	0.12
TGMB1954	5.0	60.8	NEHRP C	SS	3.8	0.2	0.02	0.03	0.02	0.02	0.02
TGMB3911	5.4	61.9	NEHRP C	SS	10.9	0.7	0.07	0.09	0.15	0.29	0.35
TGMB3910	5.4	64.5	NEHRP C	SS	7.6	0.5	0.06	0.11	0.11	0.16	0.19
TGMB0553	5.2	67.5	NEHRP C	SS	5.4	0.4	0.02	0.10	0.13	0.18	0.13
TGMB0268	5.4	68.6	NEHRP D	N	13.5	0.9	0.06	0.27	0.40	0.35	0.45
TGMB1265	5.1	70.7	NEHRP C	N	6.0	0.3	0.04	0.07	0.05	0.06	0.07
TGMB2905	5.4	73.7	NEHRP C	N	12.8	0.8	0.08	0.16	0.23	0.44	0.55
TGMB0556	5.2	76.0	NEHRP D	SS	3.1	0.3	0.02	0.06	0.08	0.12	0.09
TGMB3461	5.4	79.3	NEHRP D	N	6.2	0.5	0.03	0.15	0.10	0.09	0.14
TGMB3438	5.3	81.3	NEHRP D	N	4.7	0.3	0.02	0.07	0.09	0.05	0.05
TGMB3740	5.0	82.5	NEHRP C	N	1.9	0.1	0.01	0.02	0.02	0.03	0.03
TGMB1266	5.1	83.2	NEHRP C	N	1.8	0.1	0.01	0.01	0.02	0.04	0.03
TGMB2210	5.4	85.4	NEHRP D	N	3.0	0.2	0.02	0.08	0.08	0.07	0.05
TGMB1460	5.2	86.0	NEHRP C	SS	12.8	0.7	0.08	0.14	0.13	0.13	0.11
TGMB0547	5.2	88.2	NEHRP D	N	2.4	0.2	0.01	0.05	0.06	0.06	0.04
TGMB2613	5.3	93.6	NEHRP D	SS	18.8	2.3	0.07	0.62	0.89	1.42	1.70
TGMB0545	5.2	94.3	NEHRP D	N	2.5	0.4	0.01	0.07	0.16	0.18	0.27
TGMB3714	5.3	96.0	NEHRP D	N	3.2	0.5	0.02	0.07	0.17	0.19	0.38
TGMB4113	5.2	97.5	NEHRP C	N	2.9	0.2	0.02	0.04	0.04	0.03	0.03
TGMB2954	5.2	99.0	NEHRP C	SS	1.7	0.1	0.01	0.02	0.03	0.04	0.03

Table A1.4 M2SR

Record Name	M_w	R_{JB} (km)	Soil Type	Fault Type	PGA (cm/s^2)	PGV (cm/s)	S_d (5%, 0.3s) (cm)	S_d (5%, 0.6s) (cm)	S_d (5%, 0.9s) (cm)	S_d (5%, 1.2s) (cm)	S_d (5%, 1.5s) (cm)
PEER0136	5.9	0.0	NEHRP C	RV	141.0	11.0	0.90	2.70	2.88	2.96	4.99
PEER0150	5.7	0.4	NEHRP C	SS	363.3	34.7	1.99	4.54	6.91	10.03	10.78
PEER0235	5.7	1.4	NEHRP C	SS	406.5	23.2	2.07	2.26	2.73	3.07	3.54
PEER2387	5.9	4.1	NEHRP C	RV	137.5	9.0	0.81	1.70	5.09	4.12	2.96
PEER0637	6.0	6.0	NEHRP C	SS	155.3	10.1	0.56	2.21	3.25	3.40	2.76
PEER0148	5.7	6.8	NEHRP D	SS	244.8	23.2	1.29	2.82	7.58	9.20	7.51
ECDE0122	5.5	7.0	NEHRP D	RV	153.5	13.9	0.65	3.55	4.18	3.68	3.60
PEER2399	5.9	10.1	NEHRP C	RV	42.9	3.0	0.21	0.44	0.65	0.68	1.22
TGMB1538	5.6	10.4	NEHRP C	N	263.8	11.9	0.85	1.71	1.62	2.18	2.37
PEER0477	5.8	12.8	NEHRP C	N	100.9	3.6	0.47	0.92	1.11	1.14	0.87
PEER1646	5.6	13.9	NEHRP C	RV	217.3	16.1	1.50	1.58	2.55	3.17	4.72
PEER1740	5.7	14.1	NEHRP D	N	164.0	6.9	0.88	1.25	0.96	1.31	0.87
PEER0668	6.0	14.4	NEHRP D	SS	159.7	13.2	0.57	2.87	4.10	3.71	3.59
ECDE0120	5.5	17.0	NEHRP C	RV	88.6	4.1	0.43	0.71	0.87	0.88	1.10
TGMB0342	5.7	19.2	NEHRP C	N	140.9	5.8	0.46	1.16	1.48	1.79	2.29

Table A1.5 M2IR

Record Name	M_w	R_{JB} (km)	Soil Type	Fault Type	PGA (cm/s^2)	PGV (cm/s)	S_d (5%, 0.3s) (cm)	S_d (5%, 0.6s) (cm)	S_d (5%, 0.9s) (cm)	S_d (5%, 1.2s) (cm)	S_d (5%, 1.5s) (cm)
TGMB1379	5.8	20.5	NEHRP C	SS	46.7	2.2	0.12	0.30	0.31	0.45	0.53
ECDE0247	5.8	21.0	NEHRP C	N	40.1	2.1	0.17	0.40	0.61	0.66	0.74
PEER2426	5.9	22.5	NEHRP C	RV	29.0	1.1	0.09	0.15	0.30	0.23	0.22
PEER1643	5.6	23.7	NEHRP C	RV	100.0	5.8	0.60	0.77	1.57	1.81	2.00
PEER0135	5.9	23.8	NEHRP C	RV	48.5	4.1	0.32	0.69	1.07	1.67	2.38
TGMB1530	5.6	29.1	NEHRP C	N	36.0	1.5	0.14	0.18	0.30	0.42	0.47
PEER0480	5.8	29.6	NEHRP D	N	70.2	3.9	0.30	0.79	0.99	1.08	1.49
TGMB3617	5.5	33.1	NEHRP C	N	21.8	1.7	0.07	0.21	0.27	0.37	0.42
TGMB3163	5.7	33.2	NEHRP D	SS	54.0	4.9	0.25	1.07	1.51	2.80	2.22
PEER0151	5.7	33.7	NEHRP D	SS	43.5	3.2	0.25	0.45	1.00	0.95	0.86
PEER2259	5.9	36.2	NEHRP C	RV	38.1	2.4	0.25	0.68	0.42	0.50	0.52
TGMB2766	5.5	36.8	NEHRP C	SS	12.5	0.8	0.06	0.25	0.32	0.32	0.35
TGMB1370	5.8	40.3	NEHRP C	SS	11.8	0.9	0.07	0.09	0.09	0.13	0.25
TGMB0289	5.7	43.5	NEHRP C	SS	38.0	1.7	0.24	0.19	0.27	0.30	0.26
TGMB0294	5.6	44.3	NEHRP C	SS	25.5	1.3	0.17	0.27	0.26	0.22	0.18
TGMB3808	5.6	45.4	NEHRP C	SS	14.7	0.8	0.11	0.11	0.12	0.15	0.24
PEER0481	5.8	45.5	NEHRP D	N	36.7	3.6	0.24	0.69	1.23	1.51	1.83

Table A1.6 M2LR

Record Name	M_w	R_{JB} (km)	Soil Type	Fault Type	PGA (cm/s^2)	PGV (cm/s)	S_d (5%, 0.3s) (cm)	S_d (5%, 0.6s) (cm)	S_d (5%, 0.9s) (cm)	S_d (5%, 1.2s) (cm)	S_d (5%, 1.5s) (cm)
TGMB3858	5.8	51.3	NEHRP D	SS	20.8	1.5	0.20	0.23	0.47	0.47	0.51
TGMB3846	5.5	53.0	NEHRP D	SS	15.8	1.2	0.12	0.24	0.36	0.28	0.26
TGMB3879	5.8	54.1	NEHRP D	SS	27.5	2.4	0.14	0.47	0.82	1.11	1.17
TGMB0248	5.8	58.9	NEHRP D	SS	25.8	1.6	0.16	0.26	0.47	0.57	0.79
TGMB3765	5.6	62.3	NEHRP C	SS	8.4	1.0	0.04	0.12	0.30	0.46	0.58
PEER0609	6.0	62.6	NEHRP C	SS	32.0	2.2	0.20	0.56	0.84	0.62	0.63
PEER1744	5.7	63.8	NEHRP D	N	15.3	0.8	0.06	0.13	0.27	0.17	0.16
TGMB3864	5.8	71.8	NEHRP D	SS	8.1	0.5	0.05	0.17	0.18	0.18	0.23
TGMB3850	5.5	73.9	NEHRP D	SS	7.9	0.8	0.05	0.17	0.23	0.16	0.17
TGMB3749	5.8	75.2	NEHRP D	SS	24.3	3.2	0.16	0.65	1.25	1.95	1.66
TGMB3645	5.6	78.1	NEHRP C	SS	3.7	0.5	0.03	0.05	0.09	0.07	0.14
PEER2303	5.9	80.6	NEHRP C	RV	7.9	0.4	0.04	0.11	0.12	0.11	0.15
PEER2392	5.9	86.7	NEHRP D	RV	14.3	2.4	0.10	0.27	0.74	0.97	1.41
TGMB1374	5.8	91.3	NEHRP C	SS	14.8	0.8	0.10	0.12	0.18	0.22	0.22
PEER1745	5.7	99.4	NEHRP C	N	7.9	0.3	0.03	0.06	0.06	0.07	0.06

Table A1.7 M3SR

Record Name	M_w	R_{JB} (km)	Soil Type	Fault Type	PGA (cm/s^2)	PGV (cm/s)	S_d (5%, 0.3s) (cm)	S_d (5%, 0.6s) (cm)	S_d (5%, 0.9s) (cm)	S_d (5%, 1.2s) (cm)	S_d (5%, 1.5s) (cm)
PEER2628	6.2	0.0	NEHRP C	RV	354.7	22.4	3.08	4.80	6.23	5.34	8.80
PEER3475	6.3	0.0	NEHRP C	RV	492.5	32.0	1.39	5.07	9.24	9.32	9.38
TGMB0120	6.4	0.0	NEHRP D	N	296.1	36.4	2.61	4.03	11.61	12.83	17.37
PEER0230	6.1	1.1	NEHRP D	SS	420.7	23.2	1.84	5.30	3.91	7.23	11.00
TGMB3183	6.3	2.2	NEHRP C	SS	384.6	27.5	1.93	4.12	5.81	5.06	7.73
PEER0461	6.2	3.5	NEHRP D	SS	216.5	22.2	1.12	4.61	6.45	7.48	6.61
PEER0095	6.2	3.5	NEHRP D	SS	369.8	23.6	2.44	5.92	8.86	6.80	9.32
PEER0527	6.1	3.7	NEHRP D	SS	207.5	35.8	0.95	4.10	7.63	12.72	25.15
PEER3473	6.3	5.7	NEHRP C	RV	307.3	31.2	1.97	4.59	7.65	8.64	8.13
TGMB0001	6.1	6.4	NEHRP D	N	305.1	20.7	1.51	5.27	3.94	3.11	2.93
PEER0558	6.2	6.4	NEHRP D	SS	414.6	40.5	2.59	9.45	13.29	12.97	16.76
PEER0367	6.4	7.7	NEHRP D	RV	322.8	24.9	2.19	5.91	6.85	9.89	9.64
TGMB2361	6.0	8.2	NEHRP D	N	62.8	7.1	0.46	1.23	1.66	2.93	2.86
PEER0300	6.2	8.8	NEHRP C	N	167.6	24.4	0.73	3.61	8.25	13.85	15.97
PEER0459	6.2	9.9	NEHRP C	SS	249.9	20.5	1.45	3.24	7.12	9.10	7.68
ECDE7329	6.1	11.0	NEHRP D	SS	383.9	32.0	1.49	7.32	9.72	8.62	9.00
PEER0460	6.2	12.1	NEHRP D	SS	143.7	6.6	1.07	0.97	0.87	1.49	1.62
PEER0265	6.3	13.8	NEHRP C	SS	592.5	25.0	1.69	6.25	9.23	9.40	8.83
PEER1126	6.4	14.1	NEHRP C	N	169.5	7.9	0.82	1.16	1.65	2.49	1.94
PEER0033	6.2	16.0	NEHRP C	SS	305.7	18.0	1.56	1.56	2.66	5.10	3.85
PEER0718	6.2	17.6	NEHRP D	SS	130.3	13.1	0.59	1.79	2.19	3.76	5.34
PEER0266	6.3	18.5	NEHRP D	SS	115.0	19.7	0.65	2.84	3.99	6.93	9.64

Table A1.8 M3IR

Record Name	M_w	R_{JB} (km)	Soil Type	Fault Type	PGA (cm/s^2)	PGV (cm/s)	S_d (5%, 0.3s) (cm)	S_d (5%, 0.6s) (cm)	S_d (5%, 0.9s) (cm)	S_d (5%, 1.2s) (cm)	S_d (5%, 1.5s) (cm)
PEER0548	6.2	21.6	NEHRP D	SS	188.8	14.6	0.66	2.60	5.18	6.30	6.39
PEER0302	6.2	22.7	NEHRP C	N	95.7	10.3	0.51	1.47	3.09	5.44	5.65
PEER0534	6.1	23.0	NEHRP C	SS	239.6	9.4	0.72	2.29	2.12	2.46	2.21
PEER0463	6.2	26.4	NEHRP D	SS	90.0	10.6	0.45	1.46	3.11	6.34	5.31
PEER0815	6.1	26.8	NEHRP D	N	45.6	3.3	0.21	0.77	1.30	1.13	0.73
PEER3300	6.3	27.6	NEHRP C	RV	142.9	14.8	0.65	3.49	5.11	5.51	6.00
TGMB0117	6.4	29.0	NEHRP D	N	36.8	4.5	0.23	0.67	1.42	2.59	2.77
PEER0535	6.1	30.7	NEHRP D	SS	64.7	3.7	0.30	0.80	1.07	1.65	1.96
PEER2656	6.2	31.1	NEHRP D	RV	64.5	10.2	0.22	1.32	3.31	4.66	5.40
ECDE6329	6.4	33.0	NEHRP C	SS	55.3	5.3	0.31	1.32	1.53	1.46	1.48
PEER0555	6.2	34.9	NEHRP D	SS	44.3	2.5	0.32	0.40	0.45	0.69	0.78
PEER3496	6.3	35.1	NEHRP D	RV	69.1	11.3	0.34	1.36	3.49	5.66	8.50
TGMB0013	6.1	37.8	NEHRP C	SS	45.9	3.1	0.32	0.45	0.80	1.35	1.23
TGMB0035	6.0	38.1	NEHRP C	SS	76.2	3.9	0.28	0.60	1.17	1.31	0.89
PEER0268	6.3	39.1	NEHRP D	SS	81.7	8.4	0.45	1.40	1.73	2.60	3.59
PEER0513	6.1	42.2	NEHRP D	SS	79.9	4.8	0.40	0.87	0.80	0.92	0.77
PEER0301	6.2	43.5	NEHRP D	N	41.6	3.1	0.24	0.61	1.40	0.77	0.57
TGMB0119	6.4	43.9	NEHRP C	N	41.2	2.5	0.23	0.63	0.73	0.62	0.61
PEER3331	6.3	47.1	NEHRP D	RV	29.4	3.0	0.21	1.06	0.92	1.63	1.64
TGMB0011	6.1	47.6	NEHRP C	SS	48.9	3.5	0.30	0.54	0.96	1.20	1.13
PEER0332	6.4	49.4	NEHRP D	RV	111.2	10.4	0.60	3.54	2.99	3.05	3.04

Table A1.9 M3LR

Record Name	M_w	R_{JB} (km)	Soil Type	Fault Type	PGA (cm/s^2)	PGV (cm/s)	S_d (5%, 0.3s) (cm)	S_d (5%, 0.6s) (cm)	S_d (5%, 0.9s) (cm)	S_d (5%, 1.2s) (cm)	S_d (5%, 1.5s) (cm)
PEER0557	6.2	50.9	NEHRP D	SS	36.2	4.8	0.18	0.99	1.08	1.40	1.94
PEER0333	6.4	51.0	NEHRP D	RV	97.1	8.3	0.43	2.65	2.00	2.87	2.31
PEER0512	6.1	51.9	NEHRP C	SS	100.2	7.0	0.63	1.93	1.91	1.34	1.10
PEER0323	6.4	55.1	NEHRP C	RV	44.9	4.8	0.18	0.96	2.06	3.01	4.15
PEER1128	6.4	55.7	NEHRP D	N	28.5	2.5	0.15	0.71	0.79	1.16	1.13
TGMB0587	6.2	57.5	NEHRP C	SS	122.1	10.6	0.69	1.79	2.29	1.63	1.80
PEER3277	6.3	61.5	NEHRP D	RV	98.0	11.3	0.56	2.31	3.35	4.36	6.74
PEER0032	6.2	63.3	NEHRP C	SS	12.6	1.0	0.05	0.20	0.23	0.28	0.35
PEER0531	6.1	67.4	NEHRP C	SS	63.5	2.1	0.15	0.32	0.28	0.34	0.33
PEER3393	6.3	70.0	NEHRP C	RV	23.5	2.4	0.13	0.40	0.78	1.28	1.60
PEER0469	6.2	70.9	NEHRP D	SS	46.9	2.9	0.40	0.51	1.12	0.98	0.79
PEER0520	6.1	71.7	NEHRP D	SS	38.1	2.0	0.21	0.26	0.41	0.76	0.75
ECDE7311	6.1	72.0	NEHRP C	SS	16.3	1.0	0.09	0.35	0.37	0.25	0.26
PEER1127	6.4	74.1	NEHRP D	N	32.0	9.4	0.13	0.62	1.83	2.97	3.94
PEER3485	6.3	77.1	NEHRP C	RV	33.1	2.5	0.19	0.50	0.64	0.93	1.04
PEER1124	6.4	79.3	NEHRP D	N	19.7	2.0	0.15	0.57	0.75	1.08	0.49
PEER2921	6.2	80.0	NEHRP C	SS	14.4	1.4	0.09	0.29	0.47	0.54	0.92
PEER3030	6.2	82.7	NEHRP C	RV	39.5	3.5	0.28	0.71	1.69	1.01	0.77
TGMB3117	6.0	84.3	NEHRP C	SS	7.6	0.8	0.04	0.19	0.22	0.33	0.46
PEER3392	6.3	85.8	NEHRP C	RV	28.2	2.8	0.13	1.13	0.77	0.70	0.57
TGMB0121	6.4	86.9	NEHRP D	N	15.0	3.5	0.07	0.47	0.75	1.05	2.06
PEER2453	6.2	88.3	NEHRP D	RV	35.8	6.5	0.21	0.93	1.34	1.61	2.18
PEER2757	6.2	90.4	NEHRP D	SS	30.8	4.1	0.17	0.40	0.83	1.11	2.10
TGMB2366	6.0	90.9	NEHRP C	N	11.9	0.9	0.08	0.13	0.21	0.28	0.57
PEER2484	6.2	93.5	NEHRP D	RV	20.5	4.2	0.08	0.51	1.16	1.11	1.27
PEER2962	6.2	96.8	NEHRP D	RV	44.6	4.9	0.24	0.93	1.18	1.53	1.84
PEER2895	6.2	99.9	NEHRP D	SS	11.4	1.9	0.05	0.27	0.62	0.60	0.67

Table A1.10 M4SR

Record Name	M_w	R_{JB} (km)	Soil Type	Fault Type	PGA (cm/s^2)	PGV (cm/s)	S_d (5%, 0.3s) (cm)	S_d (5%, 0.6s) (cm)	S_d (5%, 0.9s) (cm)	S_d (5%, 1.2s) (cm)	S_d (5%, 1.5s) (cm)
PEER1078	6.7	1.7	NEHRP C	RV	254.1	16.4	1.50	3.20	4.45	5.97	7.10
PEER1052	6.7	5.3	NEHRP C	RV	354.1	40.0	2.05	8.17	13.89	14.62	15.57
PEER0165	6.5	7.3	NEHRP D	SS	257.2	27.3	1.11	6.45	8.04	8.75	10.87
PEER1042	6.7	7.9	NEHRP C	RV	278.7	23.6	1.21	3.98	5.53	11.21	9.14
PEER0313	6.6	10.3	NEHRP D	N	261.5	24.3	1.30	4.28	7.36	7.00	8.94
PEER0764	6.9	10.3	NEHRP D	SS	256.9	31.7	1.32	3.59	6.48	12.83	14.39
PEER0809	6.9	12.2	NEHRP C	SS	340.1	13.9	1.04	1.53	2.88	4.41	4.34
PEER0289	6.9	13.3	NEHRP C	N	149.5	17.4	0.99	2.36	8.41	8.54	12.00
PEER1006	6.7	13.8	NEHRP C	RV	356.0	22.0	1.18	3.42	5.40	5.39	10.15
PEER0801	6.9	14.2	NEHRP C	SS	245.3	23.4	0.95	4.46	6.64	5.99	8.83
PEER0125	6.5	15.0	NEHRP C	RV	326.2	26.1	1.61	5.46	6.24	7.21	6.40
PEER0164	6.5	15.2	NEHRP C	SS	159.7	14.7	1.34	3.61	3.95	7.68	6.01
PEER1116	6.9	19.1	NEHRP D	SS	222.7	32.5	1.04	5.82	8.29	13.81	12.67

Table A1.11 M4IR

Record Name	M_w	R_{JB} (km)	Soil Type	Fault Type	PGA (cm/s^2)	PGV (cm/s)	S_d (5%, 0.3s) (cm)	S_d (5%, 0.6s) (cm)	S_d (5%, 0.9s) (cm)	S_d (5%, 1.2s) (cm)	S_d (5%, 1.5s) (cm)
ECDE4677	6.5	20.0	NEHRP C	SS	244.1	18.9	1.45	1.81	3.60	4.39	8.80
ECDE0439	6.7	20.0	NEHRP D	RV	182.0	21.0	0.93	2.80	6.12	7.39	6.11
ECDE1796	6.5	22.0	NEHRP D	N	153.1	9.3	1.00	2.32	1.45	1.05	1.10
PEER1107	6.9	22.5	NEHRP D	SS	288.8	22.8	1.56	3.99	4.30	8.53	12.30
PEER0288	6.9	22.5	NEHRP C	N	204.1	12.6	0.70	1.87	2.19	3.82	4.22
PEER0163	6.5	23.2	NEHRP D	SS	98.4	14.3	0.66	1.02	1.94	3.30	4.09
PEER0729	6.5	23.9	NEHRP D	SS	190.0	32.2	1.03	3.29	6.12	11.07	13.94
PEER0079	6.6	25.5	NEHRP C	RV	96.7	9.2	0.75	1.49	3.95	3.26	3.26
PEER1005	6.7	28.8	NEHRP C	RV	149.3	16.7	0.86	2.79	4.57	4.74	7.29
PEER0290	6.9	29.8	NEHRP D	N	111.5	9.7	0.77	1.89	5.30	3.50	2.55
PEER0122	6.5	33.3	NEHRP D	RV	73.4	9.5	0.40	1.47	3.43	3.90	4.19
PEER0812	6.9	33.9	NEHRP C	SS	79.7	15.1	0.45	1.83	3.70	4.33	5.08
PEER0971	6.7	36.2	NEHRP D	RV	127.5	8.1	1.05	1.89	3.38	3.42	2.64
PEER0093	6.6	39.5	NEHRP D	RV	101.2	9.5	0.46	1.10	1.34	1.96	2.93
PEER0968	6.7	43.2	NEHRP D	RV	187.2	12.3	1.34	2.73	2.92	3.65	5.78
PEER0036	6.6	45.1	NEHRP D	SS	84.2	18.6	0.39	1.30	3.12	5.43	9.85

Table A1.12 M4LR

Record Name	M_w	R_{JB} (km)	Soil Type	Fault Type	PGA (cm/s^2)	PGV (cm/s)	S_d (5%, 0.3s) (cm)	S_d (5%, 0.6s) (cm)	S_d (5%, 0.9s) (cm)	S_d (5%, 1.2s) (cm)	S_d (5%, 1.5s) (cm)
TGMB3011	6.5	51.7	NEHRP D	N	103.4	10.5	0.67	2.00	3.21	5.31	5.28
ECDE0297	6.9	55.0	NEHRP C	N	40.0	6.1	0.18	0.50	0.96	1.85	3.37
PEER0051	6.6	55.2	NEHRP D	RV	31.9	4.0	0.18	0.42	1.04	1.55	1.82
PEER0069	6.6	59.0	NEHRP D	RV	28.3	8.1	0.23	0.69	0.87	1.33	1.78
TGMB0030	6.6	63.0	NEHRP C	SS	73.2	3.9	0.35	0.66	0.89	1.21	0.97
PEER1109	6.9	69.0	NEHRP C	SS	59.2	4.5	0.28	1.79	1.17	1.10	1.22
PEER1040	6.7	71.3	NEHRP D	RV	73.1	4.0	0.44	0.82	1.16	1.28	0.89
PEER0796	6.9	77.3	NEHRP C	SS	138.3	20.4	0.72	2.56	5.34	6.70	7.25
PEER1097	6.7	81.5	NEHRP D	RV	41.1	3.0	0.26	0.46	0.72	1.30	1.22
ECDE4893	6.8	84.0	NEHRP D	SS	32.5	3.3	0.14	0.53	0.56	0.93	0.96
PEER1112	6.9	86.9	NEHRP C	SS	68.2	3.9	0.40	1.10	0.78	0.72	0.67
ECDE0203	6.9	96.0	NEHRP D	RV	47.3	4.4	0.26	1.12	0.99	1.19	1.35
PEER1064	6.7	98.8	NEHRP C	RV	60.0	2.9	0.28	0.27	0.42	0.56	0.67

Table A1.13 M5SR

Record Name	M_w	R_{JB} (km)	Soil Type	Fault Type	PGA (cm/s^2)	PGV (cm/s)	S_d (5%, 0.3s) (cm)	S_d (5%, 0.6s) (cm)	S_d (5%, 0.9s) (cm)	S_d (5%, 1.2s) (cm)	S_d (5%, 1.5s) (cm)
TGMB1585	7.1	0.0	NEHRP C	SS	142.0	11.4	0.70	1.18	1.61	2.38	3.25
TGMB1594	7.1	0.0	NEHRP C	SS	654.9	26.6	3.70	2.86	2.92	3.48	5.50
TGMB1583	7.1	0.0	NEHRP D	SS	457.2	74.6	2.65	8.15	17.77	16.56	22.71
PEER0139	7.4	0.0	NEHRP C	RV	358.0	23.1	1.28	4.57	5.76	7.74	8.21
TGMB1584	7.1	3.7	NEHRP D	SS	171.0	13.6	1.22	2.10	2.48	3.57	6.47
TGMB1591	7.1	6.1	NEHRP C	SS	112.9	11.7	1.10	0.90	2.67	3.29	4.06
TGMB1104	7.6	8.3	NEHRP D	SS	337.4	59.3	2.09	6.54	10.59	15.34	20.81
PEER1546	7.6	9.4	NEHRP C	RV	234.7	38.1	1.12	4.26	6.54	11.11	13.55
TGMB1106	7.6	10.1	NEHRP C	SS	182.3	19.6	0.90	3.07	4.28	4.68	7.12
PEER0864	7.3	11.0	NEHRP C	SS	273.5	34.4	1.57	5.17	12.16	19.82	15.85
PEER1633	7.4	12.6	NEHRP C	SS	495.8	47.0	2.81	5.85	9.04	8.53	16.32
PEER0827	7.0	16.0	NEHRP C	RV	112.9	25.5	0.55	1.83	4.49	6.01	7.19
PEER1532	7.6	17.2	NEHRP C	RV	117.7	36.7	0.64	3.02	5.08	6.90	10.94
PEER0848	7.3	19.7	NEHRP D	SS	336.9	33.0	2.47	5.52	8.25	10.51	10.12

Table A1.14 M5IR

Record Name	M_w	R_{JB} (km)	Soil Type	Fault Type	PGA (cm/s^2)	PGV (cm/s)	S_d (5%, 0.3s) (cm)	S_d (5%, 0.6s) (cm)	S_d (5%, 0.9s) (cm)	S_d (5%, 1.2s) (cm)	S_d (5%, 1.5s) (cm)
PEER0138	7.4	24.1	NEHRP D	RV	95.4	15.7	0.46	1.70	3.62	4.50	7.86
PEER1628	7.5	26.5	NEHRP D	RV	129.4	26.6	0.58	2.33	6.06	10.93	15.75
PEER0880	7.3	27.0	NEHRP D	SS	123.5	12.5	0.62	1.81	2.41	3.25	3.21
TGMB1107	7.6	29.3	NEHRP D	SS	128.6	12.5	0.77	1.57	2.50	2.84	6.08
TGMB1109	7.6	29.5	NEHRP D	SS	106.6	23.4	0.63	2.09	5.03	8.54	16.18
PEER1794	7.1	31.1	NEHRP C	SS	163.1	20.4	0.90	2.63	6.26	9.81	8.19
TGMB1592	7.1	32.1	NEHRP D	SS	84.6	13.3	0.73	1.04	1.03	1.85	2.89
PEER1626	7.7	34.6	NEHRP C	SS	89.4	11.0	0.43	0.57	1.12	1.39	1.80
PEER0884	7.3	36.2	NEHRP D	SS	80.5	12.2	0.42	1.65	3.71	6.25	5.98
PEER0015	7.4	38.4	NEHRP C	RV	163.4	16.4	0.86	2.84	5.01	5.20	6.81
PEER0826	7.0	40.2	NEHRP D	RV	162.5	23.9	0.84	2.59	2.87	8.12	12.85
PEER1776	7.1	40.4	NEHRP C	SS	72.7	7.0	0.53	1.47	2.17	3.01	3.51
PEER1196	7.6	42.0	NEHRP D	RV	53.9	16.6	0.33	0.95	1.66	2.63	3.13
PEER1144	7.2	43.3	NEHRP D	SS	89.6	12.1	0.54	1.31	2.00	2.62	3.47
PEER1267	7.6	48.2	NEHRP D	RV	88.4	13.0	0.43	2.12	3.89	4.75	5.91
TGMB1108	7.6	49.3	NEHRP C	SS	50.9	8.3	0.20	0.50	1.31	1.32	2.76

Table A1.15 M5LR

Record Name	M_w	R_{JB} (km)	Soil Type	Fault Type	PGA (cm/s^2)	PGV (cm/s)	S_d (5%, 0.3s) (cm)	S_d (5%, 0.6s) (cm)	S_d (5%, 0.9s) (cm)	S_d (5%, 1.2s) (cm)	S_d (5%, 1.5s) (cm)
PEER1636	7.4	50.0	NEHRP D	SS	152.1	13.0	1.05	1.85	2.79	4.25	6.66
PEER1795	7.1	50.0	NEHRP C	SS	81.1	7.3	0.47	1.06	1.30	1.57	1.75
PEER1278	7.6	50.5	NEHRP C	RV	85.8	14.9	0.40	2.22	4.98	7.10	7.01
ECDE0153	7.0	52.0	NEHRP C	SS	83.3	5.3	0.36	0.46	0.68	0.77	1.60
TGMB1102	7.6	54.6	NEHRP C	SS	49.5	8.6	0.30	1.16	2.68	3.53	6.10
PEER0855	7.3	63.0	NEHRP D	SS	115.6	12.5	0.66	1.86	2.49	1.94	3.55
PEER1637	7.4	64.0	NEHRP D	SS	89.5	13.3	0.56	1.62	2.53	5.65	8.48
PEER1783	7.1	65.0	NEHRP D	SS	113.4	9.6	0.49	1.50	3.60	2.48	3.30
PEER1578	7.6	67.4	NEHRP C	RV	32.2	4.1	0.16	0.75	1.23	1.36	1.80
PEER0888	7.3	79.8	NEHRP D	SS	80.7	17.0	0.41	2.47	3.74	5.71	7.70
PEER0014	7.4	81.3	NEHRP C	RV	103.1	13.7	0.47	1.98	4.40	6.72	9.08
PEER0140	7.4	89.8	NEHRP D	RV	95.1	6.9	0.47	1.12	1.12	1.30	1.42
PEER1309	7.6	90.6	NEHRP D	RV	63.2	17.2	0.36	1.49	2.78	6.28	6.16
PEER1640	7.4	93.3	NEHRP D	SS	108.1	13.3	0.47	2.52	4.15	6.30	9.25
PEER1415	7.6	99.9	NEHRP D	RV	101.6	23.8	0.37	1.52	4.83	10.94	13.01

APPENDIX B

RESIDUAL SCATTERS

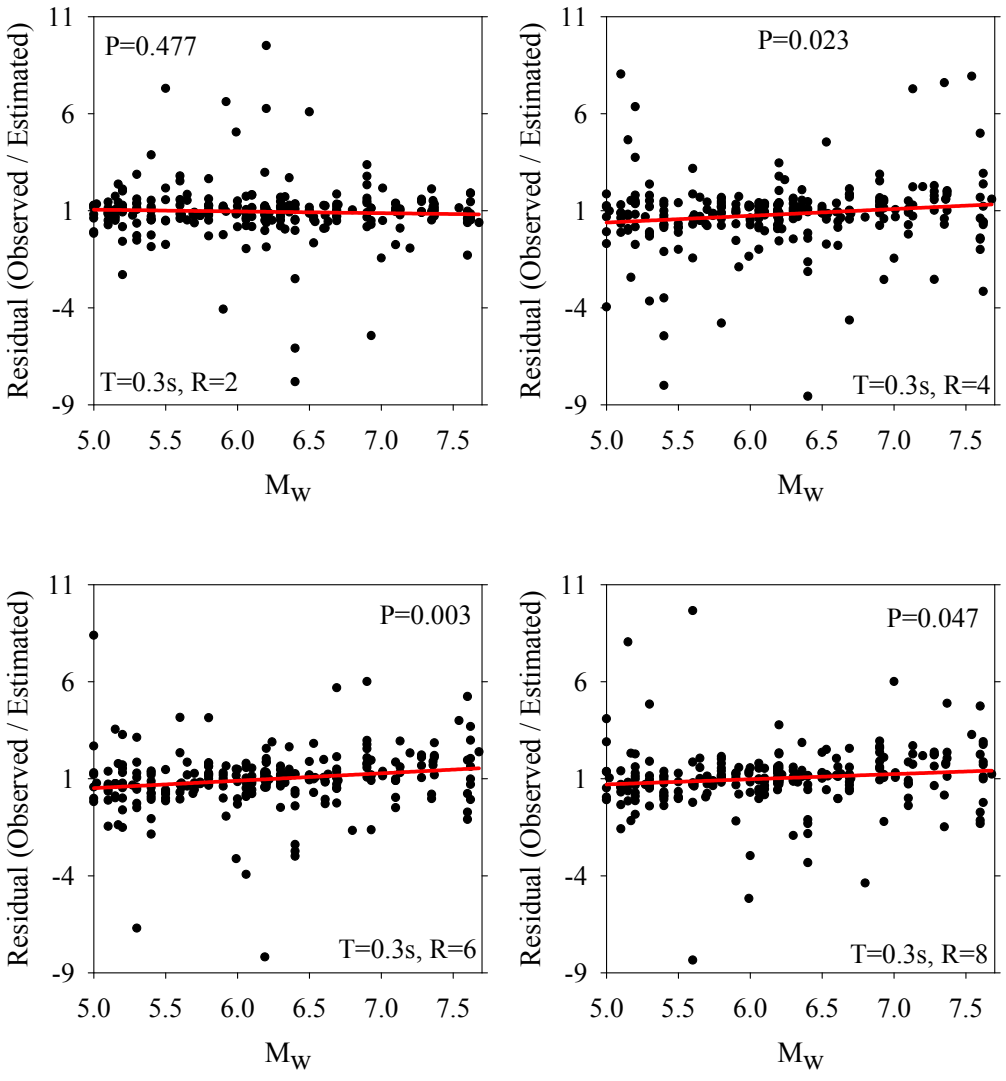

Figure B.1 Residual dependence statistics on M_w for T=0.3s

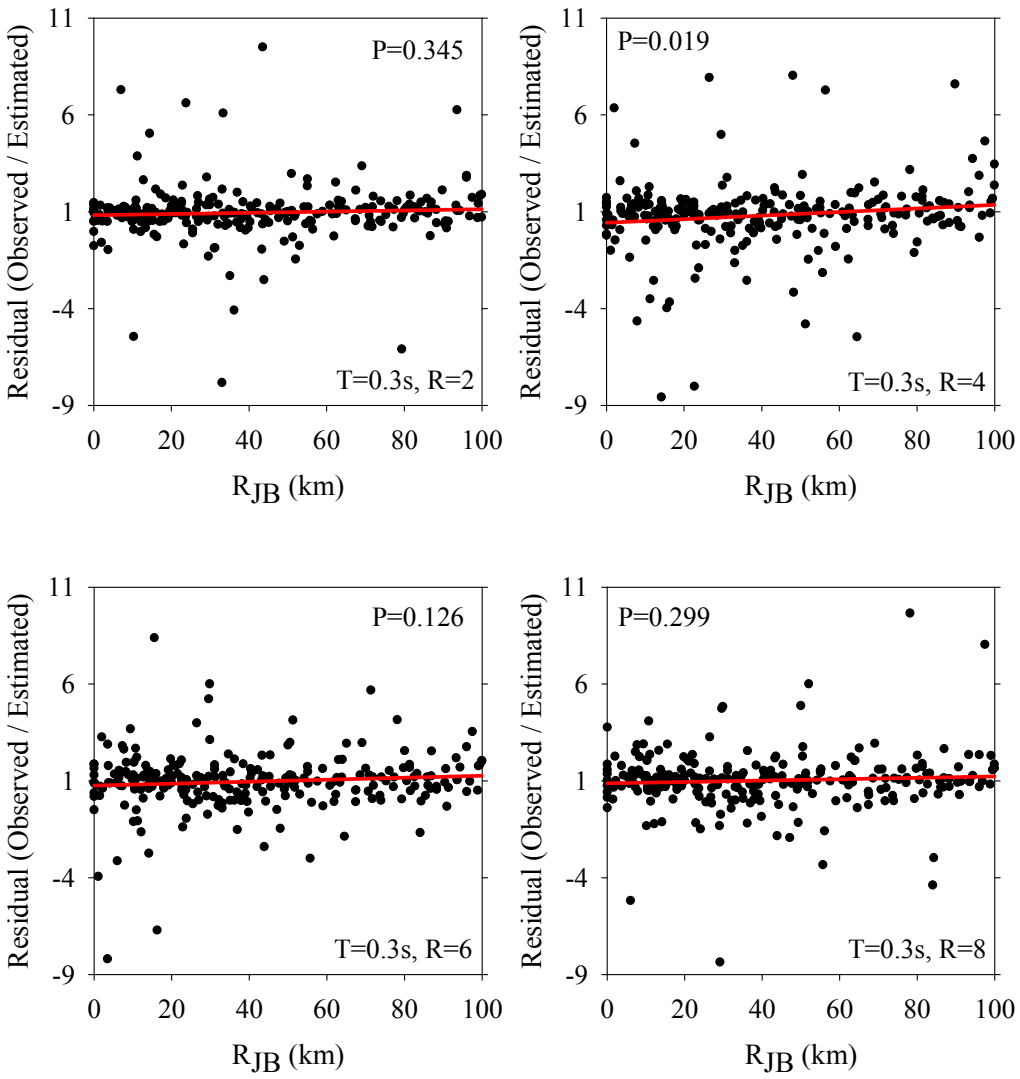

Figure B.2 Residual dependence statistics on R_{JB} for T=0.3s

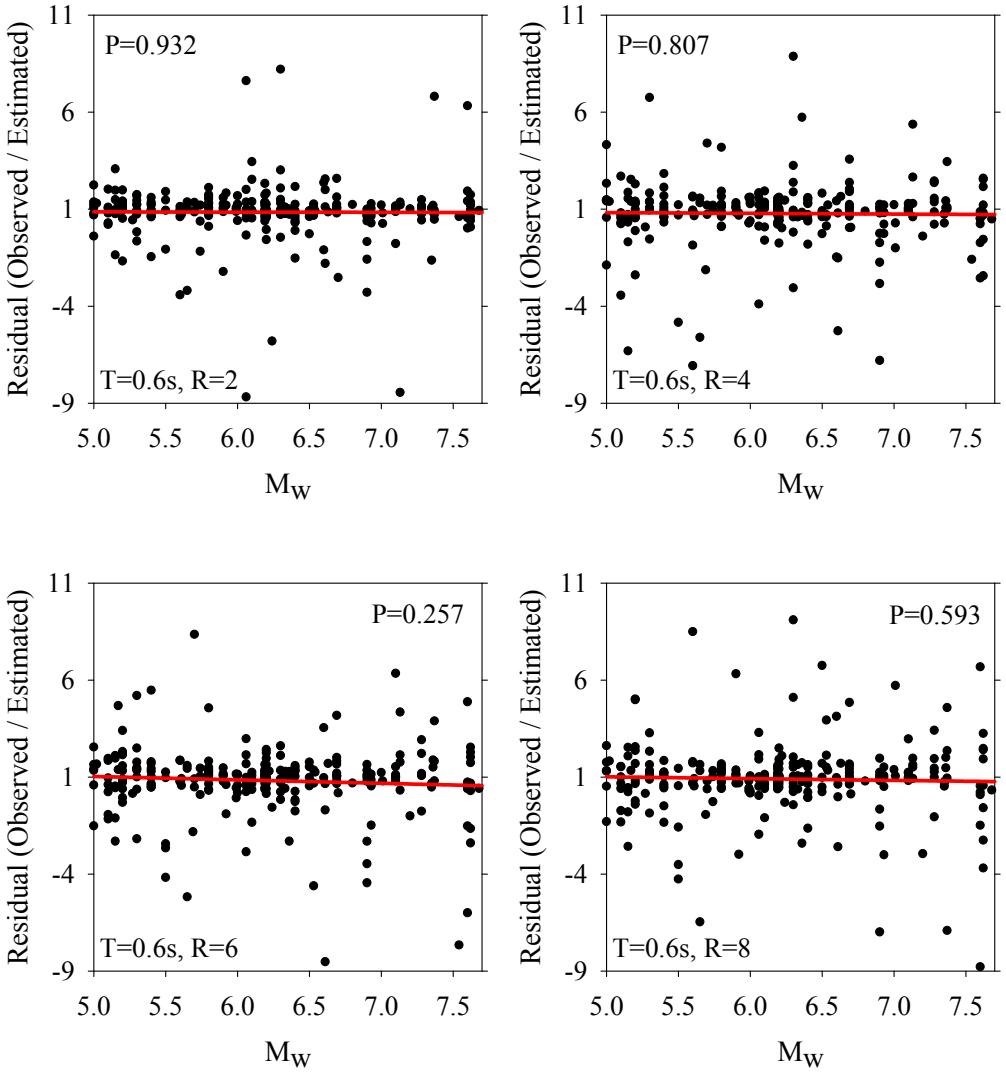

Figure B.3 Residual dependence statistics on M_w for T=0.6s

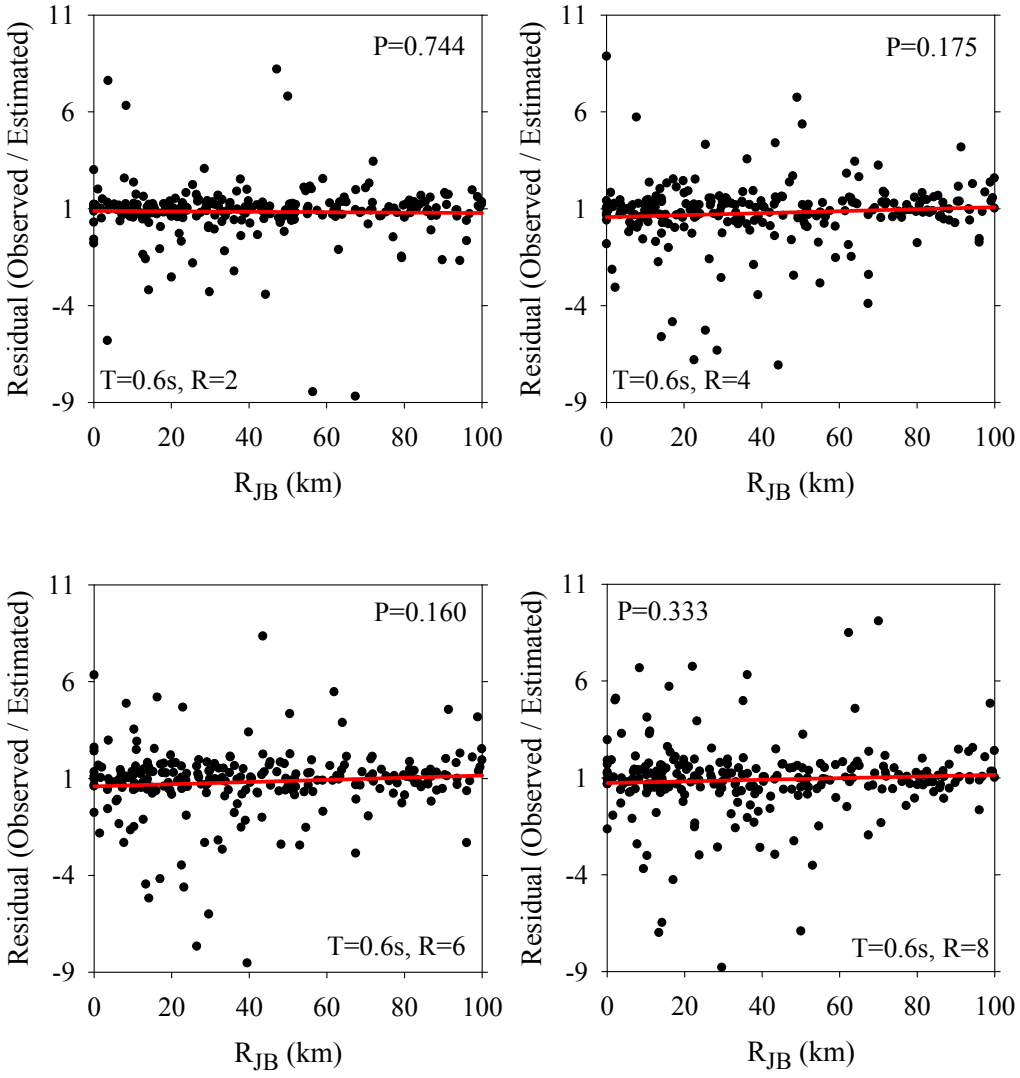

Figure B.4 Residual dependence statistics on R_{JB} for T=0.6s

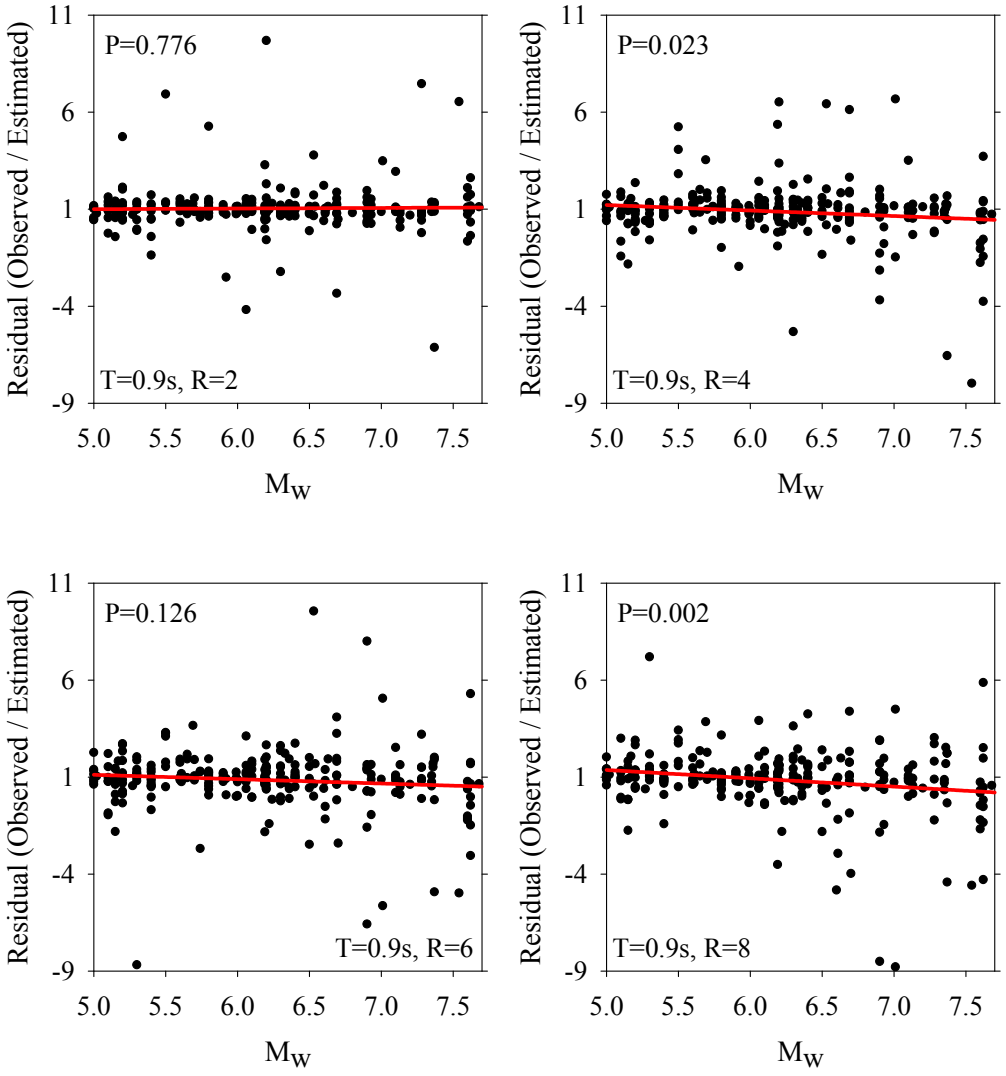

Figure B.5 Residual dependence statistics on M_w for T=0.9s

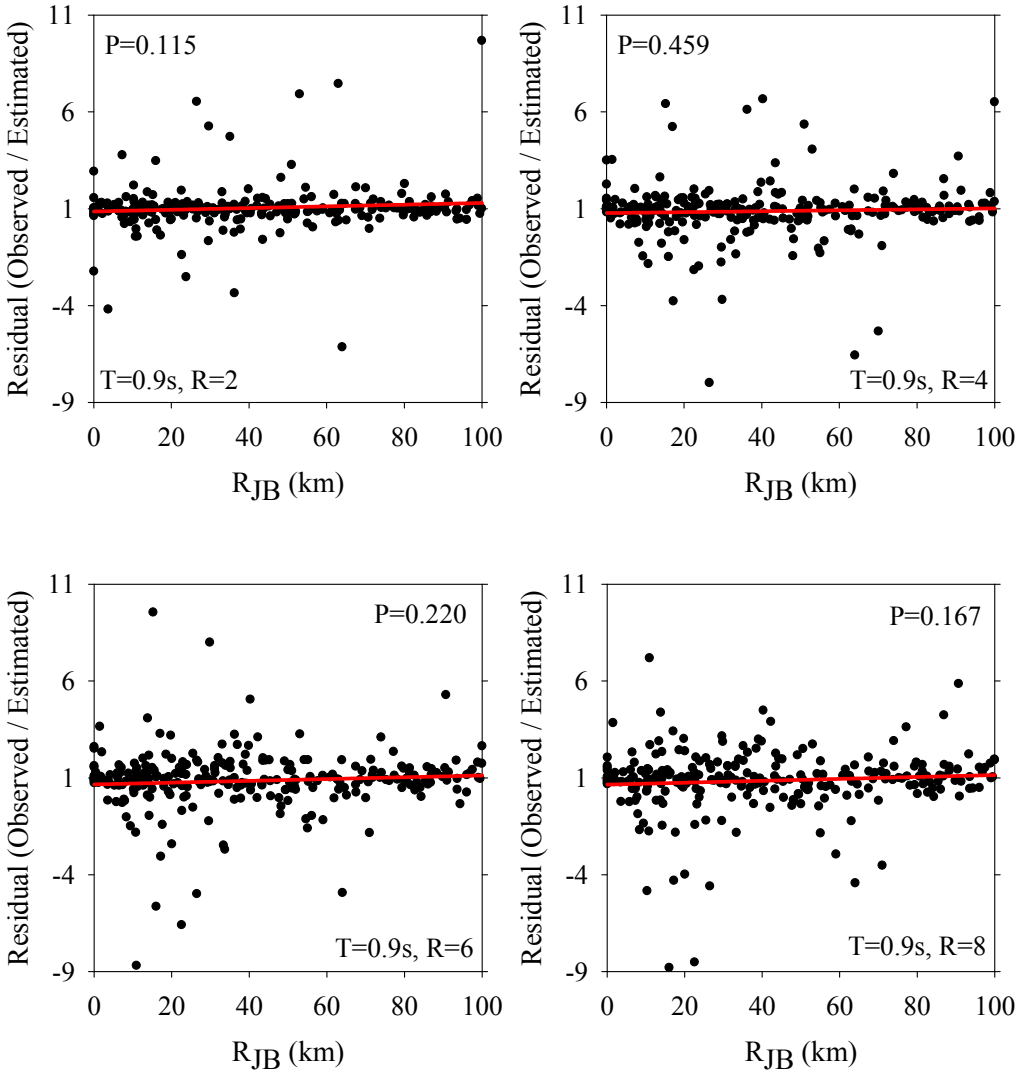

Figure B.6 Residual dependence statistics on R_{JB} for T=0.9s

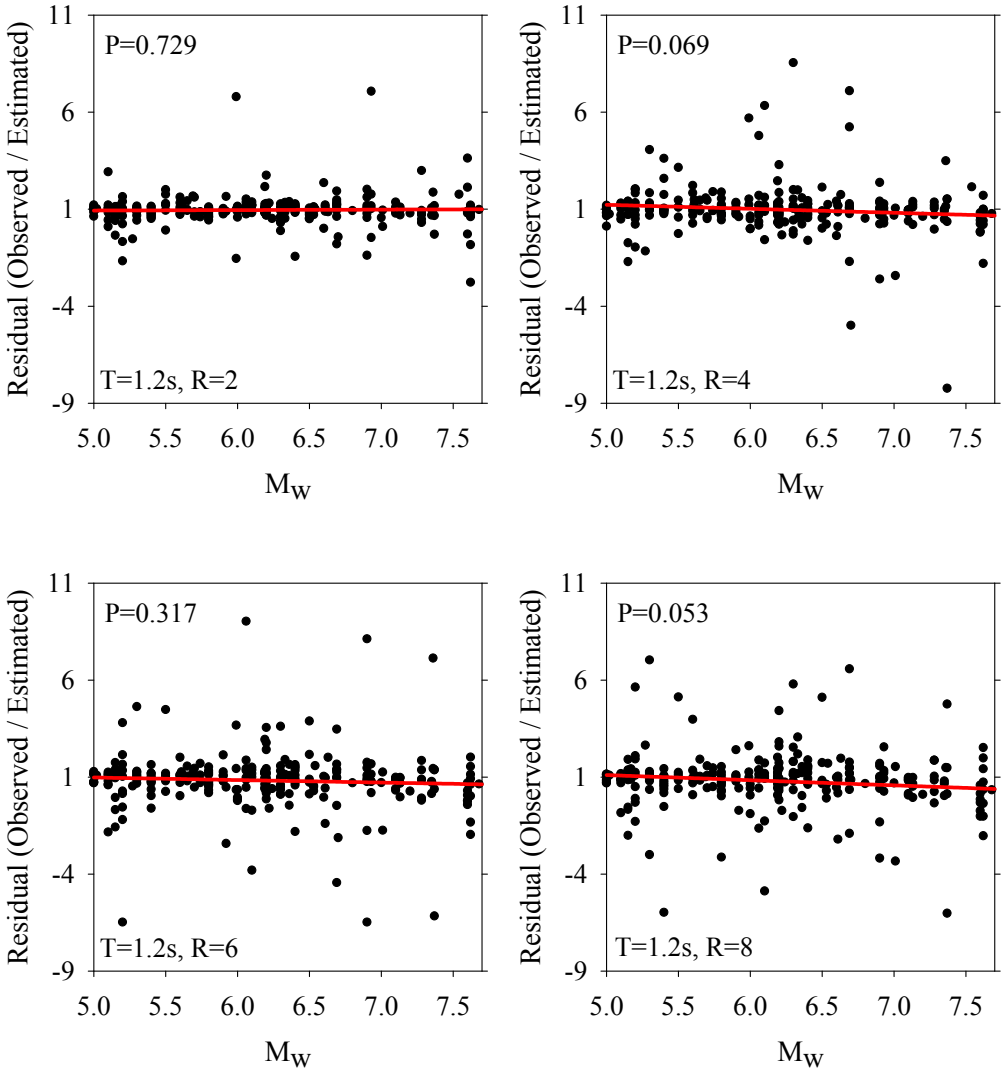

Figure B.7 Residual dependence statistics on M_w for T=1.2s

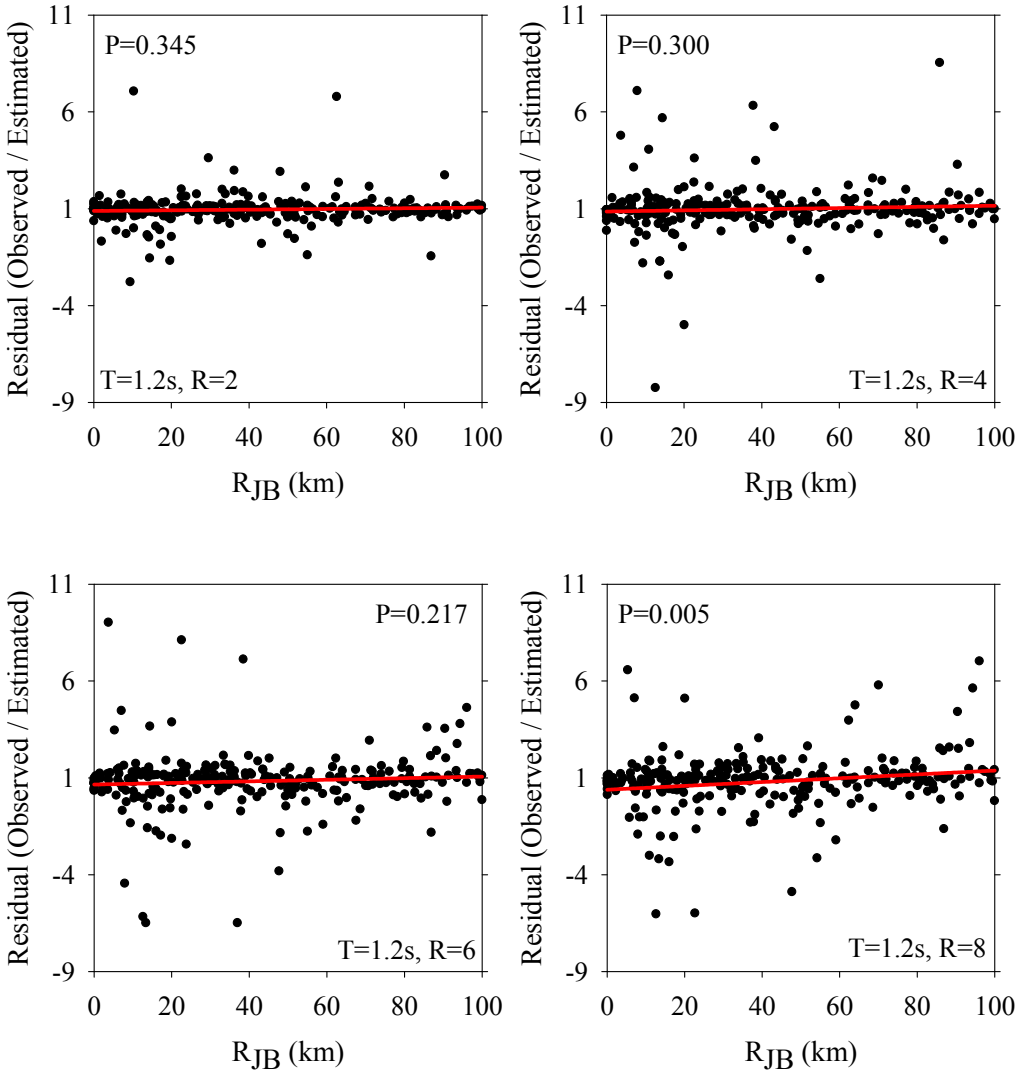

Figure B.8 Residual dependence statistics on R_{JB} for T=1.2s

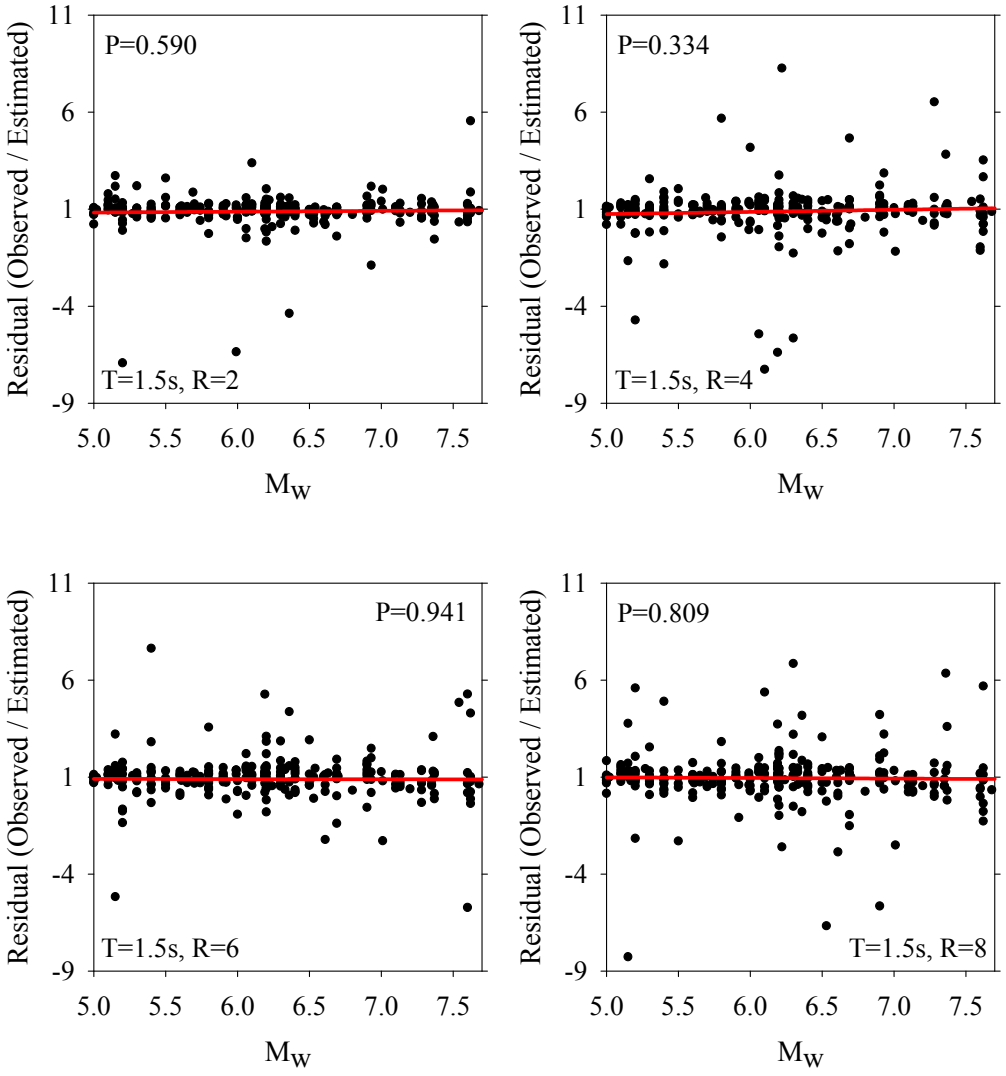

Figure B.9 Residual dependence statistics on M_w for T=1.5s

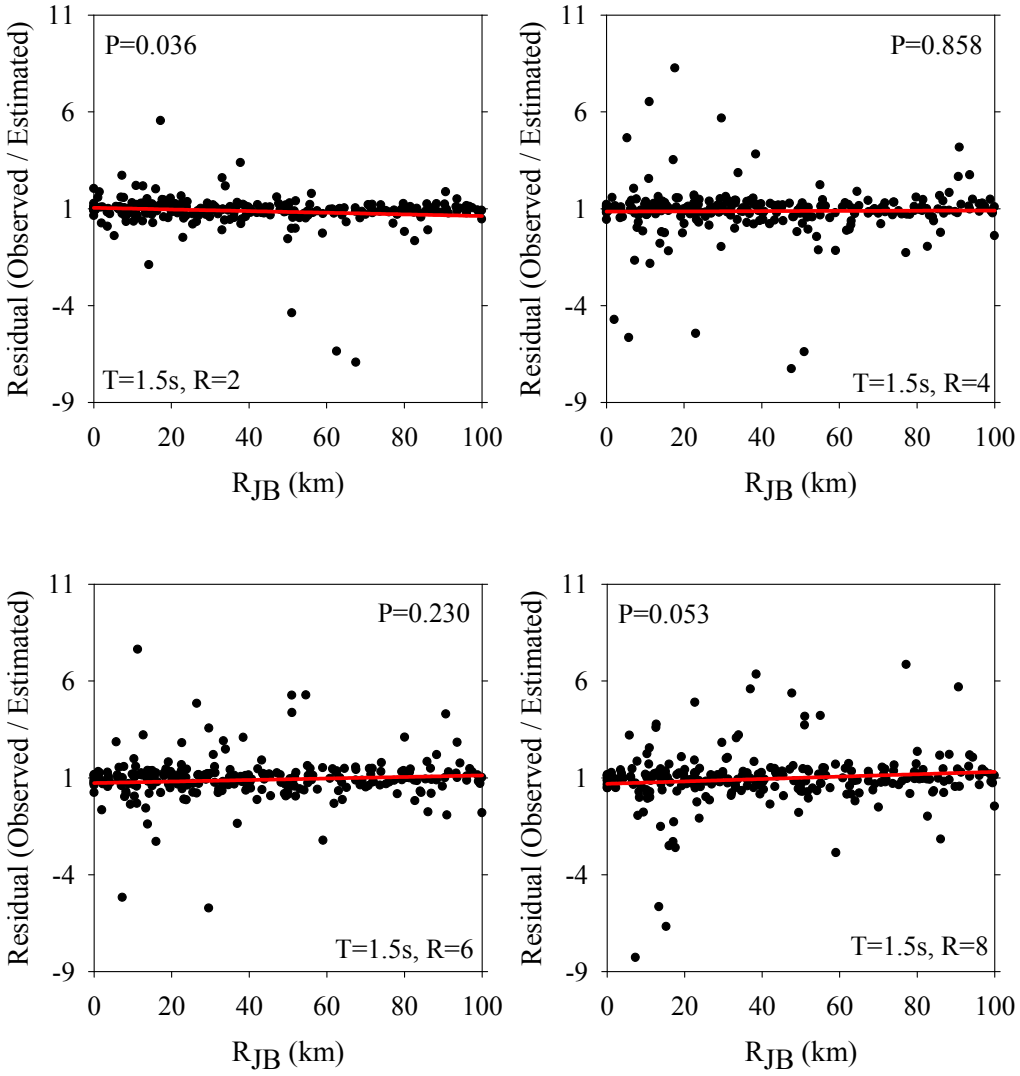

Figure B.10 Residual dependence statistics on R_{JB} for T=1.5s

APPENDIX C

STRUCTURAL MODELS

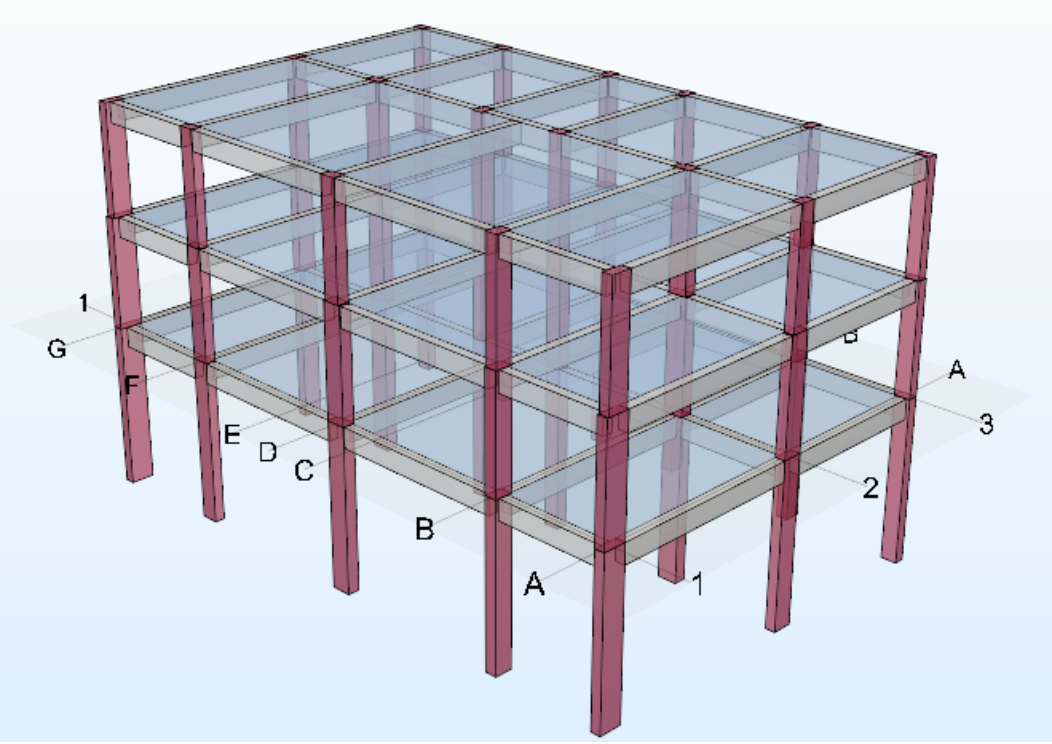

Figure C.1 3D model of 3-story building

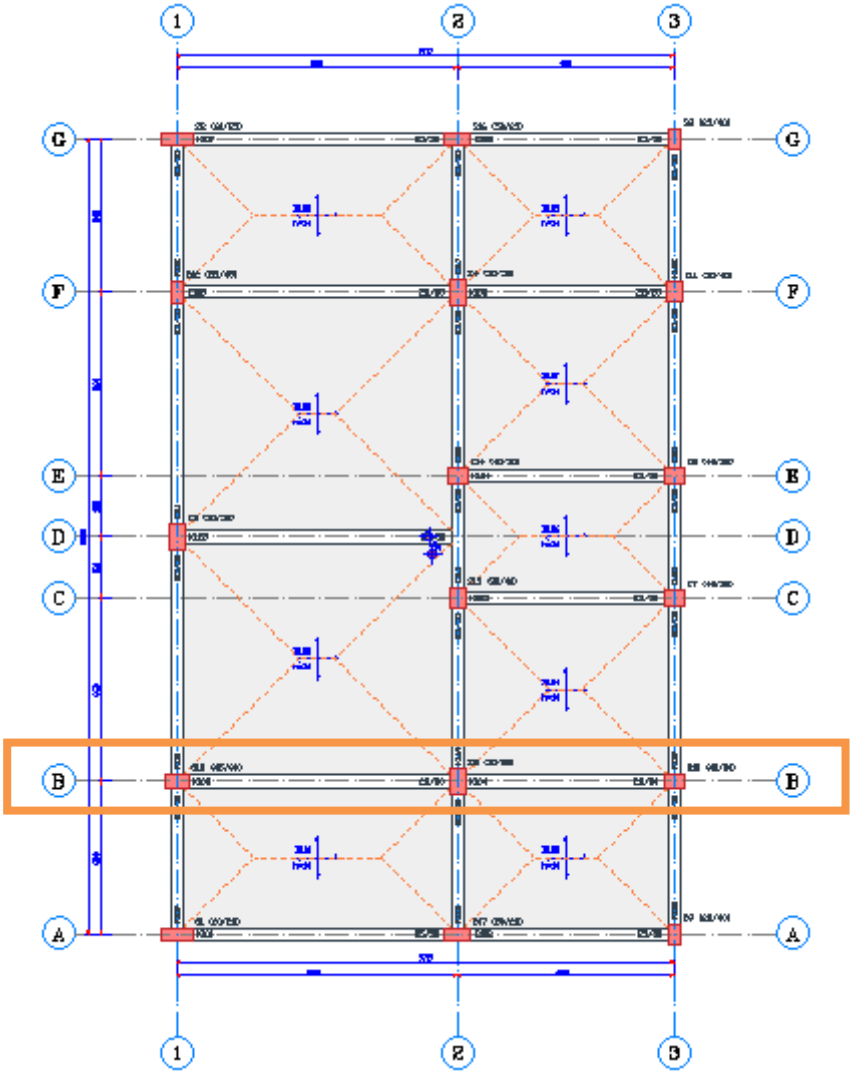

Figure C.2 Ground-story floor plan of 3-story building

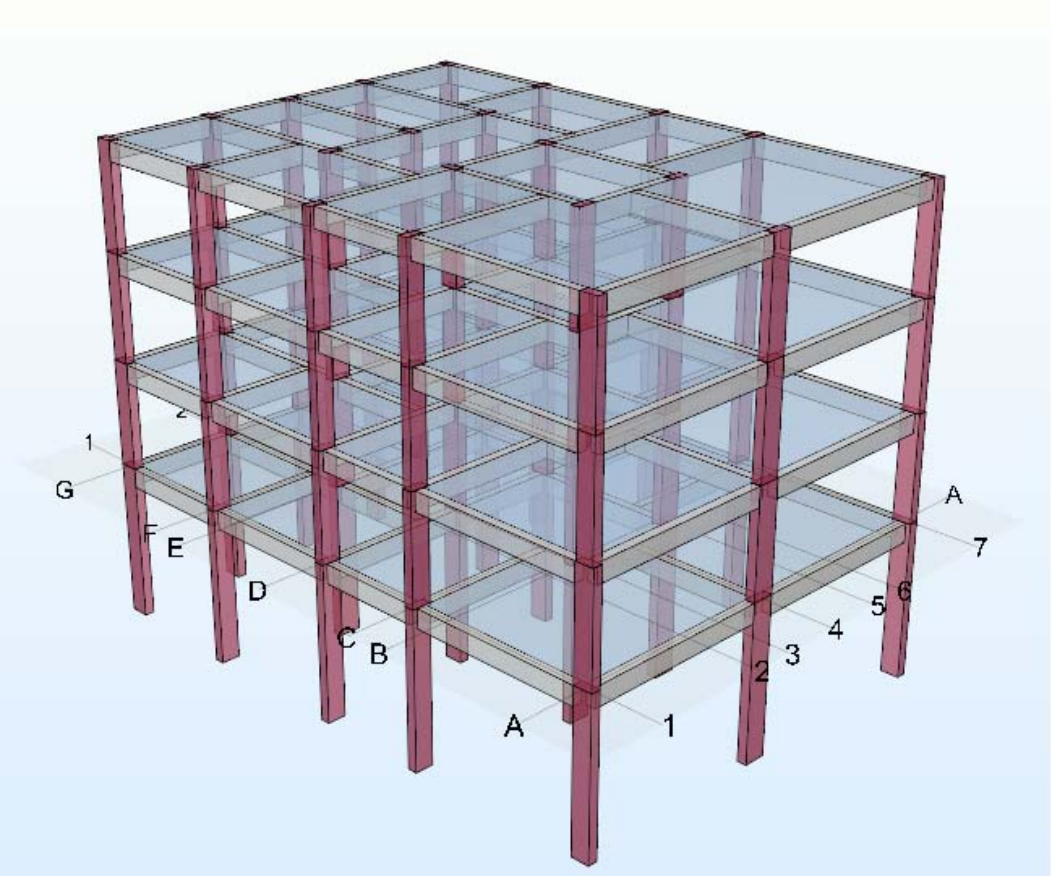

Figure C.3 3D model of 4-story building

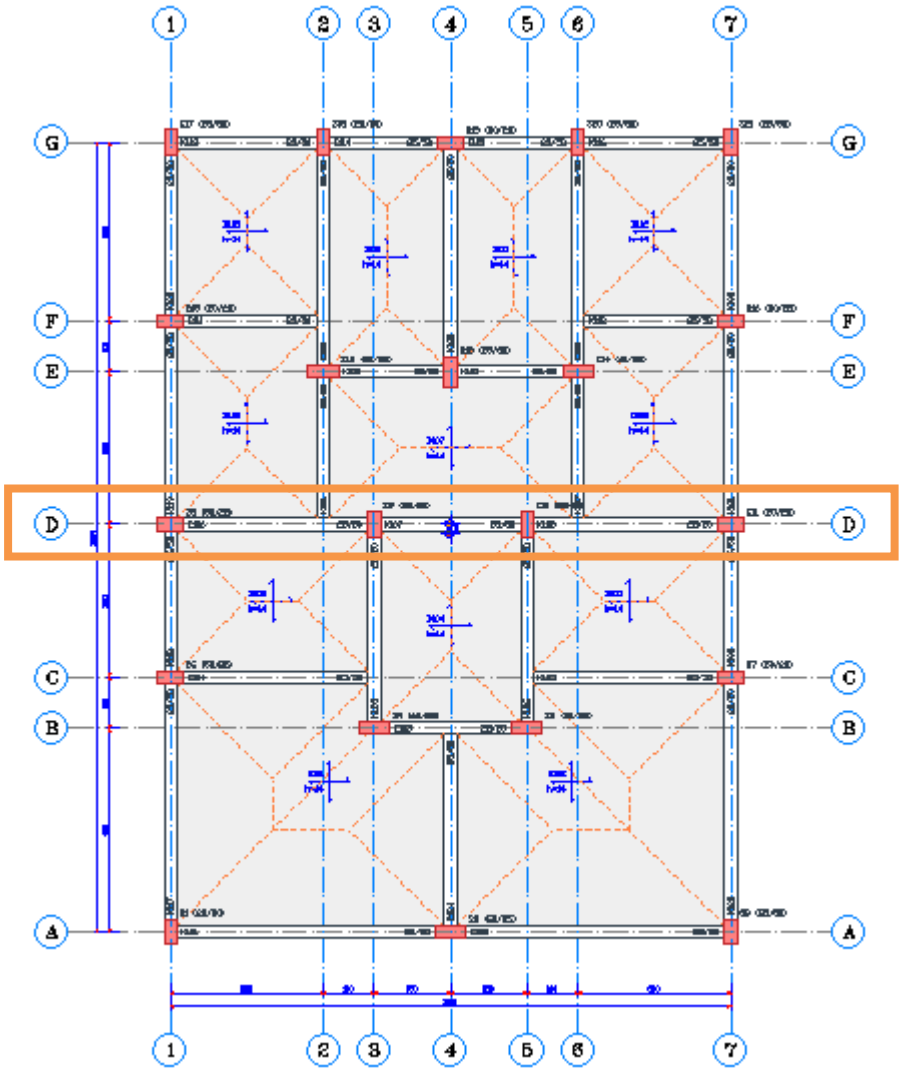

Figure C.4 Ground-story floor plan of 4-story building

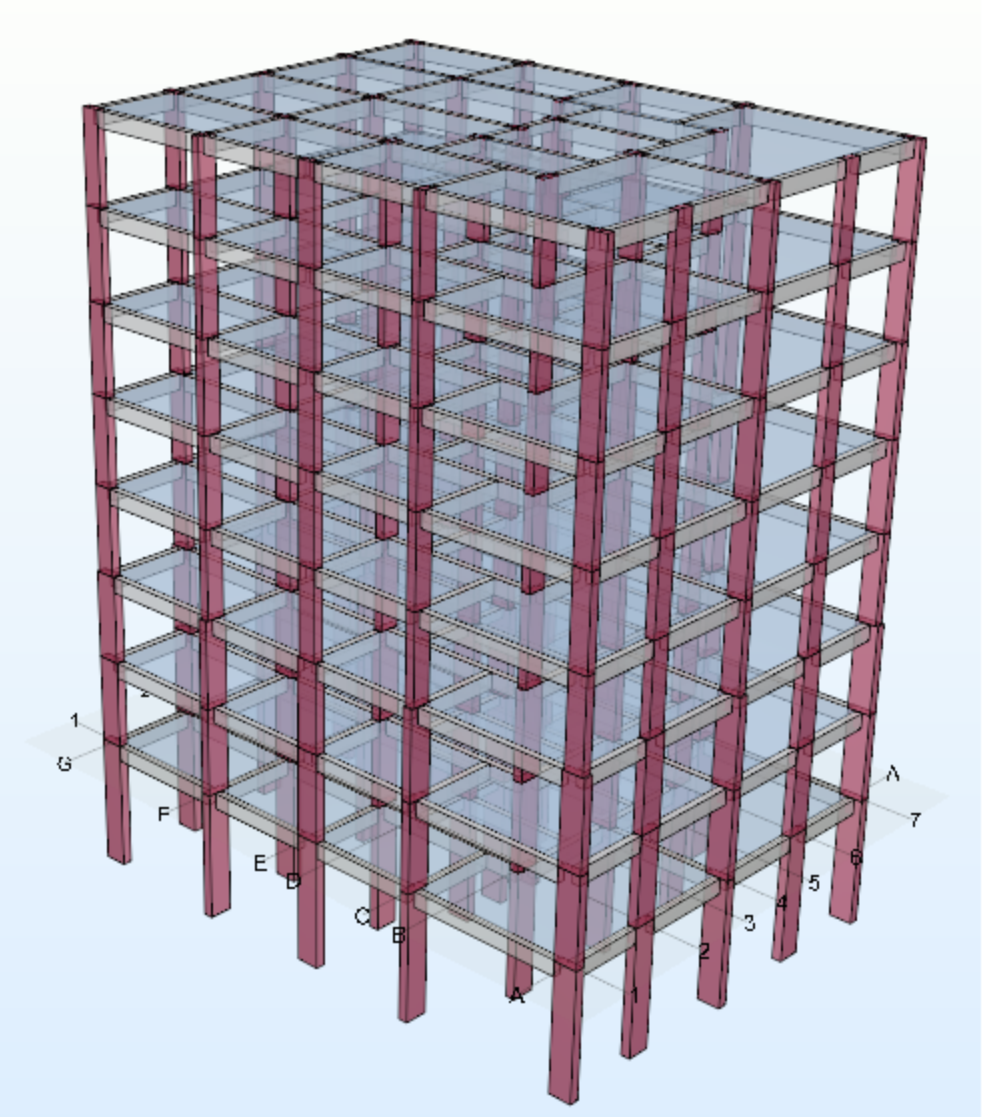

Figure C.5 3D model of 8-story building

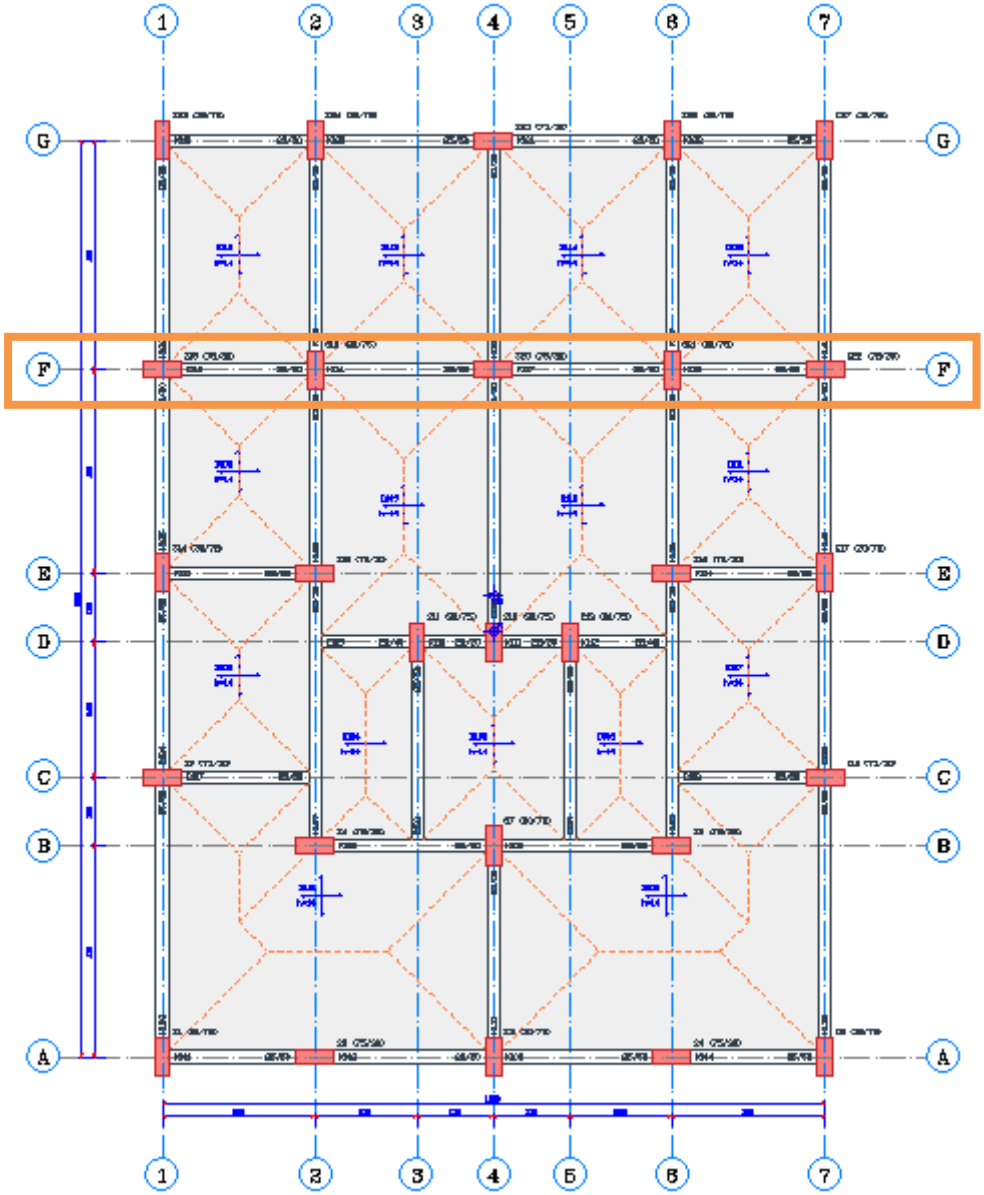

Figure C.6 Ground-story floor plan of 8-story building

CURRICULUM VITAE

PERSONAL INFORMATION

Surname, Name	: Ay, Bekir Özer
Nationality	: Turkish (TC)
Date and Place of Birth	: 13 April 1980, Karaman
Marital Status	: Married
Phone	: +90 312 210 74 44
Email	: ozer@metu.edu.tr

EDUCATION

Degree	Institution	Year of Graduation
MSc	METU Civil Engineering	2006
BSc	METU Civil Engineering	2003
High School	Ankara Anadolu High School	1998

WORK EXPERIENCE

Year	Place	Enrollment
2011 - Present	METU Dept. of Architecture	Part Time Inst.
2011 - 2012	METU Dept. of Civil Eng.	Project Assistant
2007 - 2011	METU Dept. of Civil Eng.	Research Assistant
2005 - 2007	METU Dept. of Civil Eng.	Project Assistant

FOREIGN LANGUAGES

Advanced English
Intermediate German

PUBLICATIONS

Ay, B.Ö. and Akkar, S., (2012). A Procedure on Ground Motion Selection and Scaling for Nonlinear Response of Simple Structural Systems, *Earthquake Engineering and Structural Dynamics*, Vol. 41, 1693–1707.

Ay, B.Ö. and Erberik M.A., (2008). Vulnerability of Turkish Low-Rise and Mid-Rise Reinforced Concrete Frame Structures, *Journal of Earthquake Engineering*, Vol. 12 (S2), 2–11.

Ay, B.Ö. and Akkar, S., (2012). Scaling and Selection of Ground Motion Records for Nonlinear Response History Analysis of Structures, *Proceedings of 15th World Conference on Earthquake Engineering*, Lisbon, Portugal.

Ay, B.Ö. and Akkar, S., (2010). Selecting and Scaling of Real Accelerograms, *Proceedings of 14th European Conference on Earthquake Engineering*, Ohrid, Republic of Macedonia.

Ay, B.Ö. and Akkar, S., (2010). Selecting and Scaling of Real Accelerograms to Reduce the Scatter in Dynamic Response, *Proceedings of 9th US National and 10th Canadian Conference on Earthquake Engineering: Reaching Beyond Borders*, Toronto, Canada.

Erberik, M.A., Aldemir, A. and Ay, B.Ö., (2008). A Critique on the Turkish Earthquake Code Regulations Regarding Masonry Construction, *8th International Seminar on Structural Masonry*, İstanbul, Turkey.

Ay, B.Ö. and Akkar, S., (2008). A Simplified Procedure for Estimating the Inelastic Drift Demands on Frame Structures, *Proceedings of 14th World Conference on Earthquake Engineering*, Beijing, China.

Ay, B.Ö. and Erberik, M.A., (2007). Türkiye'deki Az ve Orta Katlı Betonarme Yapıların Deprem Güvenliği Açısından İncelenmesi, *Proceedings of 6th National Conference on Earthquake Engineering*, İstanbul, Turkey.

Ay, B.Ö., Erberik M.A. and Akkar, S., (2006). Fragility Based Assessment of the Structural Deficiencies in Turkish RC Frame Structures, *Proceedings of 1st European Conference on Earthquake Engineering and Seismology*, Geneva, Switzerland.